NUMERICAL STUDY OF IMPACT INDUCED ELASTIC WAVE BASED NON-DESTRUCTIVE TEST ON REINFORCED CONCRETE STRUCTURES CONTAINING DELAMINATIONS

YONG CHEE LOK

UNVERSITI TUNKU ABDUL RAHMAN

NUMERICAL STUDY OF IMPACT-INDUCED ELASTIC WAVE BASED NON-DESTRUCTIVE TEST ON REINFORCED CONCRETE STRUCTURES CONTAINING DELAMINATION

YONG CHEE LOK

A project report submitted in partial fulfilment of the requirements for the award of Bachelor of Engineering (Honours) Civil Engineering

Lee Kong Chian Faculty of Engineering and Science
Universiti Tunku Abdul Rahman

September 2021

DECLARATION

I hereby declare that this project report is based on my original work except for citations and quotations which have been duly acknowledged. I also declare that it has not been previously and concurrently submitted for any other degree or award at UTAR or other institutions.

Signature : _____

Name : Yong Chee Lok

ID No. : 1601426

Date : 20/09/2021

APPROVAL FOR SUBMISSION

I certify that this project report entitled **"NUMERICAL STUDY OF IMPACT-INDUCED ELASTIC WAVE BASED NON-DESTRUCTIVE TEST ON REINFORCED CONCRETE STRUCTURES CONTAINING DELAMINATIONS"** was prepared by **YONG CHEE LOK** has met the required standard for submission in partial fulfilment of the requirements for the award of Bachelor of Engineering (Honours) Civil Engineering at Universiti Tunku Abdul Rahman.

Approved by,

Signature : 

Supervisor : Dr. Lee Foo Wei

Date : 20/09/2021

ACKNOWLEDGEMENTS

I would like to thank everyone who had contributed to the successful completion of this project. I would like to express my gratitude to my research supervisor, Dr. Lee Foo Wei for his invaluable advice, guidance and enormous patience throughout the development of the research.

In addition, I would also like to express my gratitude to my loving parents and friends who had helped and given me encouragement throughout the research writing process. Besides, I would like to express my gratitude to my senior, Mr. Liew Chi Hoe, for his useful information on my research.

ABSTRACT

This study presents the development of a non-destructive test method for evaluating delamination defects in reinforced concrete by the impact-induced elastic wave using four sensor accelerators and a signal acquisition unit (USB-3100 Series). A laboratory experiment was conducted to obtain the waveform result of different sizes and depths of delamination defects from different steel ball diameters. The propagated wave was interpreted numerically to determine the behaviour and characteristic of the Rayleigh wave (R-wave) by using Matrix Laboratory (MATLAB). Through the simulation of data, time-domain and frequency-domain graphs were obtained by using the highest magnitude of amplitude of the R-wave and Fast Fourier Transform, which were then used to determine the experimental measurement of concrete specimens. The correlations of velocity, amplitude attenuation and peak frequency were calculated to estimate the location, size and depth of the delamination defects with acceptable discrepancies due to the nature of reinforced concrete. Through the analysis of the result, the velocity of the R-wave has reduced from sensor 2 to sensor 3 in the sound concrete, whereas the velocity of the R-wave remains unchanged or increased along with the sensors. This phenomenon justifies the location of delamination defects. The attenuation rate of the R-wave is said to increase as the wave's frequency increases but decreases as the diameter of the steel ball increases. Furthermore, the peak frequency of R-wave is used to evaluate the depth of delamination where a greater value of peak frequency shows deeper delamination or vice versa. However, some of the results obtained are insensitive to evaluate the parameter of delamination defects. Despite the insensitive results, the study still provided a trends to evaluate R-wave behaviour in the concrete structure.

TABLE OF CONTENTS

LIST OF TABLES

LIST OF FIGURES

LIST OF SYMBOLS / ABBREVIATIONS

AE	Acoustic Emission
ASTM	American Society for Testing and Materials
CSV	Comma-Separated Values
FDM	Finite Difference Method
FEM	Finite Element Method
FFT	Fast Fourier Transform
H	Height
L	Length
MATLAB	Matrix Laboratory
NDT	Non-Destructive Test
PDE	Partial Differential Equation
PPFAC	Portland Pulverised Fuel Ash Cement
RCP	Reinforced Concrete Pipe
W	Width

LIST OF APPENDICES

CHAPTER 1

INTRODUCTION

1.1 General Introduction

Impact-induced elastic wave is a technique of Non-Destructive Test (NDT) that uses ultrasonic waves to determine a specimen's defects. Regarding the ultrasonic NDT, it is a type of wave made up of particles that eventually formed a different waves, namely longitudinal waves, transverse waves, surface waves, and Lamb waves (Ahmad and Bond, 2018). All these waves propagate effectively through a solid medium to determine the condition and characteristic of the defects. Since the waves are best for a solid medium, this study shows the impact-induced elastic wave propagates through the reinforced concrete structures containing delamination.

There are two methods for testing and inspection concrete structures ranging from large to microscopic defects: the destructive and non-destructive tests. A destructive test is a method that is carried out to the points of failure of a specimen, allowing the critical assessments for engineering evaluation. The specimen is normally destroyed or altered from its original. On the other hand, Non-Destructive Test (NDT) is the opposite of a destructive test that was carried out without causing any damage to the specimen to investigate the internal defects.

In recent decades, NDT has been developed to assess specific defects with different techniques. For example, the eddy current method can detect the concrete cover, a half-cell potential test can detect the active corrosion area of steel in reinforced concrete, and impact-induced elastic wave method which uses the surface wave or Rayleigh wave is capable of detecting the surface defect delamination-like crack in concrete structure (Maack, Villalobos and Scott, 2018). Therefore, NDT is categorised into contact and non-contact methods. Contact method requires the contact between sensor and surface of concrete structure when experimenting; while non-contact method does not require the contact between sensor and surface of concrete structures. Most of the NDT methods are contact methods such as Eddy current testing, electromagnetic testing, ultrasonic testing, liquid penetrant testing, and

penetrant testing, while the non-contact methods are radiography testing, infrared testing, holography testing, and visual inspection (Gholizadeh, 2016).

The defects that are found in the concrete structure are surface cracks, scaling and spalling, crazing, blistering, dusting, delamination, and efflorescence (Khan, 2020). Delamination is a defect that will affect the concrete strength and integrity. It is known as the separation or debonding of solids into multiple layers. The main factors that cause delamination in concrete are excessive entrapped air located in the concrete and prolonged bleeding of concrete after the concrete was cast.

1.2 Importance of the Study

The significance of this study is to enhance the knowledge of impact elastic wave-based non-destructive tests toward the engineering platform or any other similar professions. Non-destructive testing is a well-known and common technique used by almost every manufacturing, production, and engineering field that highly depend on trained professions and technicians to conduct the test. In comparison with the destructive test, NDT is more likely to be safe, efficient, accurate and cost-saving.

NDT is more appealing in terms of safe, efficient, accurate, and cost-saving because the test specimen is unharmed and remains the original after the test, thus saving resources and money. Besides, it also allows an accurate and rapid evaluation of the specimen, which is essential to ensure the performance on-site, hence, efficient and accurate. Nevertheless, according to Flyability SA's report, almost all the NDT are safe and harmless to humans or products except for Radiographic Test, which would emit radioactive isotope (Flyability SA, n.d.).

In this 21st century, the arising of technology and the evolution of materials used in this industrialized era has significantly enhanced the product's quality and quantity. This actively demonstrates that the quality control and inspection methods have led to a major impact in the engineering field and the complex nature of the products.

The contribution of this test is to ensure or guarantee the products are reliable, improved and free from any defects by limiting the room for any error production. Hence, it is called quality control and quality assurance. However,

nothing is perfect. Even with the greatest and well-inspected element, the products are still likely to contain some defections. Hence, quality control involves the testing and inspection of products and determines the defects (Testa, 1982). A well tested and defect-free structure will provide good quality control, whereas it will give advantages to the consumer and the products in terms of their lifespan, durability, and sustainability.

1.3 Problem Statement

Ever since 1300 BC, humankind has been using a composite building material called concrete. Today's concrete is made up of Portland cement, aggregates, stone, sand, water, and often mixed with some chemical component to control the concrete's setting and properties, depending on the environment and condition (Gromicko and Shepard, 2006). The lifespan of a concrete structure is normally around 50 to 100 years, depending on its mixture, reinforcement and placement (Keulemans, 2016). However, massive concrete structures such as dams, high-rise buildings, skyscrapers, and long-term bridges are easily subjected to aggressive damage by external actions. For instance, when the concrete is exposed to extreme weather conditions, chemical and physical attacks and other degradation actions, all of these processes will simultaneously act on the concrete surface and eventually minimize its durability and service life (Al Wardany, et al., 2004).

Before the deterioration of concrete, surface defects represent the early stage of the failures. Thus, it is important to test and monitor concrete's growth to maintain its life span. The implementation of NDT by the elastic wave is used to determine the defects in the concrete structures. However, the efficiency of using the contact method to detect the defects for large concrete structures is doubted. This is due to contact methods requiring a longer time to analyse the defects for large concrete structures and the proper set-up of the apparatus and sensor. Otherwise, the wave signal obtained from the experiment would be inaccurate due to the attenuation of the elastic wave. On the other hand, the cost will increase as the number of measurement points increases due to the coupling agent requirement to fix the sensor to the surface of concrete structure for the contact method.

Therefore, this study is to experiment of impact-induced elastic wave with the application of non-contact method based NDT technique on reinforced concrete containing delamination. The experiment is conducted by changing the sensor from contact method to non-contact method, while the different steel ball diameters will act as an input source of the experiment.

1.4 Aim and Objectives

The study aims to investigate the numerical study of impact-induced elastic wave-based non-destructive tests on reinforced structures containing delamination with the help of Matrix Laboratory (MATLAB) software. The objectives are:

(i) To study the changes of R-wave characteristics when propagating through concrete delamination.

(ii) To develop a methodology for R-wave signal processing and data interpretation by using MATLAB.

(iii) To statistically study the effectiveness of developed methodology on the condition of concrete delamination.

1.5 Scope and Limitation of the Study

The scope of this research is to conduct a laboratory experiment of the non-destructive test using an impact-induced elastic method on a concrete structure. The concrete structure is cast according to a special artificial defect of delamination with different diameters and depths. Then, the wavelength of the impaction is computed into the computer to generate the result in order to study the propagation velocity, attenuation rate and frequency response.

The limitation of this study in the list below:

(i) The numerical method is interpreted and limited to MATLAB software.

(ii) The dimension of the concrete specimen is constant with 4500 (L) x 1500 (W) x 1000 (H) mm with steel reinforcement.

(iii) Artificial delamination is made by polystyrene board with 5 mm thickness; while the arrangement of depth is 25 mm to 825 mm with increasing distance of 200 mm intervals and 500 mm spacing between each different delamination.

(iv) Four steel balls with different diameters of 10 mm, 15 mm, 20 mm, and 25 mm.

(v) Four sensors are placed near the surface of the concrete specimen with 10 mm of spacing.

1.6 Outline of Report

This report consists of five chapters where the first chapter describes the introduction, importance of the study, problem statement, aim and objectives, and, scope and limitation.

Chapter two discusses the appropriate literature review for this study including the method and approaches toward the experiment, destructive and non-destructive test, defects, and the past research.

Chapter three provides the methodology of this study which includes preparation and setting of the apparatus and materials, procedures, and result analysis.

Chapter four is the result and discussion of this experiment where the laboratory results of the impact-induced elastic wave on a reinforced concrete structure containing delamination are discussed thoroughly.

Chapter five is the conclusion of the study. The chapter summarises the entire study based on the result obtained from the experiment and discussion. The conclusion is made according to the objectives of the experimental study.

CHAPTER 2

LITERATURE REVIEW

2.1 Introduction

This chapter represents the literature review of related study to this topic as a whole. In summary, there are vast studies relating to the numerical study of impact-induced elastic wave based non-destructive tests on reinforced concrete structures containing delamination. It includes the analysis of the structure with different methods and different defects. Besides, this chapter also discusses different techniques used in non-destructive tests. The organisation of literature review starts with the structural analysis and followed by the destructive tests, non-destructive tests and concrete defects. Then, the last sub-topic discusses the past and similar researches.

2.2 Numerical Analysis

Numerical analysis is widely used throughout the field of engineering, sciences, medicine and business. It is the area of mathematics and computer science that uses numerical algorithms to solve the problem of continuous mathematics (Atkinson, 2007). The area of numerical analysis includes calculus, linear algebra and differential equations. With this being said, initial value and boundary value which involve either differential equation and partial differential equation, can be solved by numerical methods. The advantages of this method is easy to apply data into the equation, fast in producing results, and able to solve equations where an analytic solution is impossible. Examples of numerical methods are the finite difference method (FDM) and the finite element method (FEM). There are various types of online software to run numerical analysis such as MATLAB, Python, Octave, Julia, and etc. Hence, MATLAB is used as the general software to generate data and implement numerical methods throughout this study.

2.2.1 Finite Element Method

There are many mathematical and engineering problems that are hard and tough to solve using analytic methods, or sometimes even undergoes a tedious process

to obtain the exact solution due to vast and complex geometries and problems. Finite element method (FEM) is well known for its partial differential equations (PDE). Hence, boundary or initial conditions must be given when solving the equation (Sjodin, 2016). However, finite element analysis uses the numerical method to approximate output value. The value obtained is not an exact answer nor close to zero. Thus, the answer is said to be error to a certain degree. This is due to the factor of rounding error, truncation error and assumption error. The degree of error is depending on the type of numerical method adopted such as initial assumption and number of iterations (Strang, 2013). The major application for FEM is heat transfer, electromagnetics, frequency-domain high frequency, and structural analysis.

2.2.2 Finite Difference Method

Finite difference method (FDM) is similar to FEM which also applies the approximate method for solving PDE in a wide range of problems that include linear, non-linear, time independent and dependent problems. This method also applied to problems with irregular boundary shapes and conditions. However, comparing FDM with FEM, this method is easier to implement than FEM due to FEM requiring more sophisticated mathematical equations for its formulation. In addition, FDM is comparatively straightforward when the calculation is done under a simulation in a rectangular shaped geometry using a regular grid. However, it is difficult to solve problems with irregular or curved boundaries as the boundary conditions need to be truncated. If the boundary condition problem can be solved on irregular boundaries, thus, this method will achieve a high-quality result (Sjodin, 2016). The application of FDM is weather calculations, seismology, and astrophysics.

2.2.3 Fast Fourier Transform

Fast Fourier transform (FFT) is a complicated algorithm but a powerful analytical tool which is widely used in digital signal processing. FFT uses an application of reducing the number of computations for N values from $2N^2$ to 2N lg N, where lg is the base-2 logarithm. Thus, FFT is able to solve equations that describe dynamic responses to heat, light or electricity, and fluctuating signals.

2.3 Matrix Laboratory (MATLAB)

MATLAB is a commercial software developed by Cleve Moler in 1982. It is a programme that is used by millions of engineers and scientists to analyse data, develop algorithms, and create models. In addition, this programme also provides machine learning, image and video processing, signal processing, control system, computational finance, test and measurement, and computational biology. It is currently sold by The Math-works and can be purchased and downloaded from mathworks.com. Thus, this application allows us to translate the data and implement it into numerical methods.

2.4 Destructive Test

Destructive test refers to a methodology where a specimen is tested to a point of failure in order to understand a specimen's performance and behaviour. The aim is to determine the service life and weakness of the design which does not show under a normal working condition. Therefore, it is important to understand and determine the original specification of the specimen before undergoing the destructive test. When comparing destructive tests to non-destructive tests, it is more suitable for specimens that are produced in a large quantity due to economic factors. It is reliable but wasteful at the same time because the specimen must be destroyed or damaged during the test which could have been used for normal operations (Gupta, 2018). Figure 2.1 shows the vertical compression destructive test on a reinforced concrete pipe (RCP) in order to determine its maximum sustainable load. The disadvantages of destructive tests are being too expensive, wasteful and hard to deal with large infrastructure.

There is a lot of method to run destructive test which includes mechanical testing that perform bending, impact, and tensile test; fatigue test that perform in extreme environments to detect the endurance of a specimen; hydrogen test that perform in hydrogen exposure environment; and lastly, residual stress measurement that perform at near-surface of a specimen to detect the premature failure of a structure (TWI, 2021).

Figure 2.1: Vertical Compression Destructive Test on a DN500 RCP (Institution for Underground Infrastructure, 2020).

2.5 Non-Destructive Test

As mentioned in the introduction of chapter 1, non-destructive test is an analysis technique to evaluate the defect of a specimen without causing any damage to its original form. It is also known as non-destructive examination, non-destructive inspection, or non-destructive evaluation. The main concern of this test is to evaluate the internal flaws which are in the form of cracks and eventually lead to loss of strength, durability, and workability in a structure.

NDT is effective in detection of all types of cracks, void, and deterioration no matter how deep or tiny the defects. Besides, it can also check the integrity and quality of the structures. It is also applicable for both old and new structures. Hence, with all these effective terms, NDT is more extensive than destructive tests and greatly used by companies to examine their infrastructure such as oil rigs, nuclear plants, railroad, pipelines, and wall structures. Thus, the advantages for NDT are time and cost saving, environment safety, and highly reliability (Zetec, n.d.).

NDT has more methods to undergo the test compared to destructive tests due to the range of test specimens such as complete volumetric inspection or surface inspection, each with different types of collection data and requisite its own kind of material and apparatus. Among the most common test method, we

have Radiography NDT, Ultrasonic NDT, Eddy Current NDT, Visual NDT, Acoustic Emission NDT, Liquid Penetrant NDT, Magnetic Particle NDT and Leak Testing (Flyability SA, n.d.).

2.5.1 Acoustic Emission Testing

Acoustic emission (AE) test is a passive technique that relies on detecting short bursts of ultrasound stress waves from an emission source. The sources can be any impact of heavy loads as shown in Figure 2.2. Hence, it is also called impact acoustic testing. This technique uses sensors to convert the stress waves into electrical signals which are then processed by the software in a computer. When the stress wave travels through a medium containing defect, there will be a great release of energy, hence, a threshold as the peak amplitude will form in the software as the result of the defects (Gholizadeh, Leman and Baharudin, 2015). This method is called a transient method and it is capable of detecting cracks. On the other hand, the continuous method is capturing all the AE within a set duration and determining the average signal level. This method is capable of detecting leakage and gearboxes.

AE has the ability to detect a wide range of defects like cracking, delamination, corrosion, early stages breakages, friction and impacts. It can also conduct during the operating condition of a structure and machines. Besides, it can be conducted in a laboratory and in-situ where wireless data relay method is capable for remote testing. However, this technique is limited to assess the structural integrity when a fully diagnosed inspection is needed.

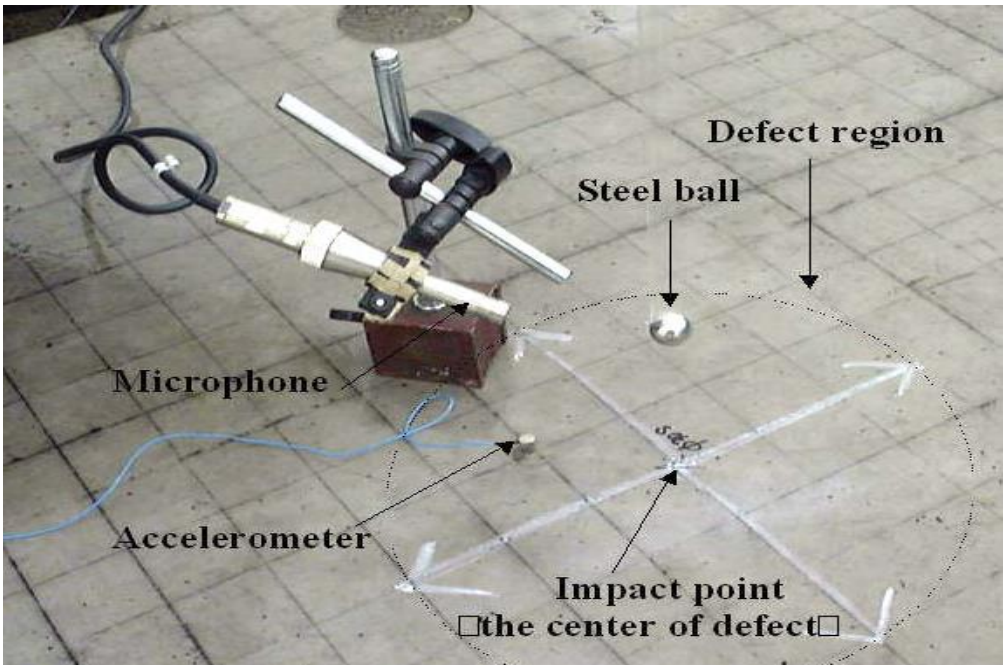

Figure 2.2: Impact Acoustic Method with a Steel Ball (Asano, et al., 2003).

2.5.2 Electromagnetic Testing

Electromagnetic testing is a method which uses the electric current with magnetic field to detect and characterise surface and near surface defects which travel through a conductive medium. Other than detecting the surface defects, it can also be used to measure the material and coating thickness, conductivity measurements, and inspection of heat exchanger tubing in the nuclear power industry. The sensitivity of electromagnetic testing has always been the advantage to detect small cracks. In addition, it can also inspect complex shapes and sizes of conductive medium, and is portable due to simple apparatus setup.

There are three types of electromagnetic testing which are the Eddy current testing, remote field testing, and alternating current field measurement. Eddy current testing is the most well-known method among the three due to the wide application in the aerospace and manufacturing industry which mainly focus on the detection of defects in conductive medium. It applies the phenomenon of electromagnetic induction where the alternating current is set at a frequency and generates a magnetic field around a coil. Then, eddy current is induced when brought closely to a conductive material. If the current detects a defect, it will disturb the circulation of eddy current as shown in Figure 2.3. Hence, the signal will be sent to the impedance plane display tester; while some

of the instruments are using the simple analogue meter displays (Nelligan and Calderwood, 2015).

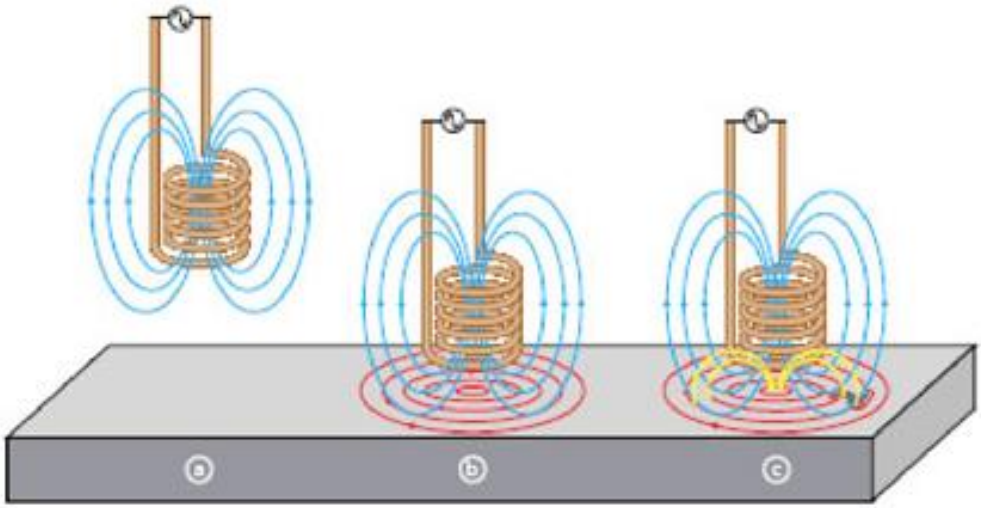

Figure 2.3: Effect of Electromagnetic Coil when Brought Closely to a Conductive Material (Nelligan and Calderwood, 2015).

2.5.3 Visual Testing

Visual testing is a kind of inspection by using the naked eye where it does not necessarily require any special tool or equipment. However, it requires a well-trained or experienced inspector to determine the quality and defect of the structures. When it comes to visual inspection of concrete structure, cracking is the easiest and most obvious to determine; while internal defects that cannot be detected with naked eye would need the help of instruments.

2.5.4 Ultrasonic Testing

Ultrasonic testing is the most common method in non-destructive tests which perform on materials like structures, pipes, aerospace, marine, and military industries. It is also used in the impact acoustic emission testing as shown in part 2.5.1 as the ultrasonic wave to determine the defect. The apparatus for this inspection normally consists of an ultrasonic transducer, receiver, and a pulser. The transducer will generate a high frequency of ultrasonic sound wave energy into the specimen when driven by the pulser that produces a high voltage electrical pulse. Then, the transducer will transform the reflected sound waves

into electrical signals to the receiver, thus, the result will show on the display unit. There are two types of transmissions which are direct and indirect transmission as shown in Figure 2.4. The sound wave is capable of travelling through any medium until it encounters a boundary with different density, it will reflect back to the source. The frequency of the sound wave is beyond the hearing limit of humans which is in the range of 500 kHz to 20 MHz.

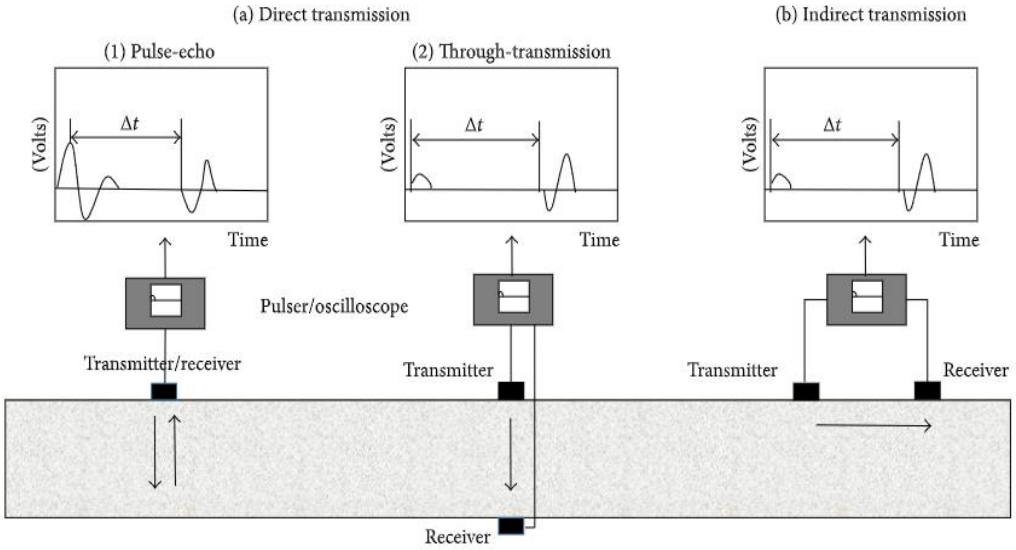

Figure 2.4: Types of Transmission (Lee and Oh, 2016).

There are two methods for ultrasound waves to receive the signal which are reflection and attenuation (Ahmad and Bond, 2018). In reflection, pulse echo inspection is a method that sends and receives the sound wave by transducer. The time interval between the reflection from a discontinuity of the sound wave is recorded. If the acoustic velocity is known, it can derive the distance travelled in the specimen. Figure 2.5 shows the scenario of the pulse echo method when the wave encounters different defects. In attenuation, through transmission testing is a method that separates the signal from sending and receiving the sound by a transducer. Each of the transducers and the transmitting probe is located at different positions. As the sound wave travels through the specimen, the porosity will attenuate within it. This method can increase the efficiency by minimizing the loss of wave energy (Sölken, 2008).

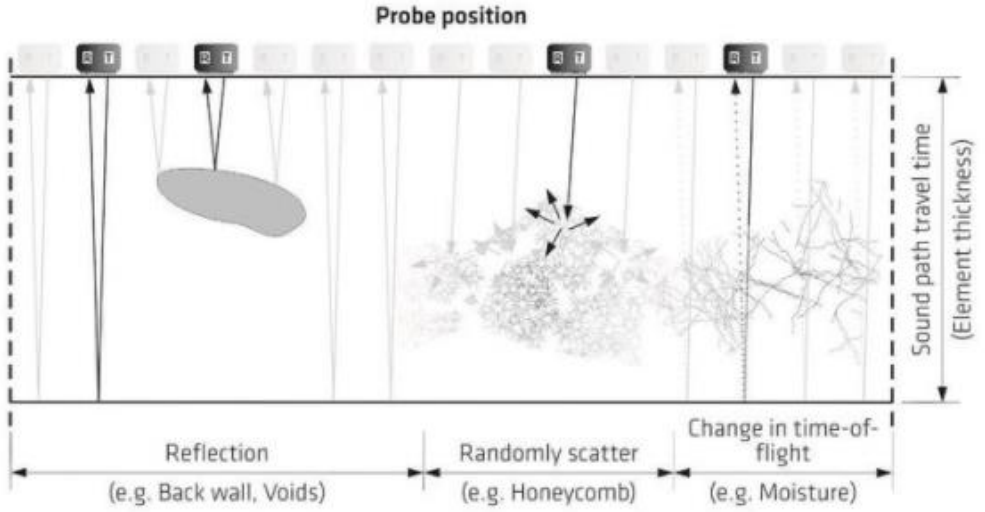

Figure 2.5: Scenario of Pulse Echo Method on Different Defects (Maack, Villalobos and Scott, 2018).

2.5.4.1 Surface Waves

Surface waves or Rayleigh Waves are a type of ultrasonic waves that travel along the surface of any medium. It is highly sensitive to flat and curved surfaces as it travels through a complex contour, it tends to reflect from a sharp edge or propagate from a rounded edge. In surface waves, the particle oscillates in an elliptical behaviour as shown in Figure 2.6. For the measurement of R-wave, velocity is the time difference between two peaks; while the wavelength is the distance for one complete cycle (Lee and Oh, 2016).

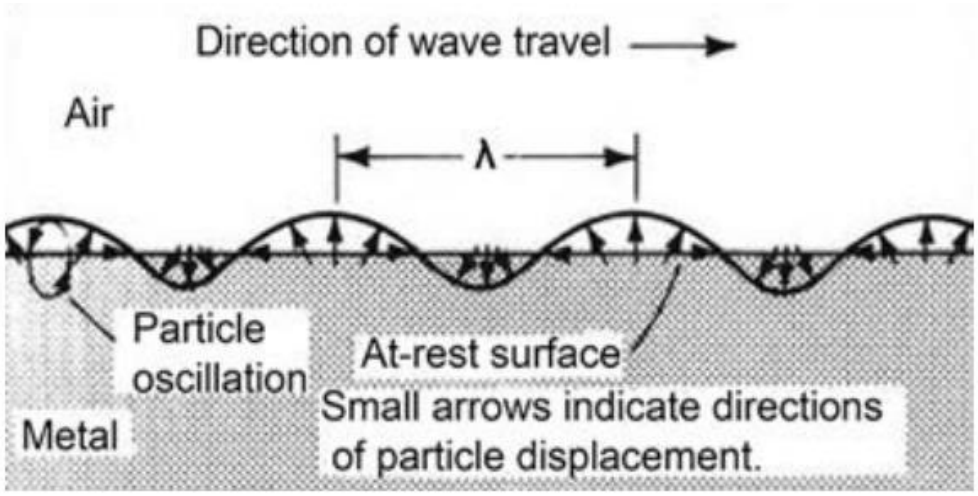

Figure 2.6: Particle Behaviour of Surface Waves when Travelling through a Medium Surface (Ahmad and Bond, 2018).

2.5.4.2 Longitudinal Waves

Longitudinal waves or compression waves are also a type of ultrasonic waves which move parallel to the direction of wave propagation. It is the most common wave used to inspect any materials. The particles in longitudinal waves will form compression and rarefactions when it travels back and forth in the direction of the travel (Ahmad and Bond, 2018). Figure 2.7 shows the schematic diagram of a longitudinal wave where, (a) the particle oscillates in compression and rarefaction. (b) amplitude of particle displacement against distance travel by wave.

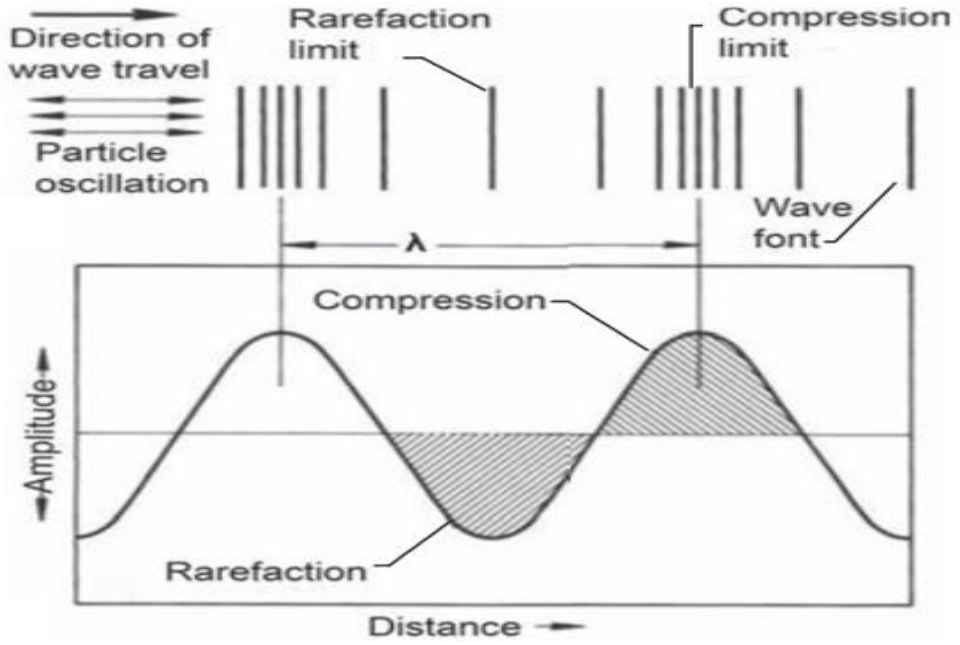

Figure 2.7: Schematic Diagram of Longitudinal Ultrasonic Waves (Ahmad and Bond, 2018).

2.5.4.3 Transverse Waves

Transverse waves or shear waves are also a type of ultrasonic waves which travel perpendicular to the direction of wave propagation. As the wave travels through a medium, the particles in the transverse wave only oscillate up and down about their equilibrium position as shown in Figure 2.8 (Russell, 1998). Unlike longitudinal waves, transverse waves exhibit a strong attraction force among each particle. Thus, the movement of the waves can apply on a solid

medium. In air and water, the attraction force between molecules is very small which is not suitable for the transmission of transverse waves.

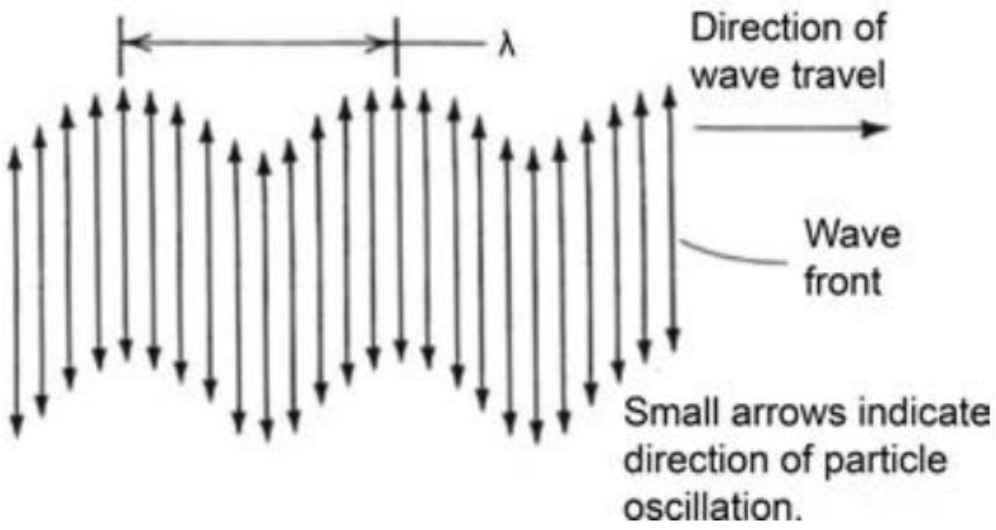

Figure 2.8: Schematic Diagram of Movement of Transverse Waves (Ahmad and Bond, 2018).

2.6 Concrete Defects

Concrete is a structure component made up of three basic ingredients that is water, aggregate and cement; while the aggregate includes rock, sand and gravel. There are a lot of different compositions to cast concrete in terms of ratio of the standard concrete mix as 1:2:4 for cement, sand and aggregates, respectively. Then, mix the concrete thoroughly and compact to remove air bubbles and voids. A good quality concrete is a high durability concrete. However, with several factors relating to durability of concrete, concrete structure is highly exposed to external conditions and extreme environments such as high humidity and rain, UV rays from sunlight, freezing and thawing, and chemical attacks. Therefore, there are different types of deterioration that can occur in concrete to lower the durability and workability of the structure. For instance, cracking, blistering, delamination, spalling, scaling, curling, dusting, and efflorescence. These defects have their specific reasons and causes.

2.6.1 Delamination in Concrete

When a fresh concrete is casted and compacted, the cement and aggregate tend to settle by gravity and lighter materials tend to float toward the surface. This

natural settlement will displace the excess water and entrapped air, or be termed as bleeding. Delamination happens when the air and water are trapped beneath the densified mortar before the surface bleeding is complete, as the concrete hardens, the subsurface voids form in the air and water is trapped. Hence, the surface will eventually detach from the structure as shown in Figure 2.9. Delamination always forms in slab structure as the concrete has a large and wide area to settle the aggregate. In order to determine delamination virtually, operators can strike the concrete with a hammer and thin mortar layers may detach (Seegebrecht, 2016).

Figure 2.9: Formation of Delamination on Concrete Slab (Khan, 2020).

Delamination may not affect the overall performance and workability of a concrete slab. It is more likely to create an awful and unattractive look on the surface. However, it will cause a severe problem to the structure if it is widespread. There are a few ways to avoid delamination:

(i) Do not seal or close the slab surface prematurely, finishing should start only after the completion of the bleeding process.

(ii) By knowing the weather condition, do use accelerators or heating devices on concrete in cooler weather.

(iii) Do not use air-entrained concrete if possible.

(iv) Do not place concrete on a vapor retarder.

(v) Do not cast the concrete on a subgrade which is less than 40 degrees Fahrenheit.

Lastly, delaminated surfaces can be cured and repaired by re-patching the surface. Extensive delaminated structure may need to be repaired by grinding and casting a new surface to it.

2.6.2 Cracking in Concrete

Cracking is the most common defect and it is normally the first sign of distress in concrete structure. It can occur in both hardened and fresh concrete when the force has exceeded its maximum tensile strength. However, according to Eurocode 2, Cl. 7.3.2 – Control of Cracking, there is an allowable crack width of 0.3mm for exposure class X0 and XC1 in quasi-permanent load. With this being said, the allowable 0.3mm crack width is maximum value to maintain the durability of a concrete structure.

Other than excessive load applied on the concrete to cause cracking, there are also reasons for cracking before the hardening process such as improper mixing of concrete composition, insufficient curing and lack of control joints. Hence, different causes will result in different types of cracks such as plastic shrinkage concrete cracks, expansion of concrete cracks, and settling concrete cracks. Plastic shrinkage cracks often happen when the water ratio is too much in the composition of concrete, hence, the concrete will shrink more than normal when it dried. Hot weather is also a reason for these plastic shrinkage cracks and expansion concrete cracks. Thus, expansion joints are often used as a point of separation and shock absorber. Besides, settling concrete cracks are caused by the force of gravity during the curing of concrete. This separates the aggregate from the surface and leaves a weaker layer near the surface where the reinforcing bar is located. Thus, during the bending of the hogging moment, the cracks tend to form at the top layer of the concrete (Giatec Scientific, 2019). Figure 2.10 shows the formation of surface cracking of plastic shrinkage cracks.

There are a few ways to prevent cracking in concrete such as start with a well compacted base in order to enhance the settling level. Then, the modification of concrete mix with a lower water-to-cement ratio or add concrete admixtures to control cracking.

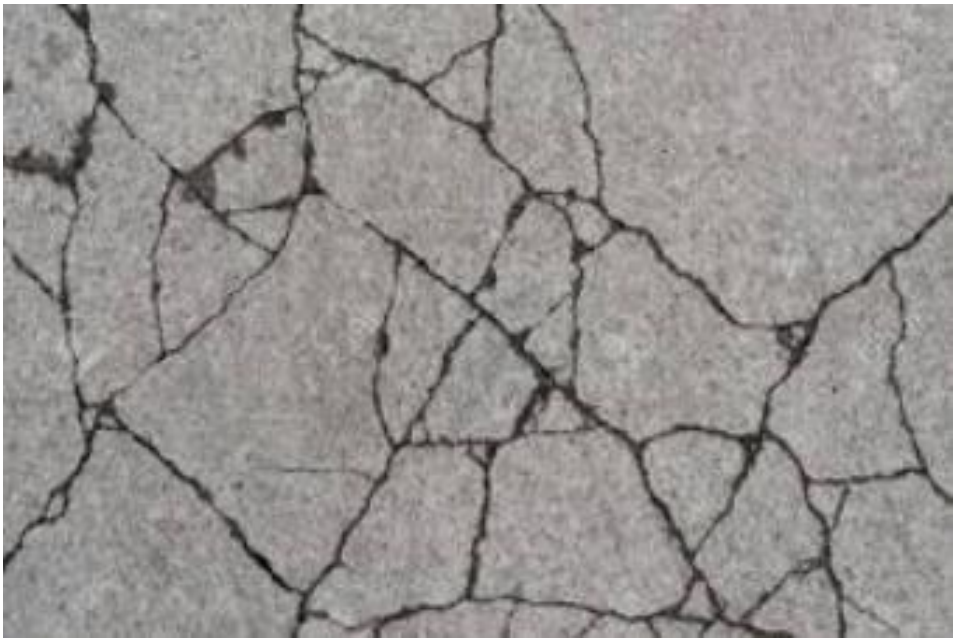

Figure 2.10: Formation of Surface Cracking (Khan, 2020).

2.6.3 Crazing in Concrete

Crazing is very similar to cracking or it is known as map cracking. It is the development of a network or random spaced hollow cracks as shown in Figure 2.11. The formation of crazing is somehow similar with cracking as the composition of concrete contains higher water content or due to insufficient curing time. However, crazing is more often to form during hot weather whereas the hardening of the surface is relatively faster than the evaporation of water content. Crazing does not deteriorate over time; hence, repair of concrete is unnecessary. However, in some cases, application of sealers and surface hardeners were used as the appearance is the main concern for the client (Tarr, 2008).

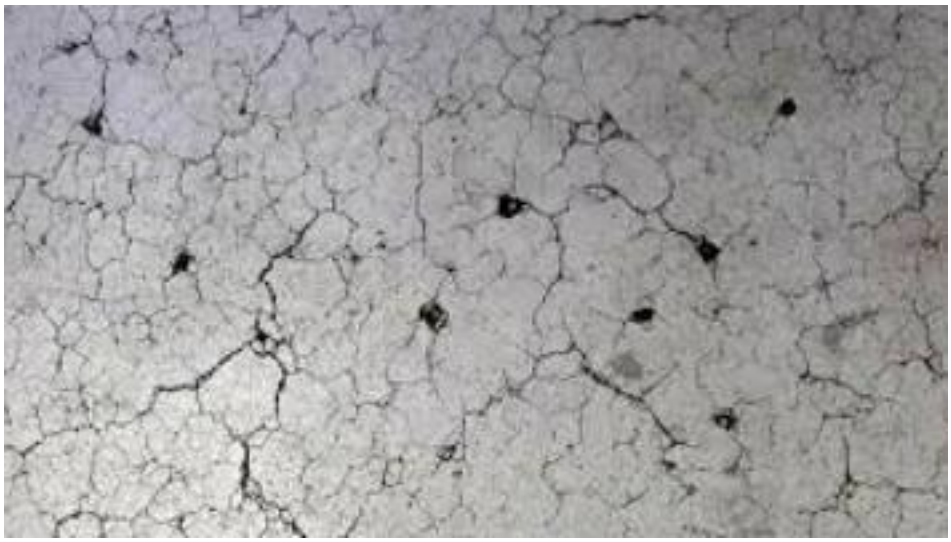

Figure 2.11: Formation of Concrete Crazing (Khan, 2020).

2.6.4 Blistering in Concrete

Concrete blisters are hollow, small, isolated, and diameter normally from 3 to 8 centimeters at the concrete surface as shown in Figure 2.12. It is very similar to delamination due to the same reason that causes these defects where air and voids are trapped under the finished concrete surface. In addition, the appearance of blistering usually shows up as bumps while delamination normally shows up as a cracked and hollow surface.

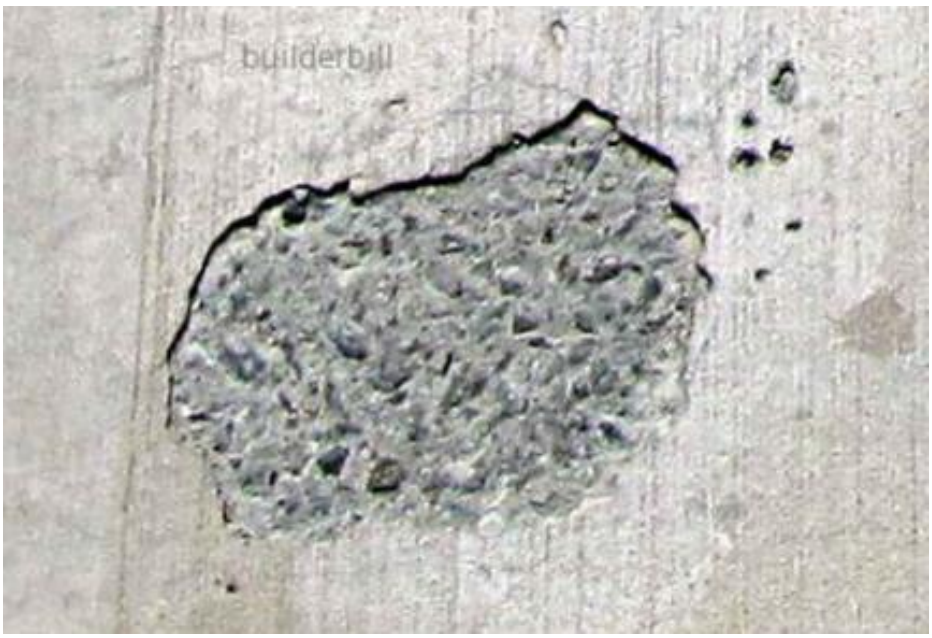

Figure 2.12: Formation of Concrete Blister (Khan, 2020).

The repairing steps are also similar with delamination such as detecting the affected area by visually inspecting or sounding with a hammer. Then, remove the affected area if it is a small defect; while grinding of surface is needed if it covers a large area of defects. Lastly, repair and recast the area with graded sand, cement, and bonding agent (Green, 2021).

2.6.5 Dusting in Concrete

Dusting is the development of fine, loose, and powdery materials on a hardened concrete by deterioration. It is also called as chalking or referred to as “Laitance” which is the weak layer of fine particles formed on the concrete surface composed of fine aggregates and hydrated cement due to excessive water during concrete curing. Figure 2.13 shows the formation of laitance scrubbed by fingers. With this being said, high water cement ratio will weaken the concrete strength and cause dusting by applying water to the surface, composition of mixing is too wet or low cement content, improper curing leads to dehydration, and unexpected rainfall during finishing.

Figure 2.13: Formation of Concrete Dusting/Laitance (Ecoratio, 2019).

Needless to say, in severe conditions, dusting could weaken the durability of the structure if the surface of the slab erodes into the harder portion of the slab, especially during a heavy rain or abrasion of a vehicle tire on a

driveway. It is time consuming and costly to repair this defect where resurfacing, overlays or removal, then replacement is needed to complete the repair progress. Lastly, in order to avoid dusting, keep out the excess water during finishing and keep in the moisture during curing (Green, 2021).

2.6.6 Efflorescence in Concrete

Efflorescence in concrete is the formation and accumulation of white powdered deposition of salts on the concrete surface as shown in Figure 2.14. Primarily, it is caused by water evaporating from the concrete and left behind soluble salts on the surface. For instance, the usage of calcium chloride admixture to accelerate the settling time during a cold weather and high slump concrete are the major factors to efflorescence (Bannister, 2020). It is not a structural but aesthetic problem as it can be cleaned by chemically unproductive aggregates.

Figure 2.14: Formation of Concrete Efflorescence (Khan, 2020).

2.6.7 Scaling and Spalling in Concrete

Scaling and spalling in concrete are the decaying and flaking of concrete surfaces where part of the surface breaks and peels away as shown in Figure 2.15. It is a result of a weak concrete surface vulnerable to damages. The main reason behind these defects is that water perforates through the concrete surface and eventually corrodes the steel reinforcement. Besides, poor finishing technique, improper curing and bad concrete mix can also lead to these defects (Sullivan, 2020).

Figure 2.15: Formation of Concrete Spalling (Albrecht, 2019).

Sealing is one of the methods to prevent spalling whereas the penetrating waterproofing sealer can be applied after 28 days of concrete placement. It can also be stopped by adding adjoined air entrainment admixtures to the concrete mix, proper finishing and curing. Additionally, scaling and spalling in concrete can also be repaired by patching, resurfacing and overlaying the defected area with cementitious compound, if the affected area is not severed.

2.6.8 Artificial Defects in Concrete

Artificial defects are produced by test engineers rather than occurring naturally, thus, it shall have a close or similar behaviour like a real defect. Artificial defects are used for various concrete testing as a calibration before the test undergoes on a real specimen. The manufacturer or professional could run a test or refer to the defected sample in order to produce artificial defects. It is then served as a reference structure where the creator of the mock-up specimen has known the area of the artificial defects. There are a few popular artificial defects which are easy and simple to produce such as honeycomb and delamination.

Normally, the artificial defect is cast differently before the main specimen. Figure 2.16 shows the artificial delamination is made by sticking two

concrete plates and leaving a small gap between each of the plates to simulate delamination. Artificial honeycomb is often tested by using a foam material but the segregation of the concrete is not realistic enough; while the mock-up honeycomb is cast by mixing an agglomeration of pebbles and stones with a constant diameter together with the concrete mixture as shown in Figure 2.17. Then, a thin layer of cement paste is coated externally. Both the foam and real honeycomb specimens are having different bulk density (Maack, Villalobos and Scott, 2018).

Figure 2.16: Simulation of Artificial Delamination with Two Fixed Concrete Plates (Maack, Villalobos and Scott, 2018).

Figure 2.17: Simulation of Artificial Honeycomb on Reinforced Bar (Maack, Villalobos and Scott, 2018).

2.7 Previous Research

There are a lot of past researches that compared different methods of non-destructive tests on reinforced concrete structure. Some of the research may be similar or close to the topic that is going to study. The researches may vary from using a different approach, technique, and defect.

2.7.1 Impact Acoustic Method

Masanori Asano (2003) and his fellow colleagues from the Department of Civil Engineering of Gifu University have done an experiment by obtaining the sound generated from a dropping steel ball to evaluate the defects in concrete. The experiment uses a concrete slab specimen with artificial defects made from styrene. The test uses a condenser microphone, an accelerometer, an amplifier, and a computer to acquire the signal of the wave. Figure 2.2 shows the set-up of the experiment. Once the test is completed, the frequency distributions were derived by using FFT.

2.7.2 Pulse Echo Technique

Maack, Villalobos, and Scott have done an experiment based on pulse echo technique in 2018. Artificial honeycomb and delamination were cast separately before placing it into the slab specimen. This technique is tested with two screening components which are B-scan and C-scan. B-scan is the inspection that scans through the side surface of the specimen; while C-scan will give a plan inspection of the specimen. The results of the measurement data process of B-scan and C-scan are shown in Figure 2.18 and Figure 2.19 respectively once the Synthetic Aperture Focusing Technique was completed.

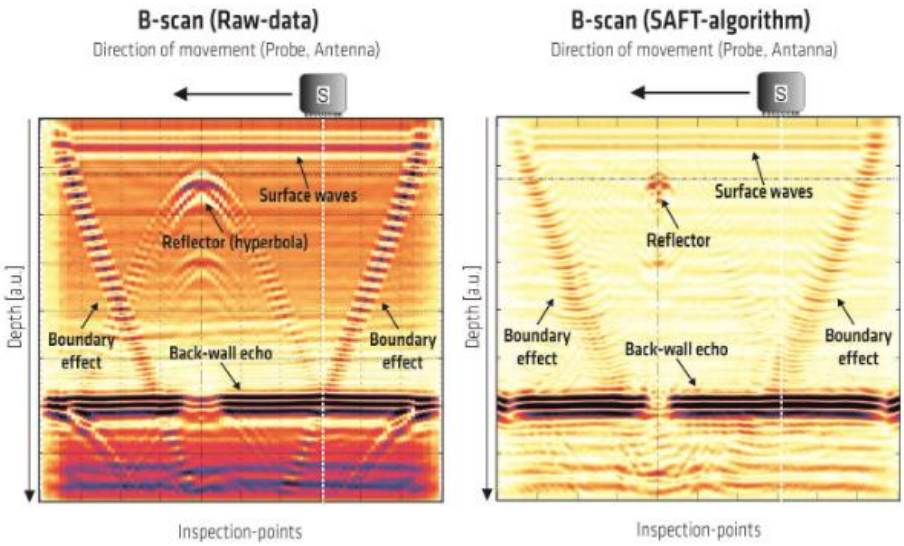

Figure 2.18: Result of B-scan by Pulse Echo Technique (Maack, Villalobos, and Scott, 2018).

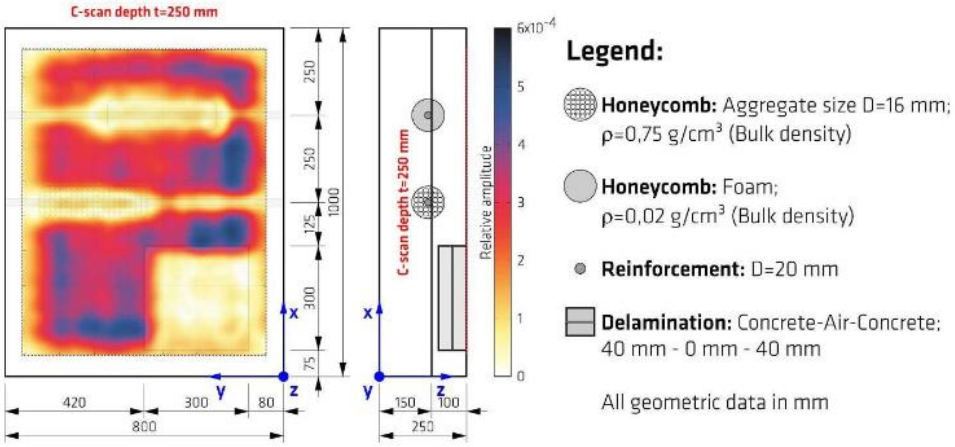

Figure 2.19: Result of C-scan by Pulse Echo Technique (Maack, Villalobos, and Scott, 2018).

In conclusion, this test requires a preliminary test to check the reality of the artificial defects in order to achieve higher NDT results compared to the real defect. Hence, it was shown that the foam-made honeycomb is not suitable to simulate the segregation phenomena in concrete.

2.8 Summary

In this chapter, the common concrete defects and the background of destructive and non-destructive tests are discussed and compared in order to obtain the best method to evaluate the reinforced concrete containing delamination. The types

of NDT method discussed are acoustic emission testing, electromagnetic testing, visual testing, and ultrasonic testing. Thus, the method that is going to be used in this study is ultrasonic testing. The study of ultrasonic testing is discussed including the longitudinal waves, transverse waves, and surface waves. Surface waves or Rayleigh waves are said to be easier to identify waveforms due to their high amplitude to propagate a longer distance and low attenuation rate.

CHAPTER 3

METHODOLOGY AND WORK PLAN

3.1 Introduction

This chapter describes the methodology and work plan in conducting the test of impact-induced elastic wave method on a reinforced concrete structure containing delamination. Figure 3.1 shows the general process of methodology and Figure 3.2 shows the procedure in conducting the experimental works for this study.

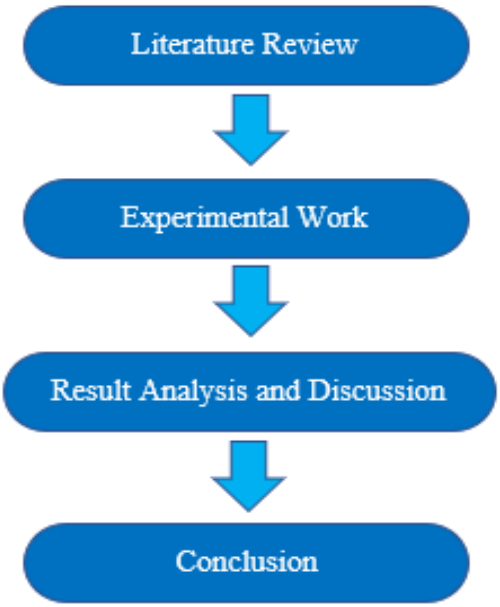

Figure 3.1: General Process of Methodology.

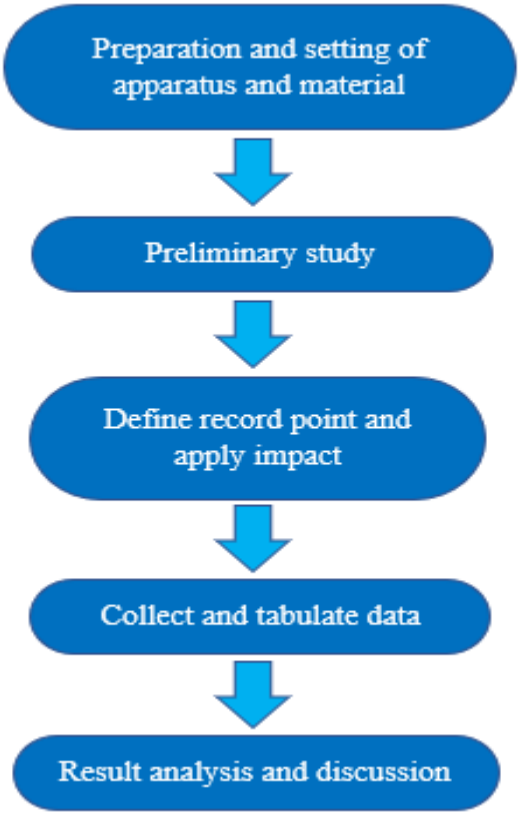

Figure 3.2: Procedure of Experimental Work.

3.2 Preparation and Setting of Apparatus and Materials

The materials used in this experiment are six concrete slab structures, each with a dimension of 4500 mm (L) x 1500 mm (W) x 1000 mm (H). The concrete specimen was cast with Portland Pulverised Fuel Ash Cement (PPFAC), coarse and fine aggregate, water, reinforced steel bar and ADVA 209 admixture. The properties of the concrete specimen are shown in Table 3.1. The density of the concrete is 2400 $\frac{kg}{m^3}$ with a concrete grade of G40. The maximum size of aggregate for the concrete mix is 20 mm.

Table 3.1: Properties of Concrete Specimen.

Mixture	Density (kg/m^3)
Cement	3150
Water	997
Fine Aggregate	1750
Coarse Aggregate	1520

The existing artificial delamination in the concrete specimen is made by using a circular shape of polystyrene board with thickness of 5 mm. There are 5 artificial delamination each with different diameters ranging from 100 mm to 500 mm. The polystyrene boards are placed in a straight line with spacing of 500 mm intervals in an increasing order of diameter from 100 mm to 500 mm as shown in Figure 3.3. There are six sets of concrete specimens each with different depth for placement of polystyrene boards in 25 mm, 225 mm, 425 mm, 625 mm, and 825 mm from the surface. The sixth concrete specimen is free from any defects which serves as the control specimen. Figure 3.4 shows the side view of concrete specimens with different depths of artificial delamination.

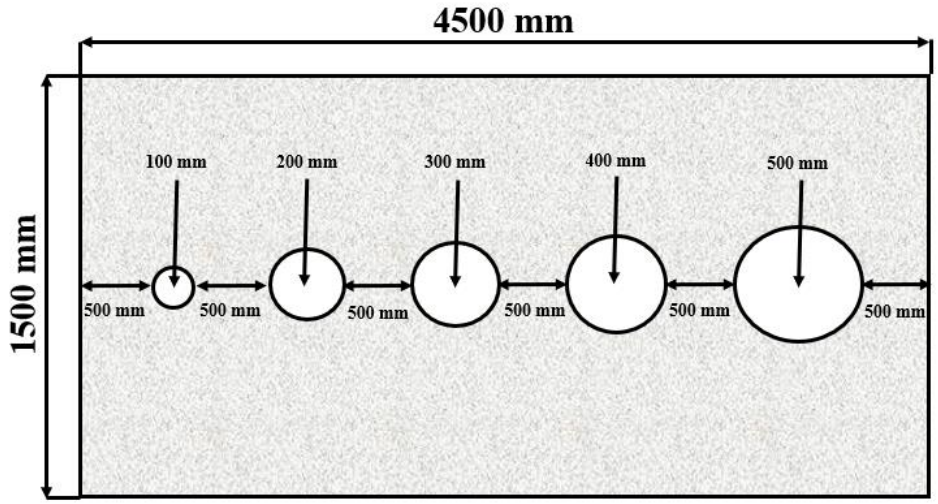

Figure 3.3: Plan View of the Placing of Polystyrene Boards in the Concrete Specimen.

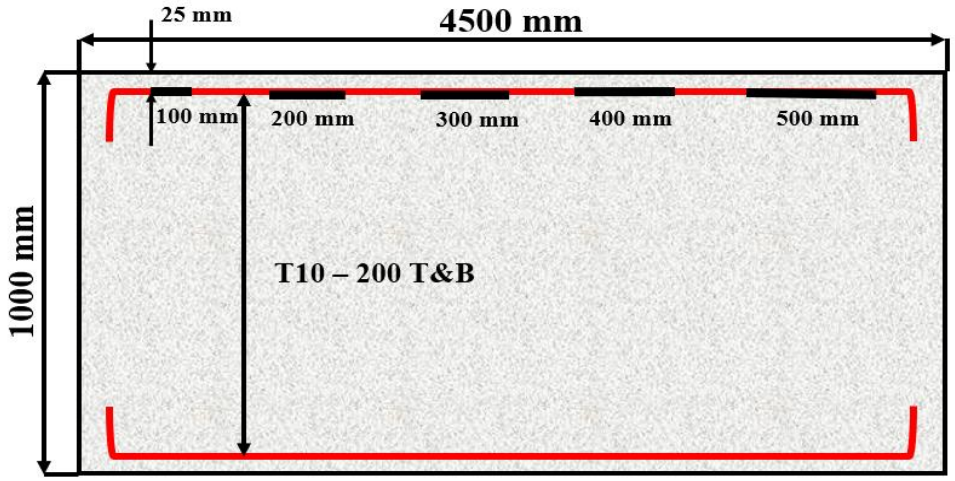
25 mm
4500 mm
100 mm
200 mm
300 mm
400 mm
500 mm
1000 mm
T10 – 200 T&B

(a)

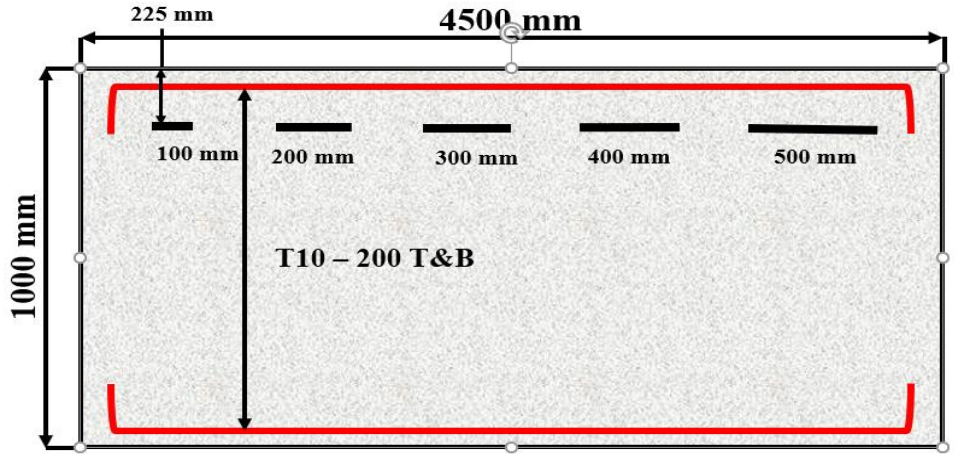
225 mm
4500 mm
100 mm
200 mm
300 mm
400 mm
500 mm
1000 mm
T10 – 200 T&B

(b)

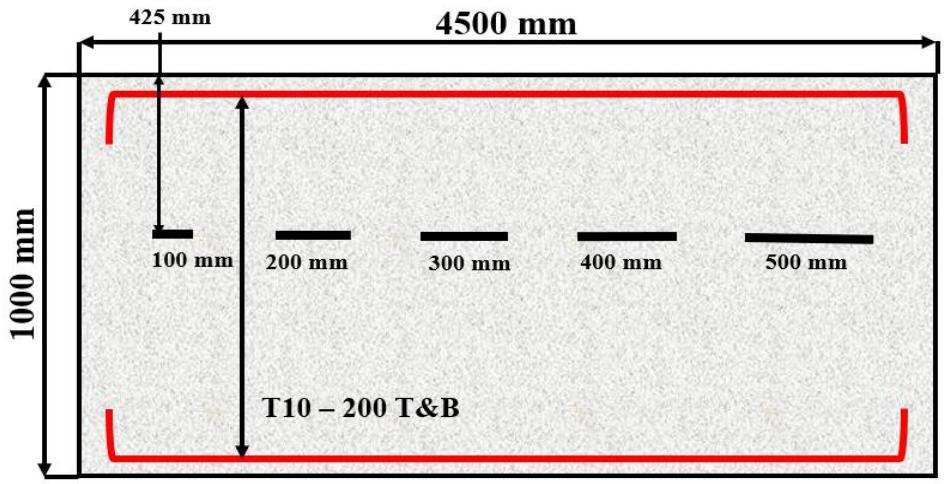
425 mm
4500 mm
100 mm
200 mm
300 mm
400 mm
500 mm
1000 mm
T10 – 200 T&B

(c)

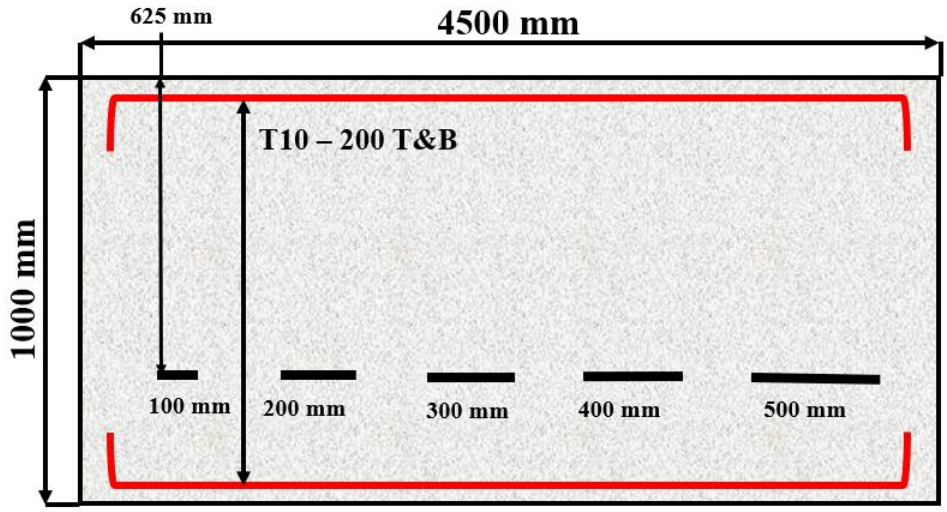

(d)

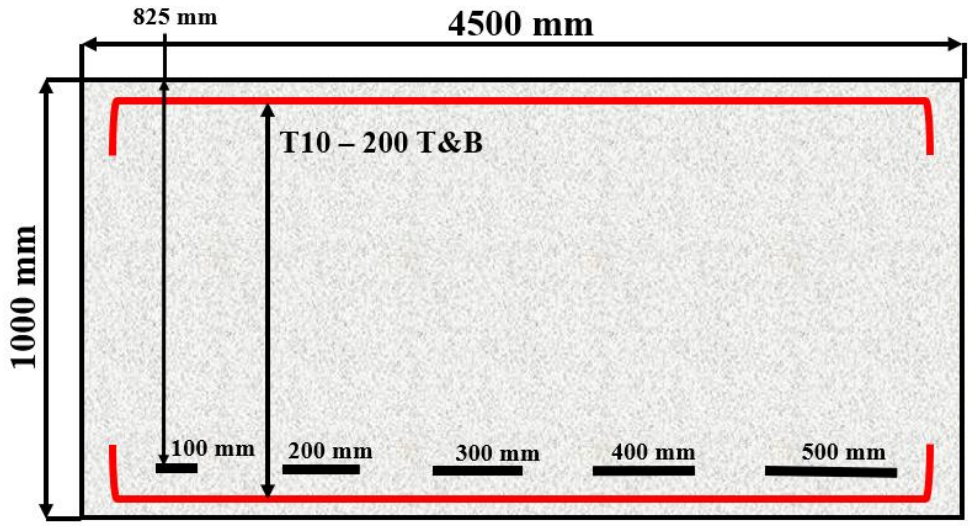

(e)

Figure 3.4: Side View of Concrete Specimens with Different Depth of Polystyrene Boards (a) 25 mm, (b) 225 mm, (c) 425 mm, (d) 625 mm, and (e) 825 mm.

The apparatus for this experiment is four sensor accelerators, a dynamic microphone, a signal acquisition unit (USB-3100 Series), a laptop, and four steel balls with different diameters of 10 mm, 15 mm, 20 mm, and 25 mm. The setting of the apparatus is shown in Figure 3.5 where four sensors are placed before and after the artificial delamination with a distance of 250 mm from the center point. Then, two of the sensors are placed with a spacing of 100 mm. The dynamic microphone with frequency ranging between 0.05 kHz to 60 kHz is placed 10

mm on top of the concrete surface as a trigger to record the waves signal. Lastly, all sensors are connected to the signal acquisition unit; while the signal acquisition unit is connected to the laptop for result processing.

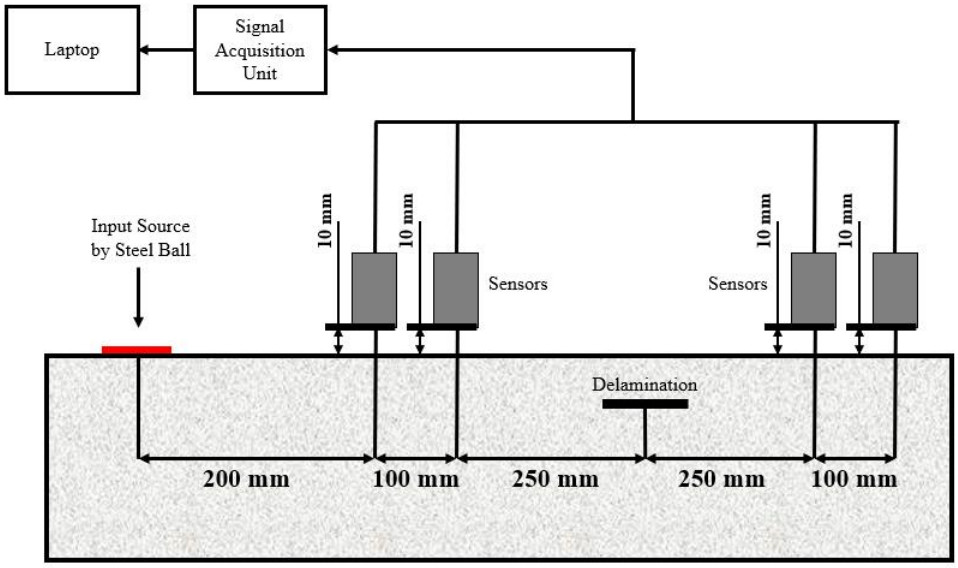

Figure 3.5: Illustration View of Apparatus Setting.

3.2.1 Materials of Concrete Specimen

The prepared concrete specimen was casted with PPFAC, water, fine and coarse aggregates, reinforced steel bar, and ADVA 209 admixture. PPFAC is compliant with the Type I Portland Cement according to ASTM C150. The cement is sieved through an opening of 300 μm and held in an air-tight container to avoid contact with air humidity.

According to ASTM C1602, the water used to cast the concrete must be free from impurities to prevent long-term impact on the hydration of cement. Hence, tap water is used to cast the concrete specimen. Furthermore, according to ASTM C778 and C33, the fine aggregate and coarse aggregate must pass through the sieve size of 600 μm and retain 4.75 mm, respectively. Hence, fine sand and crushed gravel were used in the concrete mixture. Both of the aggregates are oven-dried for at least 24 hours at a temperature of 100 ± 5 °C to remove the moisture. The method used for sieve analysis by machine complies with ASTM C136 2004. Besides, according to ASTM A663, the manufacturing of hot-wrought carbon steel should meet the standard of mechanical properties and design for non-critical construction applications. The specimens should

undergo a tension test to determine the tensile strength, yield point and elongation. Hence, 10 mm reinforced steel bars are used in the casting of concrete specimens.

3.2.2 Compressive Strength Test

During the casting of the five concrete specimens, five extra moulds are casted separately from the specimen to undergo a compressive strength test. The moulds are casted in cube shape with an equal dimension of 100 x 100 x 100 mm and oven-dried for 24 hours before the test. The test is performed under the specification of ASTM C803. The compressive test device compressed at a constant rate of 0.2 $\frac{\text{ }^{!}}{\text{ }}$with an uniaxial compression load until the mould fails.

3.3 Preliminary Study

Preliminary study is conducted to examine the repeatability of the experiment. Repeatability is the variation in measurements obtained when an individual is recording multiple measurements with the same technique and instrument. Hence, the application and calculation of mean and standard deviation is significant for this experimental measurement (Lee, et al., 2019).

3.4 Define Record Point and Apply Impact

The recording point is set-up as shown in Figure 3.5. Then, different diameters of steel ball will act as the input source of the experiment. The steel ball is dropped at a fixed height by the same operator in order to minimize inconsistencies. Then, R-waves will generate and propagate through the concrete specimen. The wave signals will be received by the sensors to the signal acquisition unit. The received wave signals are then attempted in the investigation of the relationship between dominant frequencies, amplitude attenuation and velocity of R-wave when propagating through the concrete specimen containing delamination.

3.5 Collect and Tabulate Data

There are four different diameters of steel balls to perform five average impacts on five different diameters of delamination and five different depths of

delamination in the concrete specimen. Besides, there is also a controlling specimen that does not have any delamination in order to compare the results. Hence, there are a total of 104 waveform results to collect from this experiment. The time-domain and frequency domain graphs are then plotted by using MATLAB software to ease the analysis.

3.5.1 Procedure of MATLAB Data Collection

The data collected from the experiment are named according to their parameters such as 25 mm depth of delamination with 100 mm diameter of delamination and 10 mm diameter of steel ball will be named as “25_100_10”. The excel file of the raw data is then translated into a Comma-Separated Values (CSV) file because MATLAB can only read CSV files.

After the application is opened, select “Browse for folder” to choose the respective CSV file as shown in Figure 3.6. The programmed code was prepared by a PhD student who guided me throughout the research. Figure 3.7 shows the steps to run the programmed code. Then, select “Run” and “Add to path” to browse the file that was selected previously. The code will then generate 3 different graphs which are the power spectrum, time-domain graph and peak frequency as shown in Figure 3.8. However, the arrangement of the graph is adjusted by changing the sub-plot from the code to figures in order to display a clearer value. The amendment of display will be shown in Chapter 4. Then, these steps are repeated to obtain the other parameters of data.

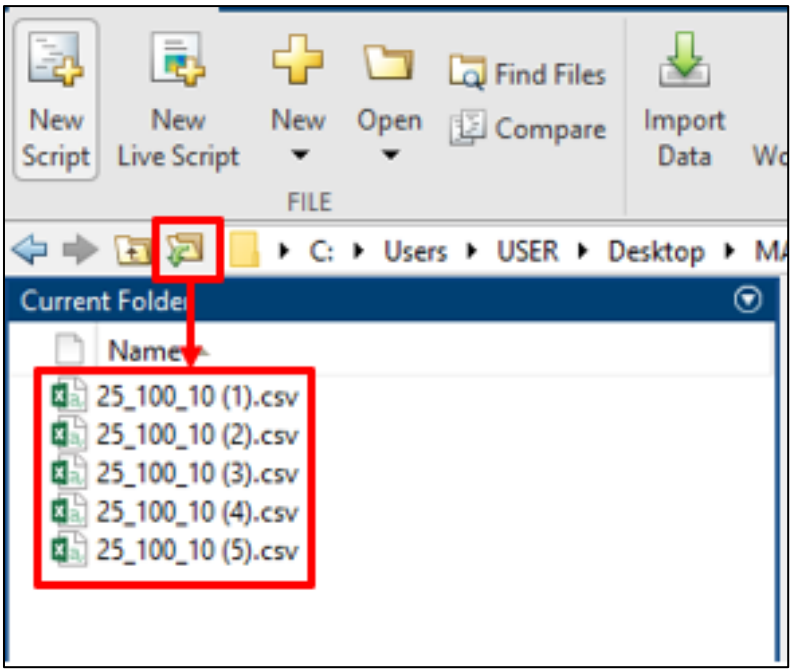

Figure 3.6: Steps to Browse Folder for each File.

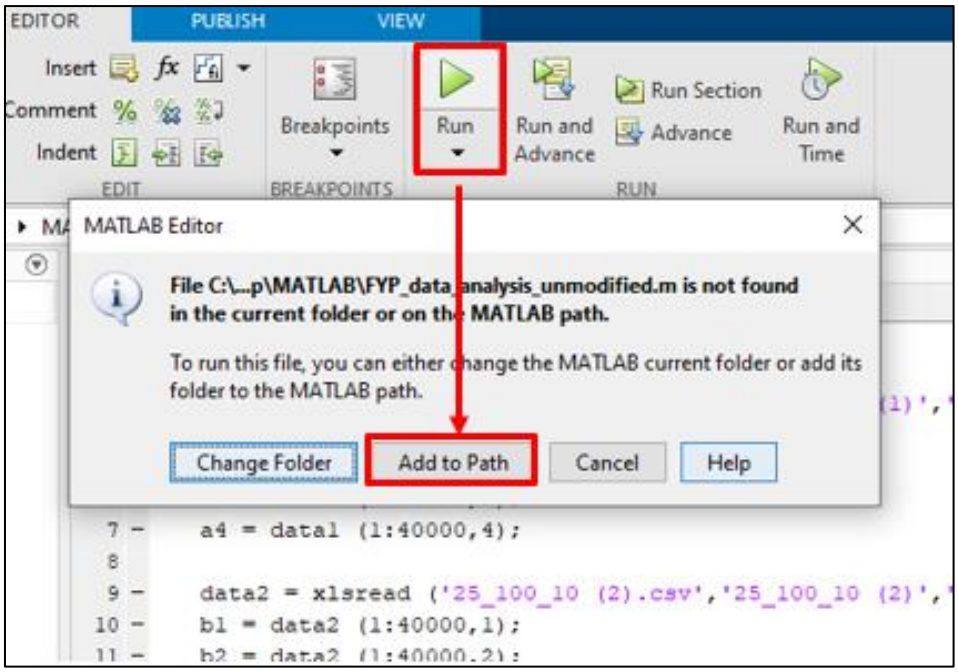

Figure 3.7: Steps to Run the Programmed Code.

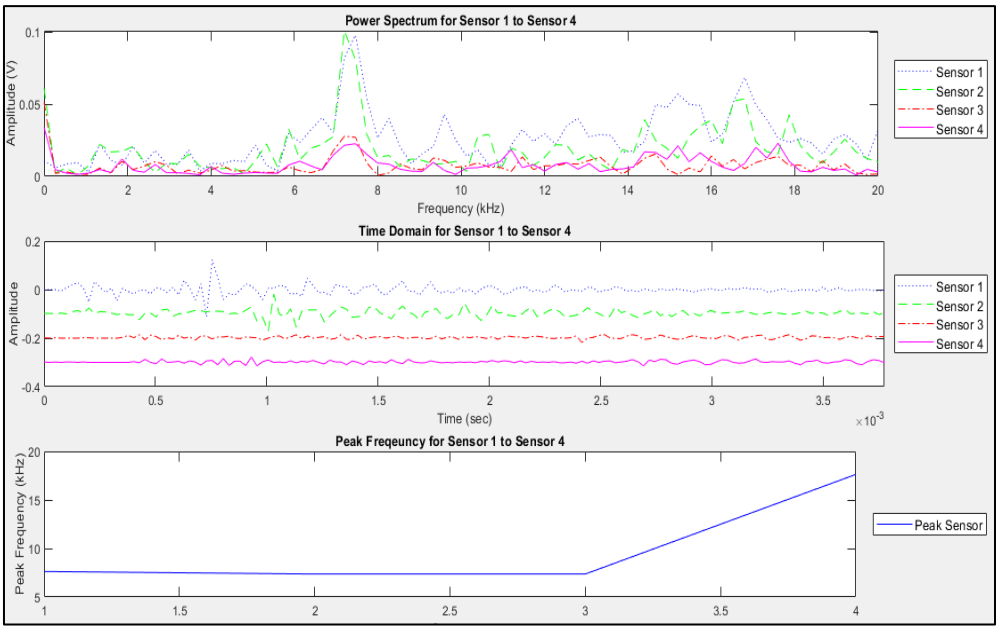

Figure 3.8: Initial Display of Result From Programmed Code.

3.6 Result Analysis and Discussion

Once the graph is plotted, the result of time-domain and frequency domain for the different delamination depth are discussed in Chapter 4 of this study. The application of FFT is used to transform the time-domain to frequency domain. Furthermore, the attenuation rate and wave velocity will also be discussed in Chapter 4.

3.7 Summary

This chapter discussed the experimental measurement and procedure of this study. The variables of this study are the different diameters and depths of the artificial delamination and the different diameters of the steel ball. The concrete specimen was prepared according to the compressive strength test under specification of ASTM C803 and cured under a water-curing condition for 28 days.

CHAPTER 4

RESULTS AND DISCUSSION

4.1 Introduction

This chapter discusses the analysis of experimental results from the changes of R-wave characteristic when propagating through the defects of concrete delamination. The different diameters of steel ball were used as the manipulated variable where different data can be obtained to compare the result. The velocity of propagated wave, ampltidue attenuation rate and frequency responses are the variables that will be obtained and determined from experimental works. The responding variables were obtained by running a programmed code via MATLAB.

4.2 Stimulation and Observation of Rayleigh Wave

When the impact of a steel ball is stimulated, the waves will scatter and attenuate with depth when propagating through the concrete sample containing delamination. Thus, it is necessary to have a proper method to determine the R-wave. Theoretically, the R-wave is a wave that contains higher energy comparing to P-wave and S-wave. Hence, the impact point and offset distance of sensors need to be aligned so that there is enough time for its preceding waves such as P wave and S wave (Zheng, et al., 2018). According to a study by Lee, Chai and Lim on 2016, the R-wave can be detected from a strong peak that followed by the first arrival of P-wave which contain a lower magnitude of amplitude compared to R-wave. Figure 4.1 shows the typical time-domain waveform acquired by the sensor and the highest magnitude of amplitude indicate the R-wave peak, which is going to determine throughout this study. Hence, Figure 4.2 shows the time-domain graph plotted by MATLAB with their indication of R-wave peak at each sensor.

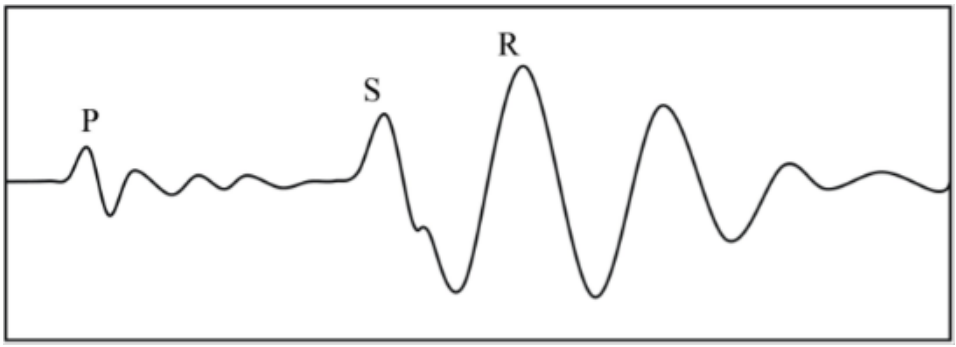

Figure 4.1: Time-domain Waveform from a Single Channel Record (Zheng, et al., 2018).

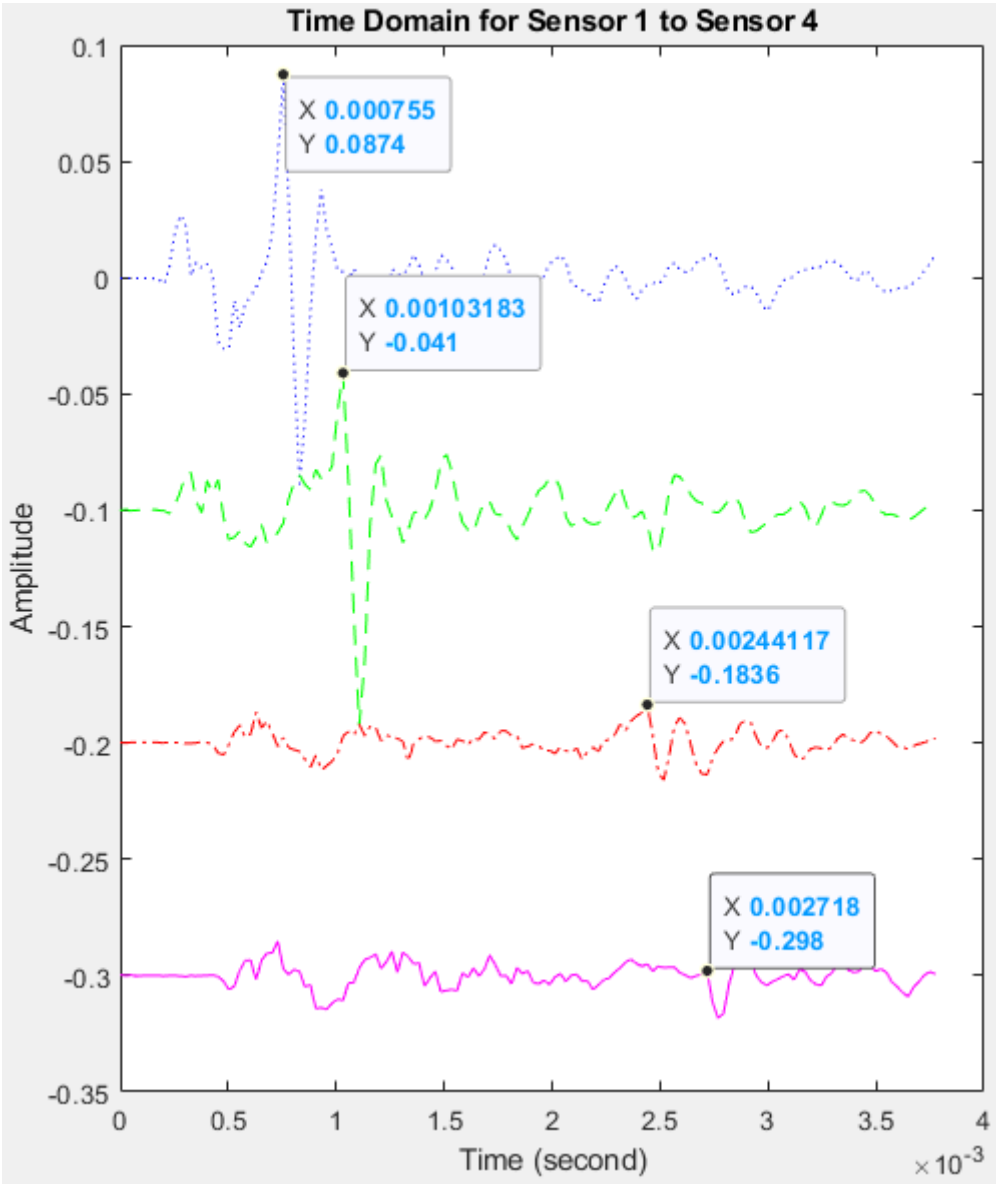

Figure 4.2: Time-domain Graph for 225 mm Depth of Delamination, 500 mm Diameter of Delamination and 25 mm Diameter of Steel Ball.

4.3 Experimental Variables

The controlling variable for this study is the 4500 mm (L) x 1500 mm (W) x 1000 mm (H) of concrete specimens containing different depths and diameters of delamination. Before the experiment was conducted on the concrete specimen containing delamination, a well-casted concrete that is free from any defects (unsound concrete) was used to conduct a test and serve as a controlling data for the experiment. Thus, the comparison between controlling data and actual data (sound concrete) can be achieved. Figure 4.3 shows the time-domain graphs, power spectrum and peak frequency that were plotted by MATLAB, which were obtained from impact of different diameters of steel balls onto the unsound concrete. Besides, the operator who conducted the impact of the steel ball is also one of the controlling variables due to the repeatability of the same force and height must be achieved.

The manipulating variable is the different diameters of steel balls used to hammer the concrete specimen in order to obtain different waveform results. The larger the diameter of the steel ball, the higher the fluctuation to the magnitude of amplitude in the time-domain graph. For each depth of delamination in terms of 25 mm, 225 mm, 425 mm, 625 mm and 825 mm, there will be 5 different diameters of delamination with 100 mm, 200 mm, 300 mm, 400 mm and 500 mm which then made up a 25 scenario for data collection. Then, the steel balls with diameter of 10 mm, 15 mm, 20 mm and 25 mm are used as the impact sources to excite the R-wave. Therefore, there are a total of 104 cases needed to perform including the controlling data. In each case, a total of 40,000 points were obtained within a time frame of 1 second and the points were then translated into comma-separated values file in order to import the data into MATLAB.

The responding variables are the parameter and the objective for this study. With the application of MATLAB, the time-domain graph, power spectrum and peak frequency are generated through a set of programmed code. Thus, the attenuation rate, velocity of wave and peak frequency can be obtained from the analysis of the graphs.

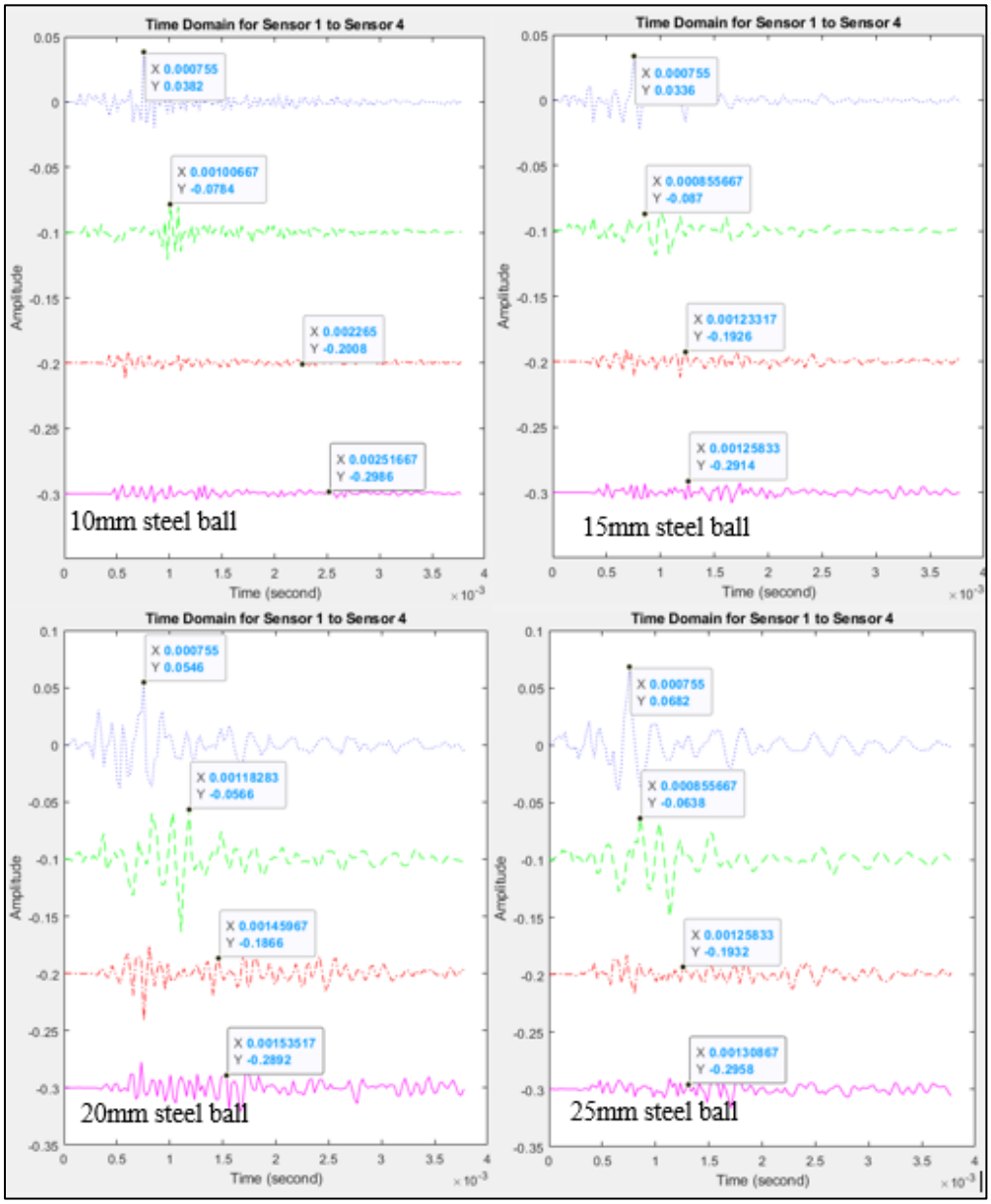
Time Domain for Sensor 1 to Sensor 4
X 0.000755
Y 0.0382
X 0.00100667
Y -0.0784
X 0.002265
Y -0.2008
X 0.00251667
Y -0.2986
10mm steel ball
Amplitude
Time (second)
Time Domain for Sensor 1 to Sensor 4
X 0.000755
Y 0.0336
X 0.000855667
Y -0.087
X 0.00123317
Y -0.1926
X 0.00125833
Y -0.2914
15mm steel ball
Amplitude
Time (second)
Time Domain for Sensor 1 to Sensor 4
X 0.000755
Y 0.0546
X 0.00118283
Y -0.0566
X 0.00145967
Y -0.1866
X 0.00153517
Y -0.2892
20mm steel ball
Amplitude
Time (second)
Time Domain for Sensor 1 to Sensor 4
X 0.000755
Y 0.0682
X 0.000855667
Y -0.0638
X 0.00125833
Y -0.1932
X 0.00130867
Y -0.2958
25mm steel ball
Amplitude
Time (second)

(a)

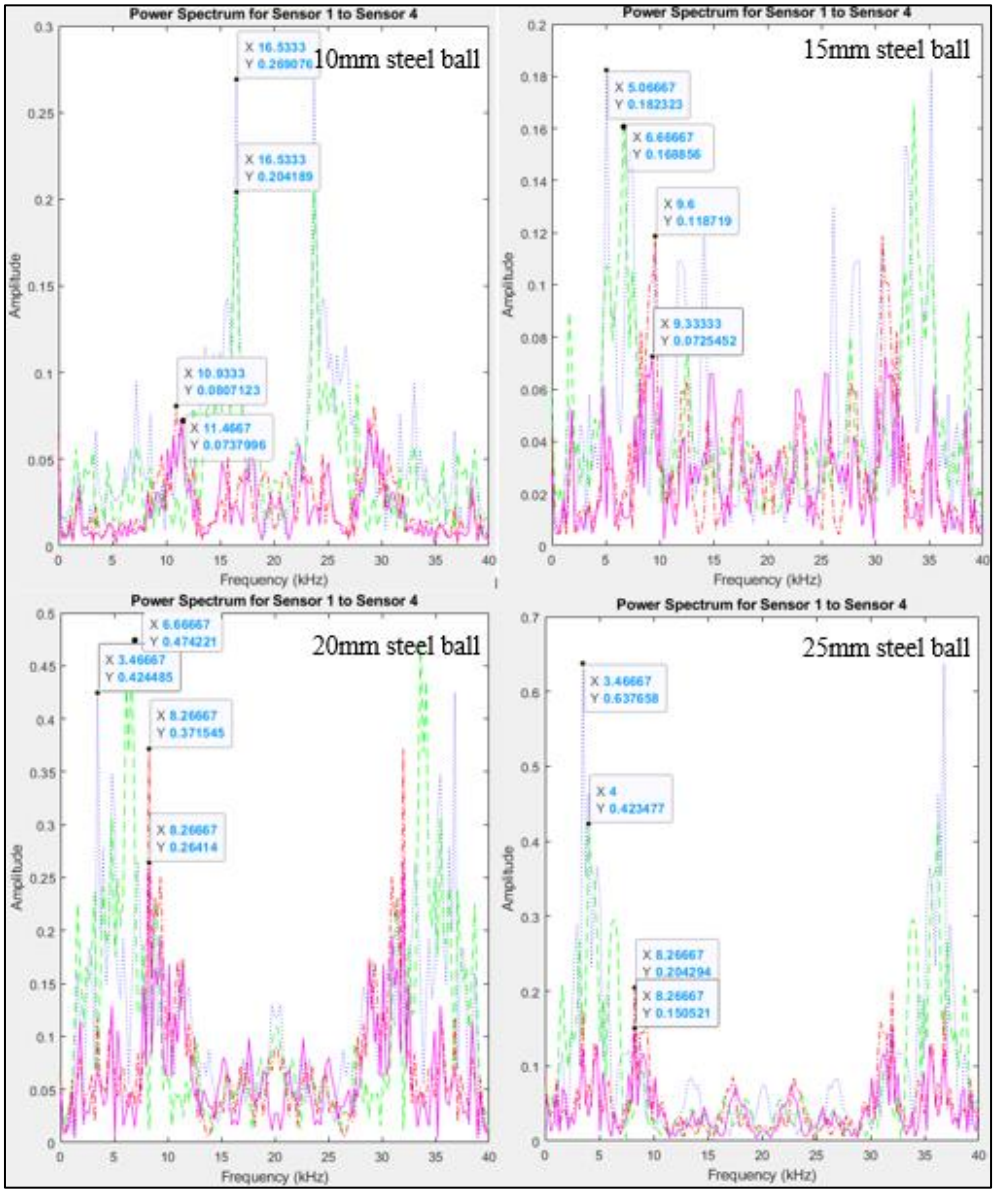
Power Spectrum for Sensor 1 to Sensor 4
10mm steel ball
X 16.5333
Y 0.269076
X 16.5333
Y 0.204189
X 10.9333
Y 0.0807123
X 11.4667
Y 0.0737096
Power Spectrum for Sensor 1 to Sensor 4
15mm steel ball
X 5.06667
Y 0.182323
X 6.66667
Y 0.168856
X 9.6
Y 0.118719
X 9.33333
Y 0.0725452
Power Spectrum for Sensor 1 to Sensor 4
20mm steel ball
X 6.66667
Y 0.474221
X 3.46667
Y 0.424485
X 8.26667
Y 0.371545
X 8.26667
Y 0.26414
Power Spectrum for Sensor 1 to Sensor 4
25mm steel ball
X 3.46667
Y 0.637658
X 4
Y 0.423477
X 8.26667
Y 0.204294
X 8.26667
Y 0.150521
Amplitude
Frequency (kHz)

(b)

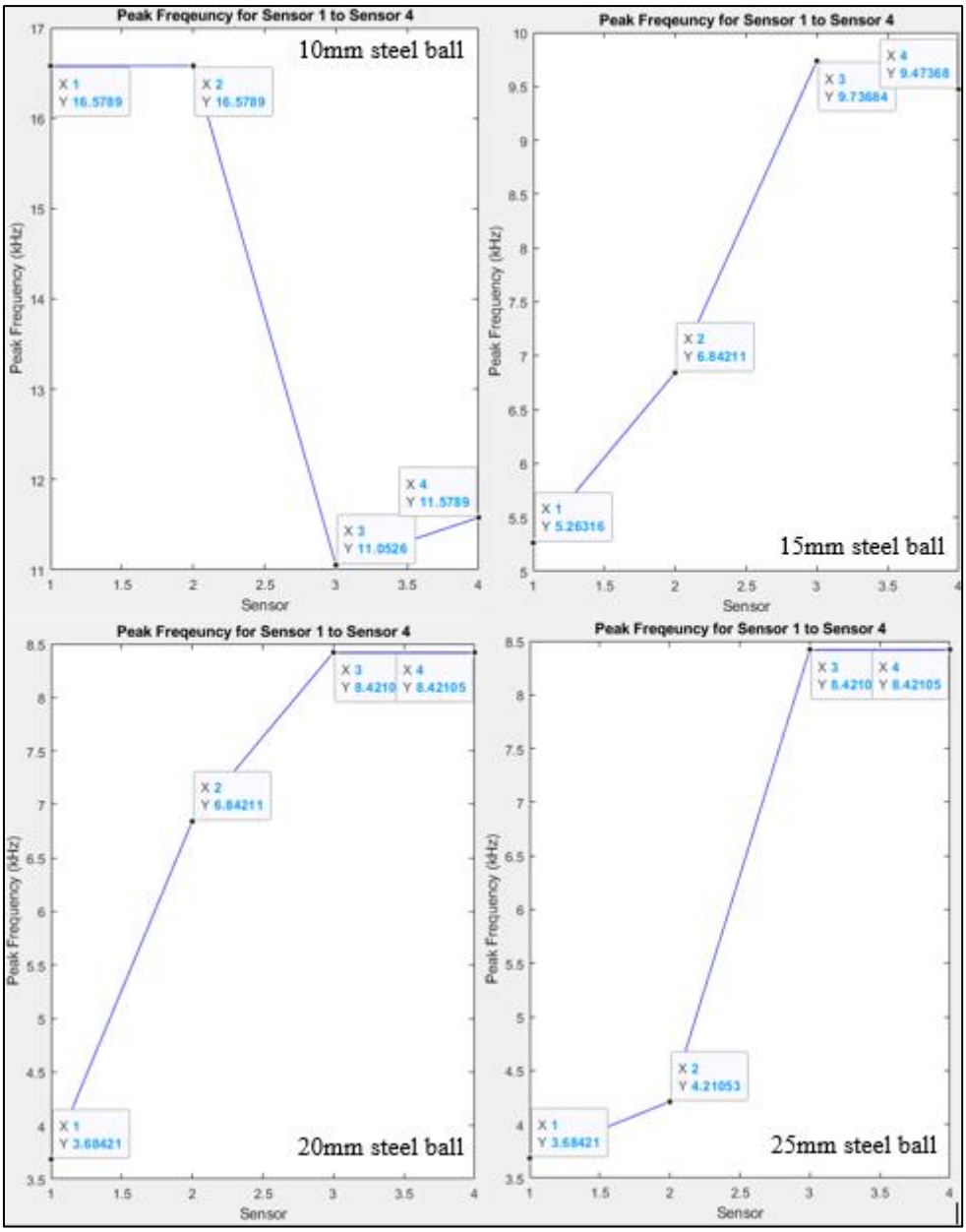

(c)

Figure 4.3: Control Graphs for (a) Time-domain, (b) Power Spectrum, and (c) Peak Frequency.

4.4 Waveform Result from Time-domain Graph

Time-domain is the analysis of mathematical function, physical signals and environmental data with respect to time. Time can be in the case of discrete or continuous while the value of the signal or function is in the case of real numbers. Thus, a time-domain graph represents the signal fluctuates with time where the amplitudes of the signal is plotted along the vertical axis and the time is plotted along the horizontal axis (Cadence, 2020). In contrast, a frequency-domain

graph is plotted against the frequency, instead of time. In general, the unit of time such as seconds, minutes, hours or its multiples are used as the measurement for the graph. In this study, the time-domain graph is based on the amplitude received by each sensor over a time frame of 1 second. The signal acquisition unit (USB-3100 Series) was used to record the signal and the data was processed by MATLAB.

Furthermore, the highest magnitude of amplitude from the time-domain graph was used as an indication to determine the R-wave signal. Additionally, the bigger the diameter of the steel ball will produce a higher magnitude of amplitude when received by each sensor. Hence, a time-domain graph with the most obvious data is selected from a total of 25 different parameters of graphs to compare the result. The other time-domain graphs will be shown in appendix A.

Figure 4.4 shows the time-domain graphs taken from 225 mm depth of delamination, 500 mm diameter of delamination and four different diameters of steel balls of 10 mm, 15 mm, 20 mm, and 25 mm. The magnitude of amplitude received by sensor 1 from a 20 mm steel ball is 0.0652 V, which is twice the value comparing to a 10 mm steel ball of 0.032 V. Besides, the 25 mm steel ball gives an amplitude of 0.0874 V, which is almost twice the value comparing to 15 mm steel ball of 0.0484 V. However, not every amplitude will display multiply of its value. For instance, the magnitude of amplitude received by sensor 4 from a 25 mm steel ball diameter is -0.298 V, but only -0.2946 V from 10 mm steel ball. The reason behind this phenomenon is caused by the amplitude attenuation which will be discussed further on.

Table 4.1 shows the amplitude and time received by each sensor from a 225 mm depth of delamination and 500 mm diameter of delamination. In sensor 1, the time is the same in every steel ball diameter when the first R-wave was determined. This phenomenon is caused by the high speed of R-wave that happens instantaneously after the impact. In contrast, Table 4.2 or Figure 4.3(a) shows the time received by sensor 3 and sensor 4 in the unsound concrete is different from the time in the sound concrete. The average time taken of the R-wave peak to reach sensor 3 and 4 in the unsound concrete is 0.00155158 second and 0.00165471 second respectively, while it is 0.0024117 second and 0.00268025 second in the sound concrete. This is one of the methods to verify

the presence of delamination in the sound concrete between sensor 2 and sensor 3. The table also shows the decrease in magnitude of amplitude from sensor 1 to sensor 4 due to the alignment of the sensors were arranged in series order. Hence, the amplitude received by each sensor will become weaker as it travels through the concrete specimen.

For more information, Figure 4.5 and 4.6 show the time-domain graphs taken from 625 mm and 825 mm depth of delamination with 500 mm diameter of delamination. Both figures show the same scenario to Figure 4.4. Moreover, Table 4.3 and 4.4 show the amplitude and time received by each sensor from 625 mm and 825 mm depth of delamination with 500 mm diameter of delamination, respectively.

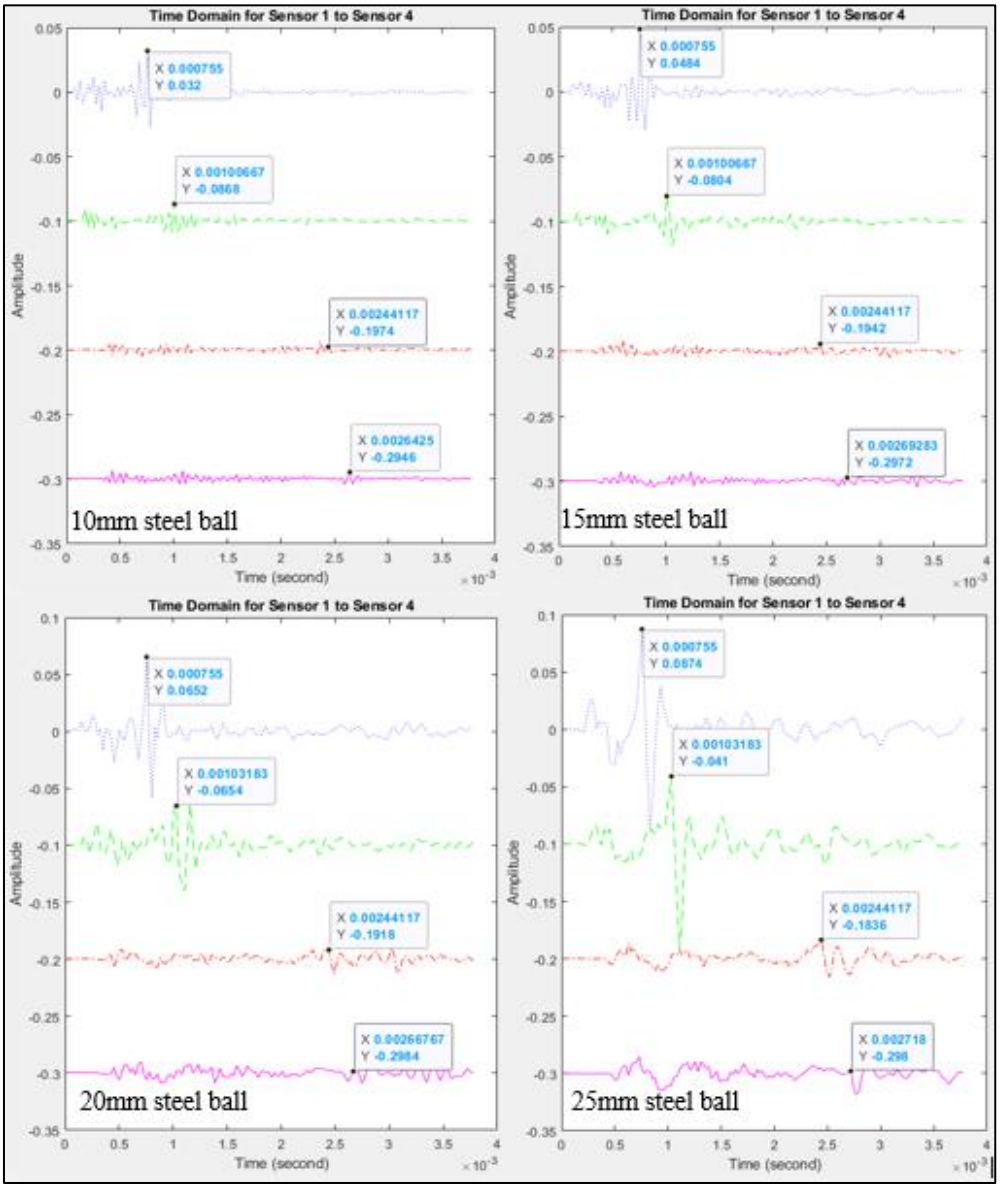

Figure 4.4: Time-domain Graphs from 225 mm Depth of Delamination and 500 mm Diameter of Delamination.

Table 4.1: Amplitude and Time Received by each Sensor from 225 mm Depth of Delamination and 500 mm Diameter of Delamination through the Change of Steel Ball Diameter.

Amplitude and time received by each sensor		Ball Diameter (mm)			
		10	15	20	25
Sensor 1	Amplitude (V)	0.032	0.0484	0.0652	0.0874
	Time (s)	0.000755	0.000755	0.000755	0.000755
Sensor 2	Amplitude (V)	-0.0868	-0.0804	-0.0654	-0.041
	Time (s)	0.00100667	0.00100667	0.00103183	0.00103183
Sensor 3	Amplitude (V)	-0.1974	-0.1942	-0.1918	-0.1836
	Time (s)	0.00244117	0.00244117	0.00244117	0.00244117
Sensor 4	Amplitude (V)	-0.2946	-0.2972	-0.2984	-0.298
	Time (s)	0.0026425	0.00269283	0.00266767	0.002718

Table 4.2: Amplitude and Time Received by each Sensor from the Controlled Data Through the Change of Steel Ball Diameter.

Amplitude and time received by each sensor		Ball Diameter (mm)			
		10	15	20	25
Sensor 1	Amplitude (V)	0.0382	0.0336	0.0546	0.0682
	Time (s)	0.000755	0.000755	0.000755	0.000755
Sensor 2	Amplitude (V)	-0.0784	-0.087	-0.0566	-0.0638
	Time (s)	0.00100667	0.0008556	0.0011828	0.0008557
Sensor 3	Amplitude (V)	-0.2008	-0.1926	-0.1866	-0.1932
	Time (s)	0.002265	0.0012233	0.0014596	0.0012583
Sensor 4	Amplitude (V)	-0.2986	-0.2914	-0.2892	-0.2958
	Time (s)	0.0025167	0.0012583	0.0015351	0.0013086

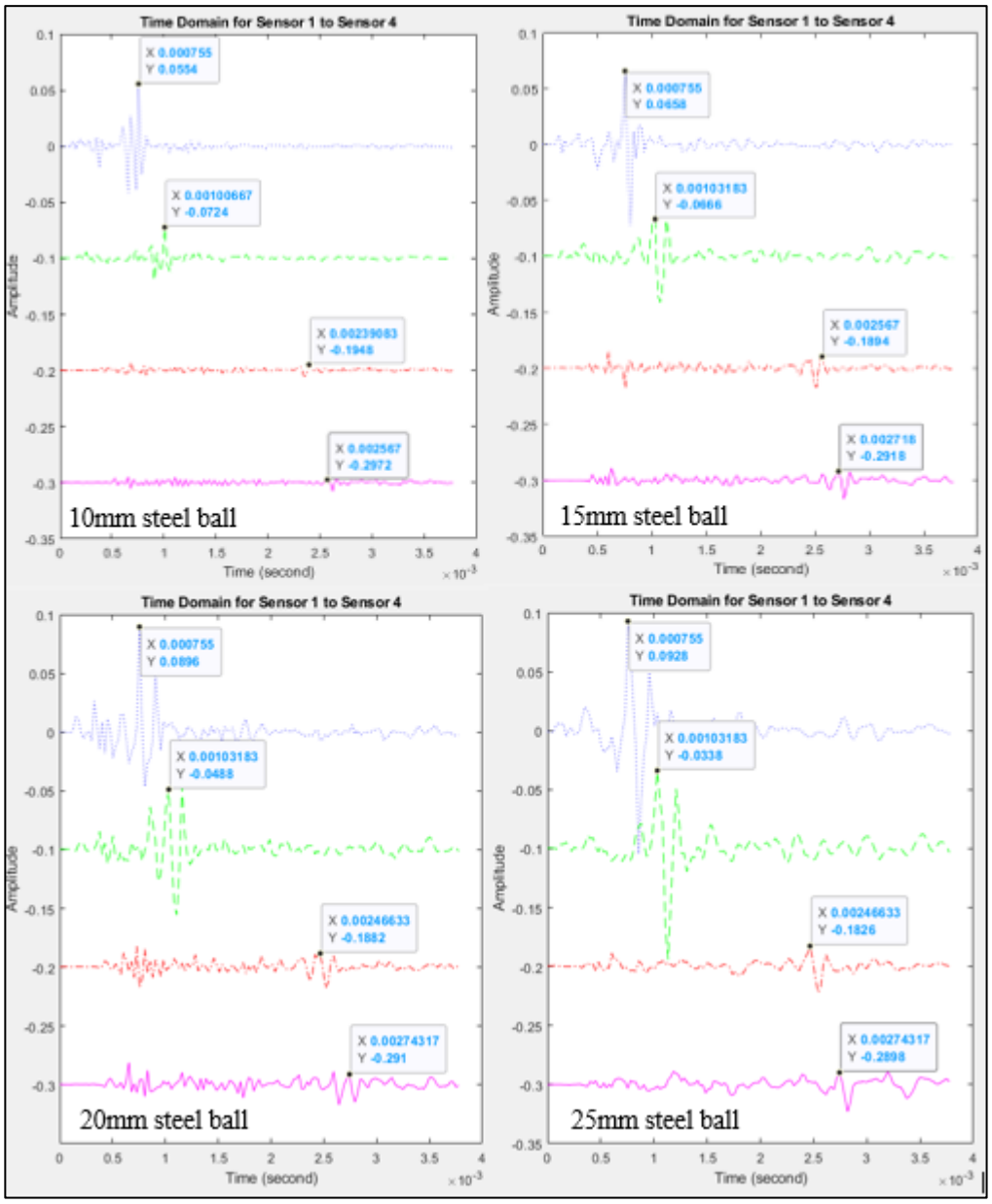

Figure 4.5: Time-domain Graphs from 625 mm Depth of Delamination and 500 mm Diameter of Delamination.

Table 4.3: Amplitude and Time Received by each Sensor from 625 mm Depth of Delamination and 500 mm Diameter of Delamination through the Change of Steel Ball Diameter.

Amplitude and time received by each sensor		Ball Diameter (mm)			
		10	15	20	25
Sensor 1	Amplitude (V)	0.0554	0.0658	0.0896	0.0928
	Time (s)	0.000755	0.000755	0.000755	0.000755
Sensor 2	Amplitude (V)	-0.0724	-0.0666	-0.0488	-0.0338
	Time (s)	0.00100667	0.00103183	0.00103183	0.00103183
Sensor 3	Amplitude (V)	-0.1948	-0.1894	-0.1882	-0.1826
	Time (s)	0.00239083	0.002567	0.00246633	0.00246633
Sensor 4	Amplitude (V)	-0.2972	-0.2918	-0.291	-0.2898
	Time (s)	0.002567	0.002718	0.00274317	0.00274317

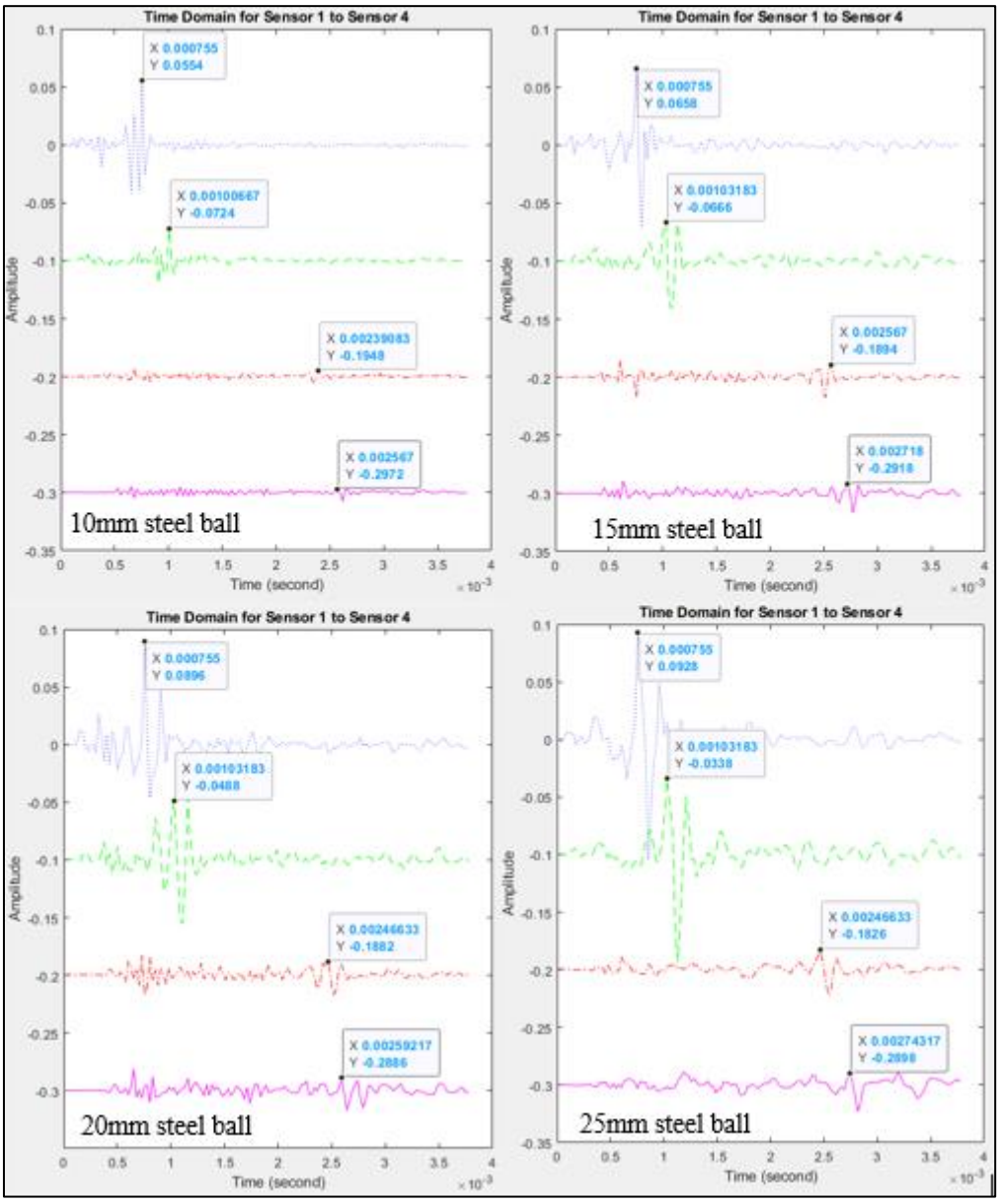

Figure 4.6: Time-domain Graphs from 825 mm Depth of Delamination and 500 mm Diameter of Delamination.

Table 4.4: Amplitude and Time Received by each Sensor from 825 mm Depth of Delamination and 500 mm Diameter of Delamination through the Change of Steel Ball Diameter.

Amplitude and time received by each sensor		Ball Diameter (mm)			
		10	15	20	25
Sensor 1	Amplitude (V)	0.0554	0.0658	0.0896	0.0928
	Time (s)	0.000755	0.000755	0.000755	0.000755
Sensor 2	Amplitude (V)	-0.0724	-0.0666	-0.0488	-0.0338
	Time (s)	0.00100667	0.00103183	0.00103183	0.00103183
Sensor 3	Amplitude (V)	-0.1948	-0.1894	-0.1882	-0.1826
	Time (s)	0.00239083	0.002567	0.00246633	0.00246633
Sensor 4	Amplitude (V)	-0.2972	-0.2918	-0.2886	-0.2898
	Time (s)	0.002567	0.002718	0.00259217	0.00274317

4.4.1 Attenuation Rate

When the wave is travelling through the concrete specimen, its intensity will decrease over time and distance due to the scattering from its impact and absorption from the wave. Thus, the combined effect is called attenuation. The attenuation rate can be obtained from the time-domain graphs where the difference of two R-waves received by the sensors are calculated and divided by the amplitude of the first sensor as shown in Equation 4.1.

$$\text{ö}_{\text{ؤ}}\ \text{سي}\ \frac{\text{كي}_{\text{ـ}}{}^{\text{٩}}\text{و}_{\text{ـ}}}{\text{و}_{\text{ـ}}}\ \text{عي}\ \rho\ \pi\ \pi\ \text{Þ} \qquad (4.1)$$

where;

$\text{ö}_{\text{ه}}$ is the amplitude of R-wave from sensor 1.

$\text{ö}_{\text{ح}}$ is the amplitude of R-wave from the other sensor.

The magnitude of amplitude of the time-domain graphs from Figure 4.4, 4.5 and 4.6 are used to calculate the attenuation rate of the R-wave by using Equation 4.1. Table 4.5 shows the percentage of the amplitude attenuation for 225 mm depth of delamination with 500 mm diameter of delamination through

the change of steel ball diameter. From Table 4.5, it can be observed that the percentage of attenuation rate of R-wave increases as it travelled through the concrete specimen. Then, the difference of attenuation rate between sensor 3 and sensor 2 is higher than the difference of attenuation rate between sensor 4 and sensor 3 as shown in Table 4.6. Thus, it can be explained by the inhomogeneous nature of materials between the concrete specimen and delamination made up of polystyrene board. This is also a method to determine the defect is in between sensor 2 to sensor 3. On the other hand, it is found that the attenuation rate decreases as the steel ball diameter increased. Hence, it can be concluded that the bigger the diameter of the steel ball will produce a lower frequency and attenuation rate. The result shows the attenuation rate is linearly proportional to the frequency of the wave while it is inversely proportional to the diameter of the steel ball.

For more data comparison, Table 4.7 and 4.9 show the percentage of the amplitude attenuation for 625 mm and 825 mm depth of delamination with 500 mm diameter of delamination through the change of steel ball diameter; while Table 4.8 and 4.10 show the difference of attenuation rate between each sensor for 625 mm and 825 mm depth of delamination with 500 mm diameter of delamination.

Table 4.5: Amplitude Attenuation Rate for 225 mm Depth of Delamination with 500 mm Diameter of Delamination through the Change of Steel Ball Diameter.

Diameter of Delamination (mm)	Ball Diameter (mm)	Attenuation Rate of each Sensor (%)		
		Sensor 2	Sensor 3	Sensor 4
500	10	371	717	1021
	15	266	501	714
	20	200	394	558
	25	147	310	441

Table 4.6: Difference of Attenuation Rate between each Sensors for 225 mm Depth of Delamination with 500 mm Diameter of Delamination through the Change of Steel Ball Diameter.

Diameter of Delamination (mm)	Ball Diameter (mm)	Difference of Attenuation Rate between Sensor (%)	
		2 to 3	3 to 4
500	10	346	304
	15	235	213
	20	194	163
	25	163	131

Table 4.7: Amplitude Attenuation Rate for 625 mm Depth of Delamination with 500 mm Diameter of Delamination through the Change of Steel Ball Diameter.

Diameter of Delamination (mm)	Ball Diameter (mm)	Attenuation Rate of each Sensor (%)		
		Sensor 2	Sensor 3	Sensor 4
500	10	231	452	636
	15	201	388	543
	20	46	310	425
	25	136	297	412

Table 4.8: Difference of Attenuation Rate between each Sensors for 625 mm Depth of Delamination with 500 mm Diameter of Delamination through the Change of Steel Ball Diameter.

Diameter of Delamination (mm)	Ball Diameter (mm)	Difference of Attenuation Rate between Sensor (%)	
		2 to 3	3 to 4
500	10	221	185
	15	187	156
	20	265	115
	25	160	116

Table 4.9: Amplitude Attenuation Rate for 825 mm Depth of Delamination with 500 mm Diameter of Delamination through the Change of Steel Ball Diameter.

Diameter of Delamination (mm)	Ball Diameter (mm)	Attenuation Rate of each Sensor (%)		
		Sensor 2	Sensor 3	Sensor 4
500	10	231	452	636
	15	201	388	543
	20	154	310	422
	25	136	297	412

Table 4.10: Difference of Attenuation Rate between each Sensors for 825 mm Depth of Delamination with 500 mm Diameter of Delamination through the Change of Steel Ball Diameter.

Diameter of Delamination (mm)	Ball Diameter (mm)	Difference of Attenuation Rate between Sensor (%)	
		2 to 3	3 to 4
500	10	221	185
	15	187	156
	20	156	112
	25	160	116

4.4.2 Velocity of Wave Propagation

The velocity of R-wave is computed by dividing the distance between two sensors and the difference between the time of R-wave peak detected from two sensors as shown in Equation 4.2. The distance between two sensors was shown in the apparatus setup in Figure 3.5 and the method to determine the R-wave peak was explained in Section 4.2.

ὠ؛ سي ت / خ٩وخو (4.2)

where;

Ὠis the distance between two sensors.

ὸ is the time of R-wave peak from the second sensor.

ὸ̧ is the time of R-wave peak from the first sensor.

Table 4.11 shows the velocity of the propagated wave for the unsound concrete. The result of the controlled data is used to compare with the sound concrete in order to determine the location of delamination. From Table 4.11, the calculated velocity for 10 mm steel ball diameter remains the same when travelling through the concrete specimen. As the diameter of the steel ball increases, the velocity becomes greater due to the time taken for the R-wave peak to reach the sensor has become shorter. Thus, Figure 4.3(a) from Section 4.3 shows the R-wave peak that causes the increment of velocity for the unsound

concrete when divided by the distance between two sensors. Figure 4.7 shows the graph plotted with the calculated value of velocity from Table 4.11.

Table 4.11: Velocity of Propagated Wave for Unsound Concrete/Controlled Data.

Ball Diameter (mm)	Velocity of propagated wave (m/s)		
	Sensor 2	Sensor 3	Sensor 4
10	397.35	397.35	397.35
15	993.37	1359.99	2856.08
20	233.74	1806.10	1324.50
25	993.37	1241.73	1986.49

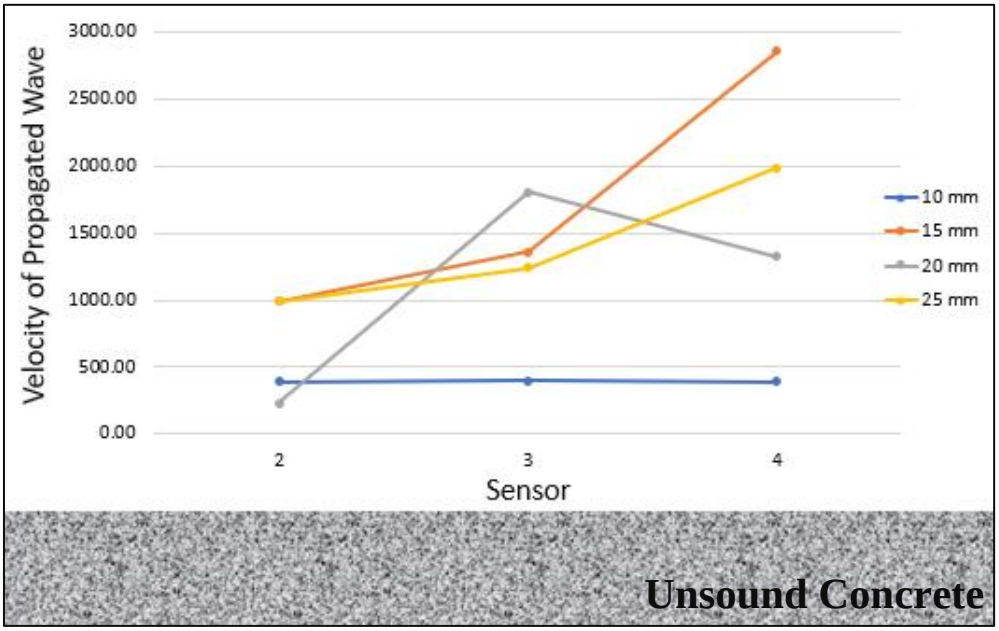

Figure 4.7: Graphs of Velocity of Propagated Wave against Sensor with Respective Diameter of Steel Ball for Unsound Concrete.

On the other hand, the velocity of propagated waves for the sound concrete of 225 mm, 625 mm and 825 mm depth of delamination with 500 mm diameter of delamination are shown in Table 4.12, 4.13 and 4.14 respectively. In addition, Figure 4.8, 4.9 and 4.10 are plotted by the calculated value from Table 4.12, 4.13 and 4.14 to show a clear observation of the decrement of velocity and its location of the delamination. By referring to the tables, the

velocity of R-wave is found in between the range of 361.23 m/s to 397.35 m/s when travelling through the concrete specimen. Then, the velocity of R-wave drops between the range of 296.53 m/s to 361.23 m/s at sensor 3, which is a huge difference comparing to the value of 397.5 m/s to 1806.10 m/s in the unsound concrete. Finally, the velocity of R-wave rises back to a value between 361.22 m/s to 1986.49 m/s.

Theoretically, the speed of Rayleigh waves is at 7800 miles per hour which is 3487 m/s according to a research by Berkeley Seismology Lab, while the R-wave velocity for reinforced concrete is between 2000 m/s to 3000 m/s (Lee, Chai and Lim, 2016). However, the R-wave velocity obtained in this study is lesser due to the scattering characteristic of R-wave is affected by the inhomogeneous nature of the reinforced concrete. As the R-wave velocity decreases from sensor 2 to sensor 3, the likelihood for the concrete specimen to possess delamination despite of the decreasing density of 2400 $\frac{kg}{m^3}$ to 1060 $\frac{kg}{m^3}$ when travelling through a different medium of concrete and polystyrene board (Park, Yoon and Oh, 2019). In addition, it takes a longer time for the R-wave to reach sensor 3 in the sound concrete due to the density of the polystyrene board that causes sound impedance along the path. In a nutshell, the presence of delamination between sensor 2 and sensor 3 will affect the velocity of the propagated waves.

Table 4.12: Velocity of Propagated Wave for 225 mm Depth of Delamination with 500 mm Diameter of Delamination.

Ball Diameter (mm)	Velocity of propagated wave (m/s)		
	Sensor 2	Sensor 3	Sensor 4
10	397.35	348.55	497.70
15	397.35	348.55	397.36
20	361.23	354.78	441.50
25	361.23	354.78	361.23

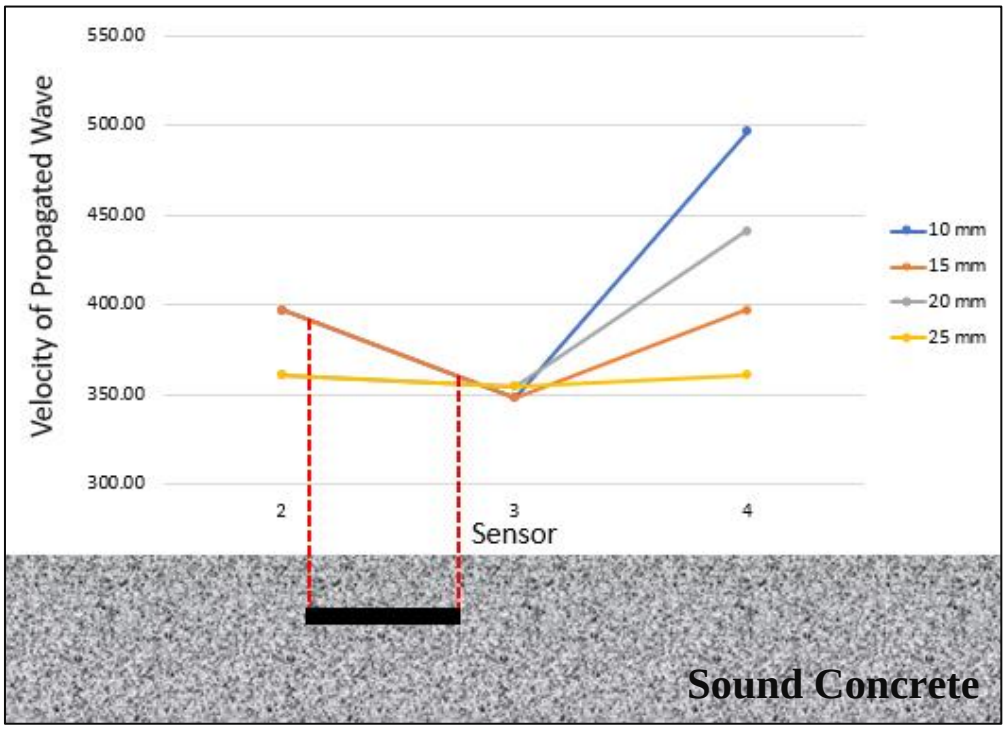

Figure 4.8: Graphs of Velocity of Propagated Wave against Sensor with Respective Diameter of Steel Ball for 225 mm Depth of Delamination and 500 mm Diameter of Delamination.

Table 4.13: Velocity of Propagated Wave for 625 mm Depth of Delamination with 500 mm Diameter of Delamination.

Ball Diameter (mm)	Velocity of propagated wave (m/s)		
	Sensor 2	Sensor 3	Sensor 4
10	361.23	348.55	397.35
15	397.35	296.53	1986.49
20	397.35	361.23	397.35
25	361.23	354.78	397.36

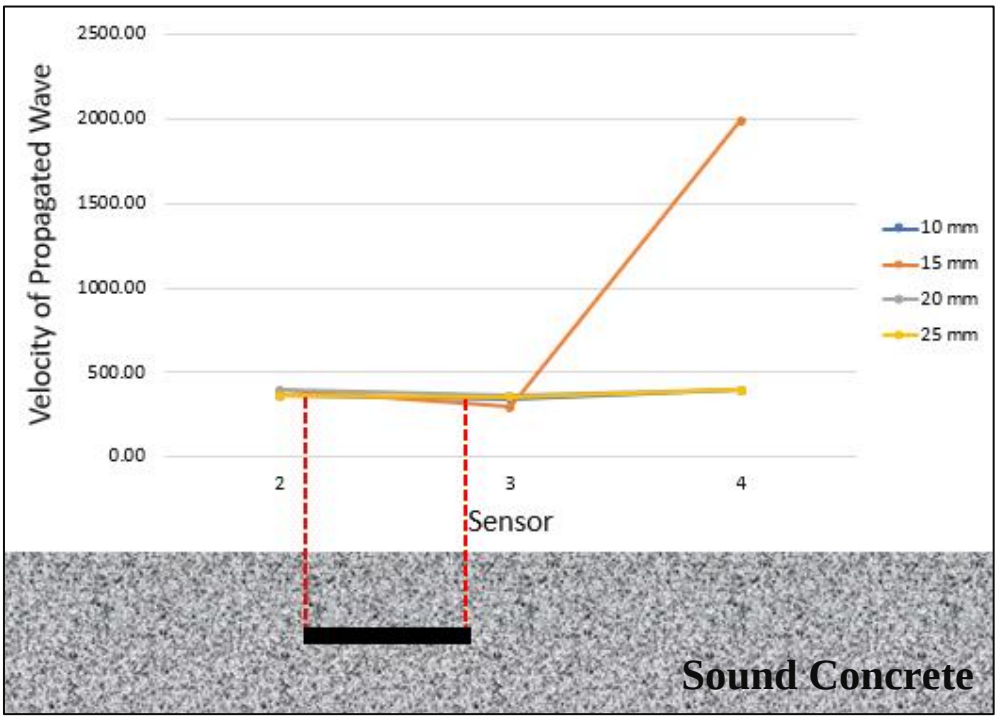

Figure 4.9: Graphs of Velocity of Propagated Wave against Sensor with Respective Diameter of Steel Ball for 625 mm Depth of Delamination and 500 mm Diameter of Delamination.

Table 4.14: Velocity of Propagated Wave for 825 mm Depth of Delamination with 500 mm Diameter of Delamination.

Ball Diameter (mm)	Velocity of propagated wave (m/s)		
	Sensor 2	Sensor 3	Sensor 4
10	397.35	361.23	567.63
15	361.23	325.70	662.25
20	361.23	348.55	794.66
25	361.23	348.55	361.23

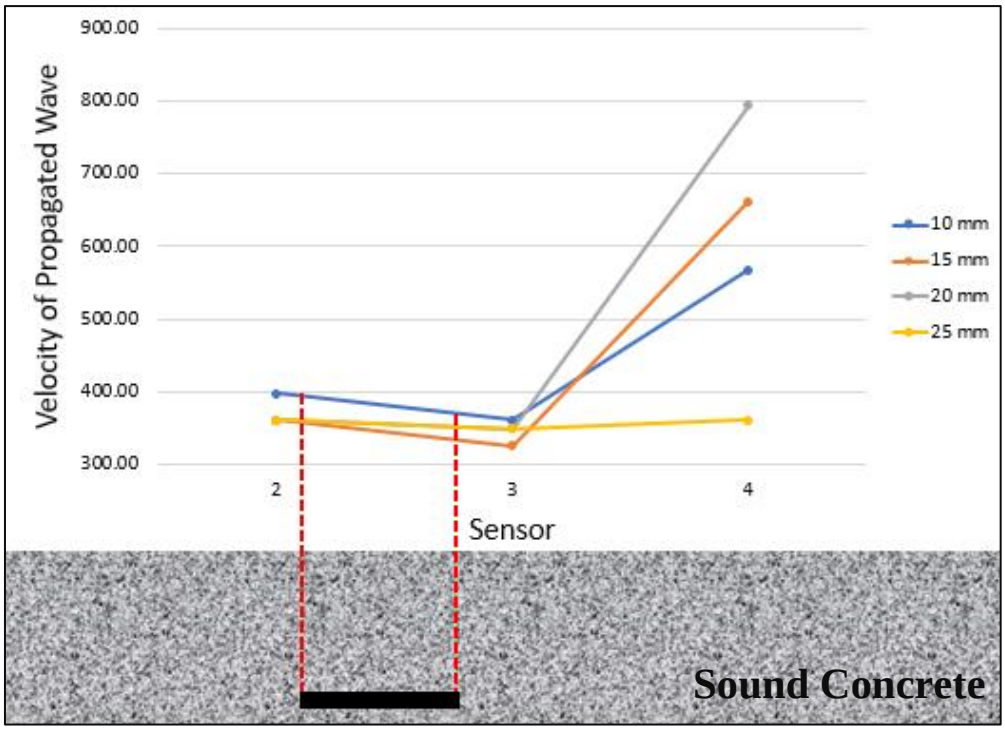

Figure 4.10: Graphs of Velocity of Propagated Wave against Sensor with Respective Diameter of Steel Ball for 825 mm Depth of Delamination and 500 mm Diameter of Delamination.

4.5 Fast Fourier Transform

The data collected from time-domain graphs are used to convert into frequency domain graphs or a power spectrum with a pair of mathematical operators called Fourier transform. The frequency formula in terms of time is shown in Equation 4.3 together with the code sample as shown in Figure 4.11.

$$\text{Ω} = \frac{1}{T} \tag{4.3}$$

where;

Ω is the frequency in Hertz.

T is the time to complete one cycle in seconds.

```
237      %----------------------FFT
238      %fs = 1/(t(2)-t(1));
239 -    t  = linspace(0,0.003775,151);
240 -    fs = 1/(0.000025)/1000;
241 -    f  = linspace(0,fs,151);
242 -    sf1 = fft(avg_sensor1);
243 -    sf2 = fft(avg_sensor2);
244 -    sf3 = fft(avg_sensor3);
245 -    sf4 = fft(avg_sensor4);
```

Figure 4.11: Code Sample for Frequency Formula in MATLAB.

4.5.1 Waveform Result from Power Spectrum

Power spectrum is the intensity of a time-varying signal that is distributed in the frequency domain. It is often generated from a time-domain input during the signal processing. Thus, it is useful for the determination of the degree of noise that is correlated with the signals. For instance, the signal can be in the form of a broadband noise measurement, a wideband signal, or in a harmonic analogue signal. Figure 4.12 shows the power spectrum generated by MATLAB for 5 different depth of delamination with 500 mm diameter of delamination through the changes of steel ball diameter. Hence, the peak frequency for each sensor in the power spectrum is determined and discussed in Section 4.5.2.

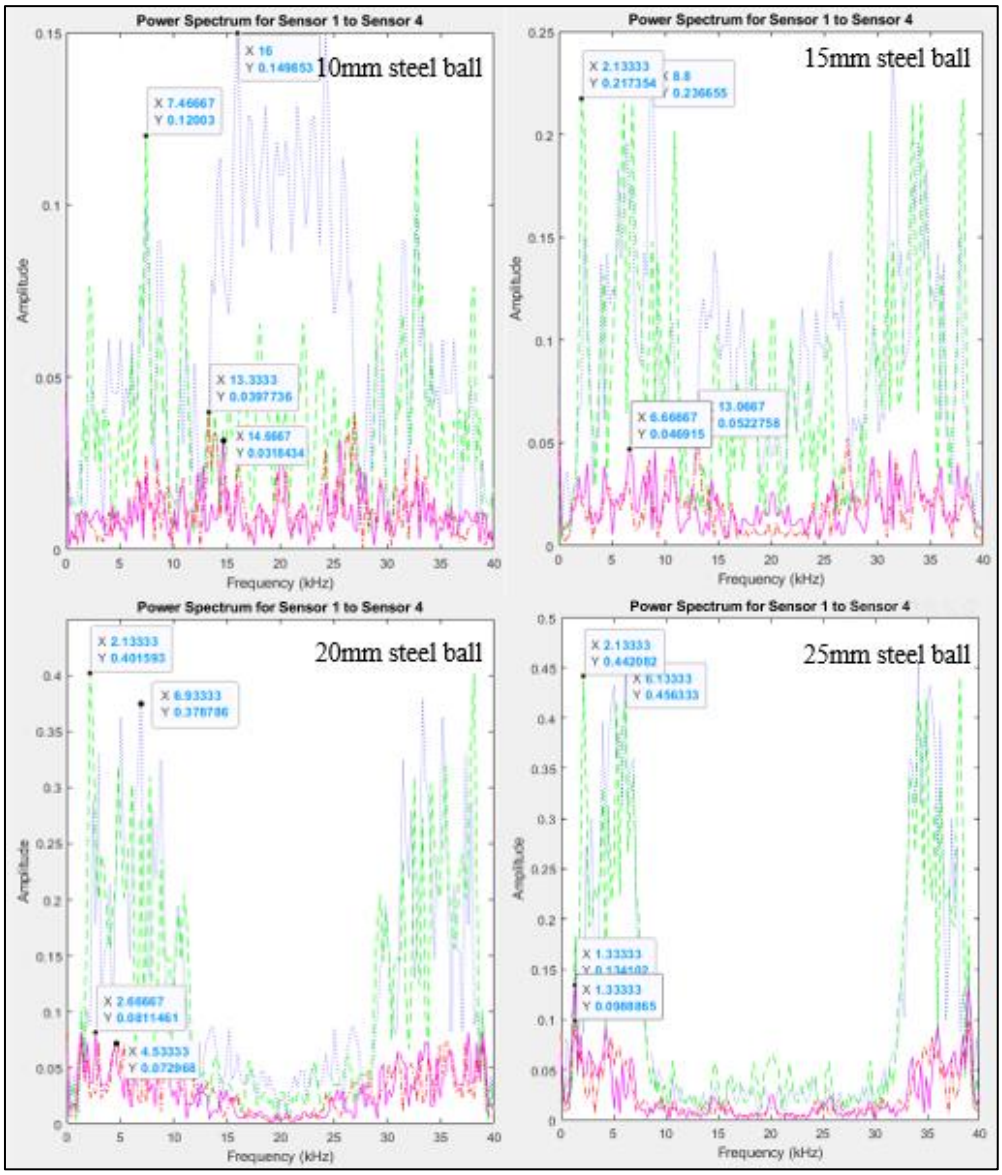
Power Spectrum for Sensor 1 to Sensor 4
10mm steel ball
X 16
Y 0.149653
X 7.46667
Y 0.12003
X 13.3333
Y 0.0397736
X 14.6667
Y 0.0316434
Amplitude
Frequency (kHz)
Power Spectrum for Sensor 1 to Sensor 4
15mm steel ball
X 2.13333
Y 0.217354
X 8.8
Y 0.236655
X 6.66667
Y 0.046915
13.0667
0.0522758
Amplitude
Frequency (kHz)
Power Spectrum for Sensor 1 to Sensor 4
20mm steel ball
X 2.13333
Y 0.401593
X 6.93333
Y 0.378786
X 2.66667
Y 0.0811461
X 4.53333
Y 0.072968
Amplitude
Frequency (kHz)
Power Spectrum for Sensor 1 to Sensor 4
25mm steel ball
X 2.13333
Y 0.442052
X 6.13333
Y 0.456333
X 1.33333
X 1.33333
Y 0.0988365
Amplitude
Frequency (kHz)

(a)

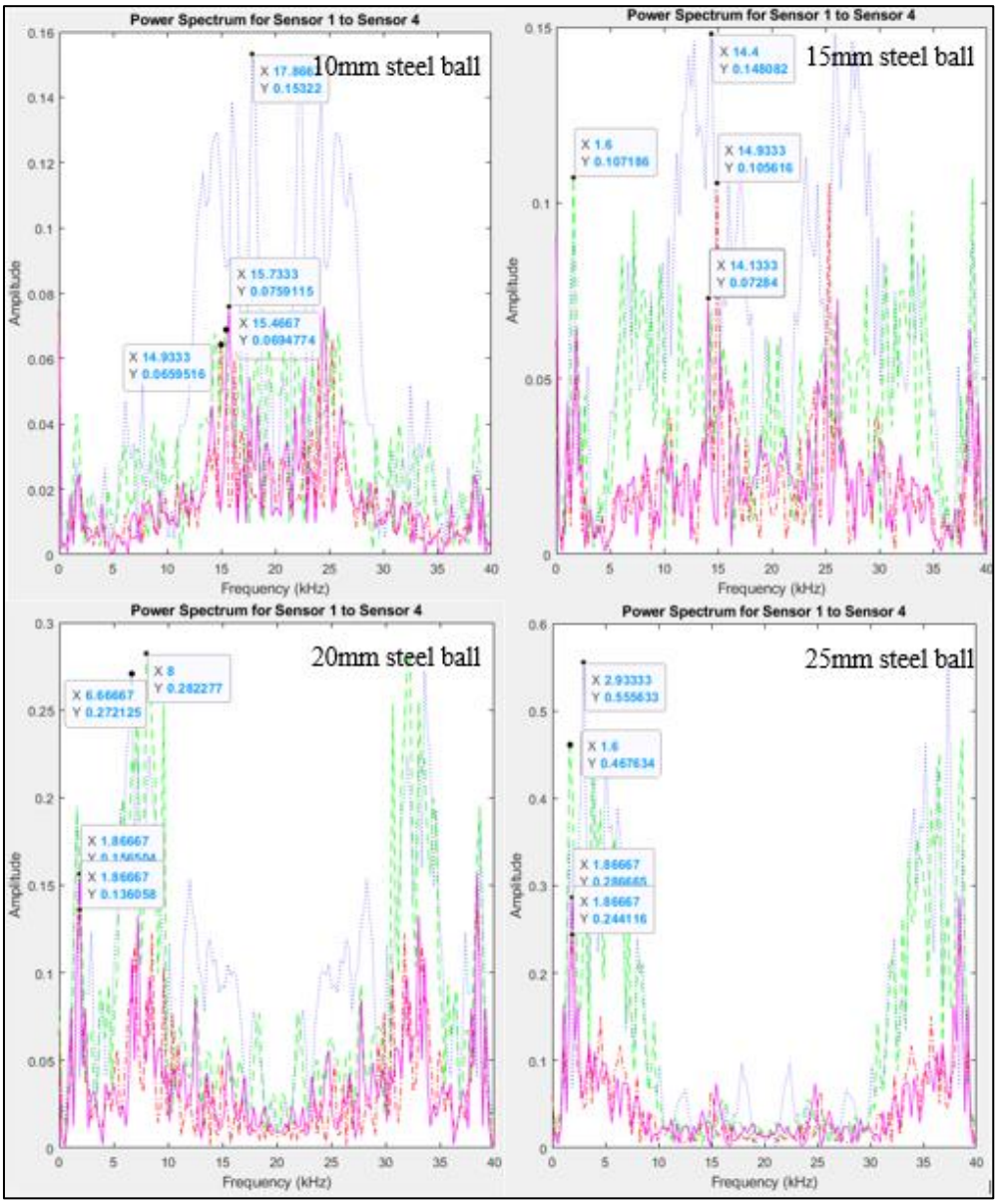
Power Spectrum for Sensor 1 to Sensor 4
10mm steel ball
X 17.866
Y 0.15322
X 15.7333
Y 0.0759115
X 15.4667
Y 0.0694774
X 14.9333
Y 0.0659516
Power Spectrum for Sensor 1 to Sensor 4
15mm steel ball
X 14.4
Y 0.148082
X 1.6
Y 0.107186
X 14.9333
Y 0.105616
X 14.1333
Y 0.07284
Power Spectrum for Sensor 1 to Sensor 4
20mm steel ball
X 8
Y 0.282277
X 6.66667
Y 0.272125
X 1.86667
X 1.86667
Y 0.136058
Power Spectrum for Sensor 1 to Sensor 4
25mm steel ball
X 2.93333
Y 0.555633
X 1.6
Y 0.467634
X 1.86667
X 1.86667
Y 0.244116
Amplitude
Frequency (kHz)

(b)

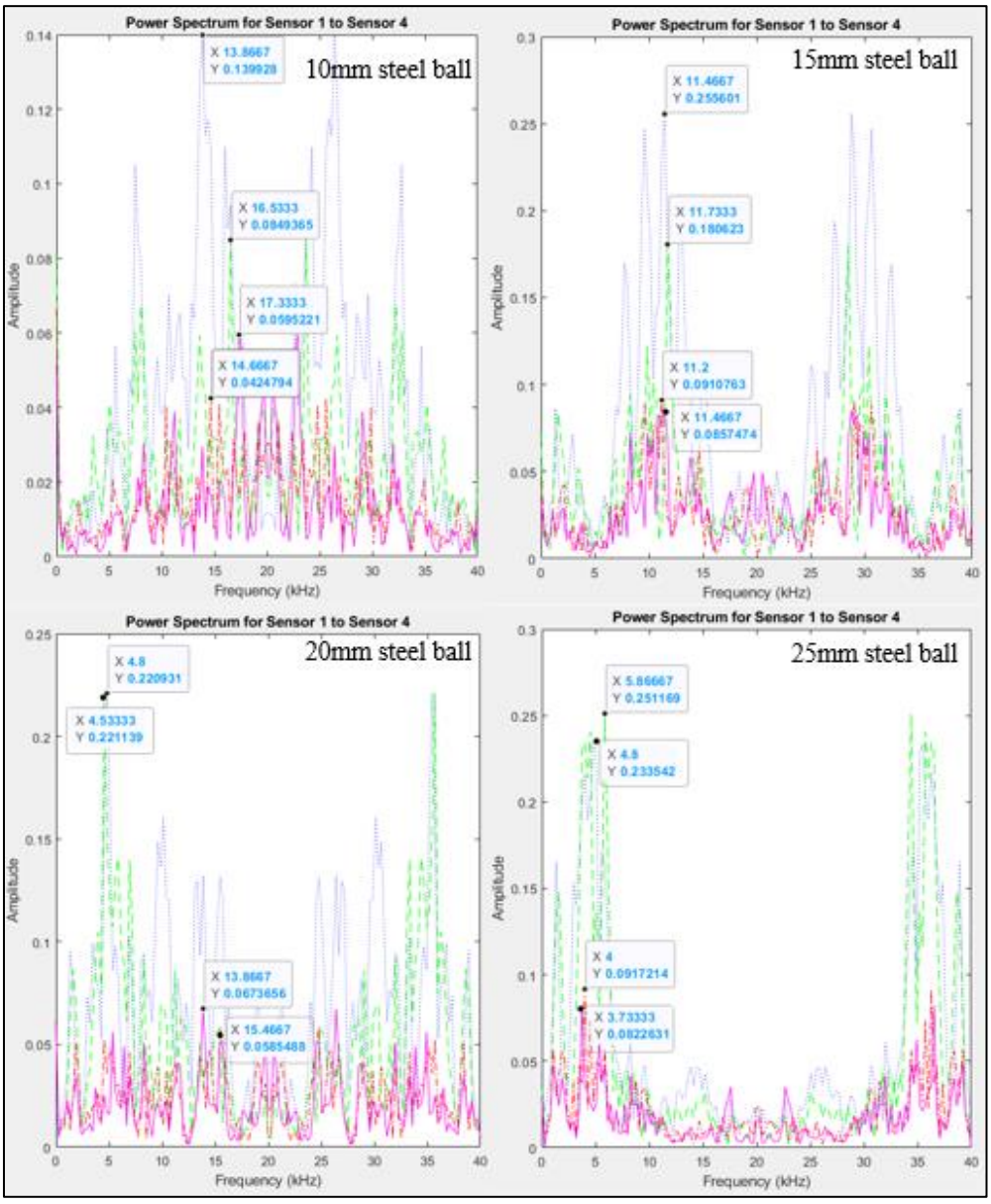
Power Spectrum for Sensor 1 to Sensor 4
10mm steel ball
X 13.8667
Y 0.139928
X 16.5333
Y 0.0849365
X 17.3333
Y 0.0595221
X 14.6667
Y 0.0424794
Amplitude
Frequency (kHz)
Power Spectrum for Sensor 1 to Sensor 4
15mm steel ball
X 11.4667
Y 0.255601
X 11.7333
Y 0.180623
X 11.2
Y 0.0910763
X 11.4667
Y 0.0857474
Amplitude
Frequency (kHz)
Power Spectrum for Sensor 1 to Sensor 4
20mm steel ball
X 4.8
Y 0.220931
X 4.53333
Y 0.221139
X 13.8667
Y 0.0673656
X 15.4667
Y 0.0585488
Amplitude
Frequency (kHz)
Power Spectrum for Sensor 1 to Sensor 4
25mm steel ball
X 5.86667
Y 0.251169
X 4.8
Y 0.233542
X 4
Y 0.0917214
X 3.73333
Y 0.0822631
Amplitude
Frequency (kHz)

(c)

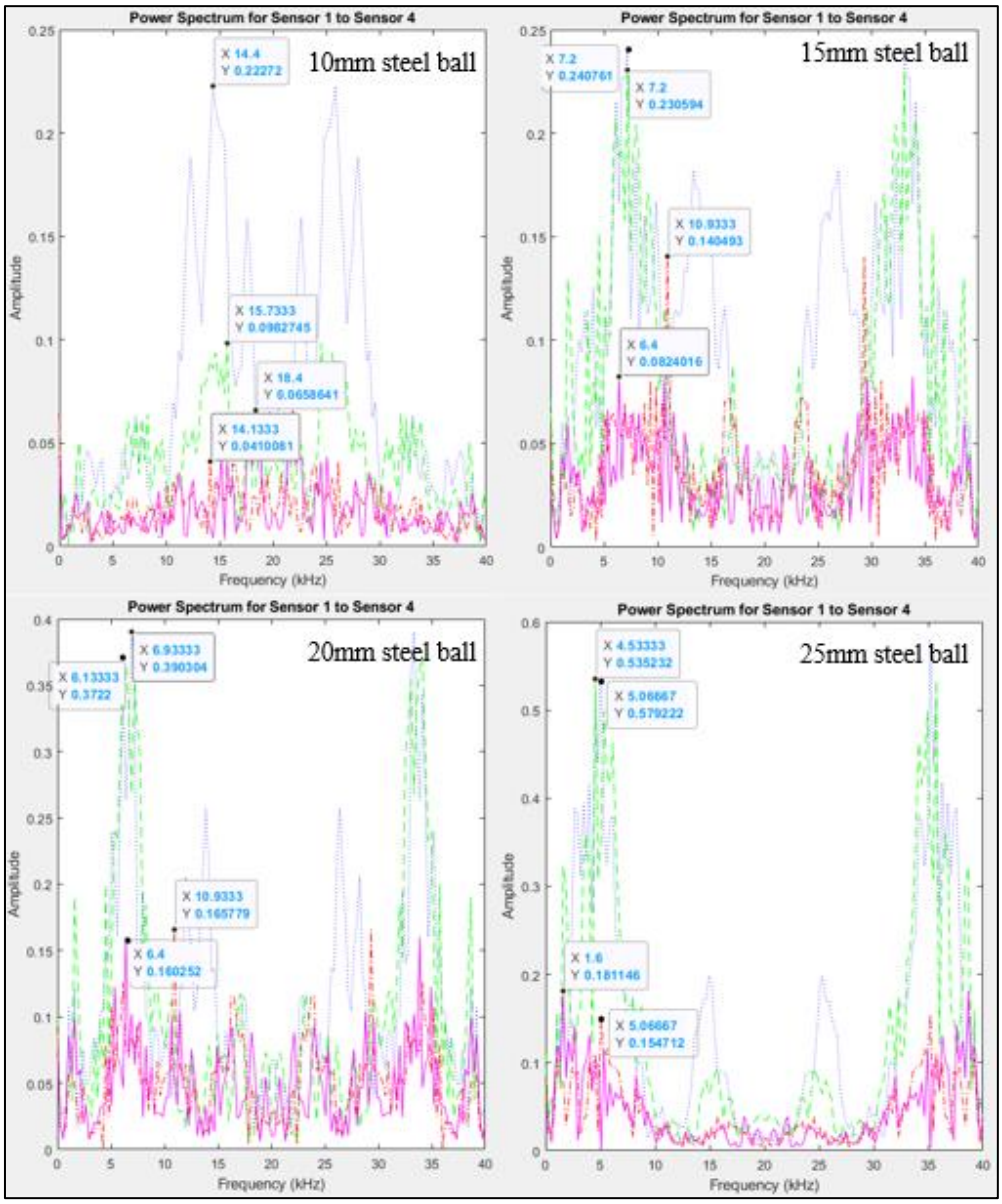
Power Spectrum for Sensor 1 to Sensor 4
10mm steel ball
X 14.4
Y 0.22272
X 15.7333
Y 0.0982745
X 18.4
Y 0.0658641
X 14.1333
Y 0.0410081
Power Spectrum for Sensor 1 to Sensor 4
15mm steel ball
X 7.2
Y 0.240761
X 7.2
Y 0.230594
X 10.9333
Y 0.140493
X 6.4
Y 0.0824016
Power Spectrum for Sensor 1 to Sensor 4
20mm steel ball
X 6.93333
Y 0.390304
X 6.13333
Y 0.3722
X 10.9333
Y 0.165779
X 6.4
Y 0.160252
Power Spectrum for Sensor 1 to Sensor 4
25mm steel ball
X 4.53333
Y 0.535232
X 5.06667
Y 0.579222
X 1.6
Y 0.181146
X 5.06667
Y 0.154712
Amplitude
Frequency (kHz)

(d)

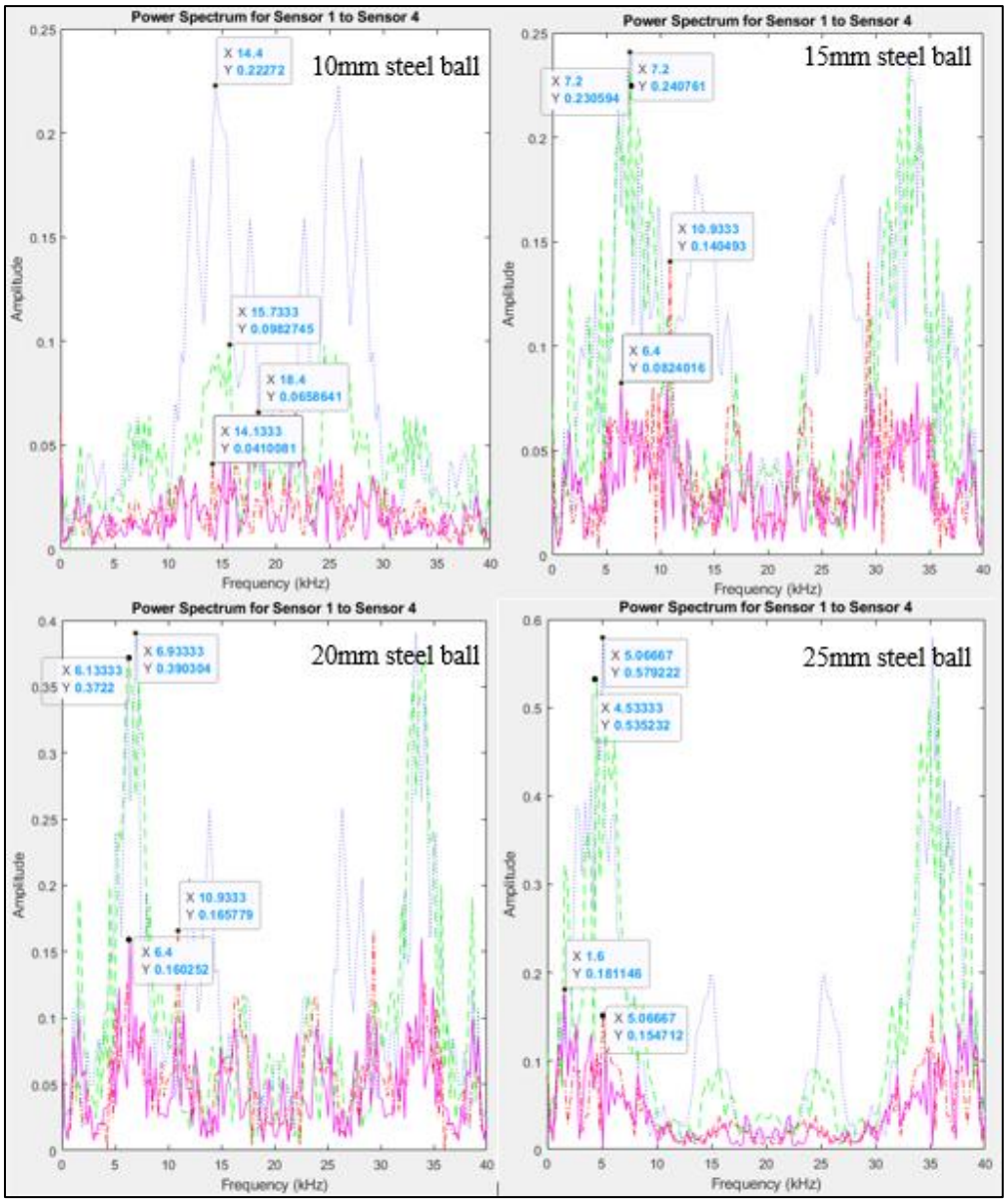

(e)

Figure 4.12: Power Spectrum for Concrete Specimen with (a) 25 mm, (b) 225 mm, (c) 425 mm, (d) 625 mm, and (e) 825 mm Depth of Delamination and 500 mm Diameter of Delamination.

4.5.2 Waveform Result from Peak Frequency

Peak frequency is associated with the maximum amplitude in the power spectrum as presented in Figure 4.12. Thus, the peak frequency is generated by MATLAB with the data from the power spectrum as shown in Figure 4.13. Then, it is compared with the data from unsound concrete in Figure 4.3(c). Table 4.15 to Table 4.20 show the tabulated data of peak frequency by Microsoft Excel in order to improve the analysis via line graph. Based on the data in Table 4.15 to

Table 4.20, the peak frequency obtained from deep delamination is higher than shallow delamination with an average of 8.96 kHz at 825 mm and 625 mm depth, 10.46 kHz at 425 mm depth, 8.63 kHz at 225 mm depth, and 7.00 kHz at 25 mm depth, whereas the average peak frequency for the unsound concrete is 8.70 kHz (Kee, Lee and Candelaria, 2019). Figure 4.14 shows the average peak frequency received by each sensor for all the concrete specimens. Therefore, the 25 mm and 225 mm depths of delamination are classified under shallow delamination, while 425 mm, 625 mm and 825 mm depths of delamination are classified under deep delamination. However, some of the peak frequency obtained from deep delamination is lower than shallow delamination due to the inhomogeneous nature of reinforced concrete which would affect the scattering characteristic of propagated wave.

Furthermore, the diameter of a steel ball does not just affect the attenuation rate, it also influences the frequency of the wave. The bigger the diameter of the steel ball, the greater the amplitude of the propagated wave, thus, the peak frequency becomes lower. However, the amplitude is found to be inconsistent as it changes from different depths of delamination. Besides, the result of amplitude and peak frequency for 625 mm and 825 mm depth of delamination is identical. This may be affected by heterogeneous nature between the reinforced concrete and polystyrene board or the position of the depth of delamination.

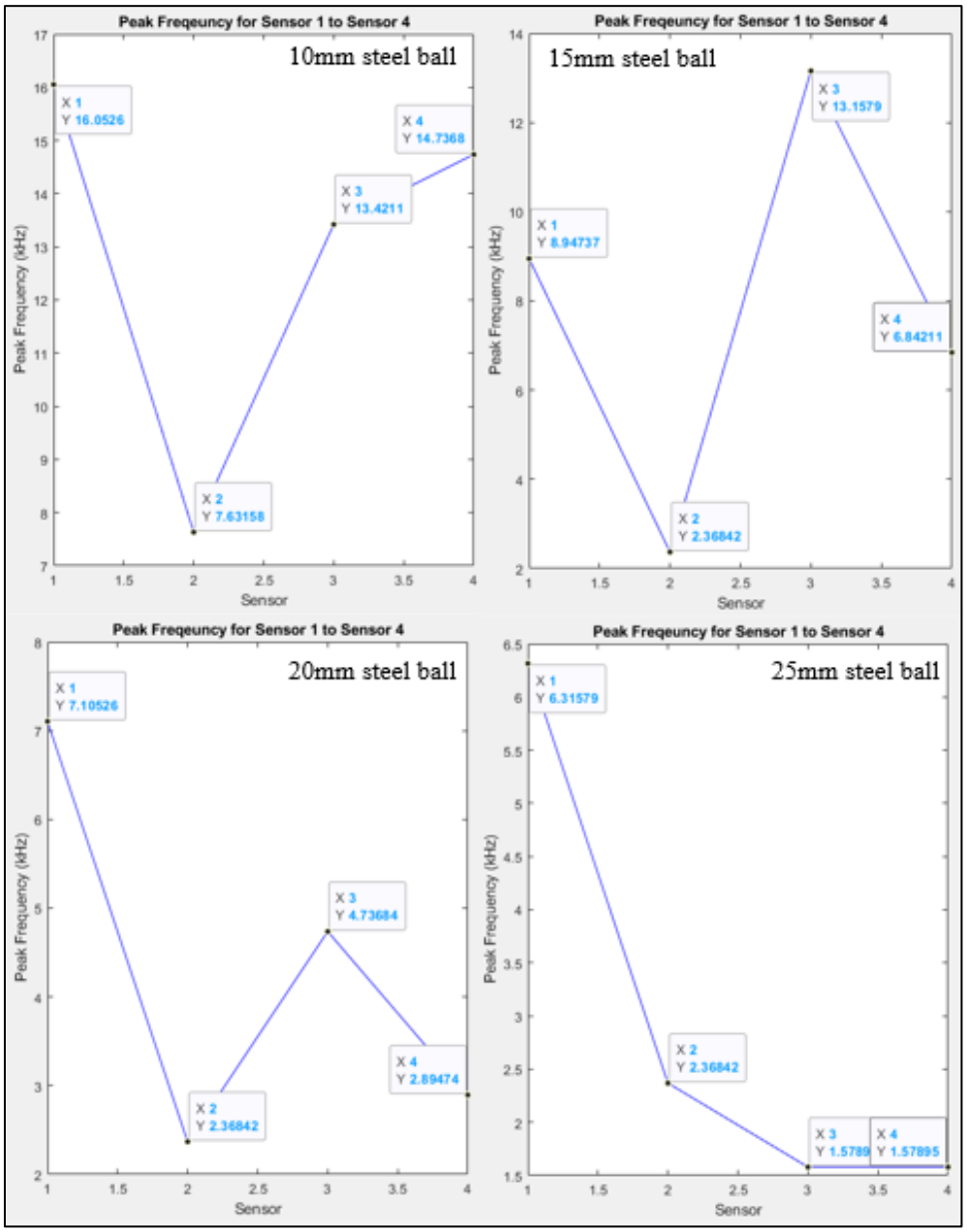
Peak Freqeuncy for Sensor 1 to Sensor 4
10mm steel ball
X 1
Y 16.0526
X 2
Y 7.63158
X 3
Y 13.4211
X 4
Y 14.7368
Peak Frequency (kHz)
Sensor
Peak Freqeuncy for Sensor 1 to Sensor 4
15mm steel ball
X 1
Y 8.94737
X 2
Y 2.36842
X 3
Y 13.1579
X 4
Y 6.84211
Peak Frequency (kHz)
Sensor
Peak Freqeuncy for Sensor 1 to Sensor 4
20mm steel ball
X 1
Y 7.10526
X 2
Y 2.36842
X 3
Y 4.73684
X 4
Y 2.89474
Peak Frequency (kHz)
Sensor
Peak Freqeuncy for Sensor 1 to Sensor 4
25mm steel ball
X 1
Y 6.31579
X 2
Y 2.36842
X 3
Y 1.5789
X 4
Y 1.57895
Peak Frequency (kHz)
Sensor

(a)

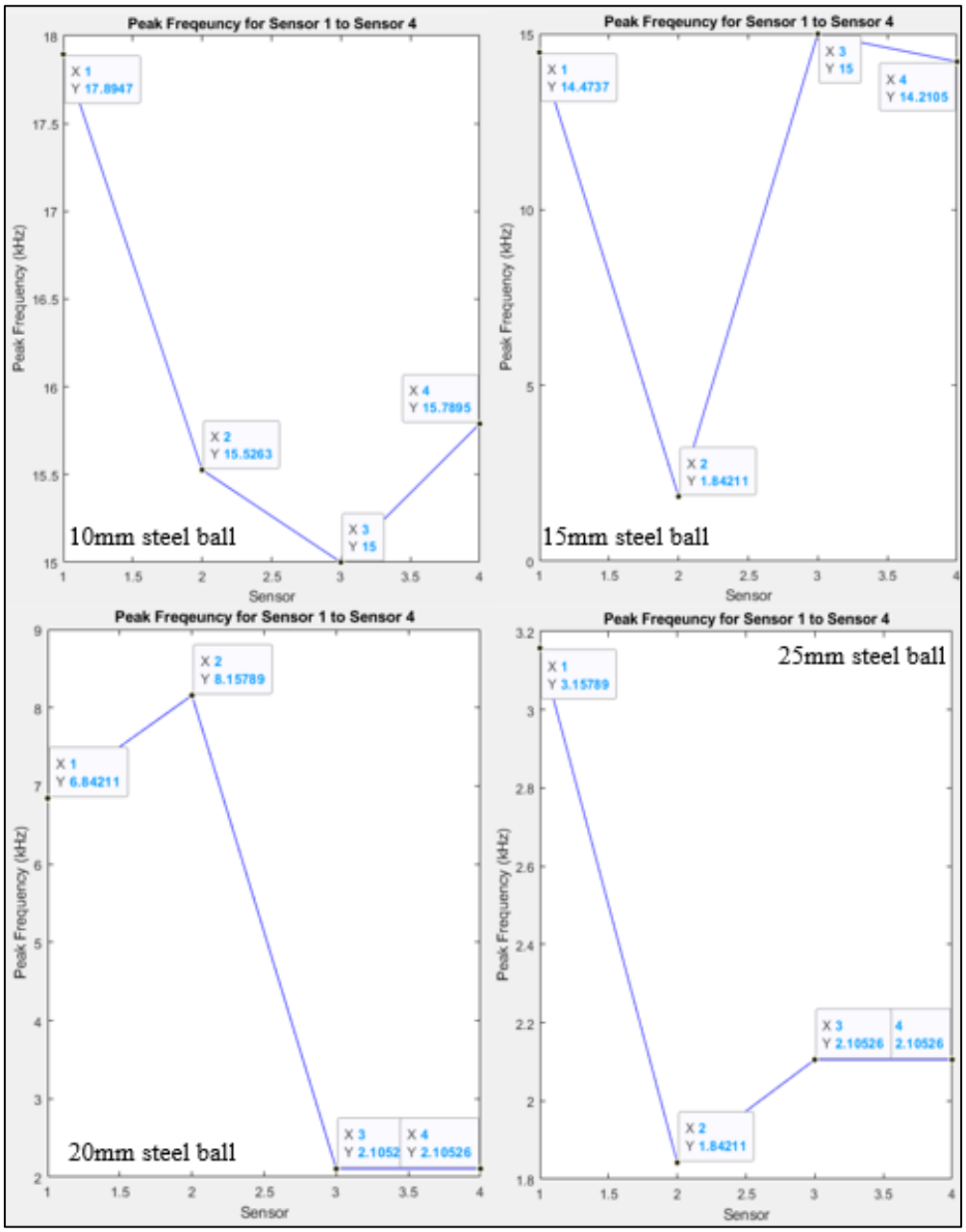
Peak Freqeuncy for Sensor 1 to Sensor 4
X 1
Y 17.8947
X 2
Y 15.5263
X 3
Y 15
X 4
Y 15.7895
10mm steel ball
Peak Frequency (kHz)
Sensor
Peak Freqeuncy for Sensor 1 to Sensor 4
X 1
Y 14.4737
X 2
Y 1.84211
X 3
Y 15
X 4
Y 14.2105
15mm steel ball
Peak Frequency (kHz)
Sensor
Peak Freqeuncy for Sensor 1 to Sensor 4
X 1
Y 6.84211
X 2
Y 8.15789
X 3
Y 2.1052
X 4
Y 2.10526
20mm steel ball
Peak Frequency (kHz)
Sensor
Peak Freqeuncy for Sensor 1 to Sensor 4
X 1
Y 3.15789
X 2
Y 1.84211
X 3
Y 2.10526
4
2.10526
25mm steel ball
Peak Frequency (kHz)
Sensor

(b)

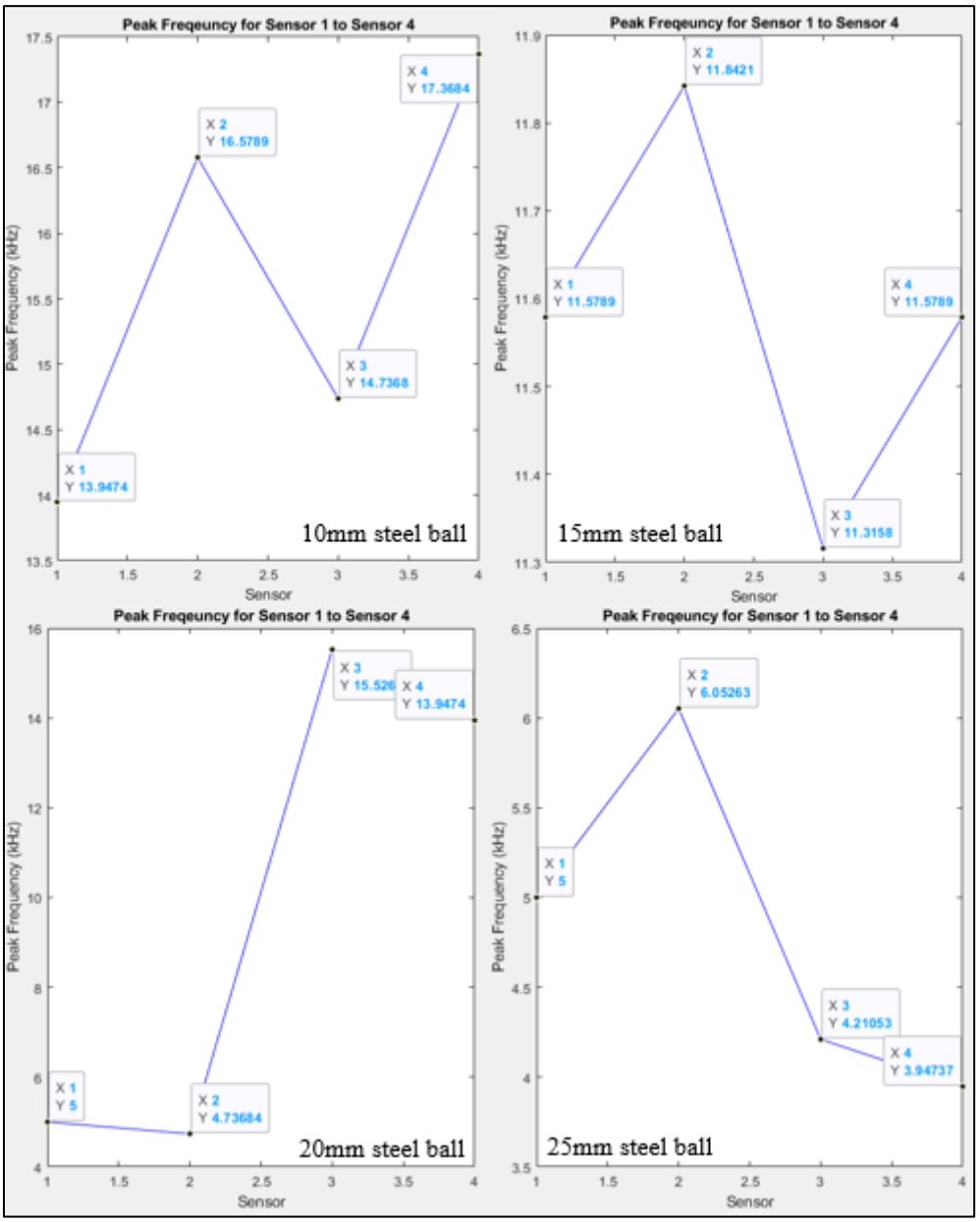
Peak Freqeuncy for Sensor 1 to Sensor 4
X 1
Y 13.9474
X 2
Y 16.5789
X 3
Y 14.7368
X 4
Y 17.3684
10mm steel ball
Peak Freqeuncy for Sensor 1 to Sensor 4
X 1
Y 11.5789
X 2
Y 11.8421
X 3
Y 11.3158
X 4
Y 11.5789
15mm steel ball
Peak Freqeuncy for Sensor 1 to Sensor 4
X 1
Y 5
X 2
Y 4.73684
X 3
Y 15.526
X 4
Y 13.9474
20mm steel ball
Peak Freqeuncy for Sensor 1 to Sensor 4
X 1
Y 5
X 2
Y 6.05263
X 3
Y 4.21053
X 4
Y 3.94737
25mm steel ball
Peak Frequency (kHz)
Sensor

(c)

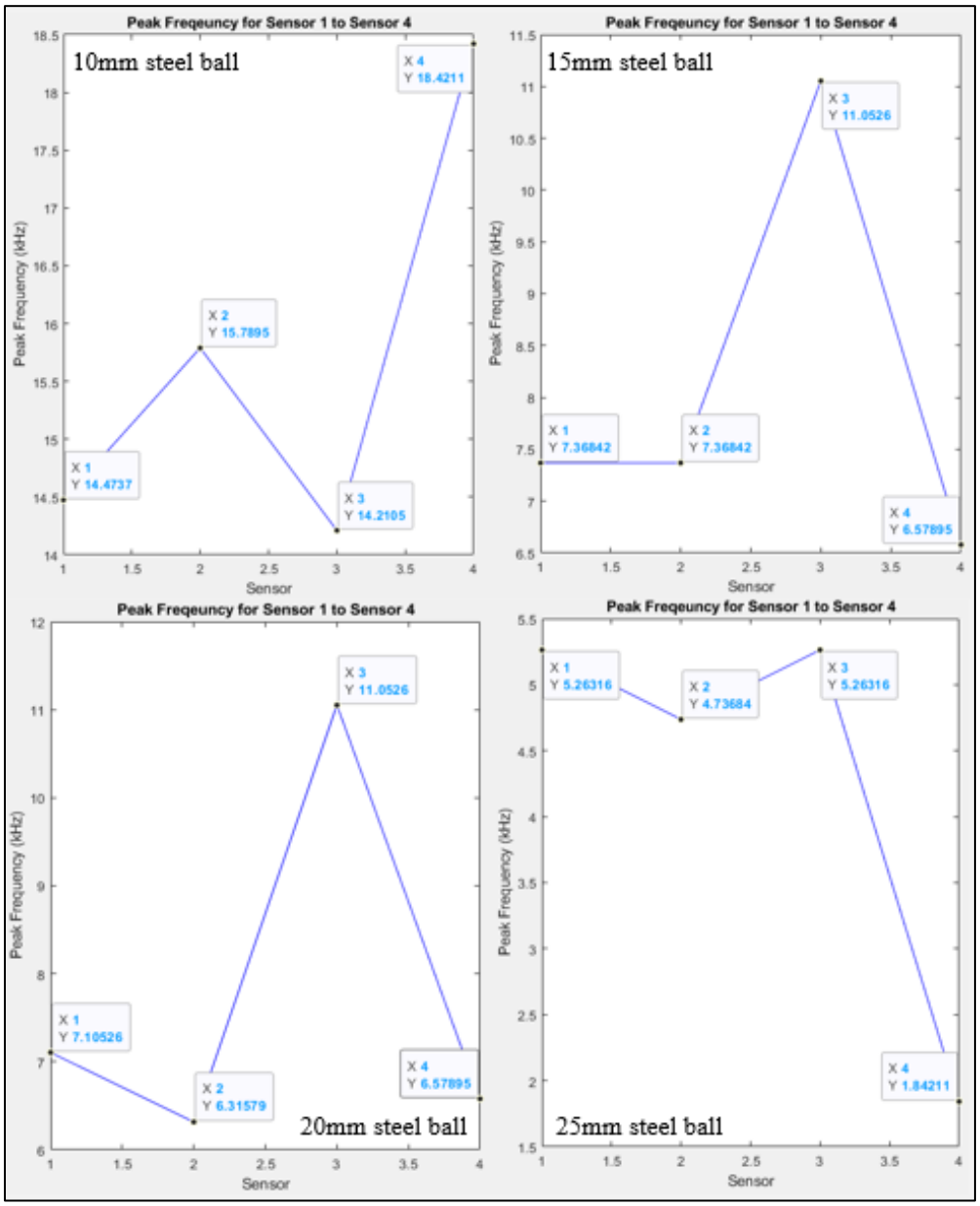
Peak Freqeuncy for Sensor 1 to Sensor 4
10mm steel ball
X 4
Y 18.4211
X 2
Y 15.7895
X 1
Y 14.4737
X 3
Y 14.2105
Peak Frequency (kHz)
Sensor
Peak Freqeuncy for Sensor 1 to Sensor 4
15mm steel ball
X 3
Y 11.0526
X 1
Y 7.36842
X 2
Y 7.36842
X 4
Y 6.57895
Peak Frequency (kHz)
Sensor
Peak Freqeuncy for Sensor 1 to Sensor 4
X 3
Y 11.0526
X 1
Y 7.10526
X 2
Y 6.31579
X 4
Y 6.57895
20mm steel ball
Peak Frequency (kHz)
Sensor
Peak Freqeuncy for Sensor 1 to Sensor 4
X 1
Y 5.26316
X 2
Y 4.73684
X 3
Y 5.26316
X 4
Y 1.84211
25mm steel ball
Peak Frequency (kHz)
Sensor

(d)

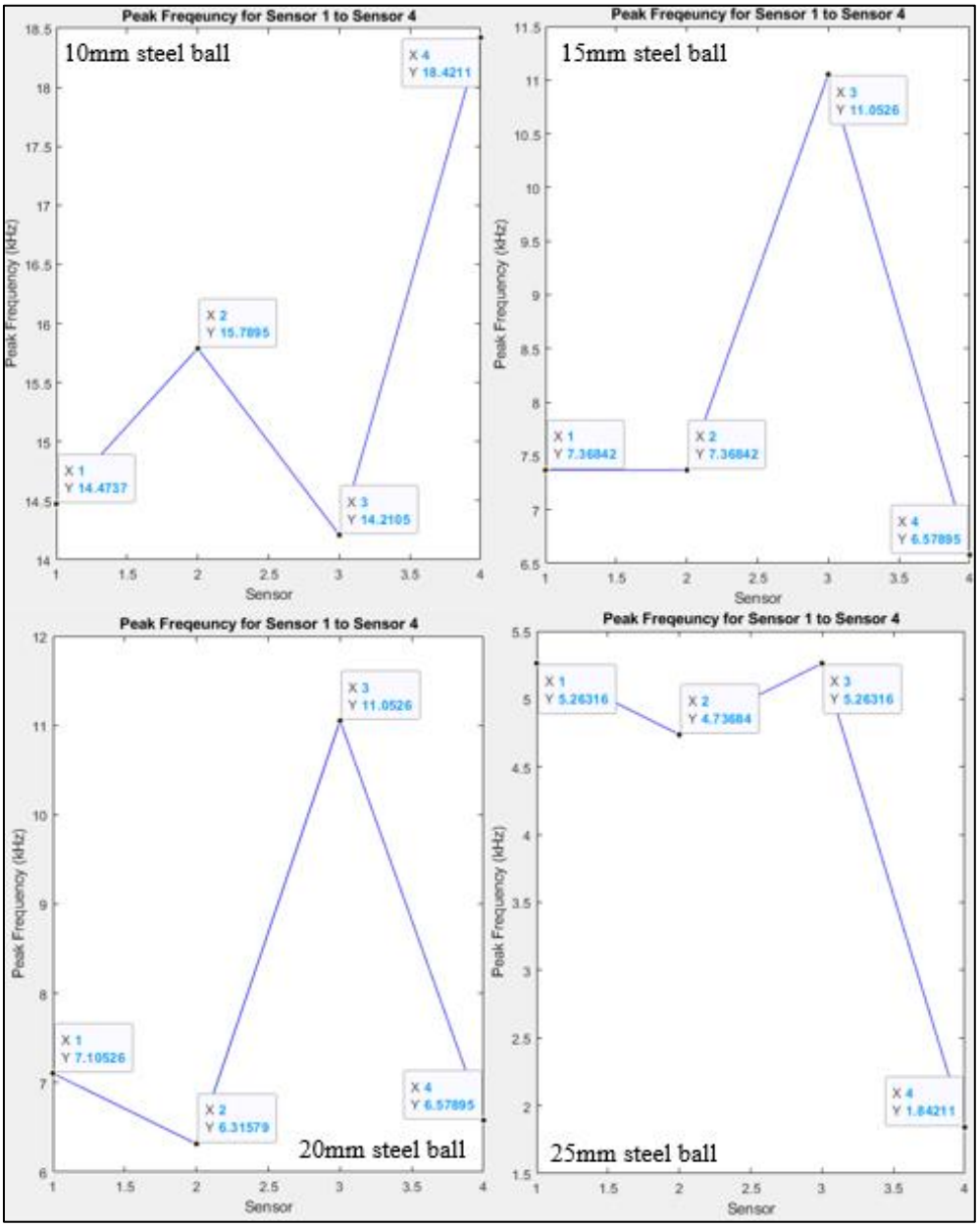

(e)

Figure 4.13: Peak Frequency for Concrete Specimen with (a) 25 mm, (b) 225 mm, (c) 425 mm, (d) 625 mm, and (e) 825 mm Depth of Delamination and 500 mm Diameter of Delamination.

Table 4.15: Amplitude and Peak Frequency for Unsound Concrete/Controlled Data.

Amplitude and peak frequency received by each sensor		Ball Diameter (mm)			
		10	15	20	25
Sensor 1	Amplitude (V)	0.260076	0.182323	0.424485	0.637658
	Peak Frequency (kHz)	16.5789	5.26316	3.68421	3.68421
Sensor 2	Amplitude (V)	0.204189	0.168856	0.474221	0.423477
	Peak Frequency (kHz)	16.5789	6.84211	6.84211	4.21053
Sensor 3	Amplitude (V)	0.0807123	0.118719	0.371545	0.204294
	Peak Frequency (kHz)	11.0526	9.73684	8.42105	8.42105
Sensor 4	Amplitude (V)	0.0737996	0.0725452	0.26414	0.150521
	Peak Frequency (kHz)	11.5789	9.47368	8.42105	8.42105

Table 4.16: Amplitude and Peak Frequency for 25 mm Depth of Delamination with 500 mm Diameter of Delamination.

Amplitude and peak frequency received by each sensor		Ball Diameter (mm)			
		10	15	20	25
Sensor 1	Amplitude (V)	0.149853	0.236655	0.378786	0.456333
	Peak Frequency (kHz)	16.0526	8.94737	7.10526	6.31579
Sensor 2	Amplitude (V)	0.12003	0.217354	0.401593	0.442082
	Peak Frequency (kHz)	7.63158	2.36842	2.36842	2.36842
Sensor 3	Amplitude (V)	0.0397736	0.0522758	0.072968	0.0988865
	Peak Frequency (kHz)	13.4211	13.1579	4.73684	1.57895
Sensor 4	Amplitude (V)	0.0318434	0.046915	0.0811461	0.134102
	Peak Frequency (kHz)	14.7368	6.84211	2.89474	1.57895

Table 4.17: Amplitude and Peak Frequency for 225 mm Depth of Delamination with 500 mm Diameter of Delamination.

Amplitude and peak frequency received by each sensor		Ball Diameter (mm)			
		10	15	20	25
Sensor 1	Amplitude (V)	0.15322	0.148082	0.272125	0.555633
	Peak Frequency (kHz)	17.8947	14.4737	6.84211	3.15789
Sensor 2	Amplitude (V)	0.0694774	0.107186	0.282277	0.467634
	Peak Frequency (kHz)	15.5263	1.84211	8.15789	1.84211
Sensor 3	Amplitude (V)	0.0659516	0.105616	0.136058	0.244116
	Peak Frequency (kHz)	15	15	2.10526	2.10526
Sensor 4	Amplitude (V)	0.0759115	0.07284	0.156504	0.286665
	Peak Frequency (kHz)	15.7895	14.2105	2.10526	2.10526

Table 4.18: Amplitude and Peak Frequency for 425 mm Depth of Delamination with 500 mm Diameter of Delamination.

Amplitude and peak frequency received by each sensor		Ball Diameter (mm)			
		10	15	20	25
Sensor 1	Amplitude (V)	0.139928	0.255601	0.220931	0.233542
	Peak Frequency (kHz)	13.9474	11.5789	5	5
Sensor 2	Amplitude (V)	0.0849365	0.180623	0.221139	0.251169
	Peak Frequency (kHz)	16.5789	11.8421	4.73684	6.05263
Sensor 3	Amplitude (V)	0.0424794	0.0910763	0.0585488	0.0917214
	Peak Frequency (kHz)	14.7368	11.3158	15.5263	4.21053
Sensor 4	Amplitude (V)	0.0595221	0.0857474	0.0673656	0.0822631
	Peak Frequency (kHz)	17.3684	11.5789	13.9474	3.94737

Table 4.19: Amplitude and Peak Frequency for 625 mm Depth of Delamination with 500 mm Diameter of Delamination.

Amplitude and peak frequency received by each sensor		Ball Diameter (mm)			
		10	15	20	25
Sensor 1	Amplitude (V)	0.22272	0.240761	0.3722	0.579222
	Peak Frequency (kHz)	14.4737	7.36842	7.10526	5.26316
Sensor 2	Amplitude (V)	0.0982745	0.0230594	0.390304	0.535232
	Peak Frequency (kHz)	15.7895	7.36842	6.31579	4.73684
Sensor 3	Amplitude (V)	0.0410081	0.140493	0.165779	0.154712
	Peak Frequency (kHz)	14.2105	11.0526	11.0526	5.26316
Sensor 4	Amplitude (V)	0.0658641	0.0824016	0.160252	0.181146
	Peak Frequency (kHz)	18.4211	6.57895	6.57895	1.84211

Table 4.20: Amplitude and Peak Frequency for 825 mm Depth of Delamination with 500 mm Diameter of Delamination.

Amplitude and peak frequency received by each sensor		Ball Diameter (mm)			
		10	15	20	25
Sensor 1	Amplitude (V)	0.22272	0.240761	0.390304	0.579222
	Peak Frequency (kHz)	14.4737	7.36842	7.10526	5.26316
Sensor 2	Amplitude (V)	0.0982745	0.230594	0.3722	0.535232
	Peak Frequency (kHz)	15.7895	7.36842	6.31579	4.73684
Sensor 3	Amplitude (V)	0.0410081	0.140493	0.165779	0.154712
	Peak Frequency (kHz)	14.2105	11.0526	11.0526	5.26316
Sensor 4	Amplitude (V)	0.0658641	0.0824016	0.160252	0.181146
	Peak Frequency (kHz)	18.4211	6.57895	6.57895	1.84211

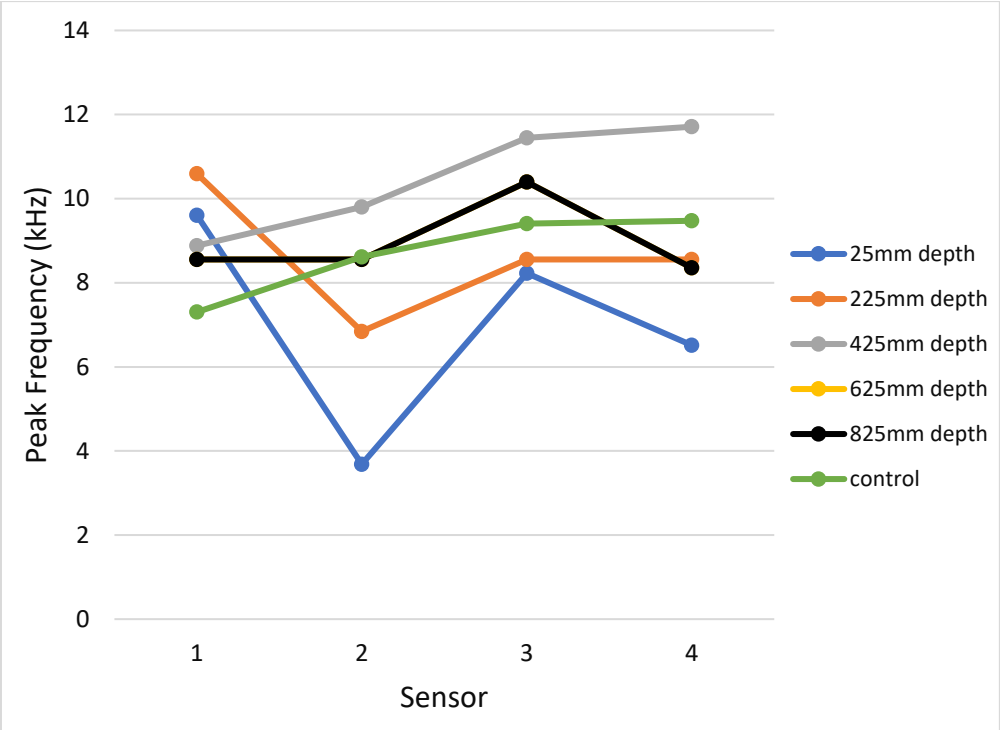

Figure 4.14: Average Peak Frequency Received by each Sensor.

4.6 Summary

Time-domain graph shows how a signal changes with time. It is very important for this study where the R-wave, amplitude attenuation and velocity of the propagated wave are determined and calculated. The R-wave is determined by the highest magnitude of amplitude of the first arriving wave. Thus, the R-wave value was applied throughout the entire calculation. The attenuation rate is calculated by the amplitude difference between two sensors and the velocity is calculated by dividing the distance to the time interval between two sensors. Besides, the bigger diameter of the steel ball will produce a greater magnitude of amplitude. It is easier to determine the R-wave signal with a bigger diameter of steel ball.

The percentage of attenuation rate for the R-wave increases as it travels from sensor 1 to sensor 4, but decreases as the diameter of the steel ball increases. Additionally, the difference of attenuation rate between sensor 2 to sensor 3 is higher than sensor 3 to sensor 4. The difference of attenuation rate in the unsound concrete is higher than the sound concrete with an average of 244% and 228.6%, respectively. Furthermore, the velocity of the propagated wave is manipulated by the time received by each sensor. It is found that the velocity

has decreased from sensor 2 to sensor 3 and increased from sensor 3 to sensor 4 in every sound concrete due to the time taken for the R-wave to reach sensor 3 is longer than it took to reach sensor 4. This is also affected by the distinct density between the reinforced concrete and the polystyrene board. However, the velocity either remains the same at 397.35 m/s or increases from sensor 2 to sensor 4 in the unsound concrete. Therefore, the defects can be estimated within the area between sensor 2 and sensor 3.

Moreover, the power spectrum and peak frequency are generated from the time-domain graph by using FFT. The frequency of the wave is affected by the difference of time from two sensors as shown in Equation 4.3 and the amplitude of the wave. Besides, the frequency of the wave is also affected by the depth of delamination where the shallow delamination has lower frequency than the deep delamination, while the frequency of the unsound concrete is in between 225 mm and 425 mm depth of delamination. Hence, 25 mm and 225 mm depth of delamination are categorised under shallow delamination and others are deep delamination.

Finally, the attenuation rate is linearly proportional to the frequency of the wave while it is inversely proportional to the diameter of steel ball, whereas the velocity of the propagated wave is inversely proportional to the time taken for R-wave to reach the sensor. The depth of defects can also be estimated by its peak frequency where the greater the value of peak frequency will detect a deep delamination. However, some of the data acquired are inconsistent due to the inhomogeneous nature of the reinforced concrete that changes the scattering characteristic of the propagated wave.

CHAPTER 5

CONCLUSION AND RECOMMENDATIONS

5.1 Introduction

This chapter discusses the conclusion and overall summary based on the aim and objective of this study. Recommendations are provided to enhance similar types of research in the time to come.

5.2 Conclusion

This experiment is to study the impact-induced elastic wave based non-destructive test on reinforced concrete containing delamination. The behaviour and characteristic of the propagated wave is studied both experimentally by non-contact method and numerically by MATLAB throughout this study. The analysis focuses on determining the position and depth of the delamination with parameters of velocity, amplitude attenuation and peak frequency which are extracted and calculated from the time-domain and frequency domain data. The comparison of data between sound and unsound concrete was studied throughout the analysis.

The first and third objectives regarding to the changes of R-wave characteristic when propagating through the concrete delamination and the effectiveness of the developed methodology on the condition of concrete delamination were both discussed in chapter 4. The second objective regarding the development of a methodology for R-wave signal processing and data interpretation by using MATLAB was discussed in chapter 3.

Based on the experimental results, the velocity of R-wave is between the range of 361. 23 m/s to 397.35 m/s when travelling through the concrete specimen and then dropped to 296.53 m/s to 361.23 m/s at sensor 3, and rose back to the range between 361.22 m/s to 1986.49 m/s at sensor 4. Comparing it to the unsound concrete, the velocity either remains unchanged or keeps increasing when travelling through the specimen. This can justify the presence of delamination between sensor 2 and sensor 3 will affect the velocity of the propagated waves.

For attenuation rate of R-wave, the percentage is found to be increasing as it travels through the concrete specimen due to the magnitude of amplitude received by each sensor has become weaker. The difference of attenuation rate between sensor 3 and sensor 2 is higher than the difference between sensor 4 and sensor 3 to justify the presence of delamination and the inhomogeneous nature of the concrete specimen and polystyrene board. In addition, the attenuation rate is also affected by the diameter of the steel ball where a bigger diameter of steel ball will produce a lower attenuation rate.

For peak frequency that generated from power spectrum, it is higher at deep delamination comparing to the shallow delamination with an average value of 8.96 kHz, 8.96 kHz, 10.46 kHz, 8.63 kHz, and 7.00 kHz at descending order from 825 mm to 25 mm respectively. Therefore, the 25 mm and 225 mm depth of delamination are classified under shallow delamination, while 425 mm, 625 mm and 825 mm depth of delamination are classified under deep delamination. Furthermore, the diameter of the steel ball will also affect the frequency of the wave where the bigger diameter of the steel ball will produce greater amplitude of propagated wave and lower frequency. The inconsistency of amplitude and peak frequency from the results are mainly due to the heterogeneous nature between the reinforced concrete and polystyrene board.

5.3 Recommendations for future work

By considering the preliminary study of non-contact method of impact-induced elastic wave based non-destructive test on reinforced concrete containing delamination, the recommendation for user of similar materials and apparatus in the future is comparing non-contact method to contact method in order to improve the feasibility of R-wave in non-contact method.

Furthermore, there are many numerical methods to simulate engineering problems such as FDM and FEM. Thus, the feasibility of non-contact R-wave can be improved with the comparison of more numerical simulation in order to characterise the depth and size of delamination within the same environment.

The arrangement of sensors in this experiment is fixed to a distance which could be manipulated in further study. This function could obtain a wider

variety of data and establish a multi-functional technique that is adaptable to all sorts of experiments by using non-contact methods.

REFERENCES

Ahmad, A. and Bond, L., 2018. Fundamental of Ultrasonic Inspection. *ASM Handbook, Volume 17, Nondestructive Evaluation of Materials*, [online] Available at: https://www.asminternational.org/documents/10192/22533690/05511G_SampleArticle.pdf/a8c3979c-3b35-f304-68f2-151271f2e3b8 [Accessed 28 February 2021].

Al Wardany, R., Rhazi, J., Gallias, J. L. and Saleh, K., 2004. *Use of Rayleigh wave methods to detect near surface concrete damage*. [online] Available at: https://www.researchgate.net/publication/239586012_USE_OF_RAYLEIGH_WAVE_METHODS_TO_DETECT_NEAR_SURFACE_CONCRETE_DAMAGE [Accessed 20 February 2021].

Albrecht, L., 2019. *Concrete surface defects: when temperature attack*. PowerBlanker [blog] 17 September. Available at: https://www.powerblanket.com/blog/common-concrete-surface-defects-caused-cold-weather/ [Accessed 22 February].

Aqua calculator, 2021. *Density of Polystyrene (material)*. [online] Worldwide: AVCalc LLC. Available at: https://www.aqua-calc.com/page/density-table/substance/polystyrene

Asano, M., Kamada, T., Kunieda, M. and Rokugo, K., 2003. Impact Acoustics Methods for Defect Evaluation Concrete. *Non-destructive testing in civil engineering 2003*, [online] Available at: https://www.ndt.net/article/ndtce03/papers/v040/v040.htm [Accessed 11 March 2021].

Atkinson, K. E., 2007. Numerical analysis. *Scholarpedia*. [e-journal] http://dx.doi.org/10.4249/scholarpedia.3163

Bannister, D., 2020. *A guide to concrete efflorescence*. [online] USA: ConcreteNetwork.com. Available at: https://www.concretenetwork.com/doug_bannister/efflorescence.htm [Accessed 25 February 2021].

Cadence PCB solutions, 2020. *Power Spectrum vs. Power Spectral Density: What Are You Measuring?* [online] Ireland: Cadence Design Systems, Inc. Available at: https://resources.pcb.cadence.com/blog/2020-power-spectrum-vs-power-spectral-density-what-are-you-measuring [Accessed 7 July 2021].

Cadence PCB solutions, 2020. *Time Domain Analysis vs Frequency Domain Analysis: A Guide and Comparison*. [online] Ireland: Cadence Design Systems, Inc. Available at: https://resources.pcb.cadence.com/blog/2020-time-domain-analysis-vs-frequency-domain-analysis-a-guide-and-comparison [Accessed 7 July 2021].

Ecoratio, 2019. *Tips on how to stop concrete dusting*. Ecoratio the release agent company blog, [blog] 15 January. Available at: https://blog.ecoratio.com/stop-concrete-dusting [Accessed 22 February].

Flyability, (in press) *NDT: What it is, common methods & industries, and how drones can help*. [online] Switzerland: Flyability SA. Available at: https://www.flyability.com/ndt

Gholizadeh, S., 2016. A review of non-destructive testing methods of composite materials. *Procedia Structural Integrity*, [e-journal] 1, pp.50-57. https://doi.org/10.1016/j.prostr.2016.02.008

Gholizadeh, S., Leman, Z. and Baharudin, B. T. H. T., 2015. A review of the application of acoustic emission technique in engineering. *Structural Engineering and Mechanics*, [e-journal] Volume 54 – Issue 6,pp.1075-1095. https://doi.org/10.12989/sem.2015.54.6.1075

Giatec, 2019. *Evaluating Cracking in Concrete Procedures*. [online] Canada: Giatec Scientific Inc. Available at: https://www.giatecscientific.com/education/cracking-in-concrete-procedures/ [Accessed 24 February 2021].

Green, D., 2021. *Delamination and Blisters*. [online] Available at: https://concretesouth.com/tech-center/tech-topics-ready-mix/delamination-and-blisters [Accessed 22 February].

Gromicko, N. and Shepard, K., 2006. *The History of Concrete*. [online] Available at: https://www.nachi.org/history-of-concrete.htm#:~:text=The%20precursor%20to%20concrete%20was,form%20a%20hard%2C%20protective%20surface [Accesed 16 February 2021].

Gupta, S., 2018. Comparison of Non-Destructive and Destructive Testing on Concrete: A Review. *Trends in Civil Engineering and its Architecture*, [e-journal] Volume 3 – Issue 1,pp.1-7. http://dx.doi.org/10.32474/TCEIA.2018.03.000154

Hashimoto, K., Shiotani, T. and Ohtsu, M., 2020. Application of Impact-Echo Method to 3D SIBIE Procedure for Damage Detection in Concrete. *Nondestructive Testing (NDT)*, [e-journal] Volume 10 – Issue 8,pp.2-16. https://doi.org/10.3390/app10082729

Institute for Underground Infrastructure, 2020. *Concrete, component and method tests*. [online] Germany: Institute for Underground Infrastructure. Available at: https://www.ikt-online.org/test-centre/concrete/ [Accessed 25 February 2021].

Kee, S.H., Lee, J.W. and Candelaria, M.D, 2019. Evaluation of Delamination in Concrete by IE Testing Using Multi-Channel Elastic Wave Data. *Journal of Physical Sensors*, [e-journal] 20(1), 201. https://doi.org/10.3390/s20010201

Keulemans, G., 2016. *The problem with reinforced concrete*. [online] Australia: University of New South Wales. Available at: https://theconversation.com/the-problem-with-reinforced-concrete-56078 [Accessed 15 February 2021].

Khan, M., 2020. *Defects in Concrete Structures ï Its Causes, Types, and Prevention*. [online] Available at: https://civilmint.com/defects-in-concrete-structures/ [Accessed 25 February 2021].

Lee, F.W., Chai, H.K. and Lim, K.S., 2016. Assessment of Reinforced Concrete Surface Breaking Crack Using Rayleigh Wave Measurement. *Journal of Physical Sensors*, [e-journal] 16(3), 337. https://doi.org/10.3390/s16030337.

Lee, Y. H. and Oh, T., 2016. The Measurement of P-, S-, and R-Wave Velocities to Evaluate the Condition of Reinforced and Prestressed Concrete Slabs. *Advances in Materials Science and Engineering*, [e-journal] Volume 2016, pp.2-15. https://doi.org/10.1155/2016/1548215

Liew, C. H., Lee, F. W., Tan, D. S., Lim, J. H., Yew, M. K. and Woon, Y. B., 2019. Behavioural study of surface Rayleigh waves in concrete structure containing delamination. *Journal of Civil Structural Health Monitoring*, [online] Available at: https://www.researchgate.net/publication/335637839_Behavioural_study_of_surface_Rayleigh_waves_in_concrete_structure_containing_delamination [Accessed 3 March 2021].

Maack, S., Villalobos, S. and Scott, D., 2018. Validation of artificial defects for Non-destructive testing measurements on a reference structure. *MATEC Web of Conferences*, [e-journal] Volume 199, pp.2-9. https://doi.org/10.1051/matecconf/201819906006

Nelligan, T. and Calderwood, C., 2015. *Introduction to Eddy Current Testing*. [online] Global: Olympus Industrial Resources. Available at: https://www.olympus-ims.com/en/eddycurrenttesting/ [Accessed 23 February 2021].

Russell, D., 1998. *Acoustics and Vibration Animations*. Graduate Program in Acoustics. The Pennsylvania State University. Available at: https://www.acs.psu.edu/drussell/Demos/waves/wavemotion.html [Accessed 27 February 2021].

Seegebrecht, G., 2016. *Delamination in concrete slabs*. [online] Available at: https://www.concretenetwork.com/concrete-delamination.html [Accessed 25 February 2021].

Seismo Blog, 2009. *Lord Rayleigh and the Love Waves*. [blog] 27 July. Available at: https://seismo.berkeley.edu/blog/2009/07/27/lord-rayleigh-and-the-love-waves.html [Accessed 11 July 2021].

Sjodin, B., 2016. *Wh a t ô s T h e D i f f e r e n c e B e t w e e n F E*
[online] Available at: https://www.machinedesign.com/3d-printing-cad/fea-

and-simulation/article/21832072/whats-the-difference-between-fem-fdm-and-fvm#:~:text=The%20finite%2Ddifference%20method%20is,to%20discretizing%20partial%20differential%20equations.&text=There%20is%20a%20connection%20with,method%20on%20the%20same%20grid. [Accessed 21 February 2021].

Sölken, W., 2008. *Ultrasonic Testing*. [online] USA: Explore the World of Piping. Available at: http://www.wermac.org/others/ndt_ut.html

Strang, G., 2013. *Mathematician Gilbert Strang on differential equations, history of finite elements, and problems of the method*.

Sullivan, C., 2020. *Repair spalling concrete*. [online] USA: ConcreteNetwork.com. Available at: https://www.concretenetwork.com/fix-spalled-concrete/#:~:text=Spalling%20concrete%20is%20a%20common,Freeze%2Dthaw%20cycles&text=A%20bad%20concrete%20mix [Accessed 25 February 2021].

Tarr, S., 2008. *Surface crazing*. [online] USA: Concrete Construction. Available at: https://www.concreteconstruction.net/how-to/concrete-production-precast/surface-crazing_o [Accessed 25 February 2021].

Testa, A. J., 1982. Nondestructive measurement of surface cracks using ultrasonic Rayleigh waves. *Retrospective Theses and Dissertations*, [e-journal] https://doi.org/10.31274/rtd-180813-8038

TWI, 2021. *What is destructive testing? ï Methods, Definition and Examples*. [online] UK: The Welding Institute. Available at: https://www.twi-global.com/technical-knowledge/faqs/what-is-destructive-testing#:~:text=Destructive%20testing%20is%20undertaken%20in,to%20reproduce%20set%20service%20conditions. [Accessed 19 February 2021].

Zetec, 2018. *Destructive and Nondestructive Testing Methods: A Comparison*. [online] Washington: Zetec Inc. Available at: https://www.zetec.com/blog/destructive-and-nondestructive-testing-methods-a-comparison/ [Accessed 20 February 2021].

Zheng, X.H., Liu, L., Sun, J.Z., Li, G., Zhou, F.B. and Xu, J.M, 2018. Imaging of underground karst water channels using an improved multichannel transient Rayleigh wave detecting method. PLoS ONE 13(6): e0199030. https://doi.org/10.1371/journal.pone.0199030

APPENDICES

APPENDIX A: Time-domain Graph (Section 4.4).

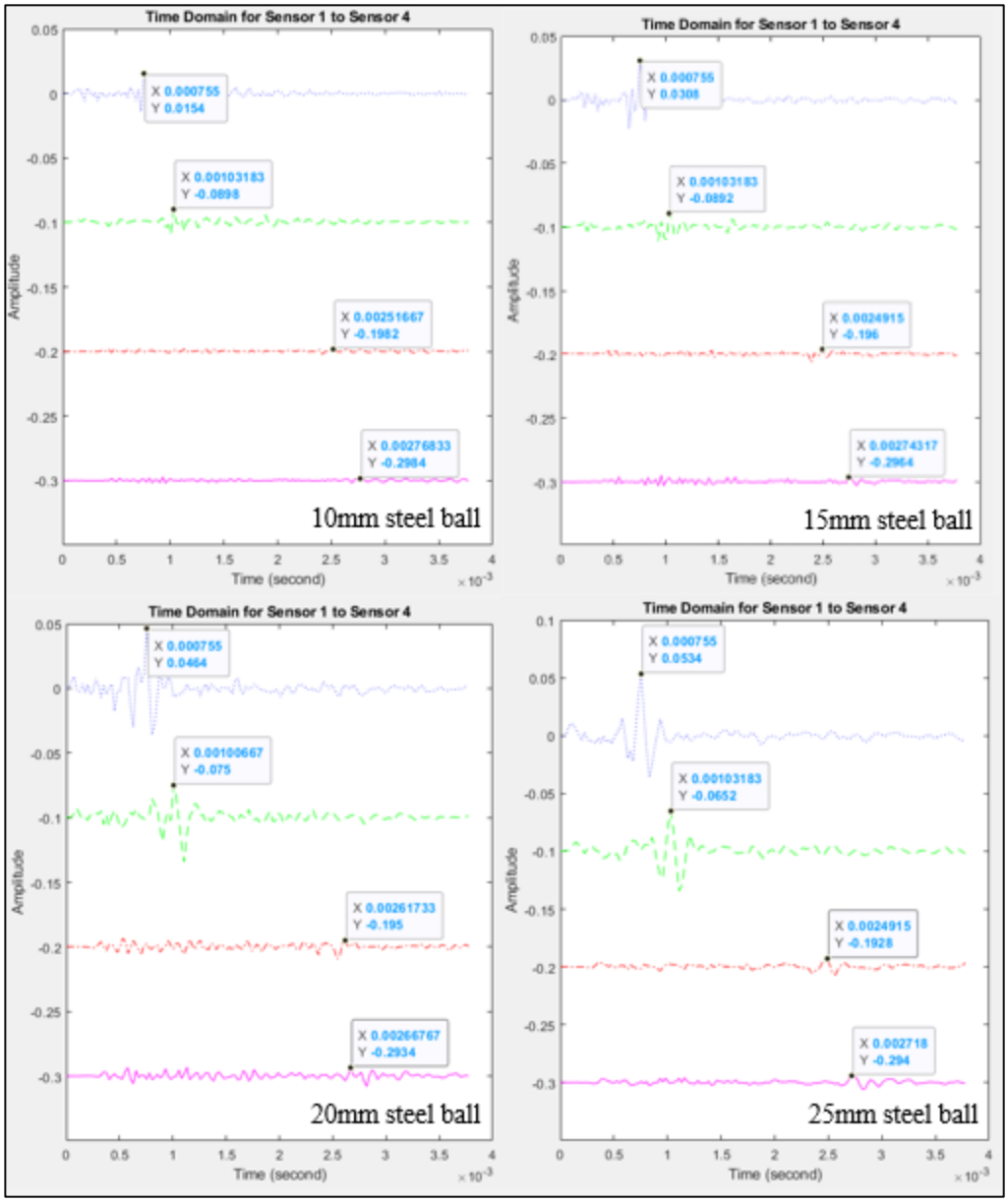

(a)

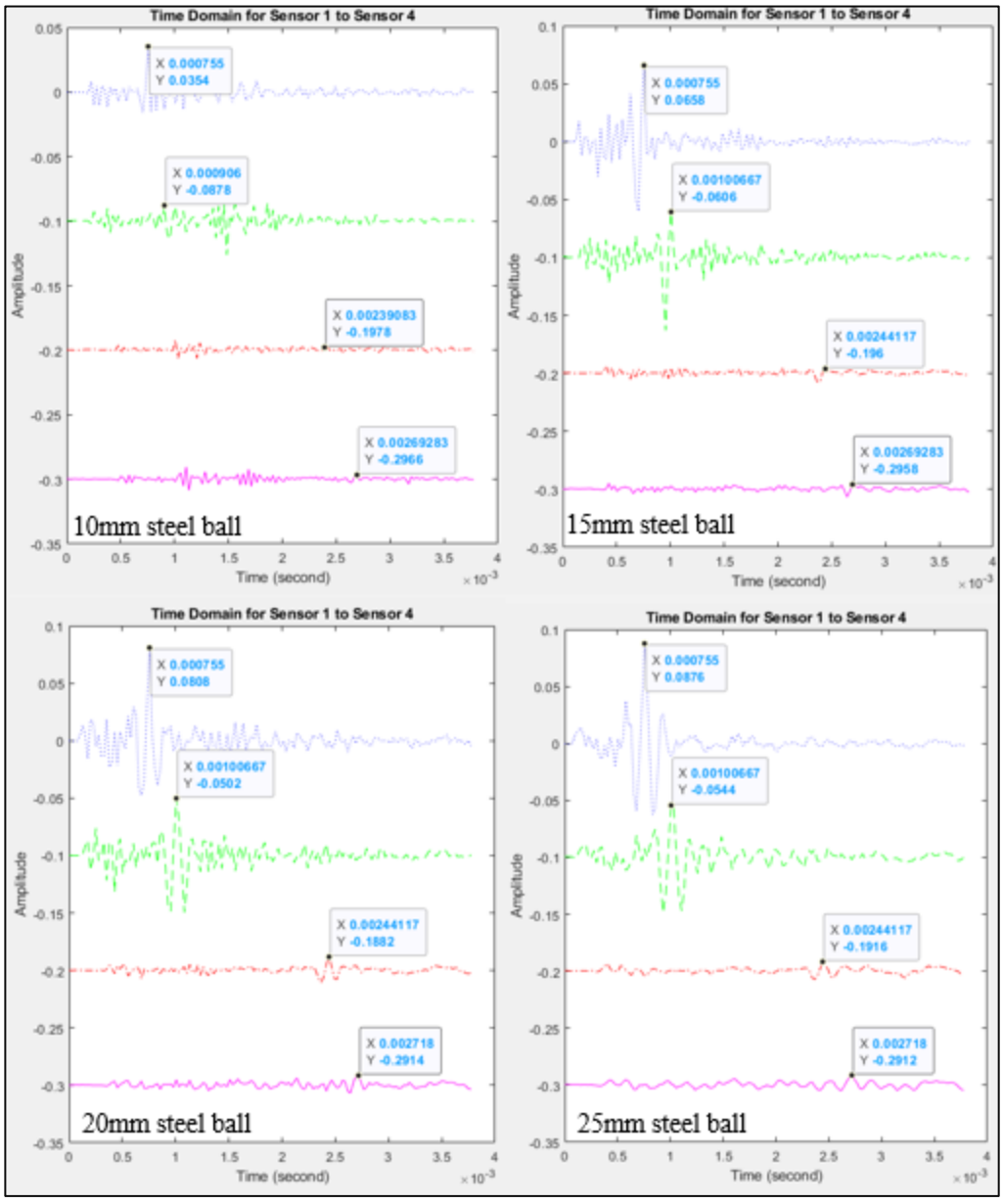
Time Domain for Sensor 1 to Sensor 4
X 0.000755
Y 0.0354
X 0.000906
Y -0.0878
X 0.00239083
Y -0.1978
X 0.00269283
Y -0.2966
10mm steel ball
Amplitude
Time (second)
Time Domain for Sensor 1 to Sensor 4
X 0.000755
Y 0.0658
X 0.00100667
Y -0.0606
X 0.00244117
Y -0.196
X 0.00269283
Y -0.2958
15mm steel ball
Amplitude
Time (second)
Time Domain for Sensor 1 to Sensor 4
X 0.000755
Y 0.0808
X 0.00100667
Y -0.0502
X 0.00244117
Y -0.1882
X 0.002718
Y -0.2914
20mm steel ball
Amplitude
Time (second)
Time Domain for Sensor 1 to Sensor 4
X 0.000755
Y 0.0876
X 0.00100667
Y -0.0544
X 0.00244117
Y -0.1916
X 0.002718
Y -0.2912
25mm steel ball
Amplitude
Time (second)

(b)

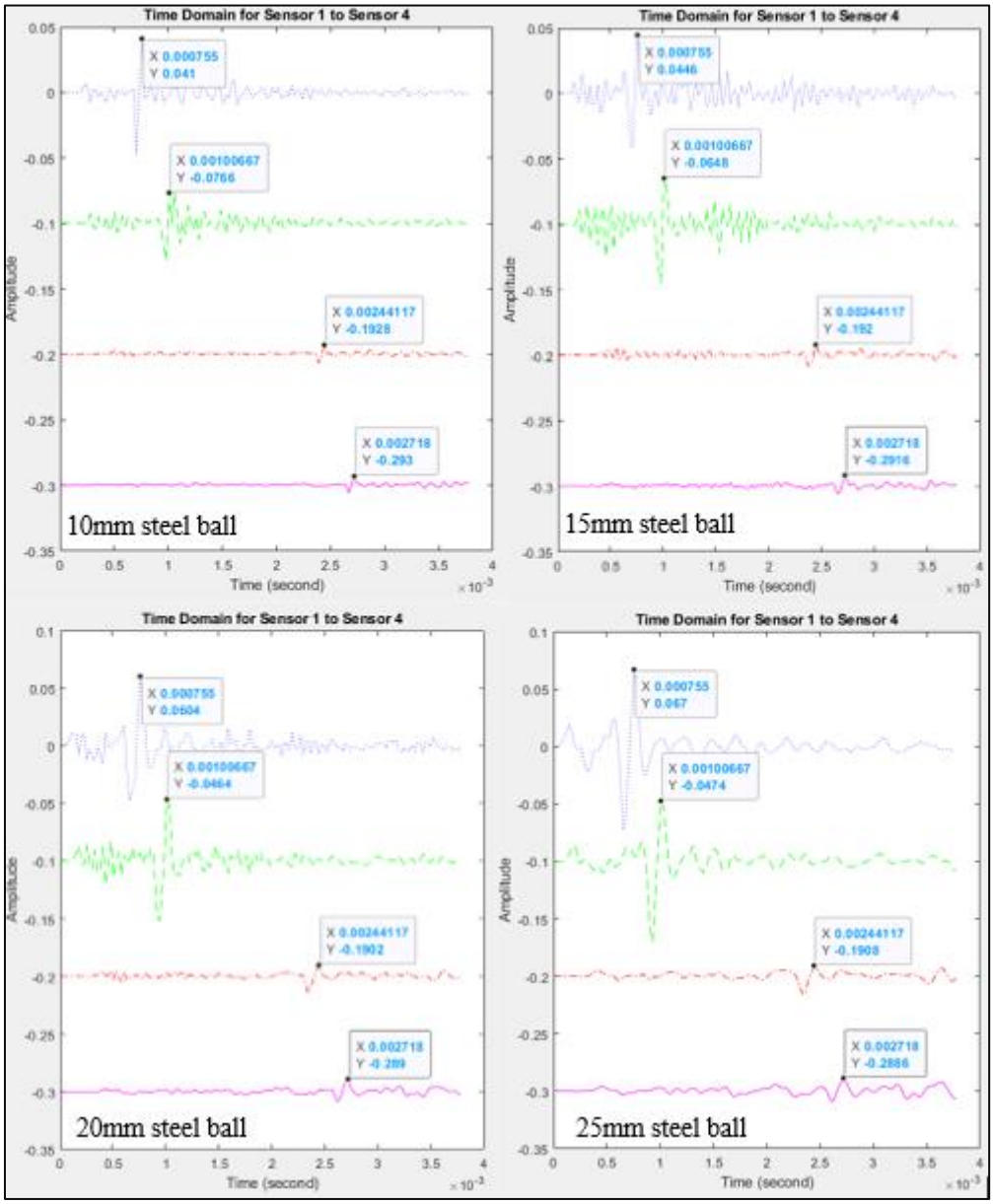
Time Domain for Sensor 1 to Sensor 4
X 0.000755
Y 0.041
X 0.00100667
Y -0.0766
X 0.00244117
Y -0.1928
X 0.002718
Y -0.293
10mm steel ball
Amplitude
Time (second)
Time Domain for Sensor 1 to Sensor 4
X 0.000755
Y 0.0446
X 0.00100667
Y -0.0648
X 0.00244117
Y -0.192
X 0.002718
Y -0.2916
15mm steel ball
Amplitude
Time (second)
Time Domain for Sensor 1 to Sensor 4
X 0.000755
Y 0.0504
X 0.00100667
Y -0.0464
X 0.00244117
Y -0.1902
X 0.002718
Y -0.289
20mm steel ball
Amplitude
Time (second)
Time Domain for Sensor 1 to Sensor 4
X 0.000755
Y 0.067
X 0.00100667
Y -0.0474
X 0.00244117
Y -0.1908
X 0.002718
Y -0.2886
25mm steel ball
Amplitude
Time (second)

(c)

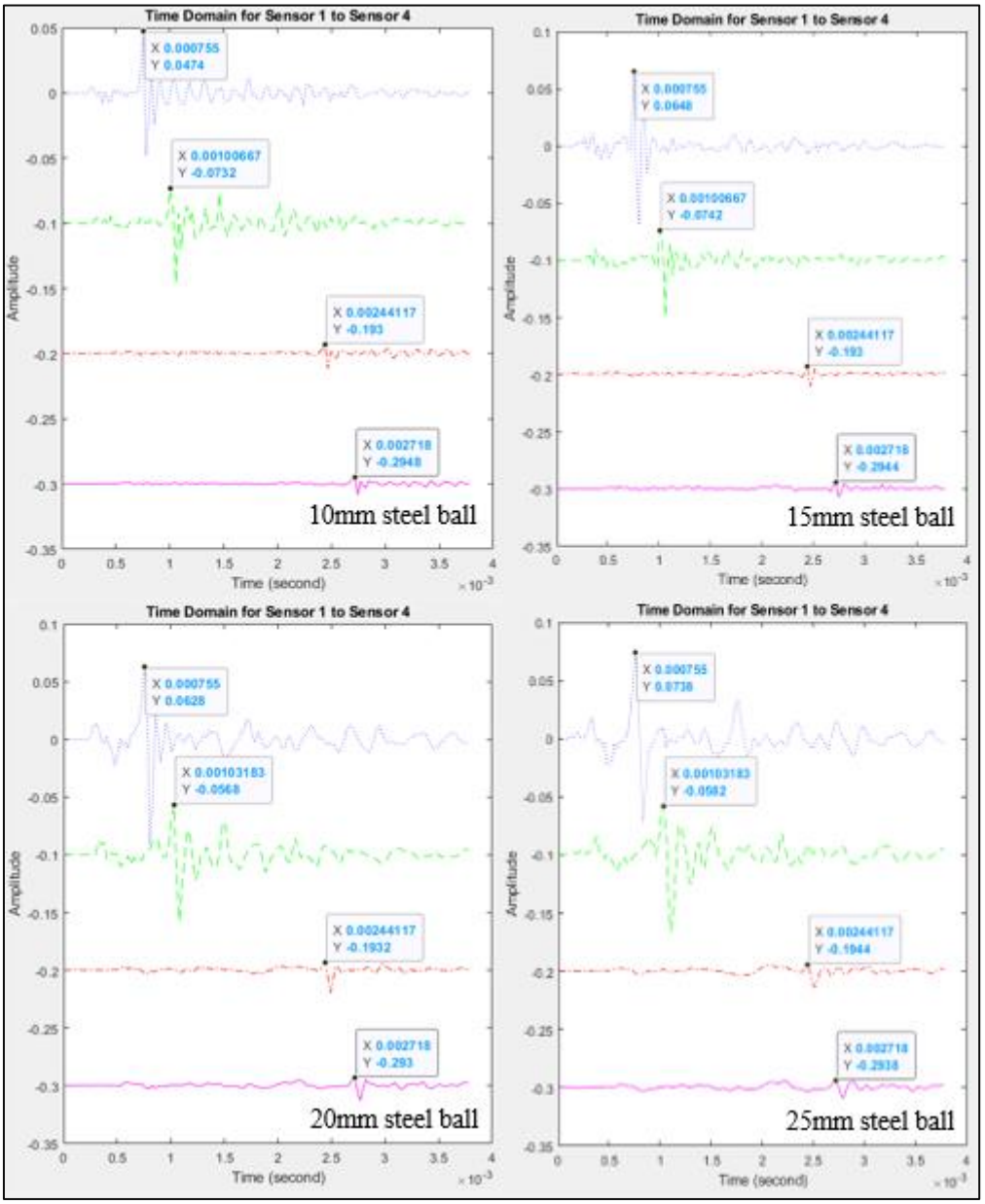
Time Domain for Sensor 1 to Sensor 4
X 0.000755
Y 0.0474
X 0.00100667
Y -0.0732
X 0.00244117
Y -0.193
X 0.002718
Y -0.2948
10mm steel ball
Amplitude
Time (second)
Time Domain for Sensor 1 to Sensor 4
X 0.000755
Y 0.0648
X 0.00100667
Y -0.0742
X 0.00244117
Y -0.193
X 0.002718
Y -0.2944
15mm steel ball
Amplitude
Time (second)
Time Domain for Sensor 1 to Sensor 4
X 0.000755
Y 0.0628
X 0.00103183
Y -0.0568
X 0.00244117
Y -0.1932
X 0.002718
Y -0.293
20mm steel ball
Amplitude
Time (second)
Time Domain for Sensor 1 to Sensor 4
X 0.000755
Y 0.0738
X 0.00103183
Y -0.0582
X 0.00244117
Y -0.1944
X 0.002718
Y -0.2938
25mm steel ball
Amplitude
Time (second)

(d)

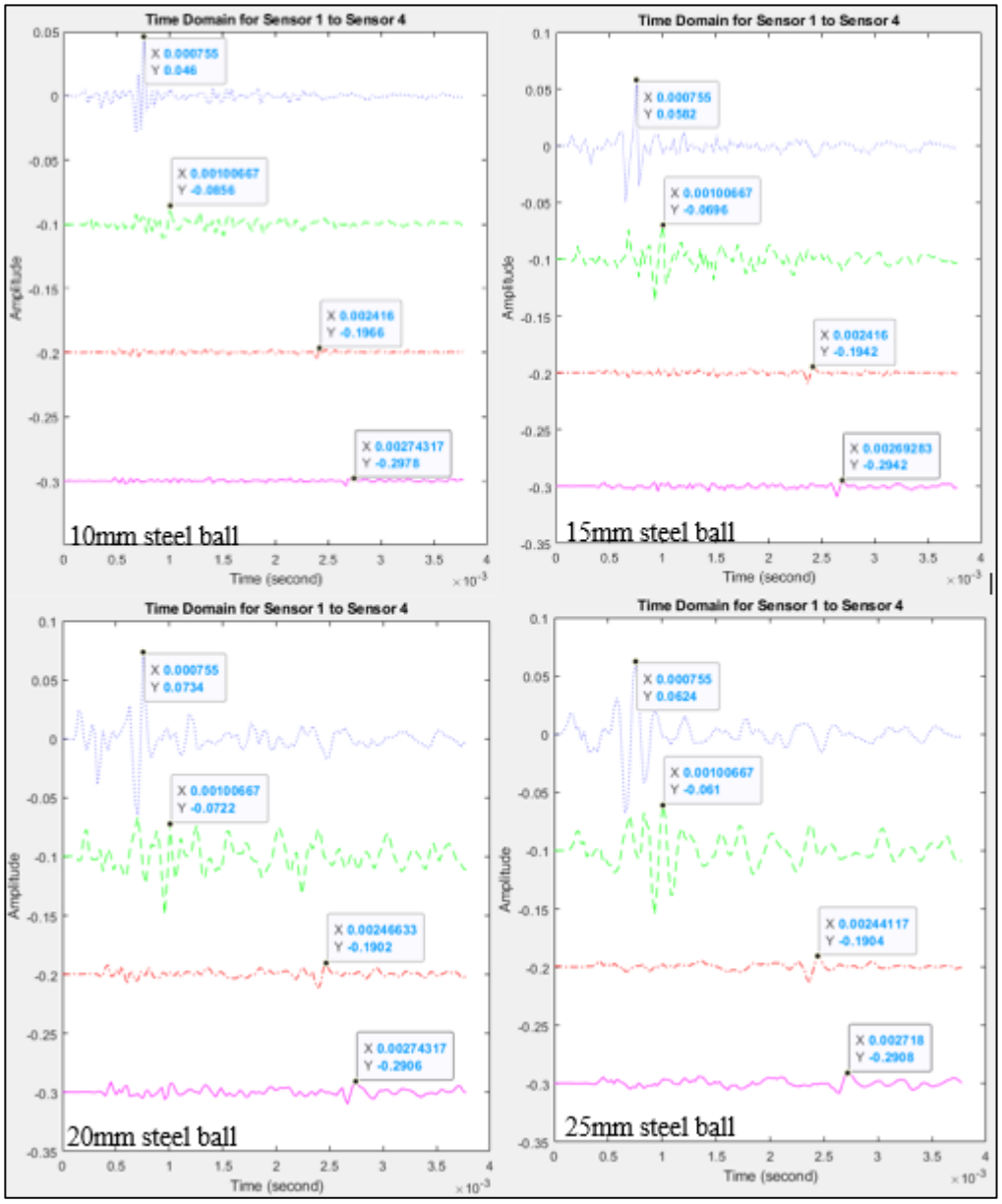

(e)

Appendix A-1: Time-domain Graph for 25 mm Depth of Delamination and (a) 100 mm, (b) 200 mm, (c) 300 mm, (d) 400 mm, and (e) 500 mm Diameter of Delamination.

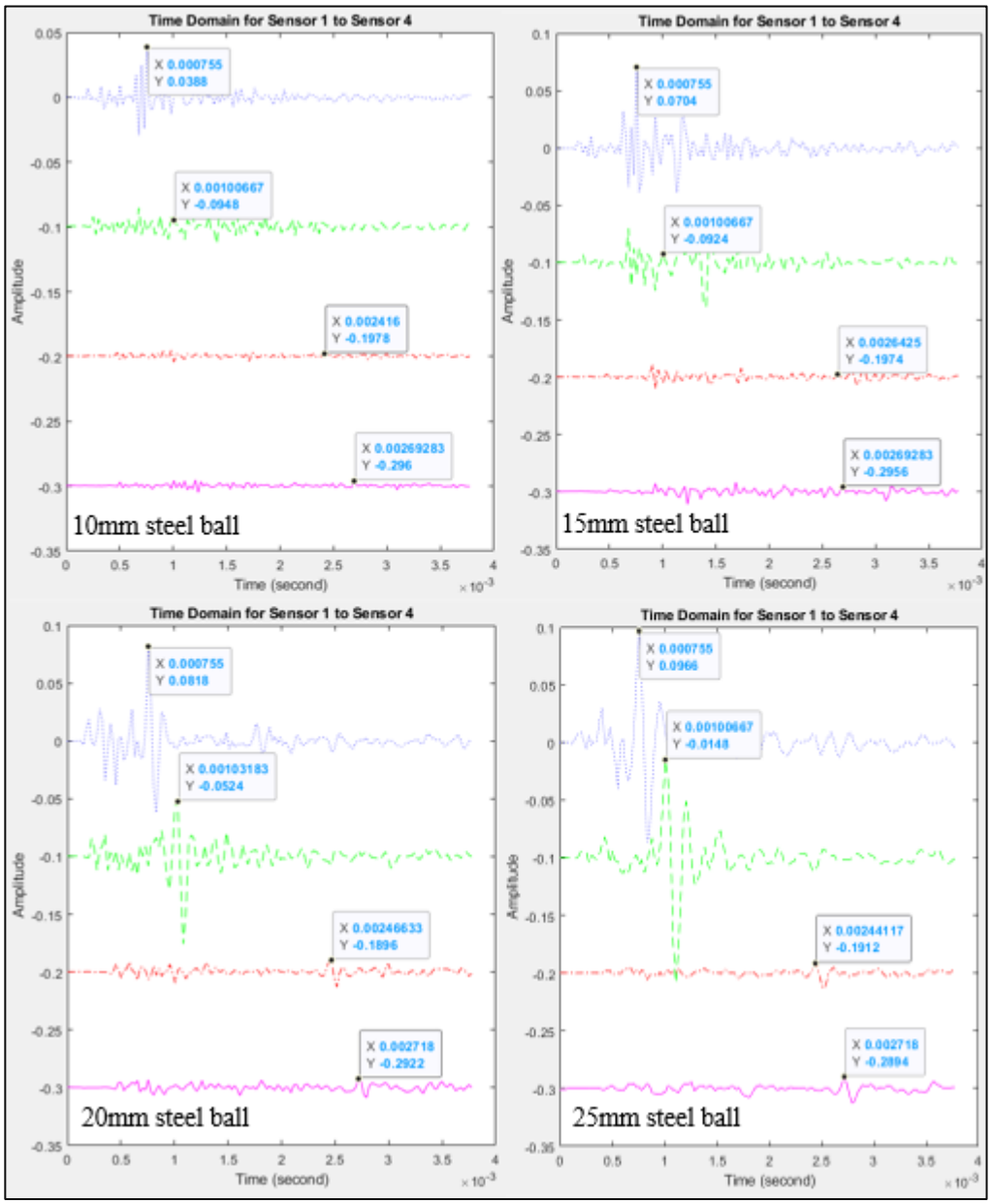
Time Domain for Sensor 1 to Sensor 4
X 0.000755
Y 0.0388
X 0.00100667
Y -0.0948
X 0.002416
Y -0.1978
X 0.00269283
Y -0.296
10mm steel ball
Amplitude
Time (second)
Time Domain for Sensor 1 to Sensor 4
X 0.000755
Y 0.0704
X 0.00100667
Y -0.0924
X 0.0026425
Y -0.1974
X 0.00269283
Y -0.2956
15mm steel ball
Amplitude
Time (second)
Time Domain for Sensor 1 to Sensor 4
X 0.000755
Y 0.0818
X 0.00103183
Y -0.0524
X 0.00246633
Y -0.1896
X 0.002718
Y -0.2922
20mm steel ball
Amplitude
Time (second)
Time Domain for Sensor 1 to Sensor 4
X 0.000755
Y 0.0966
X 0.00100667
Y -0.0148
X 0.00244117
Y -0.1912
X 0.002718
Y -0.2894
25mm steel ball
Amplitude
Time (second)

(a)

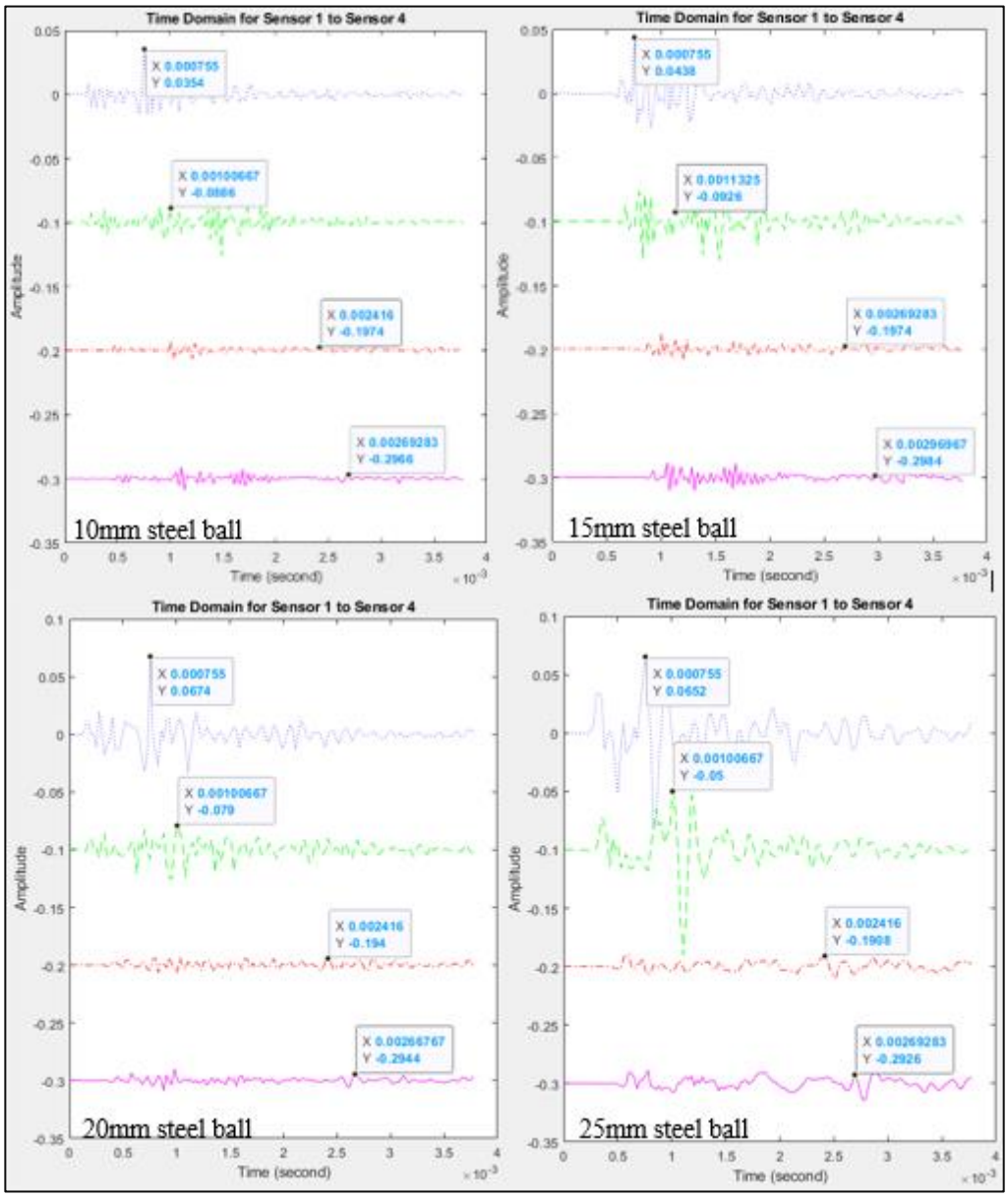
Time Domain for Sensor 1 to Sensor 4
X 0.000755
Y 0.0354
X 0.00100667
Y -0.0886
X 0.002416
Y -0.1974
X 0.00269283
Y -0.2966
10mm steel ball
Amplitude
Time (second)
Time Domain for Sensor 1 to Sensor 4
X 0.000755
Y 0.0438
X 0.0011325
Y -0.0926
X 0.00269283
Y -0.1974
X 0.00296967
Y -0.2984
15mm steel ball
Amplitude
Time (second)
Time Domain for Sensor 1 to Sensor 4
X 0.000755
Y 0.0674
X 0.00100667
Y -0.079
X 0.002416
Y -0.194
X 0.00266767
Y -0.2944
20mm steel ball
Amplitude
Time (second)
Time Domain for Sensor 1 to Sensor 4
X 0.000755
Y 0.0652
X 0.00100667
Y -0.05
X 0.002416
Y -0.1908
X 0.00269283
Y -0.2926
25mm steel ball
Amplitude
Time (second)

(b)

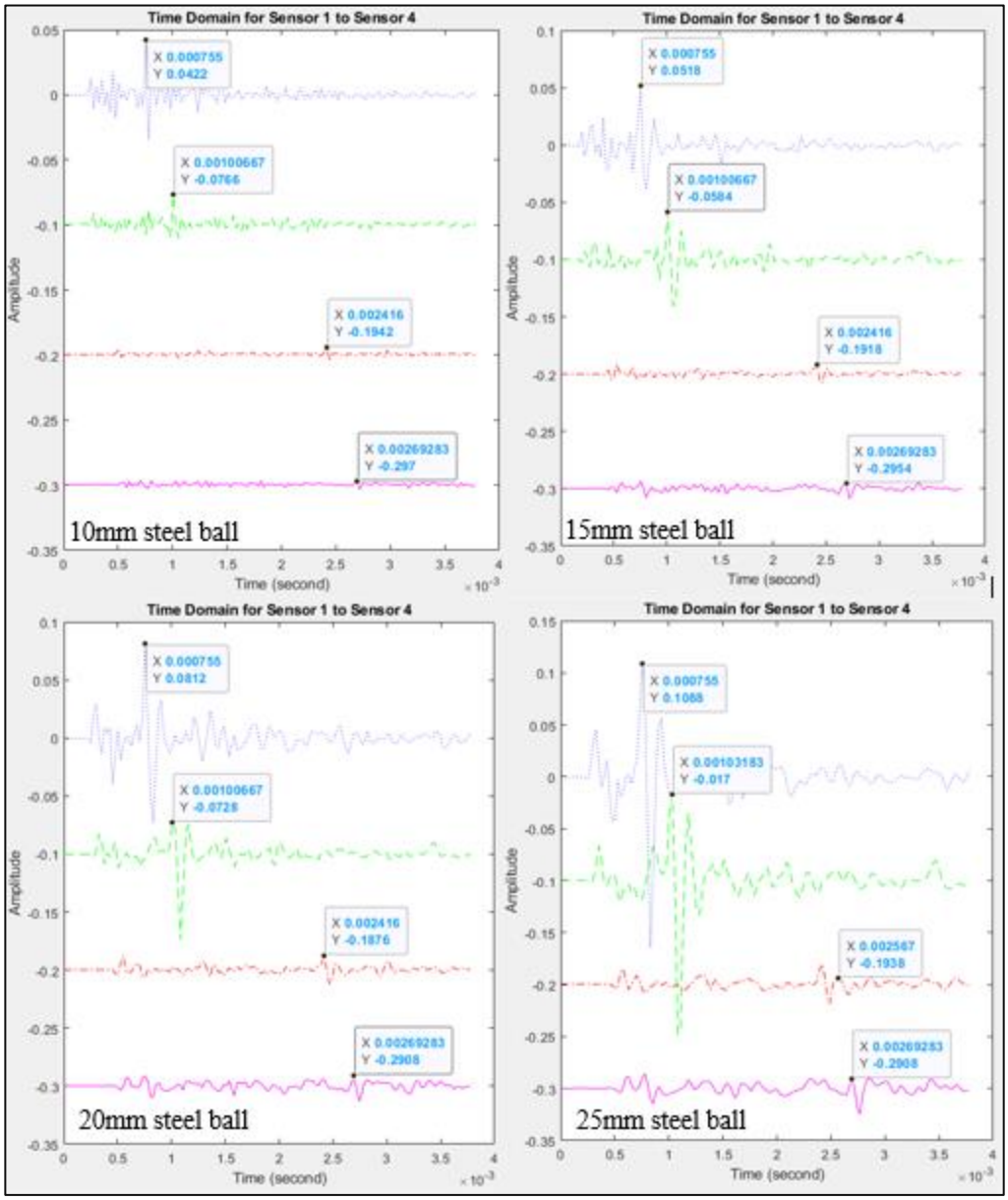
Time Domain for Sensor 1 to Sensor 4
X 0.000755
Y 0.0422
X 0.00100667
Y -0.0766
X 0.002416
Y -0.1942
X 0.00269283
Y -0.297
10mm steel ball
Amplitude
Time (second)
Time Domain for Sensor 1 to Sensor 4
X 0.000755
Y 0.0518
X 0.00100667
Y -0.0584
X 0.002416
Y -0.1918
X 0.00269283
Y -0.2954
15mm steel ball
Amplitude
Time (second)
Time Domain for Sensor 1 to Sensor 4
X 0.000755
Y 0.0812
X 0.00100667
Y -0.0728
X 0.002416
Y -0.1876
X 0.00269283
Y -0.2908
20mm steel ball
Amplitude
Time (second)
Time Domain for Sensor 1 to Sensor 4
X 0.000755
Y 0.1088
X 0.00103183
Y -0.017
X 0.002567
Y -0.1938
X 0.00269283
Y -0.2908
25mm steel ball
Amplitude
Time (second)

(c)

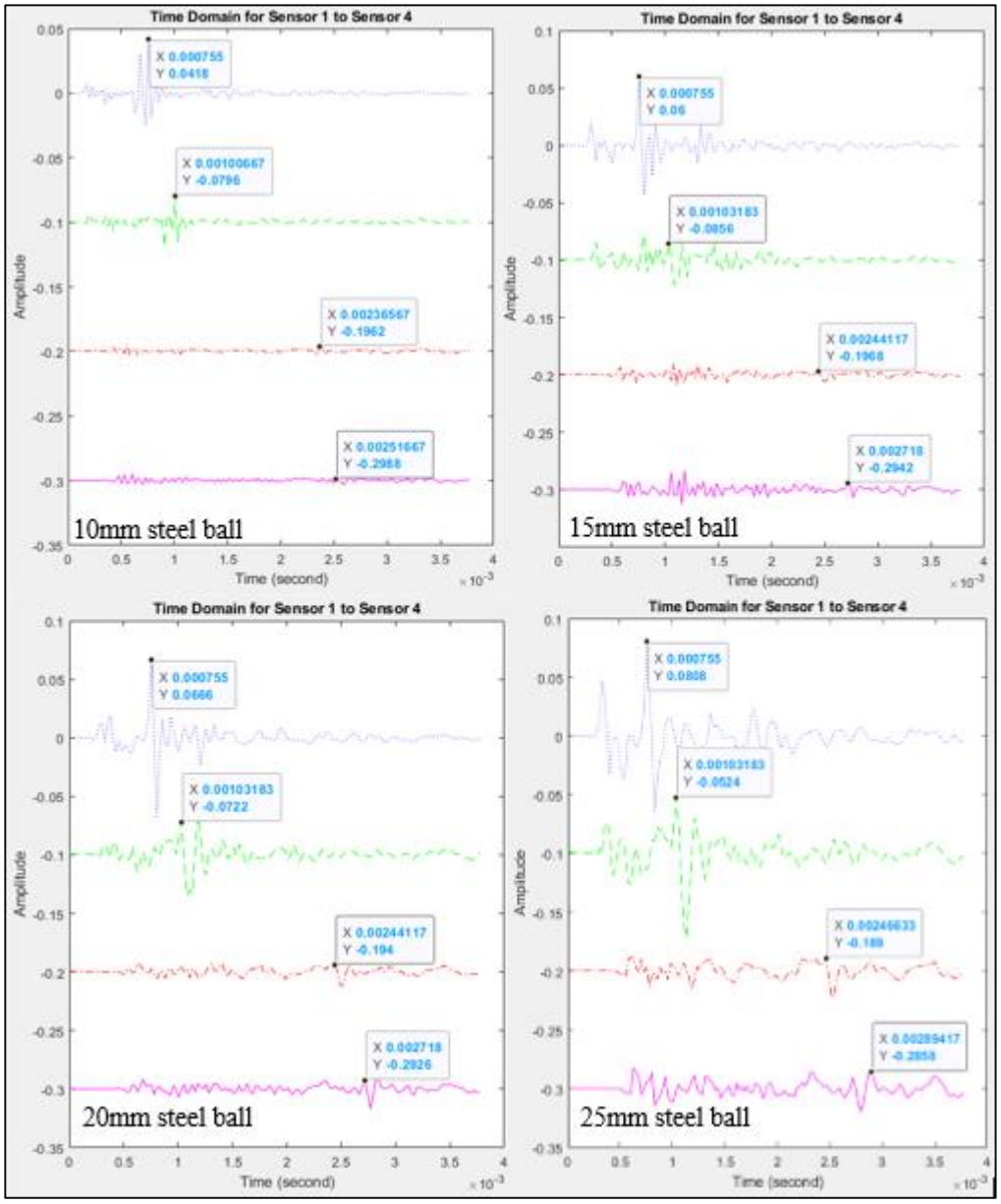

(d)

Appendix A-2: Time-domain Graph for 225 mm Depth of Delamination and (a) 100 mm, (b) 200 mm, (c) 300 mm, and (d) 400 mm Diameter of Delamination.

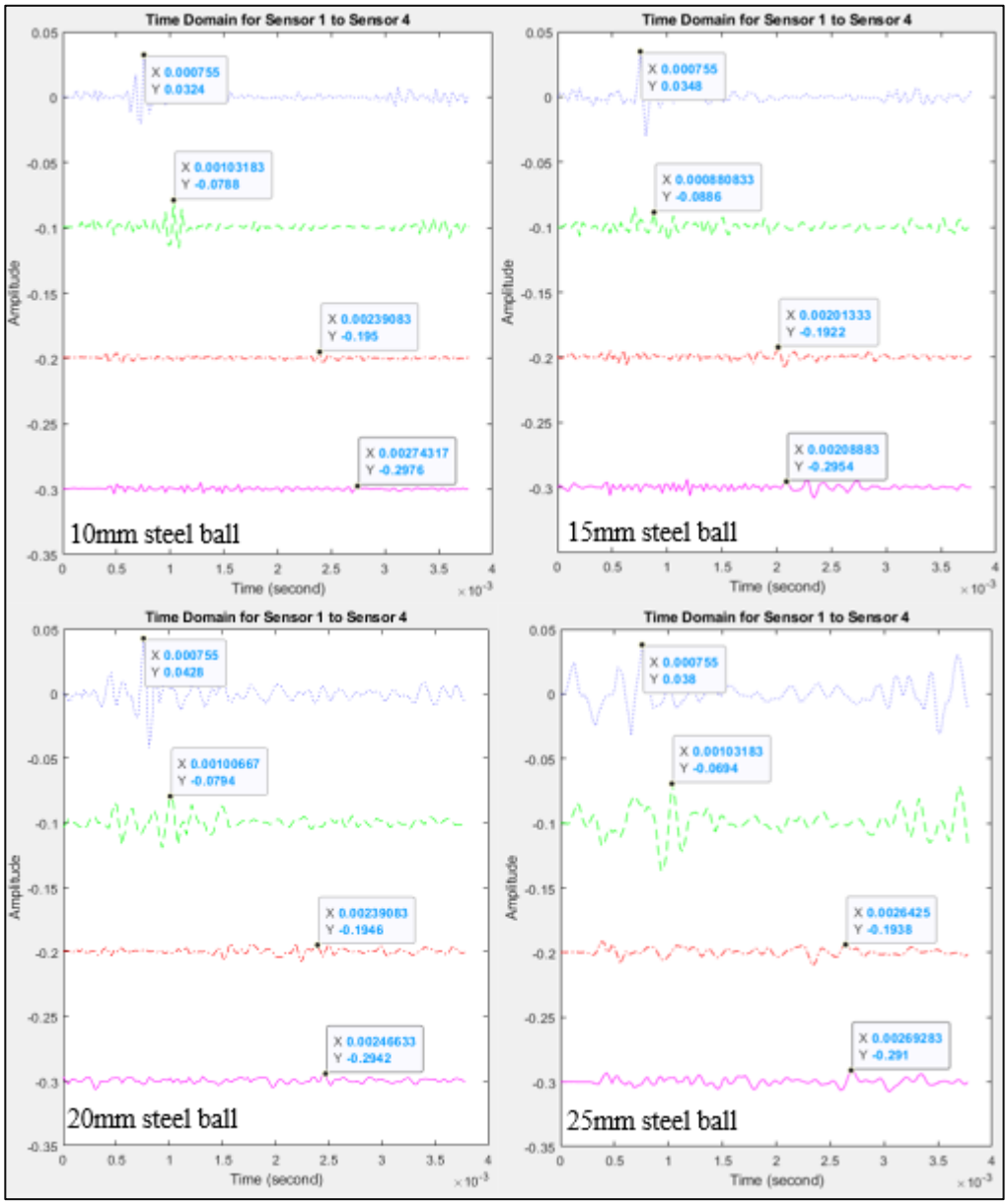
Time Domain for Sensor 1 to Sensor 4
X 0.000755
Y 0.0324
X 0.00103183
Y -0.0788
X 0.00239083
Y -0.195
X 0.00274317
Y -0.2976
10mm steel ball
Amplitude
Time (second)
Time Domain for Sensor 1 to Sensor 4
X 0.000755
Y 0.0348
X 0.000880833
Y -0.0886
X 0.00201333
Y -0.1922
X 0.00288883
Y -0.2954
15mm steel ball
Amplitude
Time (second)
Time Domain for Sensor 1 to Sensor 4
X 0.000755
Y 0.0428
X 0.00100667
Y -0.0794
X 0.00239083
Y -0.1946
X 0.00246633
Y -0.2942
20mm steel ball
Amplitude
Time (second)
Time Domain for Sensor 1 to Sensor 4
X 0.000755
Y 0.038
X 0.00103183
Y -0.0694
X 0.0026425
Y -0.1938
X 0.00269283
Y -0.291
25mm steel ball
Amplitude
Time (second)

(a)

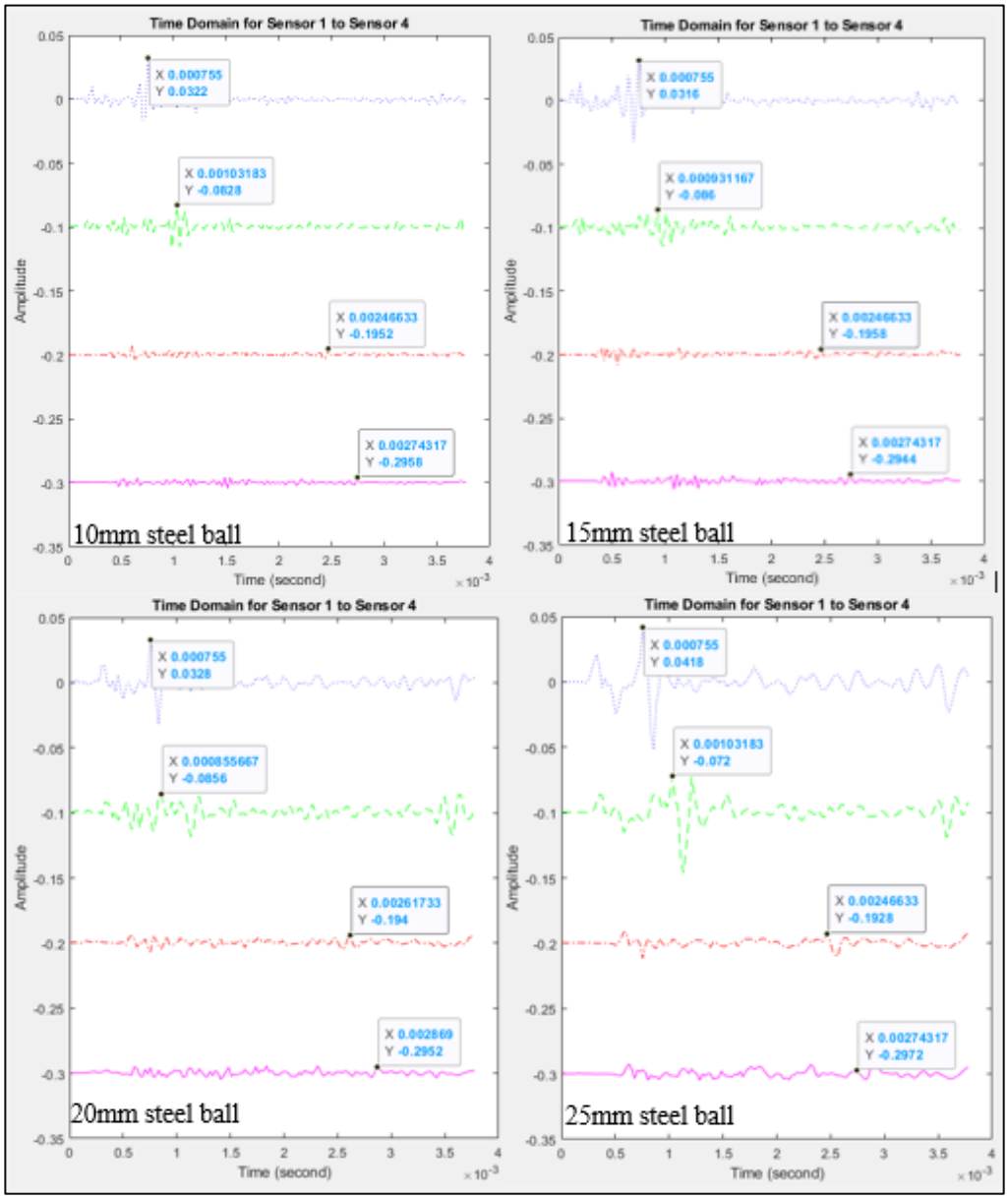
Time Domain for Sensor 1 to Sensor 4
X 0.000755
Y 0.0322
X 0.00103183
Y -0.0628
X 0.00246633
Y -0.1952
X 0.00274317
Y -0.2958
10mm steel ball
Amplitude
Time (second)
Time Domain for Sensor 1 to Sensor 4
X 0.000755
Y 0.0316
X 0.000931167
Y -0.066
X 0.00246633
Y -0.1958
X 0.00274317
Y -0.2944
15mm steel ball
Amplitude
Time (second)
Time Domain for Sensor 1 to Sensor 4
X 0.000755
Y 0.0328
X 0.000855667
Y -0.0856
X 0.00261733
Y -0.194
X 0.002869
Y -0.2952
20mm steel ball
Amplitude
Time (second)
Time Domain for Sensor 1 to Sensor 4
X 0.000755
Y 0.0418
X 0.00103183
Y -0.072
X 0.00246633
Y -0.1928
X 0.00274317
Y -0.2972
25mm steel ball
Amplitude
Time (second)

(b)

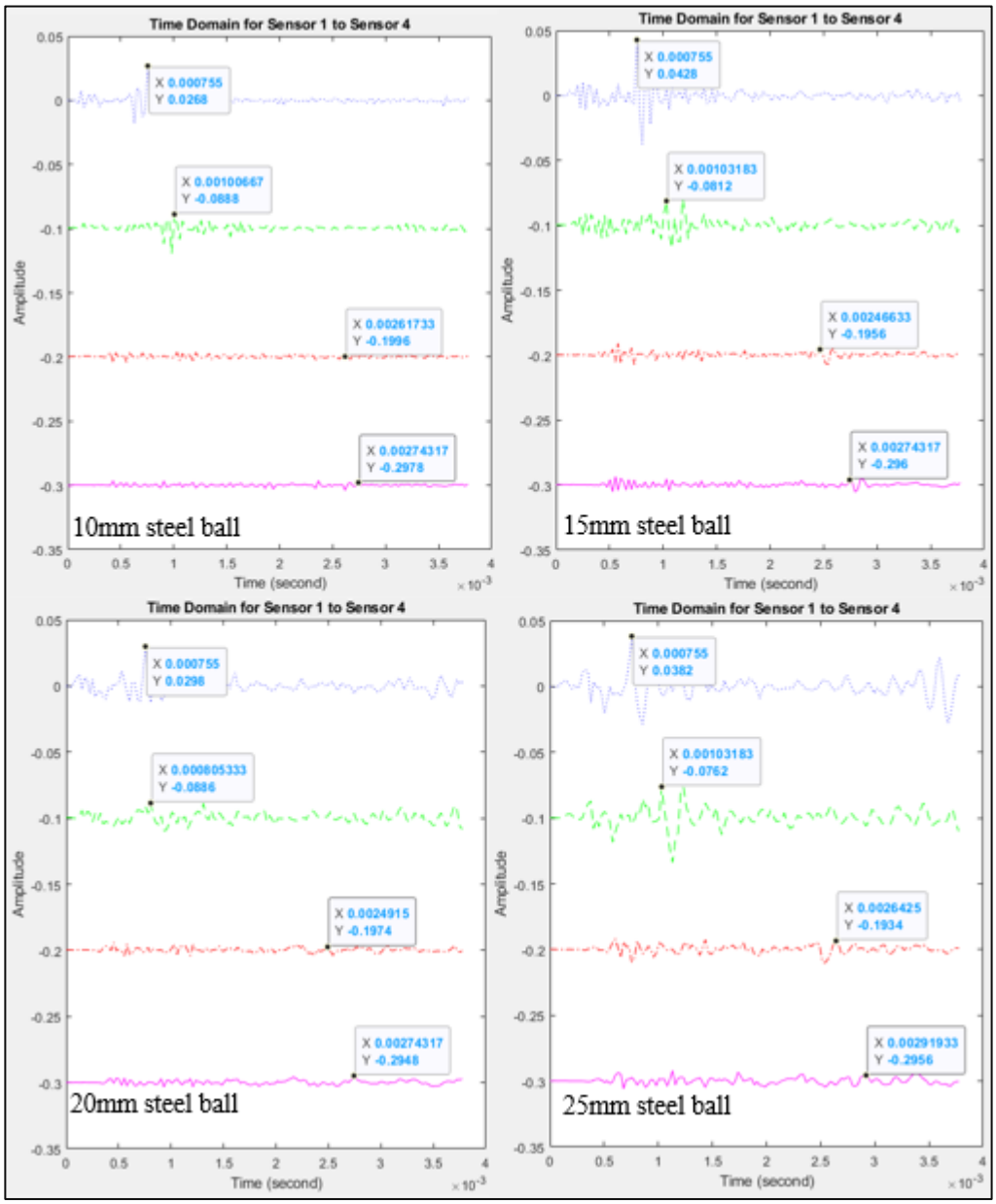
Time Domain for Sensor 1 to Sensor 4
X 0.000755
Y 0.0268
X 0.00100667
Y -0.0888
X 0.00261733
Y -0.1996
X 0.00274317
Y -0.2978
10mm steel ball
Amplitude
Time (second)
Time Domain for Sensor 1 to Sensor 4
X 0.000755
Y 0.0428
X 0.00103183
Y -0.0812
X 0.00246633
Y -0.1956
X 0.00274317
Y -0.296
15mm steel ball
Amplitude
Time (second)
Time Domain for Sensor 1 to Sensor 4
X 0.000755
Y 0.0298
X 0.000805333
Y -0.0886
X 0.0024915
Y -0.1974
X 0.00274317
Y -0.2948
20mm steel ball
Amplitude
Time (second)
Time Domain for Sensor 1 to Sensor 4
X 0.000755
Y 0.0382
X 0.00103183
Y -0.0762
X 0.0026425
Y -0.1934
X 0.00291933
Y -0.2956
25mm steel ball
Amplitude
Time (second)

(c)

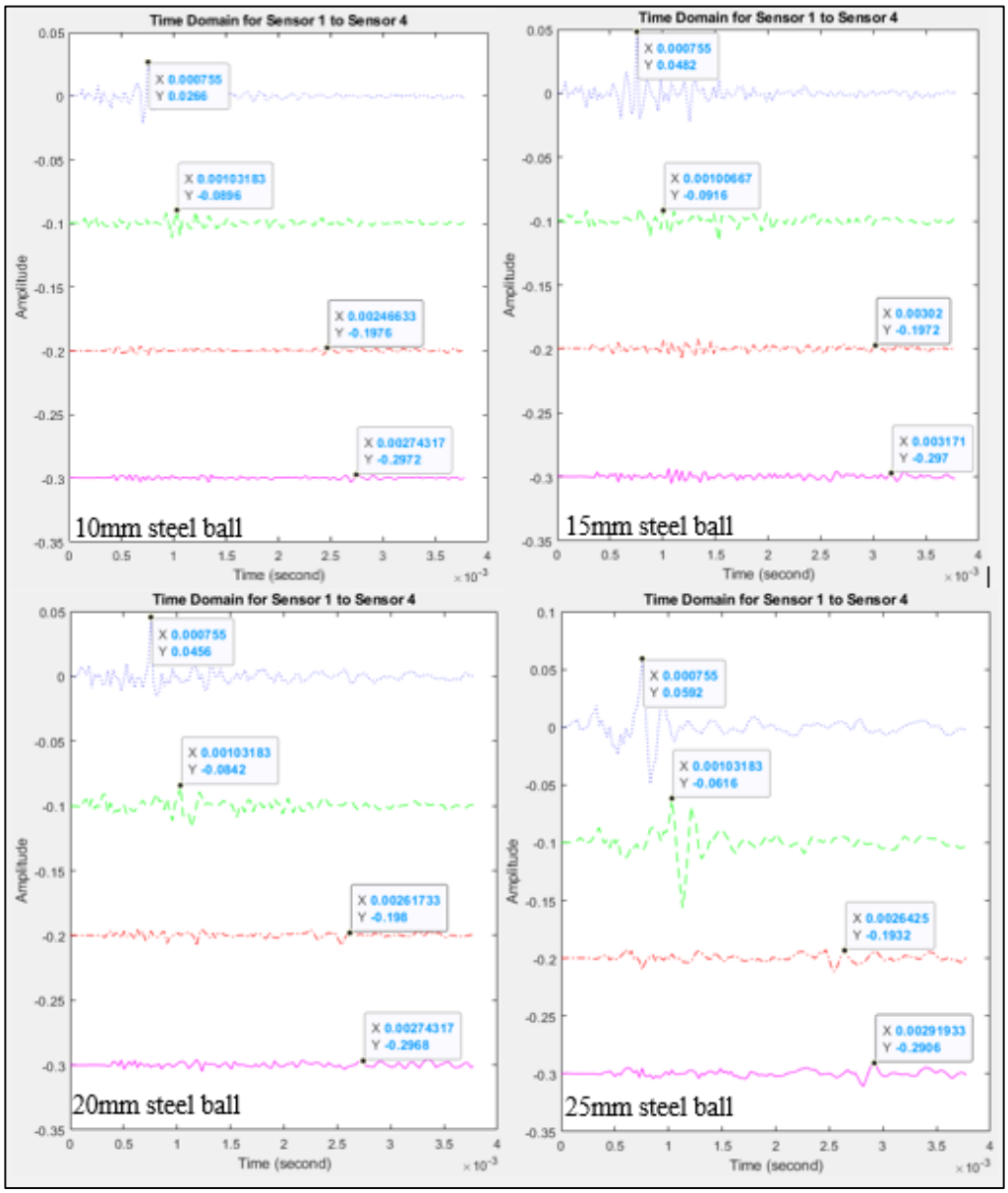
Time Domain for Sensor 1 to Sensor 4
X 0.000755
Y 0.0266
X 0.00103183
Y -0.0896
X 0.00246633
Y -0.1976
X 0.00274317
Y -0.2972
10mm steel ball
Amplitude
Time (second)
Time Domain for Sensor 1 to Sensor 4
X 0.000755
Y 0.0482
X 0.00100667
Y -0.0916
X 0.00302
Y -0.1972
X 0.003171
Y -0.297
15mm steel ball
Amplitude
Time (second)
Time Domain for Sensor 1 to Sensor 4
X 0.000755
Y 0.0456
X 0.00103183
Y -0.0842
X 0.00261733
Y -0.198
X 0.00274317
Y -0.2968
20mm steel ball
Amplitude
Time (second)
Time Domain for Sensor 1 to Sensor 4
X 0.000755
Y 0.0592
X 0.00103183
Y -0.0616
X 0.0026425
Y -0.1932
X 0.00291933
Y -0.2906
25mm steel ball
Amplitude
Time (second)

(d)

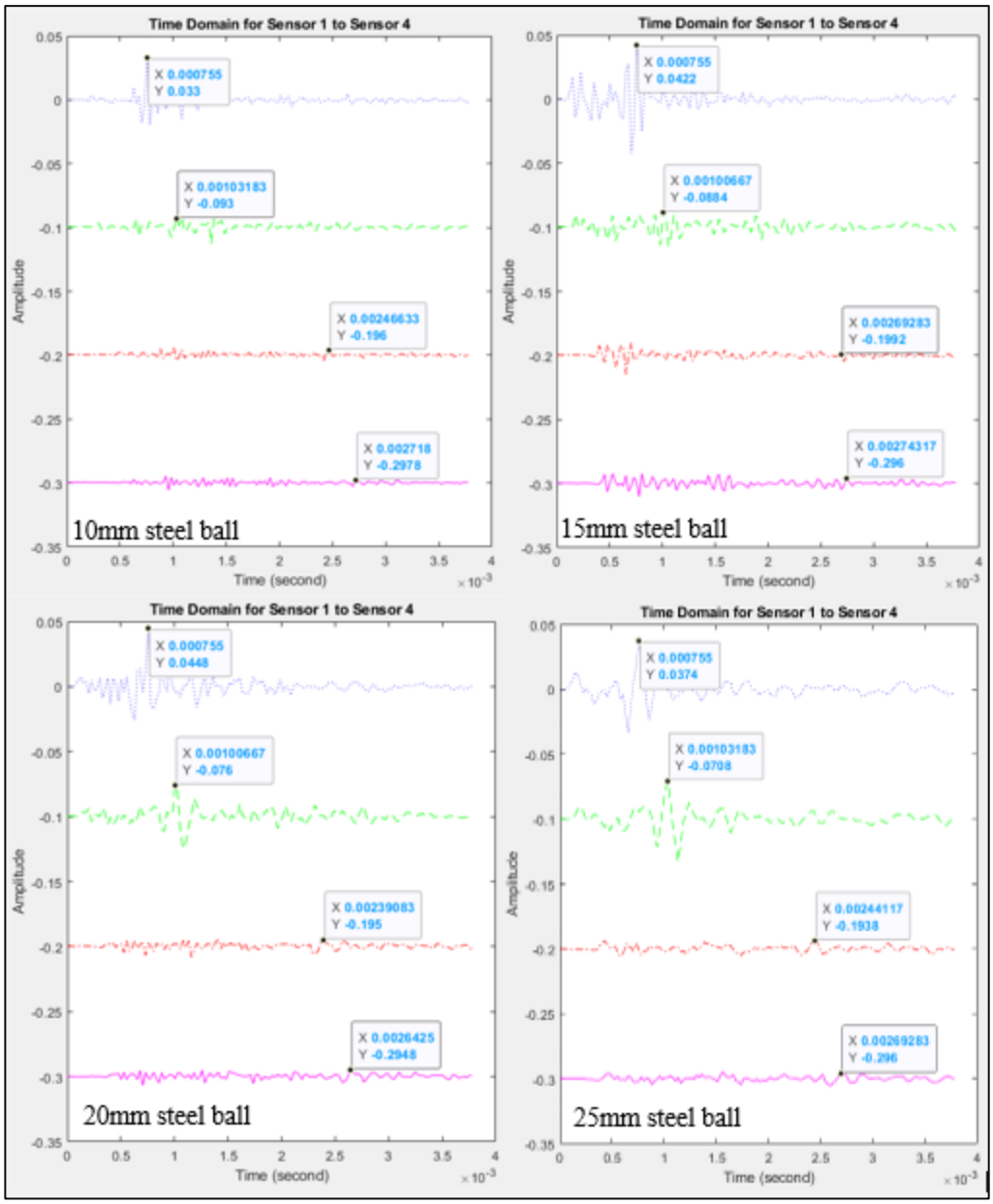

(e)

Appendix A-3: Time-domain Graph for 425 mm Depth of Delamination and (a) 100 mm, (b) 200 mm, (c) 300 mm, (d) 400 mm, and (e) 500 mm Diameter of Delamination.

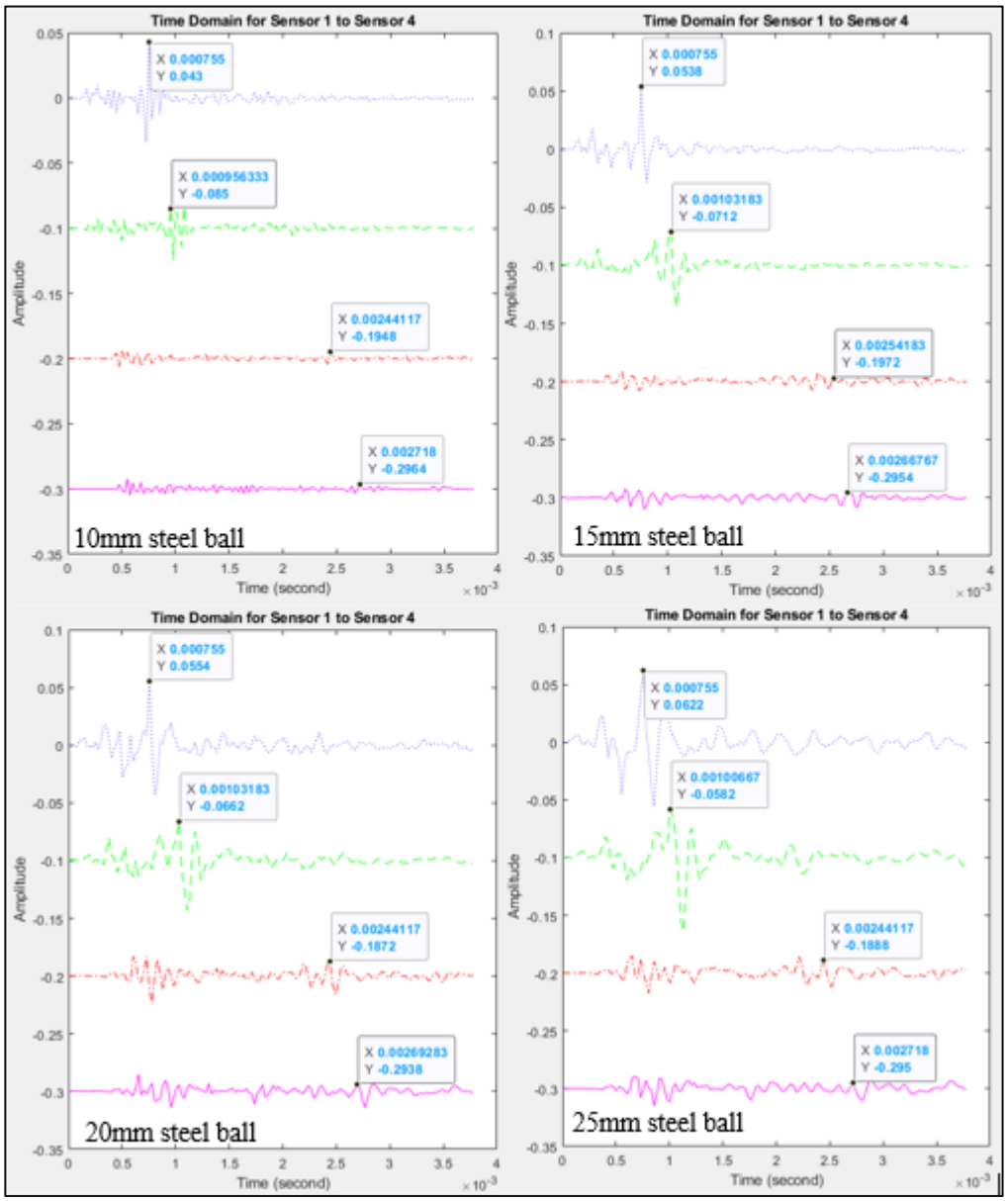
Time Domain for Sensor 1 to Sensor 4
X 0.000755
Y 0.043
X 0.000956333
Y -0.085
X 0.00244117
Y -0.1948
X 0.002718
Y -0.2964
10mm steel ball
Amplitude
Time (second)
Time Domain for Sensor 1 to Sensor 4
X 0.000755
Y 0.0538
X 0.00103183
Y -0.0712
X 0.00254183
Y -0.1972
X 0.00266767
Y -0.2954
15mm steel ball
Amplitude
Time (second)
Time Domain for Sensor 1 to Sensor 4
X 0.000755
Y 0.0554
X 0.00103183
Y -0.0662
X 0.00244117
Y -0.1872
X 0.00269283
Y -0.2938
20mm steel ball
Amplitude
Time (second)
Time Domain for Sensor 1 to Sensor 4
X 0.000755
Y 0.0622
X 0.00100667
Y -0.0582
X 0.00244117
Y -0.1888
X 0.002718
Y -0.295
25mm steel ball
Amplitude
Time (second)

(a)

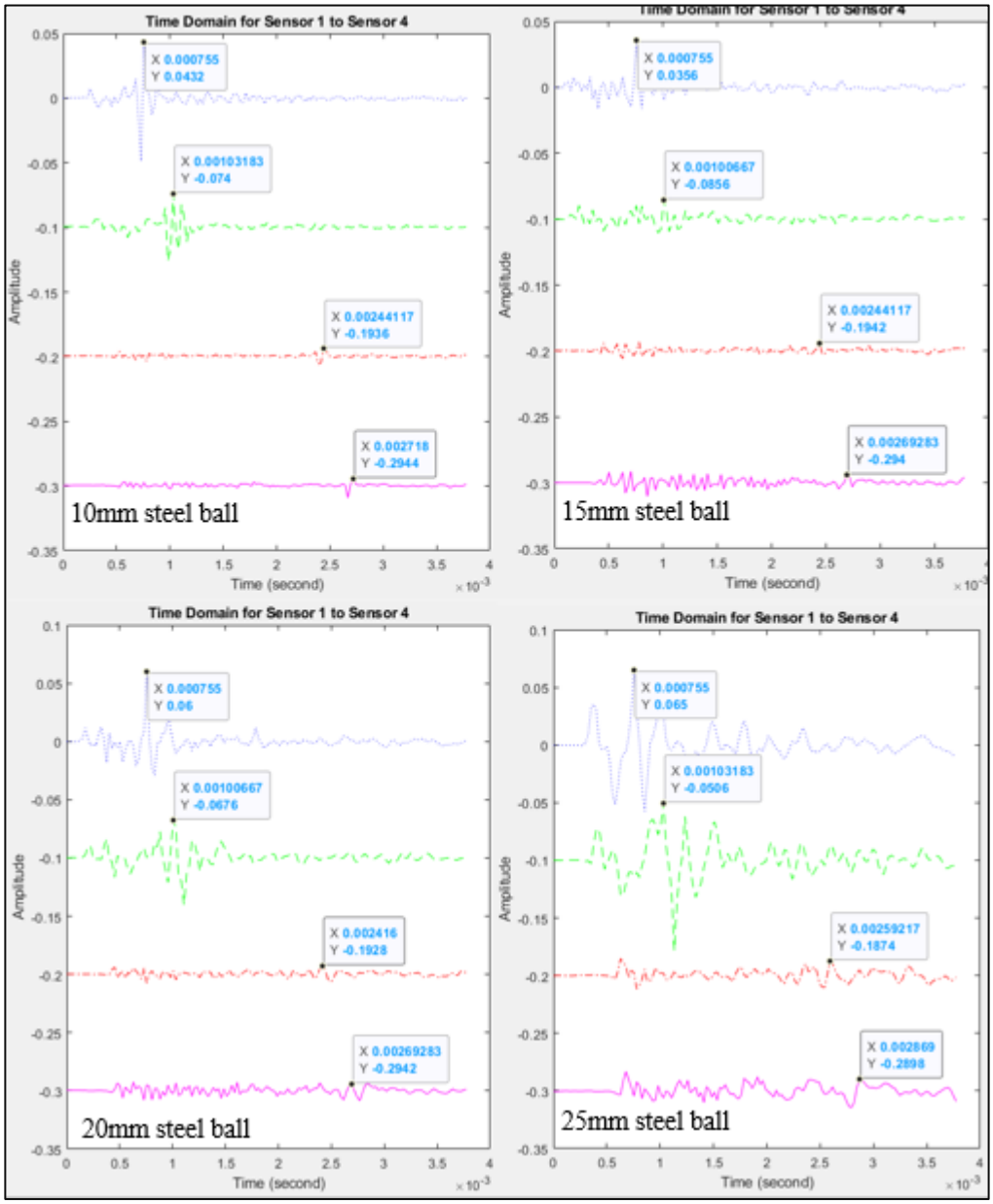
Time Domain for Sensor 1 to Sensor 4
X 0.000755
Y 0.0432
X 0.00103183
Y -0.074
X 0.00244117
Y -0.1936
X 0.002718
Y -0.2944
10mm steel ball
Amplitude
Time (second)
Time Domain for Sensor 1 to Sensor 4
X 0.000755
Y 0.0356
X 0.00100667
Y -0.0856
X 0.00244117
Y -0.1942
X 0.00269283
Y -0.294
15mm steel ball
Amplitude
Time (second)
Time Domain for Sensor 1 to Sensor 4
X 0.000755
Y 0.06
X 0.00100667
Y -0.0676
X 0.002416
Y -0.1928
X 0.00269283
Y -0.2942
20mm steel ball
Amplitude
Time (second)
Time Domain for Sensor 1 to Sensor 4
X 0.000755
Y 0.065
X 0.00103183
Y -0.0506
X 0.00259217
Y -0.1874
X 0.002869
Y -0.2898
25mm steel ball
Amplitude
Time (second)

(b)

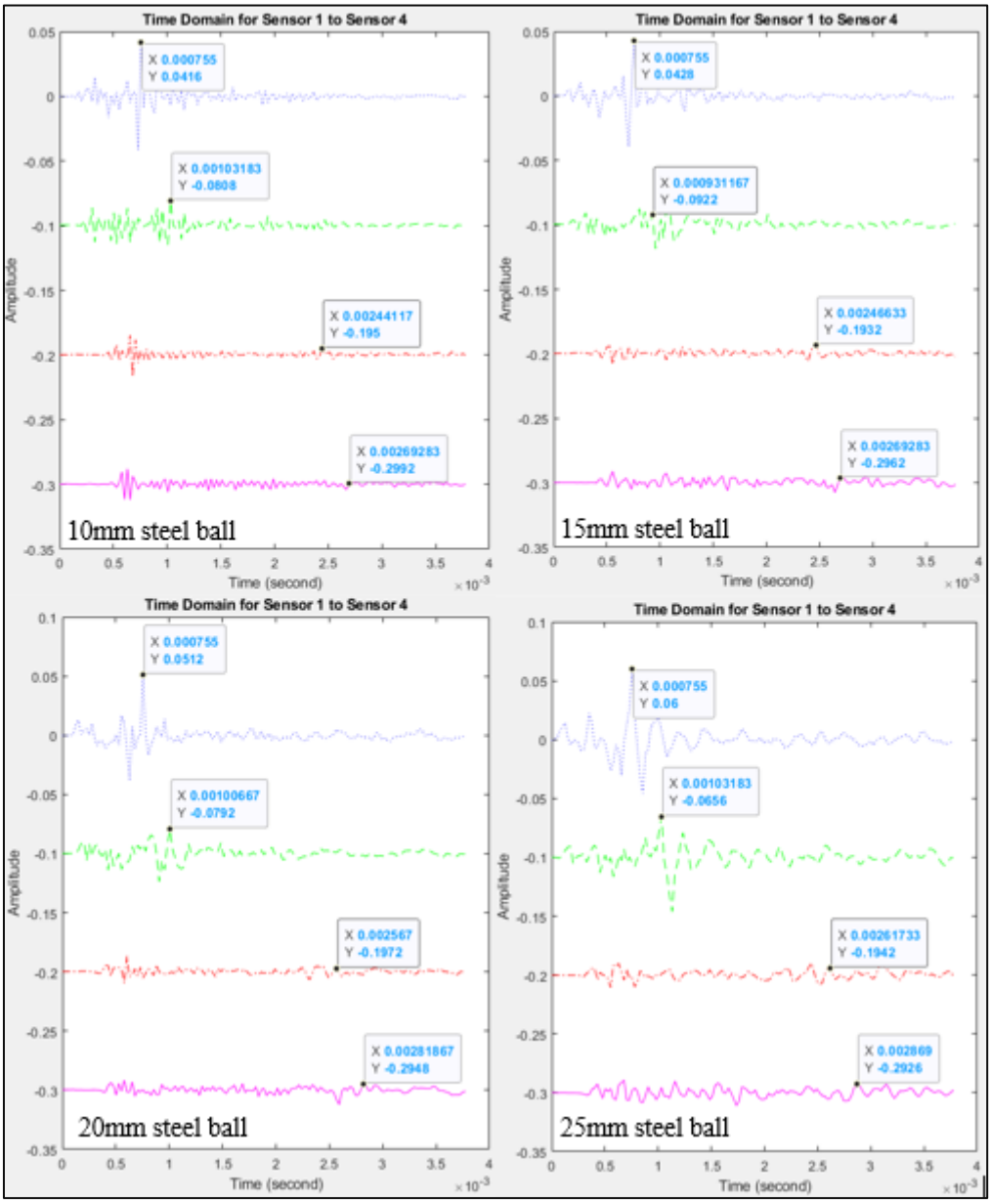
Time Domain for Sensor 1 to Sensor 4
X 0.000755
Y 0.0416
X 0.00103183
Y -0.0808
X 0.00244117
Y -0.195
X 0.00269283
Y -0.2992
10mm steel ball
Amplitude
Time (second)
Time Domain for Sensor 1 to Sensor 4
X 0.000755
Y 0.0428
X 0.000931167
Y -0.0922
X 0.00246633
Y -0.1932
X 0.00269283
Y -0.2962
15mm steel ball
Amplitude
Time (second)
Time Domain for Sensor 1 to Sensor 4
X 0.000755
Y 0.0512
X 0.00100667
Y -0.0792
X 0.002567
Y -0.1972
X 0.00281867
Y -0.2948
20mm steel ball
Amplitude
Time (second)
Time Domain for Sensor 1 to Sensor 4
X 0.000755
Y 0.06
X 0.00103183
Y -0.0656
X 0.00261733
Y -0.1942
X 0.002869
Y -0.2926
25mm steel ball
Amplitude
Time (second)

(c)

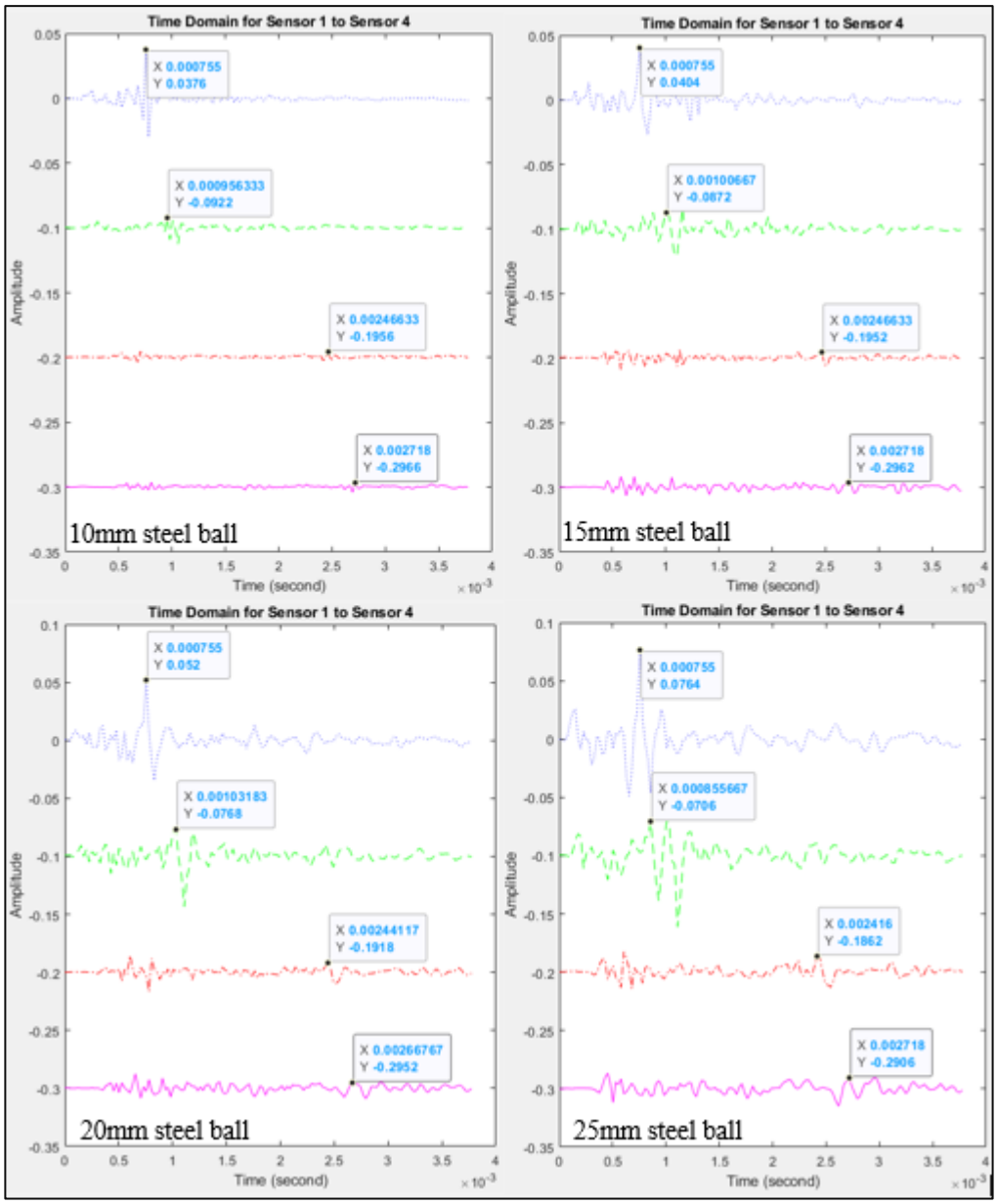

(d)

Appendix A-4: Time-domain Graph for 625 mm Depth of Delamination and (a) 100 mm, (b) 200 mm, (c) 300 mm, and (d) 400 mm Diameter of Delamination.

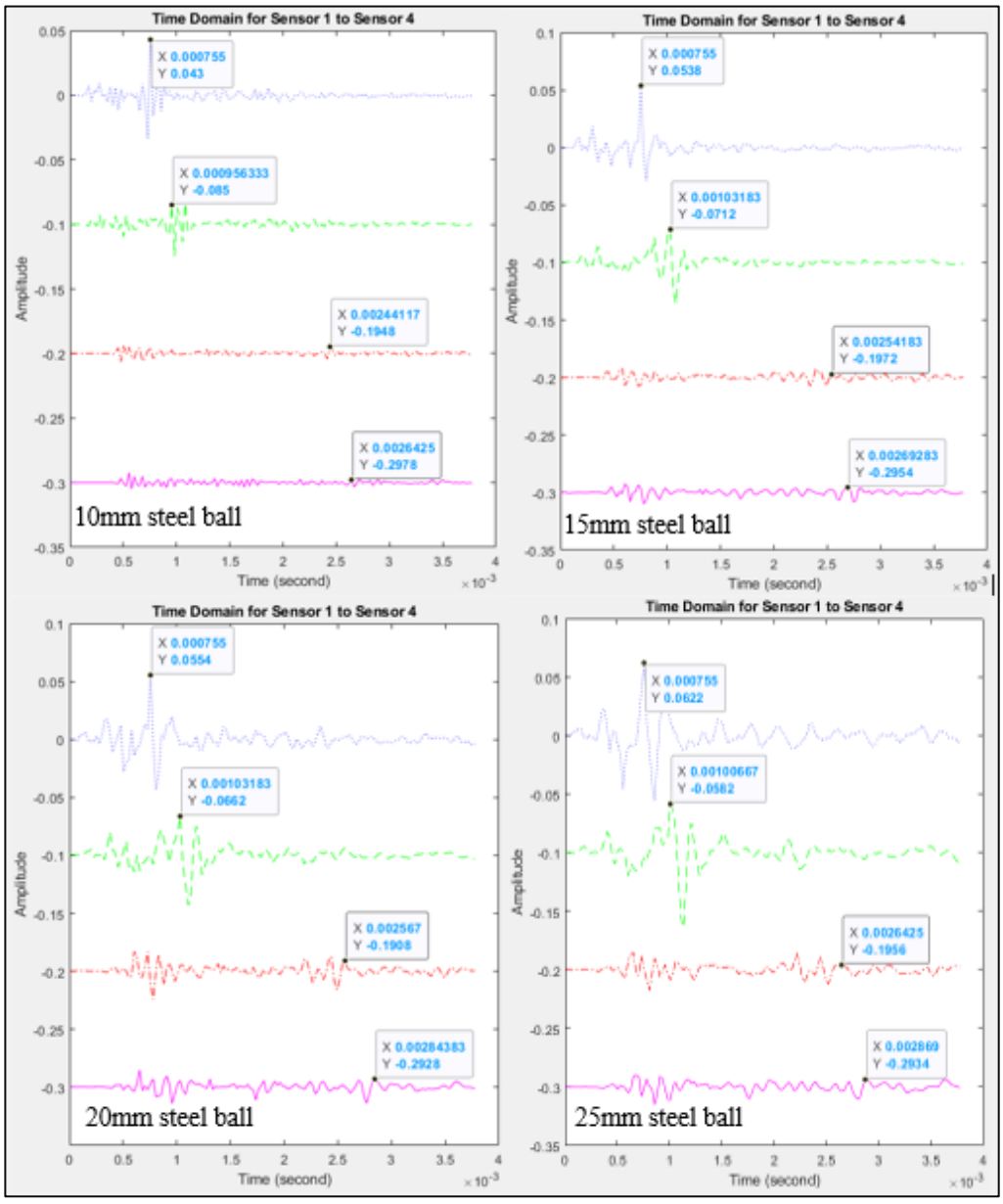
Time Domain for Sensor 1 to Sensor 4
X 0.000755
Y 0.043
X 0.000956333
Y -0.085
X 0.00244117
Y -0.1948
X 0.0026425
Y -0.2978
10mm steel ball
Amplitude
Time (second)
Time Domain for Sensor 1 to Sensor 4
X 0.000755
Y 0.0538
X 0.00103183
Y -0.0712
X 0.00254183
Y -0.1972
X 0.00269283
Y -0.2954
15mm steel ball
Amplitude
Time (second)
Time Domain for Sensor 1 to Sensor 4
X 0.000755
Y 0.0554
X 0.00103183
Y -0.0662
X 0.002567
Y -0.1908
X 0.00284383
Y -0.2928
20mm steel ball
Amplitude
Time (second)
Time Domain for Sensor 1 to Sensor 4
X 0.000755
Y 0.0622
X 0.00100667
Y -0.0582
X 0.0026425
Y -0.1956
X 0.002869
Y -0.2934
25mm steel ball
Amplitude
Time (second)

(a)

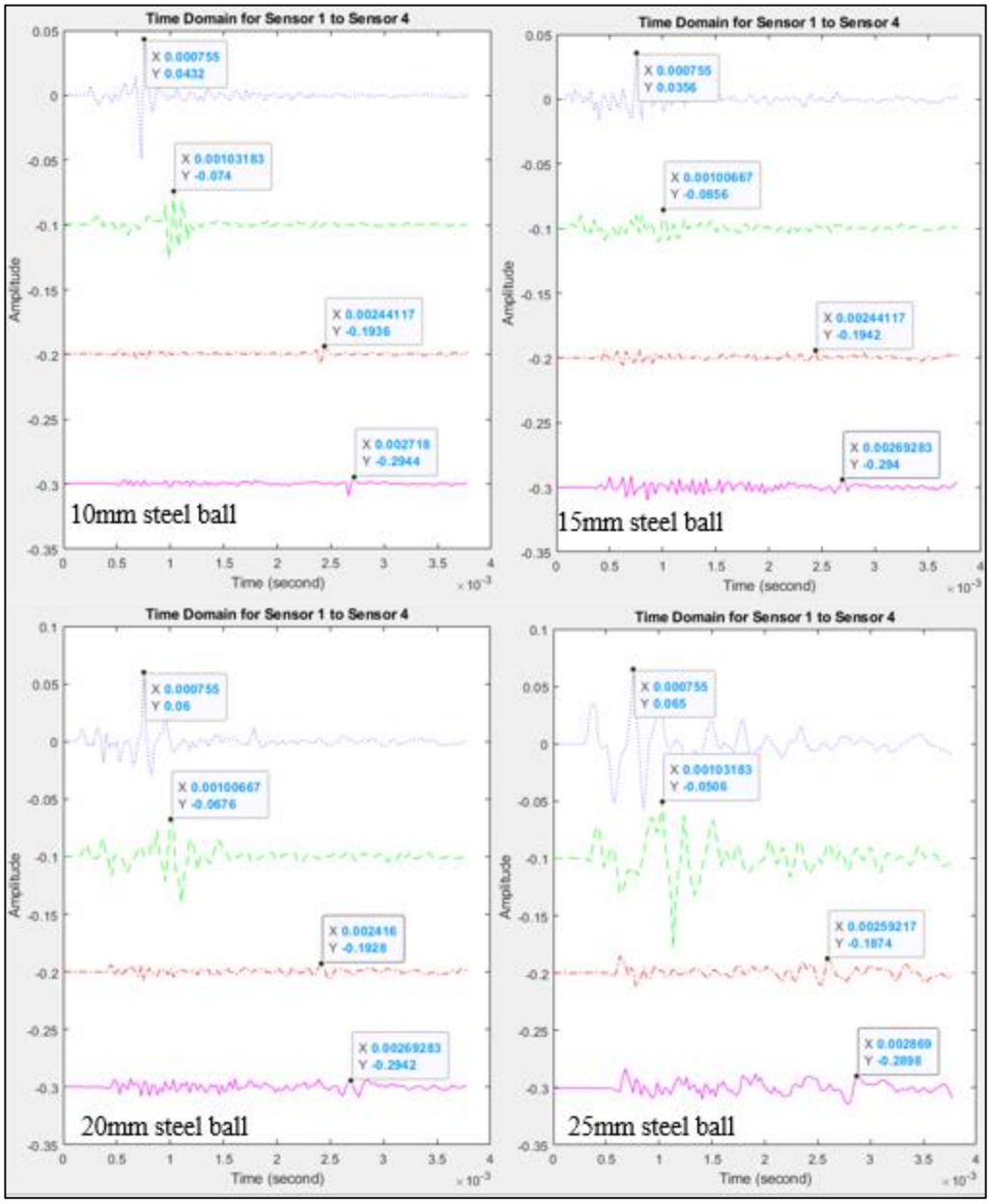
Time Domain for Sensor 1 to Sensor 4
X 0.000755
Y 0.0432
X 0.00103183
Y -0.074
X 0.00244117
Y -0.1936
X 0.002718
Y -0.2944
10mm steel ball
Amplitude
Time (second)
Time Domain for Sensor 1 to Sensor 4
X 0.000755
Y 0.0356
X 0.00100667
Y -0.0856
X 0.00244117
Y -0.1942
X 0.00269283
Y -0.294
15mm steel ball
Amplitude
Time (second)
Time Domain for Sensor 1 to Sensor 4
X 0.000755
Y 0.06
X 0.00100667
Y -0.0676
X 0.002416
Y -0.1928
X 0.00269283
Y -0.2942
20mm steel ball
Amplitude
Time (second)
Time Domain for Sensor 1 to Sensor 4
X 0.000755
Y 0.065
X 0.00103183
Y -0.0506
X 0.00259217
Y -0.1874
X 0.002869
Y -0.2898
25mm steel ball
Amplitude
Time (second)

(b)

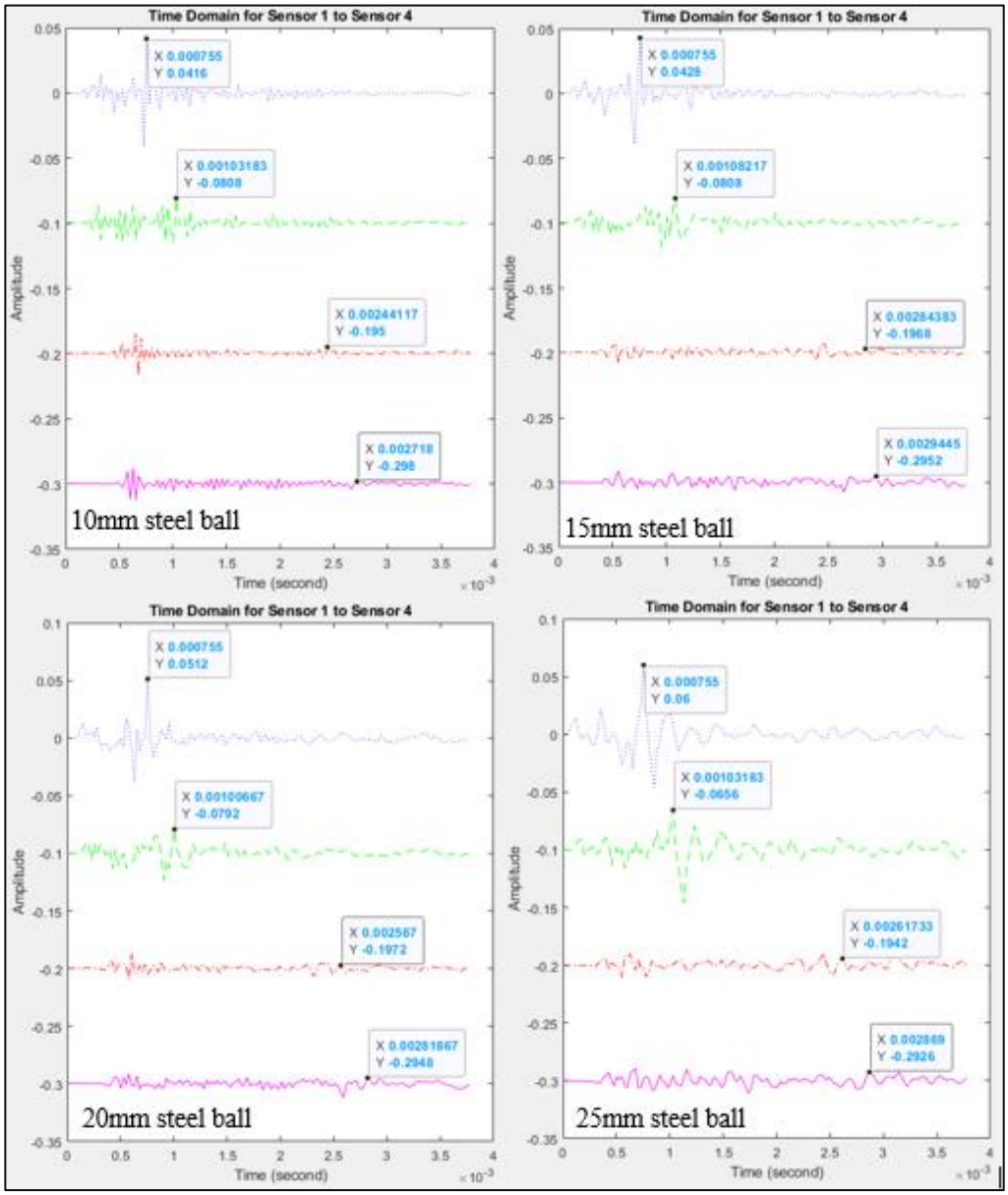
Time Domain for Sensor 1 to Sensor 4
X 0.000755
Y 0.0416
X 0.00103183
Y -0.0808
X 0.00244117
Y -0.195
X 0.002718
Y -0.298
10mm steel ball
Amplitude
Time (second)
Time Domain for Sensor 1 to Sensor 4
X 0.000755
Y 0.0428
X 0.00108217
Y -0.0808
X 0.00284383
Y -0.1968
X 0.0029445
Y -0.2952
15mm steel ball
Amplitude
Time (second)
Time Domain for Sensor 1 to Sensor 4
X 0.000755
Y 0.0512
X 0.00100667
Y -0.0792
X 0.002567
Y -0.1972
X 0.00281867
Y -0.2948
20mm steel ball
Amplitude
Time (second)
Time Domain for Sensor 1 to Sensor 4
X 0.000755
Y 0.06
X 0.00103183
Y -0.0656
X 0.00261733
Y -0.1942
X 0.002869
Y -0.2926
25mm steel ball
Amplitude
Time (second)

(c)

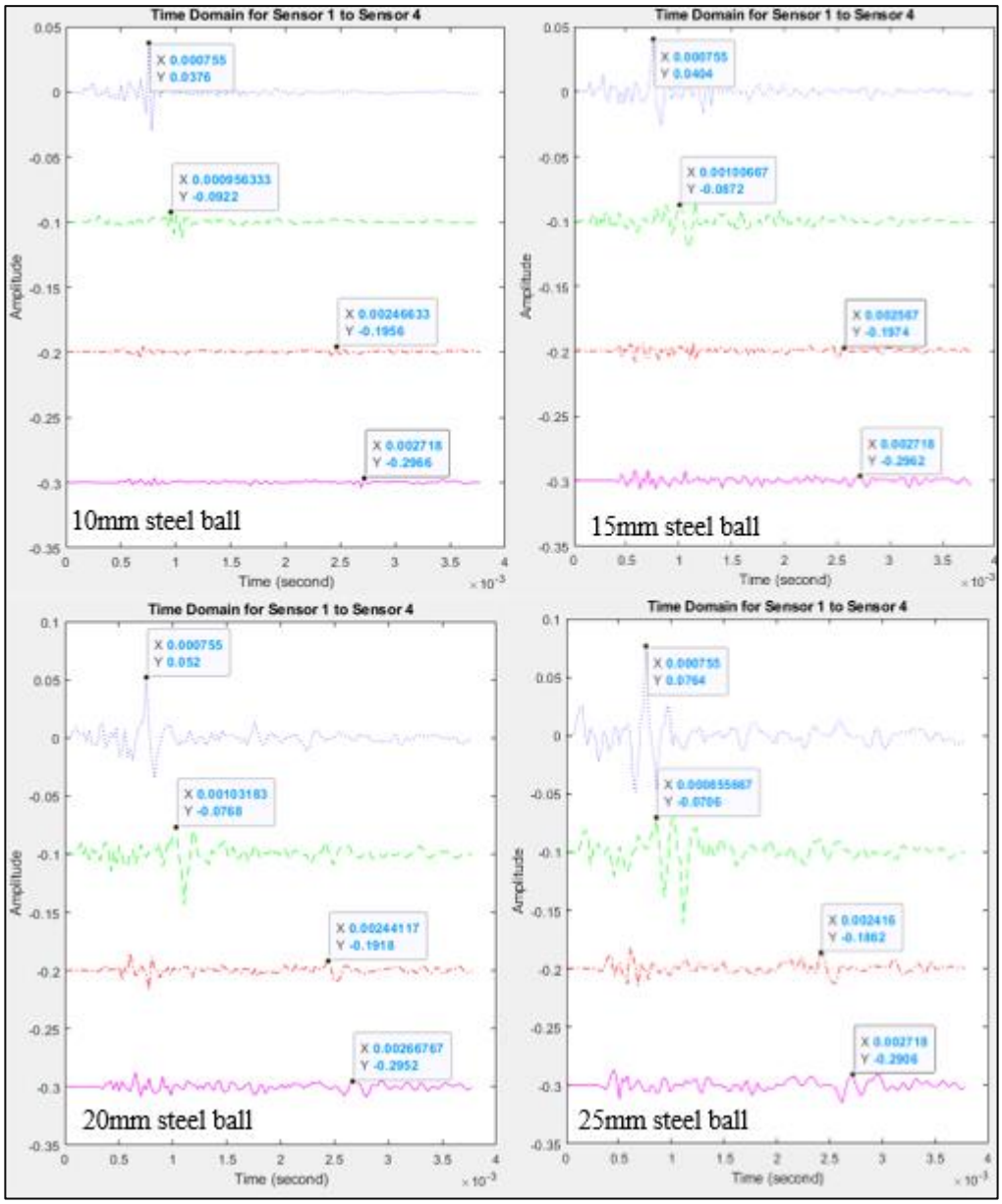

(d)

Appendix A-5: Time-domain Graph for 825 mm Depth of Delamination and (a) 100 mm, (b) 200 mm, (c) 300 mm, and (d) 400 mm Diameter of Delamination.

APPENDIX B: Power Spectrum (Section 4.5.1).

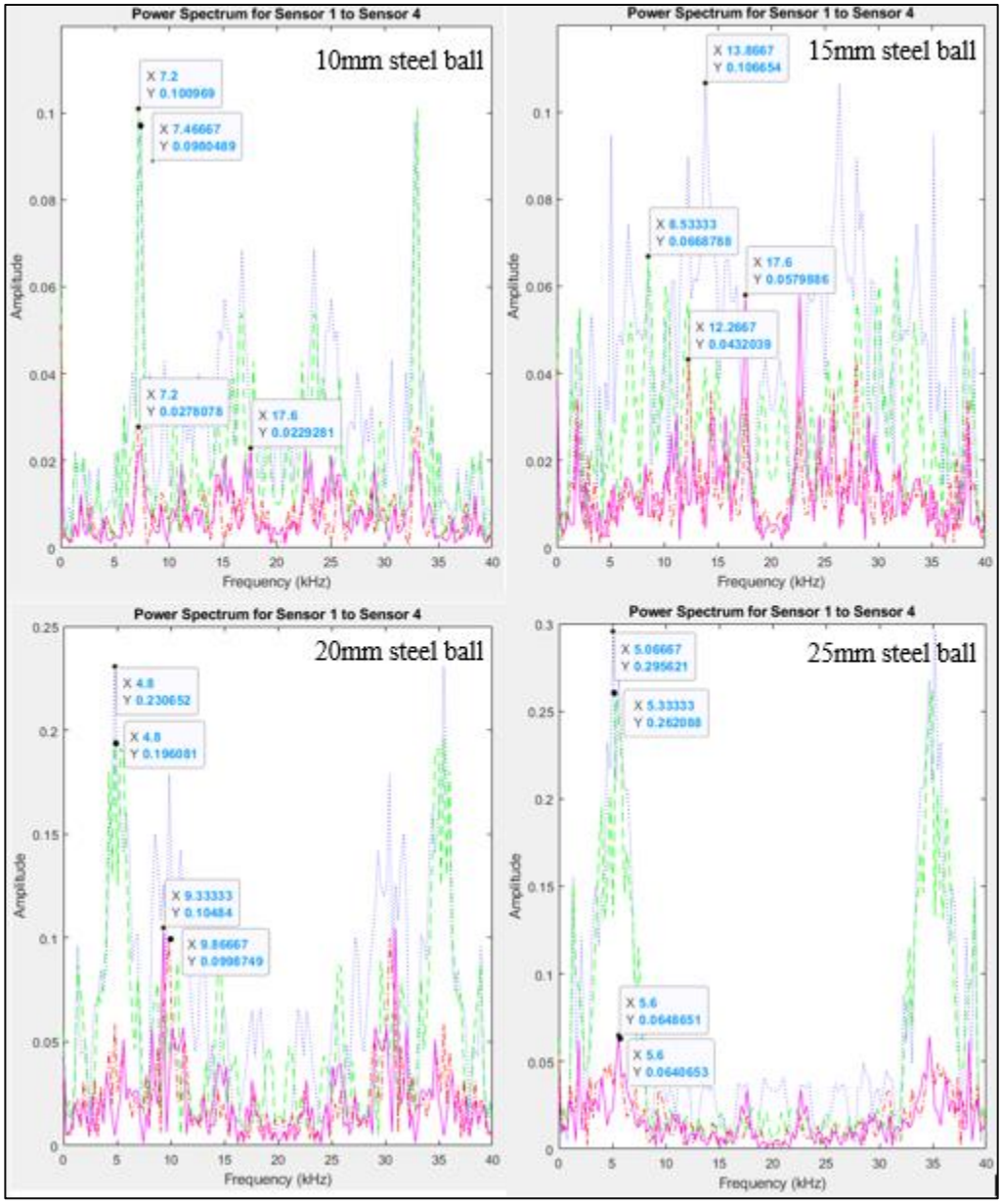

(a)

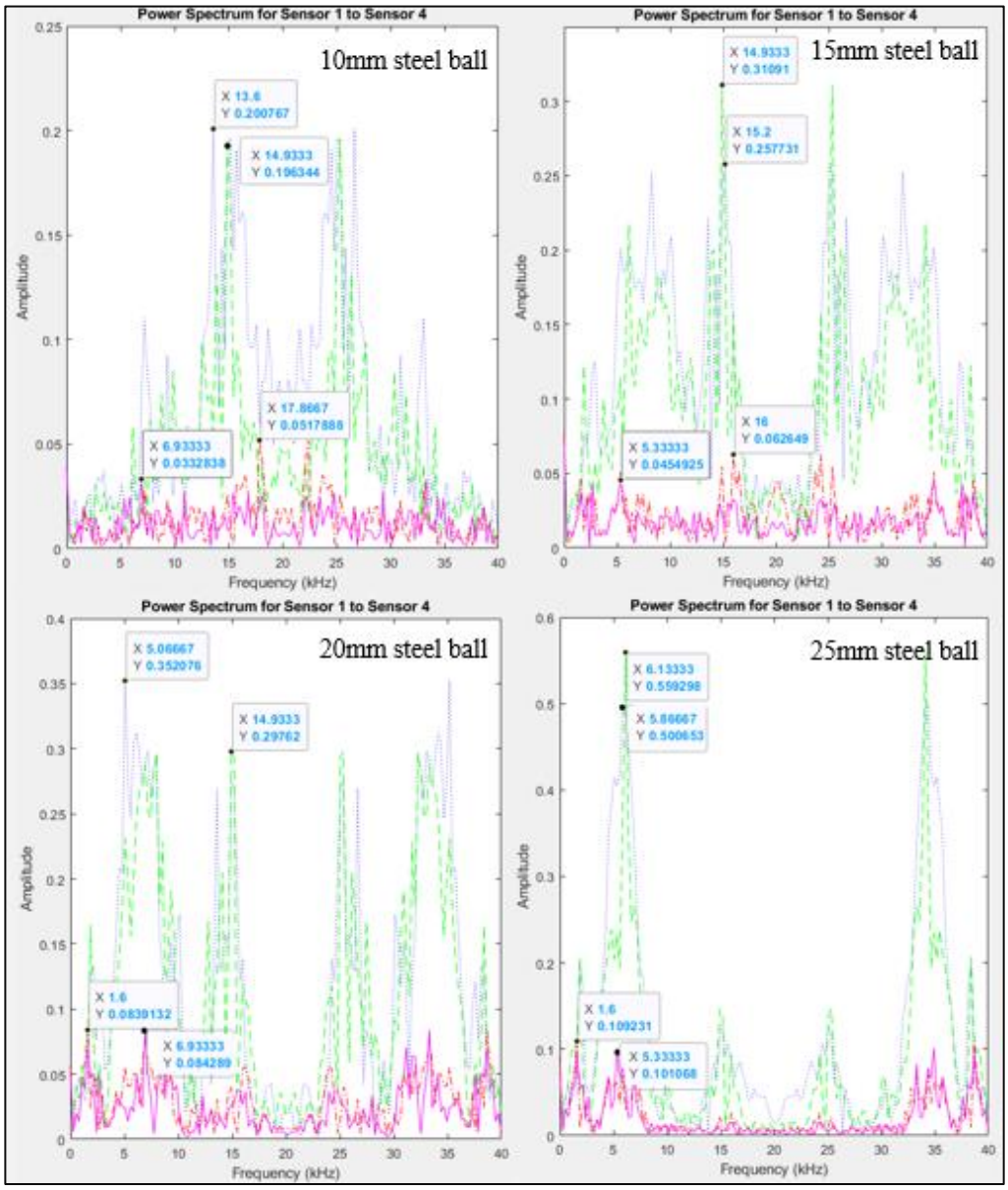
Power Spectrum for Sensor 1 to Sensor 4
10mm steel ball
X 13.6
Y 0.200767
X 14.9333
Y 0.196344
X 17.8667
Y 0.0517888
X 6.93333
Y 0.0332838
Power Spectrum for Sensor 1 to Sensor 4
15mm steel ball
X 14.9333
Y 0.31091
X 15.2
Y 0.257731
X 16
Y 0.062649
X 5.33333
Y 0.0454925
Power Spectrum for Sensor 1 to Sensor 4
20mm steel ball
X 5.06667
Y 0.352076
X 14.9333
Y 0.29762
X 1.6
Y 0.0839132
X 6.93333
Y 0.084289
Power Spectrum for Sensor 1 to Sensor 4
25mm steel ball
X 6.13333
Y 0.559298
X 5.86667
Y 0.500653
X 1.6
Y 0.109231
X 5.33333
Y 0.101068
Amplitude
Frequency (kHz)

(b)

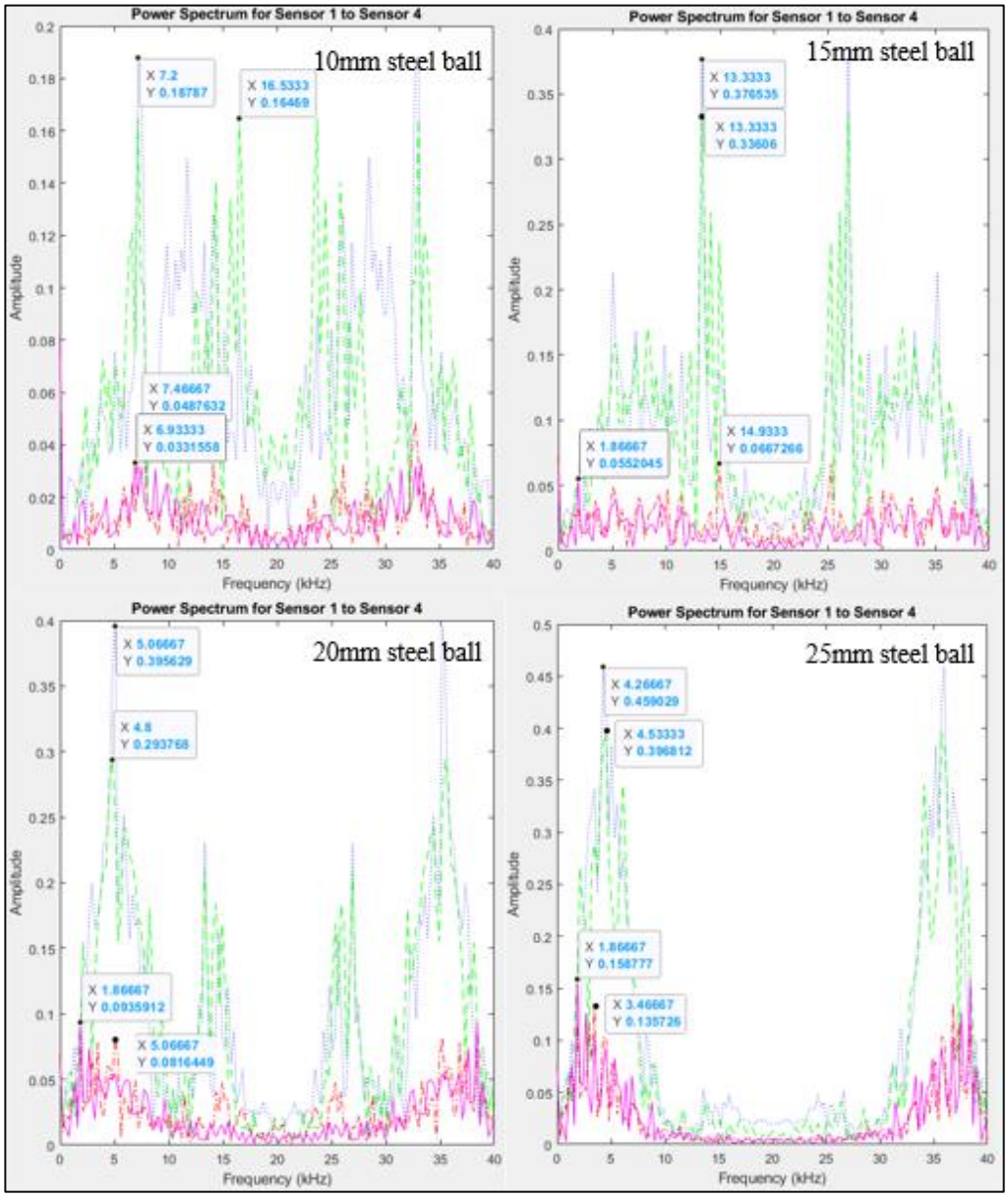
Power Spectrum for Sensor 1 to Sensor 4
10mm steel ball
X 7.2
Y 0.18787
X 16.5333
Y 0.16469
X 7.46667
Y 0.0487632
X 6.93333
Y 0.0331558
Power Spectrum for Sensor 1 to Sensor 4
15mm steel ball
X 13.3333
Y 0.376535
X 13.3333
Y 0.33606
X 1.86667
Y 0.0552045
X 14.9333
Y 0.0667266
Power Spectrum for Sensor 1 to Sensor 4
20mm steel ball
X 5.06667
Y 0.395629
X 4.8
Y 0.293768
X 1.86667
Y 0.0935912
X 5.06667
Y 0.0816449
Power Spectrum for Sensor 1 to Sensor 4
25mm steel ball
X 4.26667
Y 0.459029
X 4.53333
Y 0.396812
X 1.86667
Y 0.158777
X 3.46667
Y 0.135726
Amplitude
Frequency (kHz)

(c)

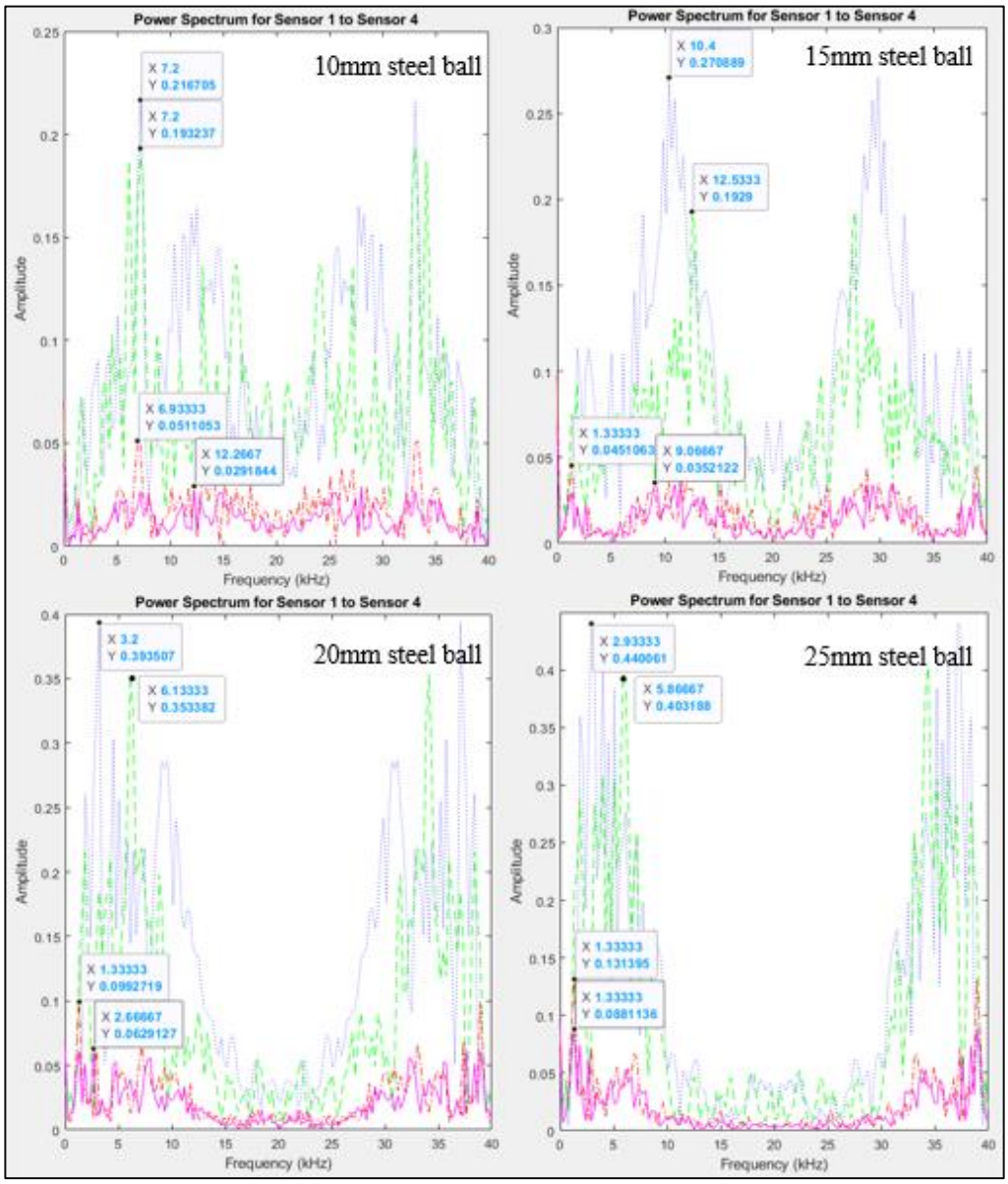
Power Spectrum for Sensor 1 to Sensor 4
10mm steel ball
X 7.2
Y 0.216705
X 7.2
Y 0.193237
X 6.93333
Y 0.0511053
X 12.2667
Y 0.0291844
Amplitude
Frequency (kHz)
Power Spectrum for Sensor 1 to Sensor 4
15mm steel ball
X 10.4
Y 0.270889
X 12.5333
Y 0.1929
X 1.33333
Y 0.0451063
X 9.06667
Y 0.0352122
Amplitude
Frequency (kHz)
Power Spectrum for Sensor 1 to Sensor 4
20mm steel ball
X 3.2
Y 0.393507
X 6.13333
Y 0.353382
X 1.33333
Y 0.0992719
X 2.66667
Y 0.0629127
Amplitude
Frequency (kHz)
Power Spectrum for Sensor 1 to Sensor 4
25mm steel ball
X 2.93333
Y 0.440061
X 5.86667
Y 0.403188
X 1.33333
Y 0.131395
X 1.33333
Y 0.0881136
Amplitude
Frequency (kHz)

(d)

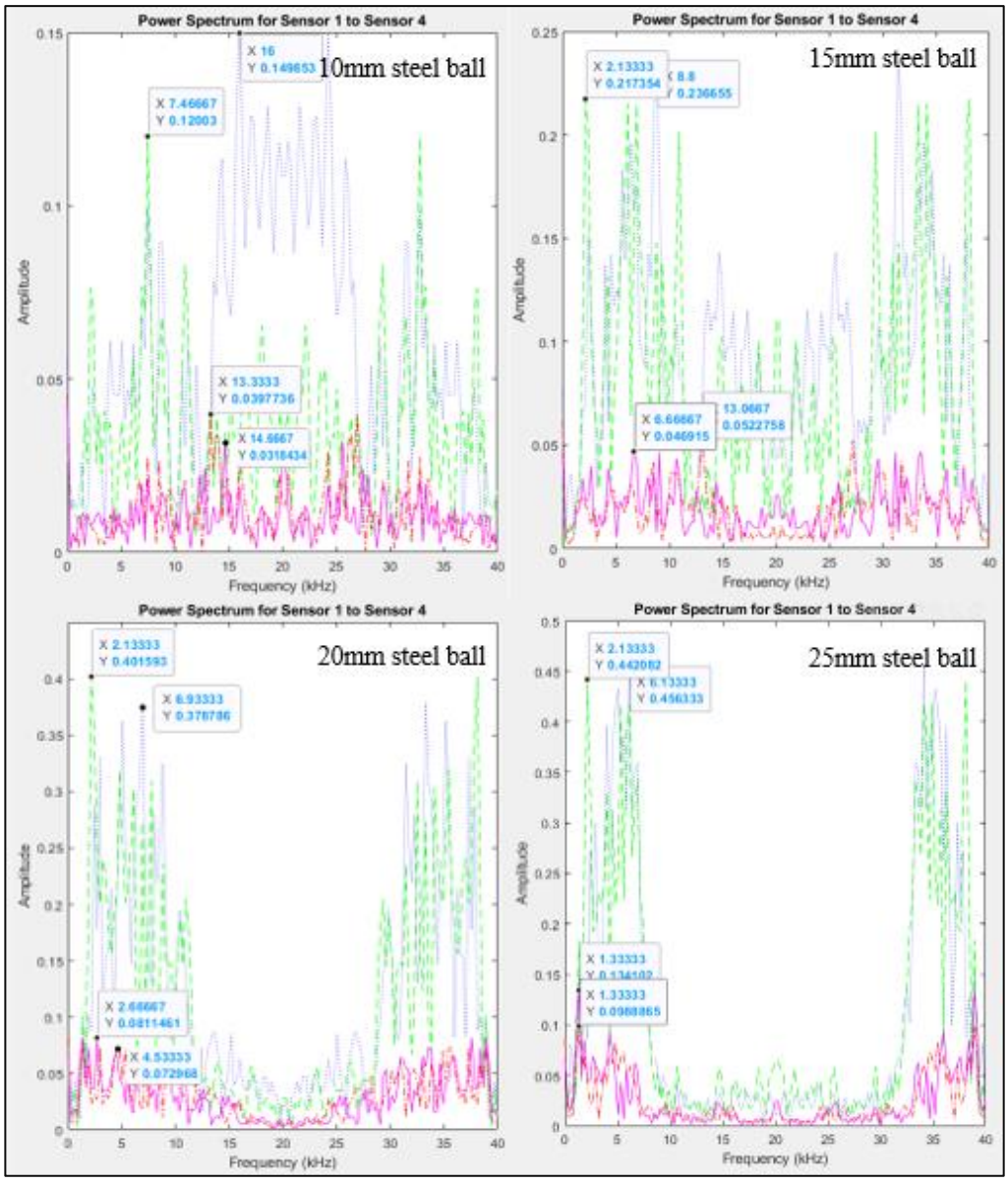

(e)

Appendix B-1: Power Spectrum for 25 mm Depth of Delamination and (a) 100 mm, (b) 200 mm, (c) 300 mm, (d) 400 mm, and (e) 500 mm Diameter of Delamination.

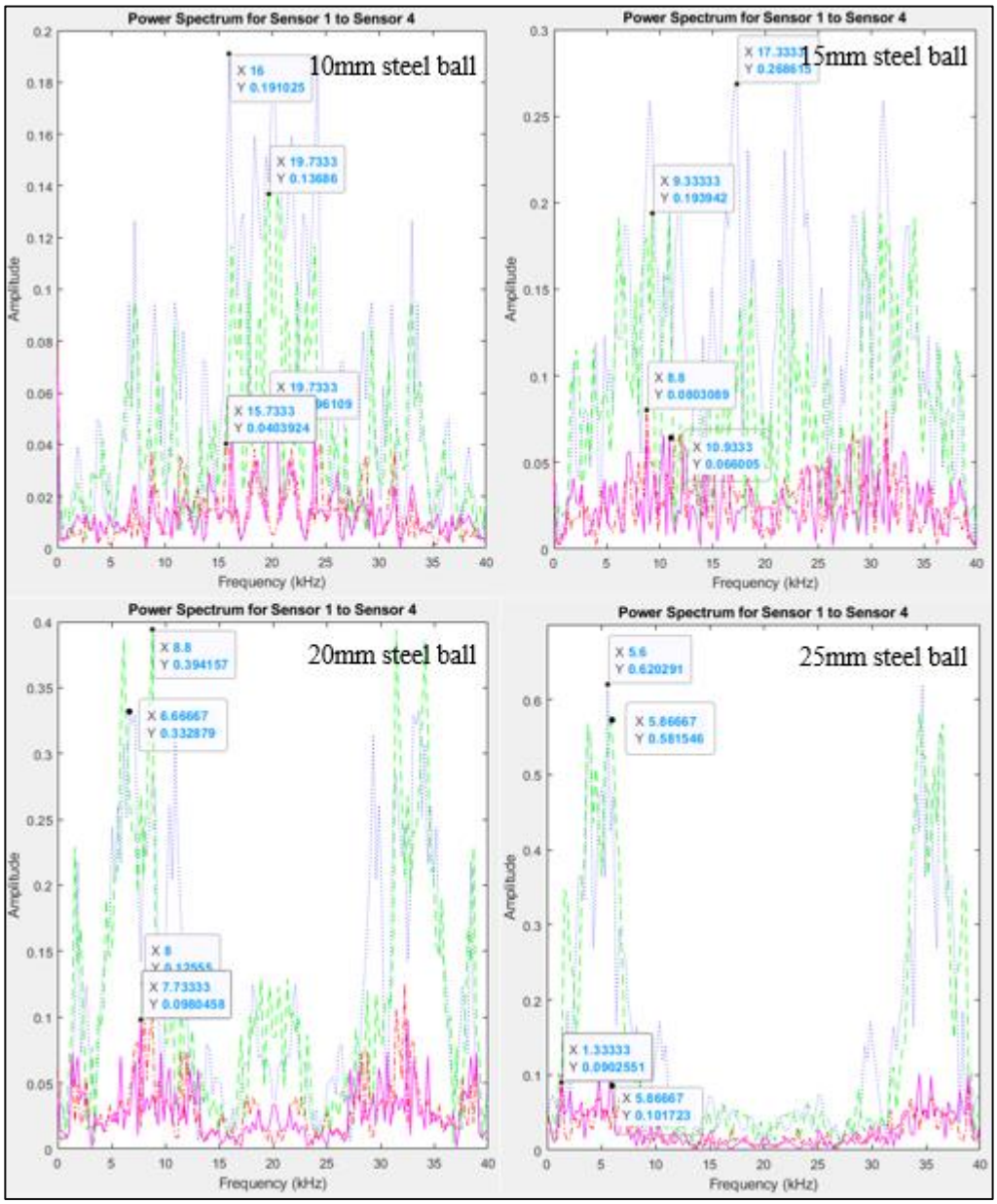
Power Spectrum for Sensor 1 to Sensor 4
10mm steel ball
X 16
Y 0.191025
X 19.7333
Y 0.13686
X 19.7333
X 15.7333
Y 0.0403924
Amplitude
Frequency (kHz)
Power Spectrum for Sensor 1 to Sensor 4
15mm steel ball
X 17.3333
Y 0.268615
X 9.33333
Y 0.193942
X 8.8
Y 0.0803089
X 10.9333
Y 0.066005
Amplitude
Frequency (kHz)
Power Spectrum for Sensor 1 to Sensor 4
20mm steel ball
X 8.8
Y 0.394157
X 6.66667
Y 0.332879
X 8
X 7.73333
Y 0.0980458
Amplitude
Frequency (kHz)
Power Spectrum for Sensor 1 to Sensor 4
25mm steel ball
X 5.6
Y 0.620291
X 5.86667
Y 0.581546
X 1.33333
Y 0.0902551
X 5.86667
Y 0.101723
Amplitude
Frequency (kHz)

(a)

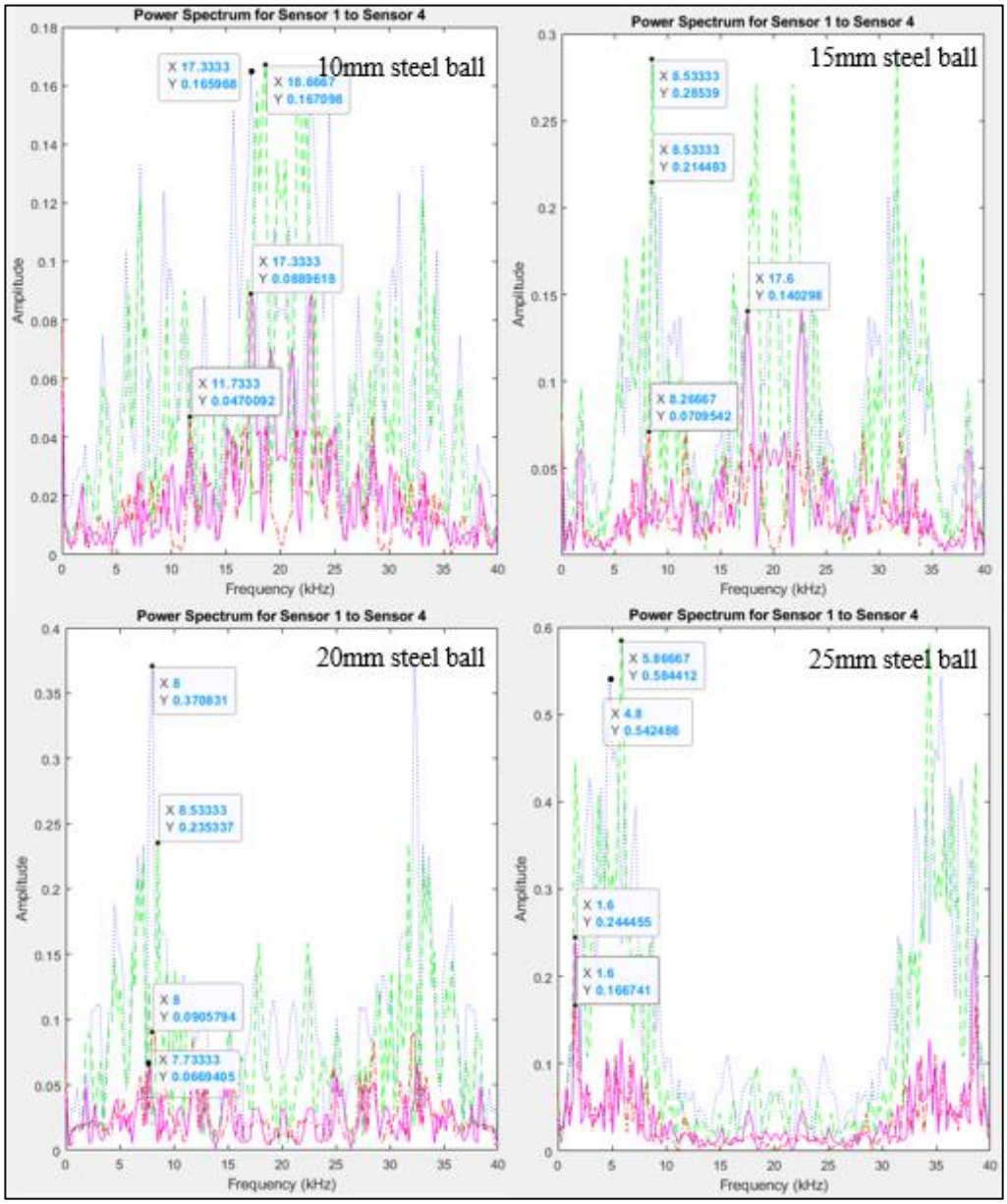
Power Spectrum for Sensor 1 to Sensor 4
10mm steel ball
X 17.3333
Y 0.165968
X 18.6667
Y 0.167096
X 17.3333
Y 0.0889618
X 11.7333
Y 0.0470092
Power Spectrum for Sensor 1 to Sensor 4
15mm steel ball
X 8.53333
Y 0.28539
X 8.53333
Y 0.214483
X 17.6
Y 0.140298
X 8.26667
Y 0.0709542
Power Spectrum for Sensor 1 to Sensor 4
20mm steel ball
X 8
Y 0.370831
X 8.53333
Y 0.235337
X 8
Y 0.0905794
X 7.73333
Y 0.0669405
Power Spectrum for Sensor 1 to Sensor 4
25mm steel ball
X 5.86667
Y 0.584412
X 4.8
Y 0.542486
X 1.6
Y 0.244455
X 1.6
Y 0.166741
Amplitude
Frequency (kHz)

(b)

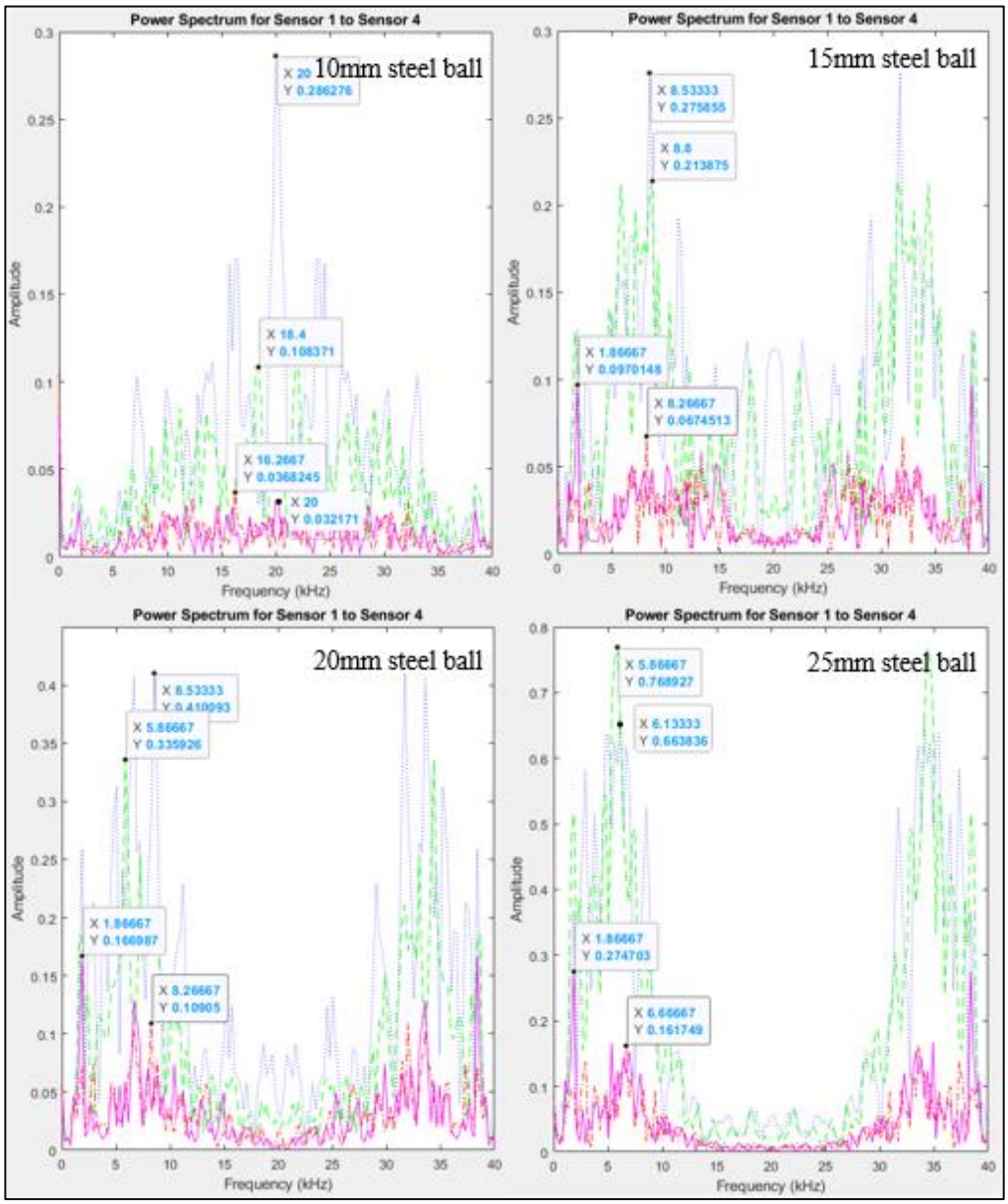
Power Spectrum for Sensor 1 to Sensor 4
10mm steel ball
X 20
Y 0.286276
X 18.4
Y 0.108371
X 16.2667
Y 0.0368245
X 20
Y 0.032171
Power Spectrum for Sensor 1 to Sensor 4
15mm steel ball
X 8.53333
Y 0.275855
X 8.8
Y 0.213875
X 1.86667
Y 0.0970148
X 8.26667
Y 0.0674513
Power Spectrum for Sensor 1 to Sensor 4
20mm steel ball
X 8.53333
Y 0.410093
X 5.86667
Y 0.335926
X 1.86667
Y 0.166987
X 8.26667
Y 0.10905
Power Spectrum for Sensor 1 to Sensor 4
25mm steel ball
X 5.86667
Y 0.768927
X 6.13333
Y 0.663836
X 1.86667
Y 0.274703
X 6.66667
Y 0.161749
Amplitude
Frequency (kHz)

(c)

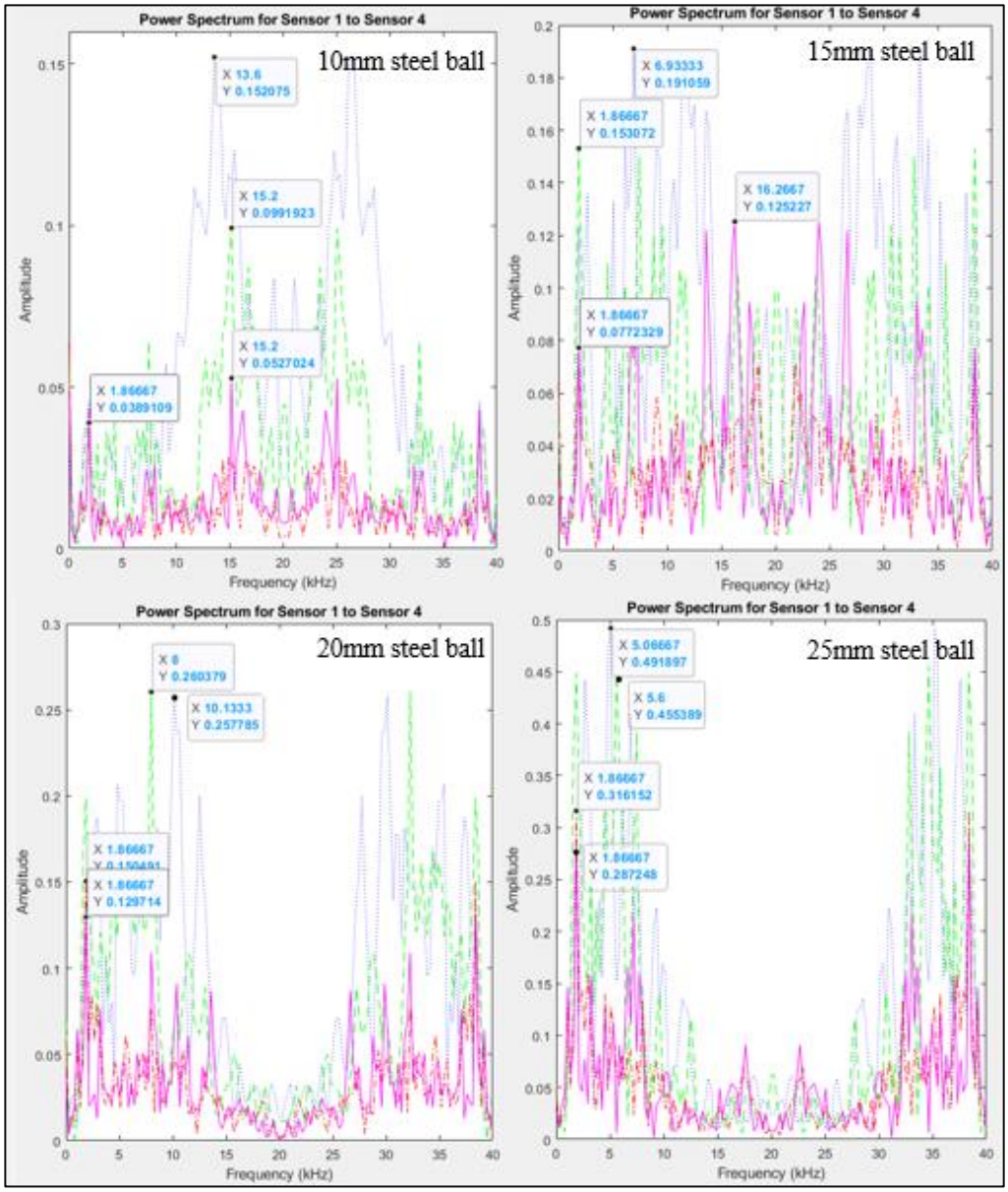

(d)

Appendix B-2: Power Spectrum for 225 mm Depth of Delamination and (a) 100 mm, (b) 200 mm, (c) 300 mm, and (d) 400 mm Diameter of Delamination.

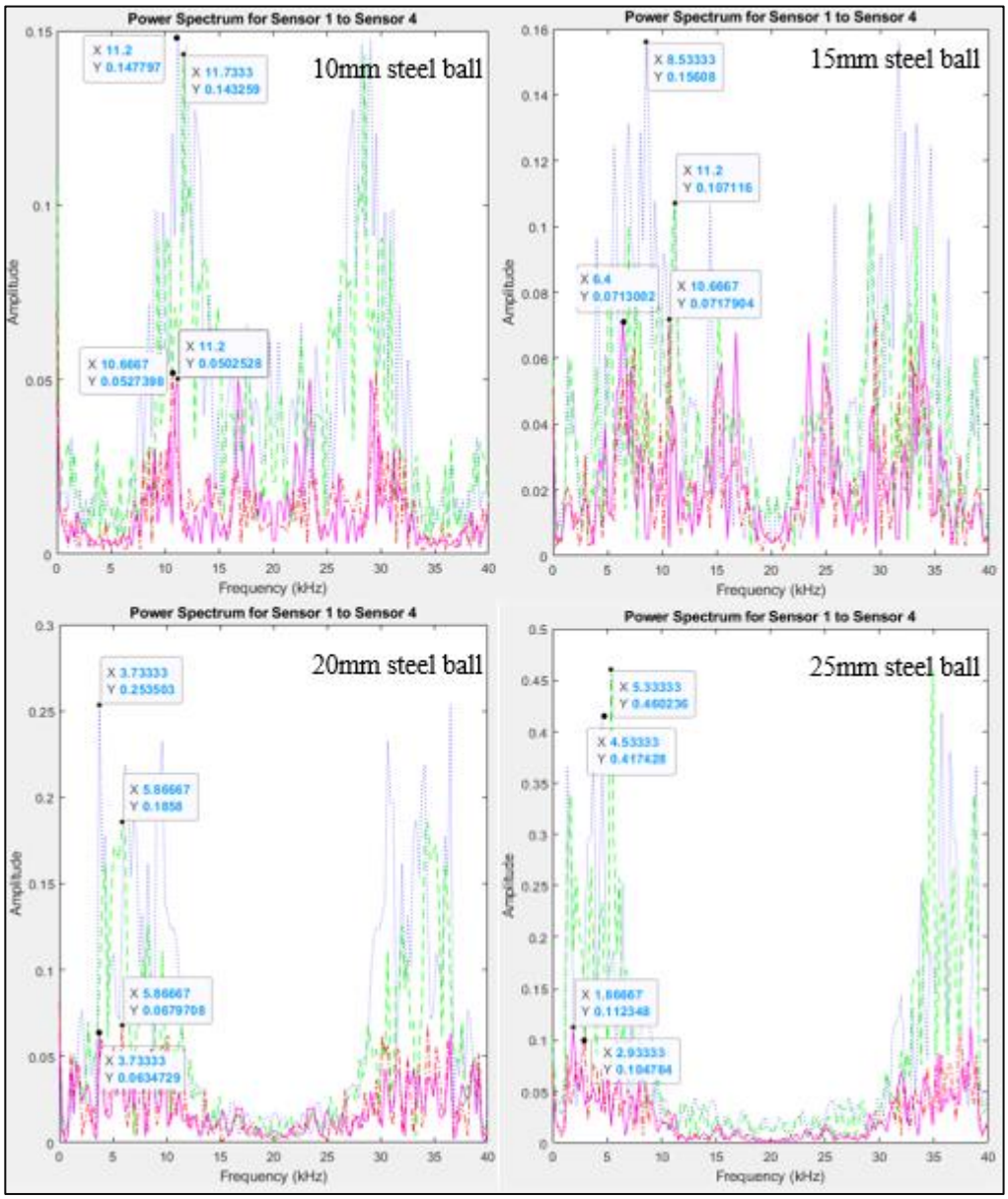
Power Spectrum for Sensor 1 to Sensor 4
10mm steel ball
X 11.2
Y 0.147797
X 11.7333
Y 0.143259
X 11.2
Y 0.0502528
X 10.6667
Y 0.0527398
Power Spectrum for Sensor 1 to Sensor 4
15mm steel ball
X 8.53333
Y 0.15608
X 11.2
Y 0.107116
X 6.4
Y 0.0713002
X 10.6667
Y 0.0717904
Power Spectrum for Sensor 1 to Sensor 4
20mm steel ball
X 3.73333
Y 0.253503
X 5.86667
Y 0.1858
X 5.86667
Y 0.0679708
X 3.73333
Y 0.0634729
Power Spectrum for Sensor 1 to Sensor 4
25mm steel ball
X 5.33333
Y 0.460236
X 4.53333
Y 0.417428
X 1.86667
Y 0.112348
X 2.93333
Y 0.104784
Amplitude
Frequency (kHz)

(a)

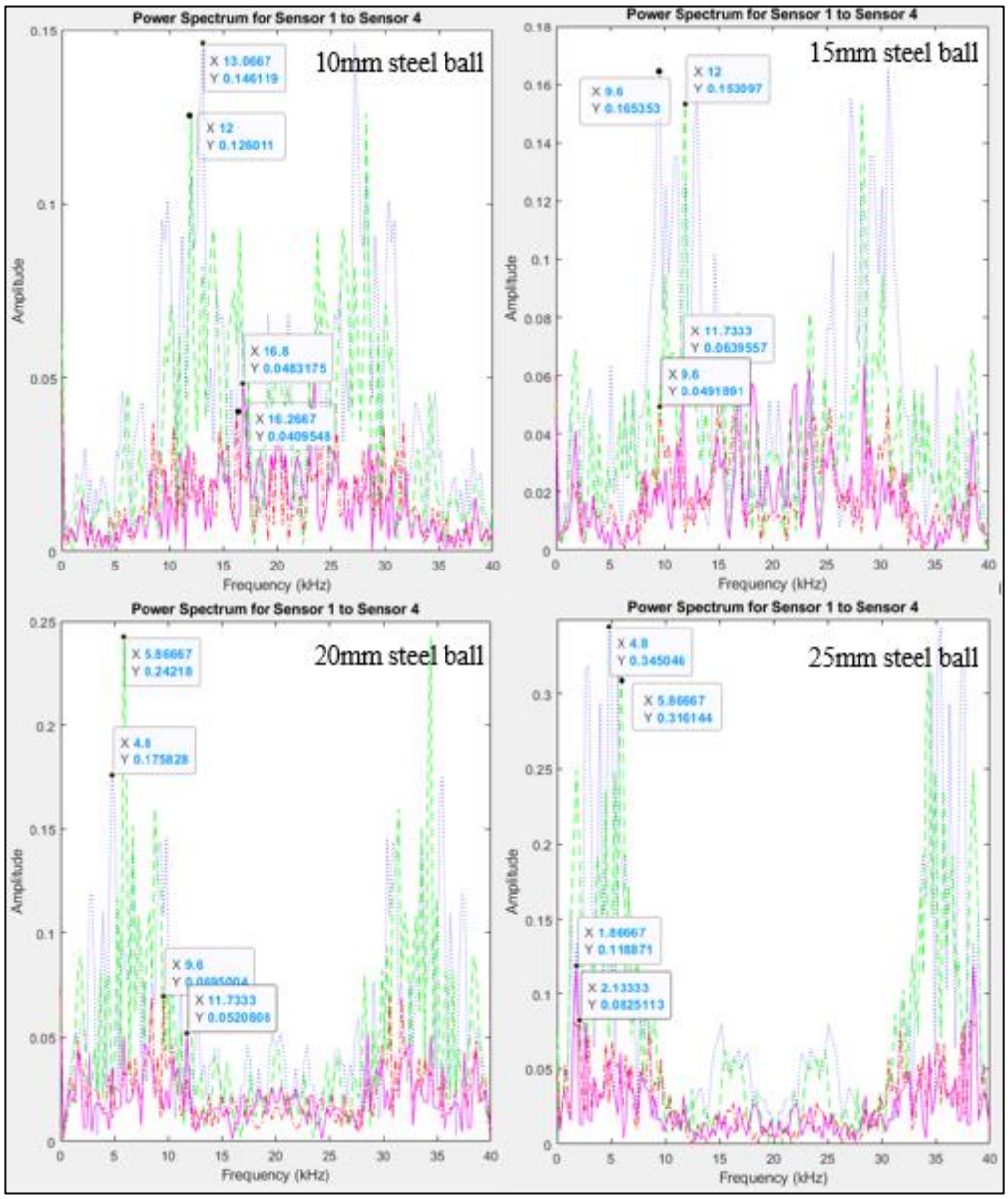
Power Spectrum for Sensor 1 to Sensor 4
10mm steel ball
X 13.0667
Y 0.146119
X 12
Y 0.126011
X 16.8
Y 0.0483175
X 16.2667
Y 0.0409548
Power Spectrum for Sensor 1 to Sensor 4
15mm steel ball
X 9.6
Y 0.165353
X 12
Y 0.153097
X 11.7333
Y 0.0639557
X 9.6
Y 0.0491891
Power Spectrum for Sensor 1 to Sensor 4
20mm steel ball
X 5.86667
Y 0.24218
X 4.8
Y 0.175828
X 11.7333
Y 0.0520808
Power Spectrum for Sensor 1 to Sensor 4
25mm steel ball
X 4.8
Y 0.345046
X 5.86667
Y 0.316144
X 1.86667
Y 0.118871
X 2.13333
Y 0.0825113
Amplitude
Frequency (kHz)

(b)

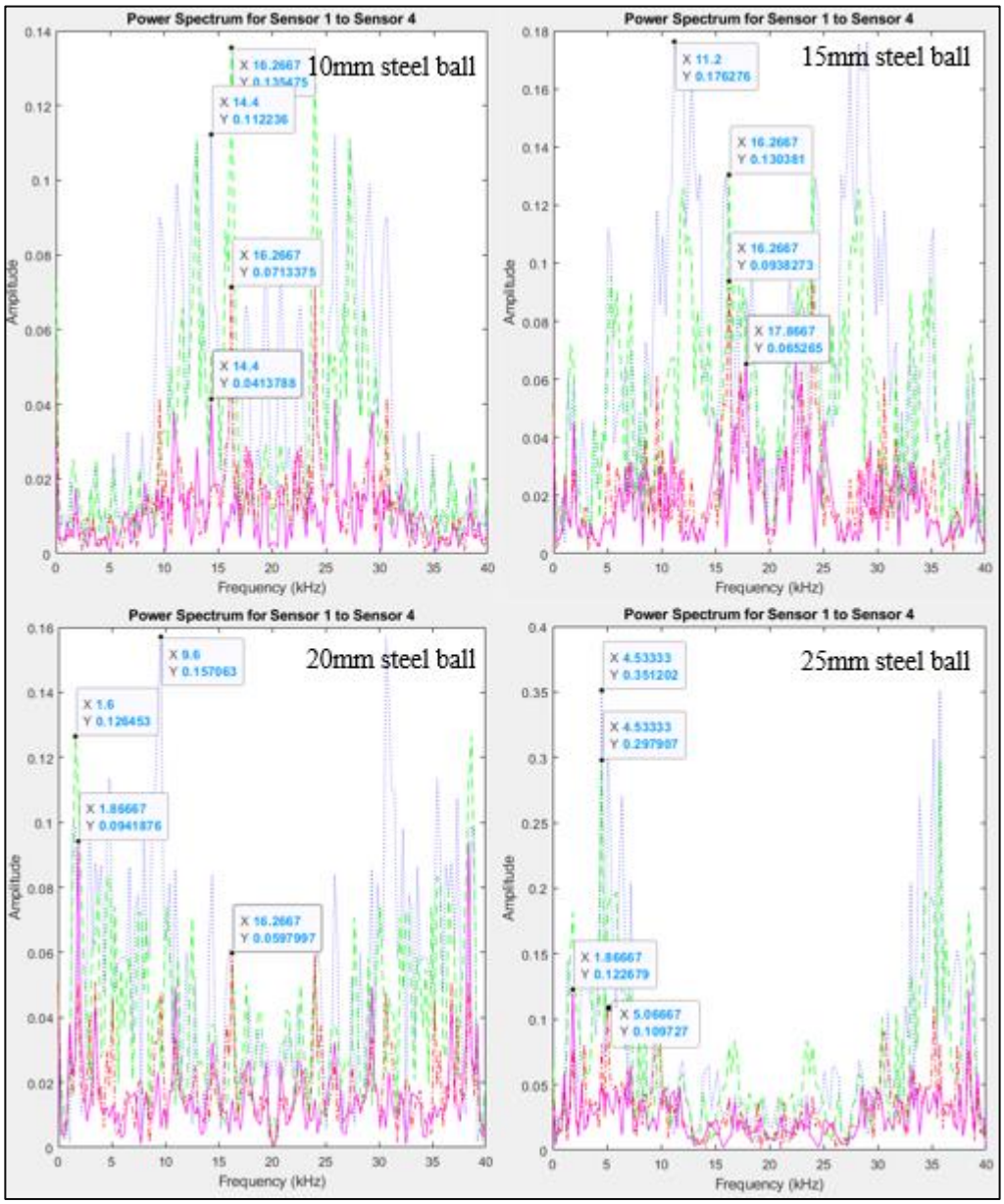
Power Spectrum for Sensor 1 to Sensor 4
10mm steel ball
X 16.2667
Y 0.135475
X 14.4
Y 0.112236
X 16.2667
Y 0.0713375
X 14.4
Y 0.0413788
Power Spectrum for Sensor 1 to Sensor 4
15mm steel ball
X 11.2
Y 0.176276
X 16.2667
Y 0.130381
X 16.2667
Y 0.0938273
X 17.8667
Y 0.065265
Power Spectrum for Sensor 1 to Sensor 4
20mm steel ball
X 9.6
Y 0.157063
X 1.6
Y 0.126453
X 1.86667
Y 0.0941876
X 16.2667
Y 0.0597997
Power Spectrum for Sensor 1 to Sensor 4
25mm steel ball
X 4.53333
Y 0.351202
X 4.53333
Y 0.297987
X 1.86667
Y 0.122679
X 5.06667
Y 0.109727
Amplitude
Frequency (kHz)

(c)

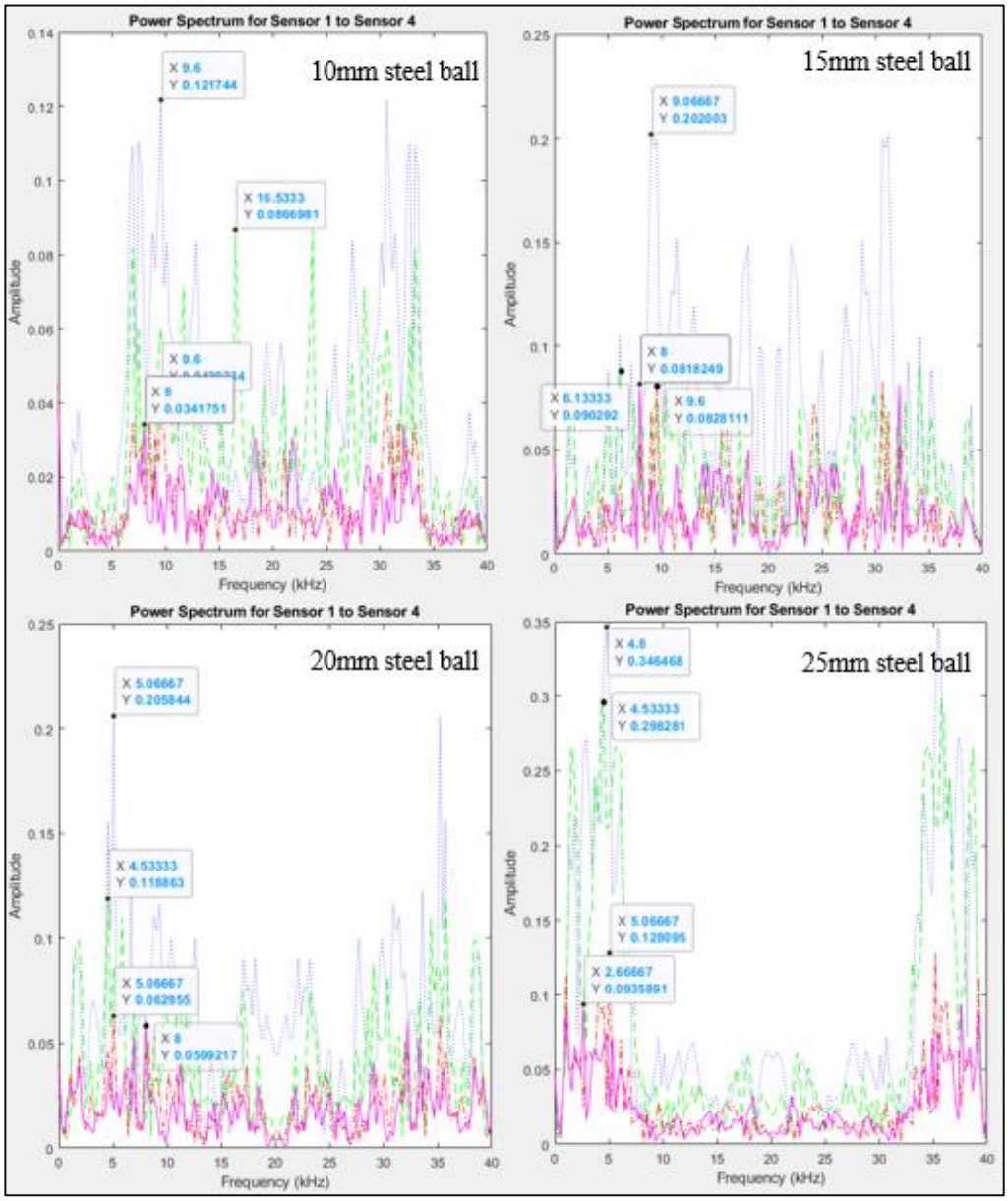
Power Spectrum for Sensor 1 to Sensor 4
10mm steel ball
X 9.6
Y 0.121744
X 16.5333
Y 0.0866981
X 8
Y 0.0341751
Power Spectrum for Sensor 1 to Sensor 4
15mm steel ball
X 9.06667
Y 0.202003
X 8
Y 0.0818249
X 6.13333
Y 0.090292
X 9.6
Y 0.0828111
Power Spectrum for Sensor 1 to Sensor 4
20mm steel ball
X 5.06667
Y 0.205844
X 4.53333
Y 0.116863
X 5.06667
Y 0.062955
X 8
Y 0.0509217
Power Spectrum for Sensor 1 to Sensor 4
25mm steel ball
X 4.8
Y 0.346468
X 4.53333
Y 0.298281
X 5.06667
Y 0.128095
X 2.66667
Y 0.0935891
Amplitude
Frequency (kHz)

(d)

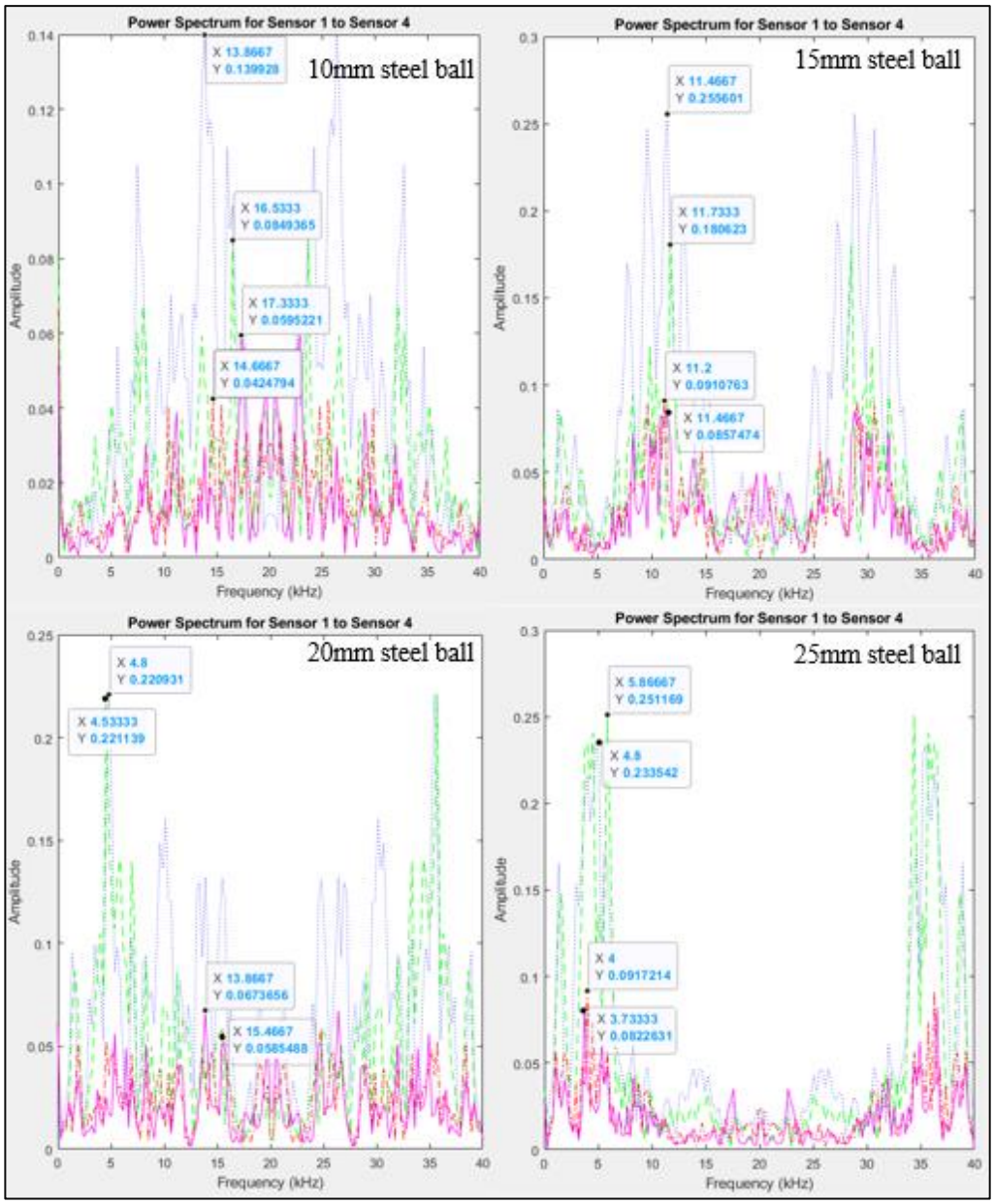

(e)

Appendix B-3: Power Spectrum for 425 mm Depth of Delamination and (a) 100 mm, (b) 200 mm, (c) 300 mm, (d) 400 mm, and (e) 500 mm Diameter of Delamination.

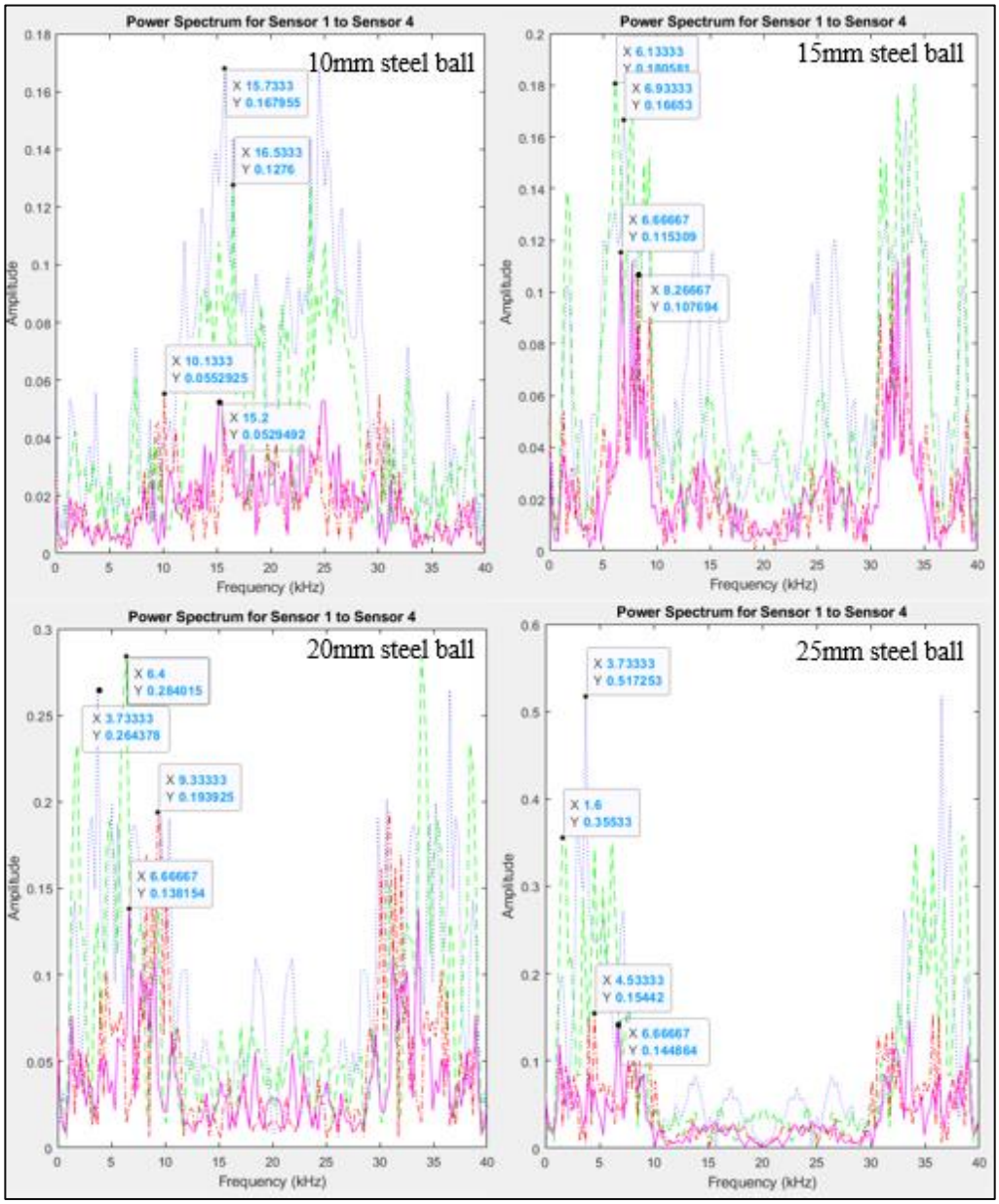
Power Spectrum for Sensor 1 to Sensor 4
10mm steel ball
X 15.7333
Y 0.167955
X 16.5333
Y 0.1276
X 10.1333
Y 0.0552925
X 15.2
Y 0.0529492
Amplitude
Frequency (kHz)
Power Spectrum for Sensor 1 to Sensor 4
15mm steel ball
X 6.13333
X 6.93333
Y 0.16653
X 6.66667
Y 0.115309
X 8.26667
Y 0.107694
Amplitude
Frequency (kHz)
Power Spectrum for Sensor 1 to Sensor 4
20mm steel ball
X 6.4
Y 0.264015
X 3.73333
Y 0.264378
X 9.33333
Y 0.193925
X 6.66667
Y 0.138154
Amplitude
Frequency (kHz)
Power Spectrum for Sensor 1 to Sensor 4
25mm steel ball
X 3.73333
Y 0.517253
X 1.6
Y 0.35533
X 4.53333
Y 0.15442
X 6.66667
Y 0.144864
Amplitude
Frequency (kHz)

(a)

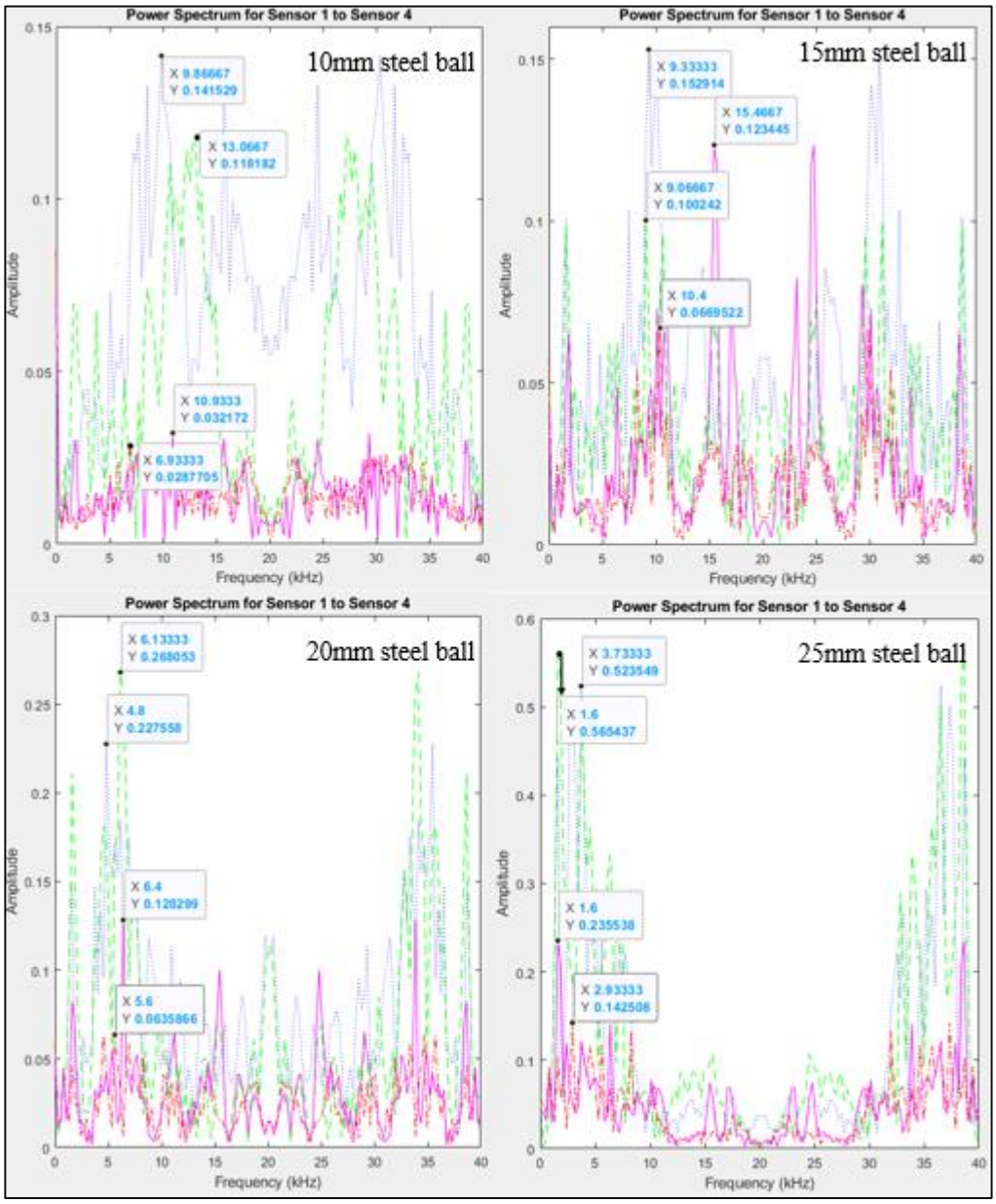
Power Spectrum for Sensor 1 to Sensor 4
10mm steel ball
X 9.86667
Y 0.141529
X 13.0667
Y 0.118182
X 10.9333
Y 0.032172
X 6.93333
Y 0.0287795
Power Spectrum for Sensor 1 to Sensor 4
15mm steel ball
X 9.33333
Y 0.152914
X 15.4667
Y 0.123445
X 9.06667
Y 0.100242
X 10.4
Y 0.0669522
Power Spectrum for Sensor 1 to Sensor 4
20mm steel ball
X 6.13333
Y 0.268053
X 4.8
Y 0.227558
X 6.4
Y 0.128299
X 5.6
Y 0.0635866
Power Spectrum for Sensor 1 to Sensor 4
25mm steel ball
X 3.73333
Y 0.523549
X 1.6
Y 0.565437
X 1.6
Y 0.235538
X 2.93333
Y 0.142508
Amplitude
Frequency (kHz)

(b)

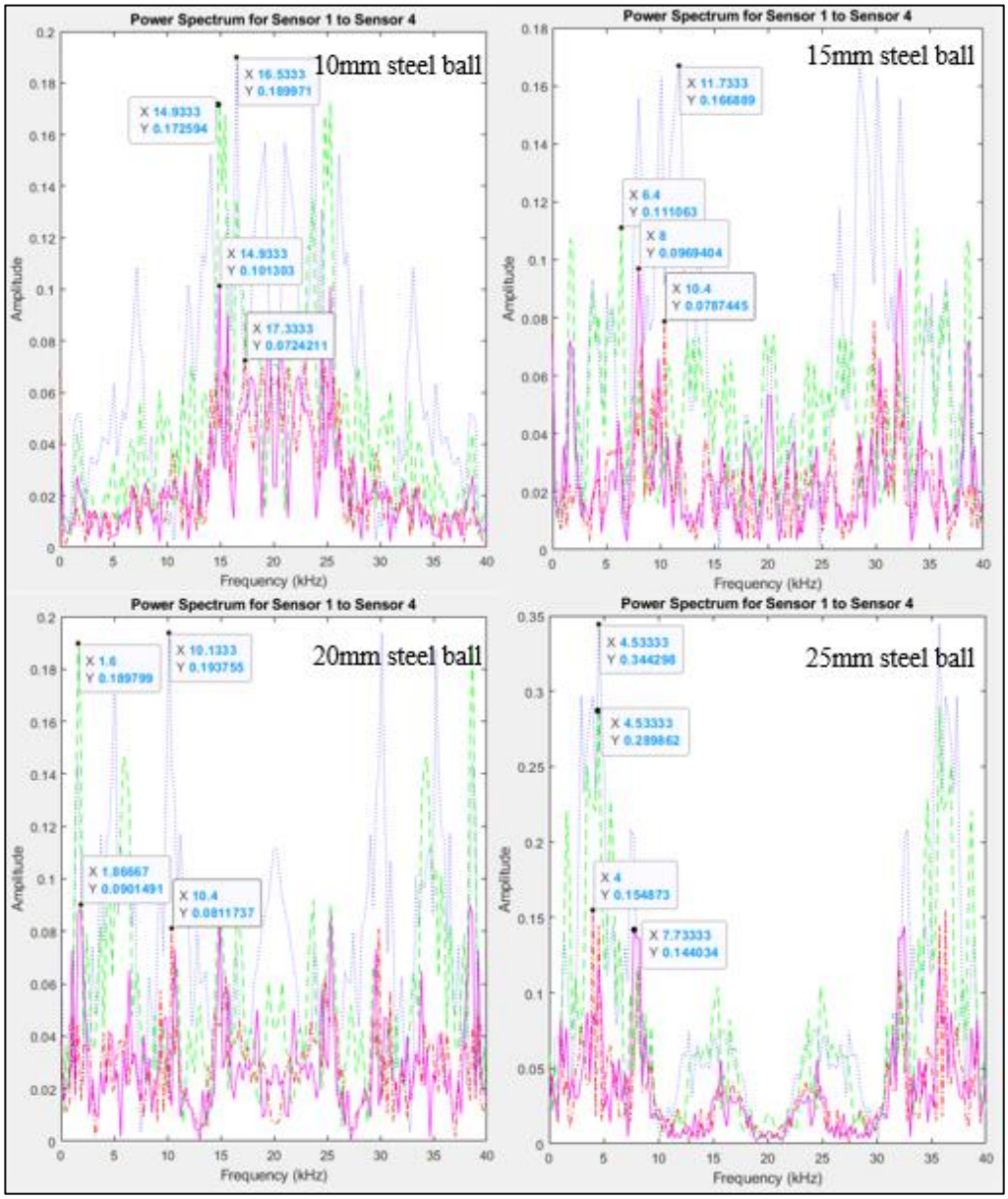
Power Spectrum for Sensor 1 to Sensor 4
10mm steel ball
X 16.5333
Y 0.189971
X 14.9333
Y 0.172594
X 14.9333
Y 0.101303
X 17.3333
Y 0.0724211
Power Spectrum for Sensor 1 to Sensor 4
15mm steel ball
X 11.7333
Y 0.166889
X 6.4
Y 0.111063
X 8
Y 0.0969404
X 10.4
Y 0.0787445
Power Spectrum for Sensor 1 to Sensor 4
20mm steel ball
X 1.6
Y 0.189799
X 10.1333
Y 0.193755
X 1.86667
Y 0.0901491
X 10.4
Y 0.0811737
Power Spectrum for Sensor 1 to Sensor 4
25mm steel ball
X 4.53333
Y 0.344298
X 4.53333
Y 0.289862
X 4
Y 0.154873
X 7.73333
Y 0.144034
Amplitude
Frequency (kHz)

(c)

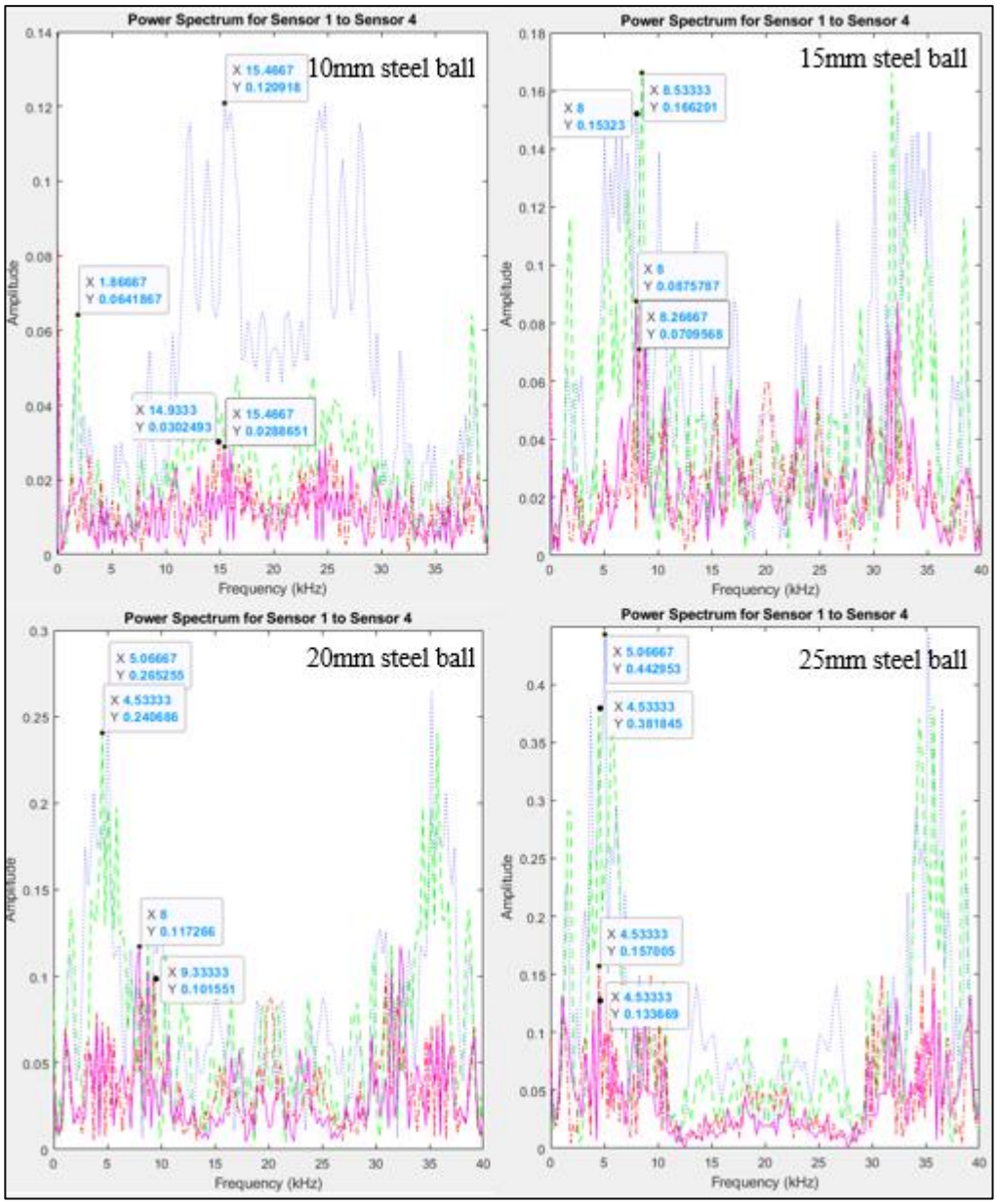

(d)

Appendix B-4: Power Spectrum for 625 mm Depth of Delamination and (a) 100 mm, (b) 200 mm, (c) 300 mm, and (d) 400 mm Diameter of Delamination.

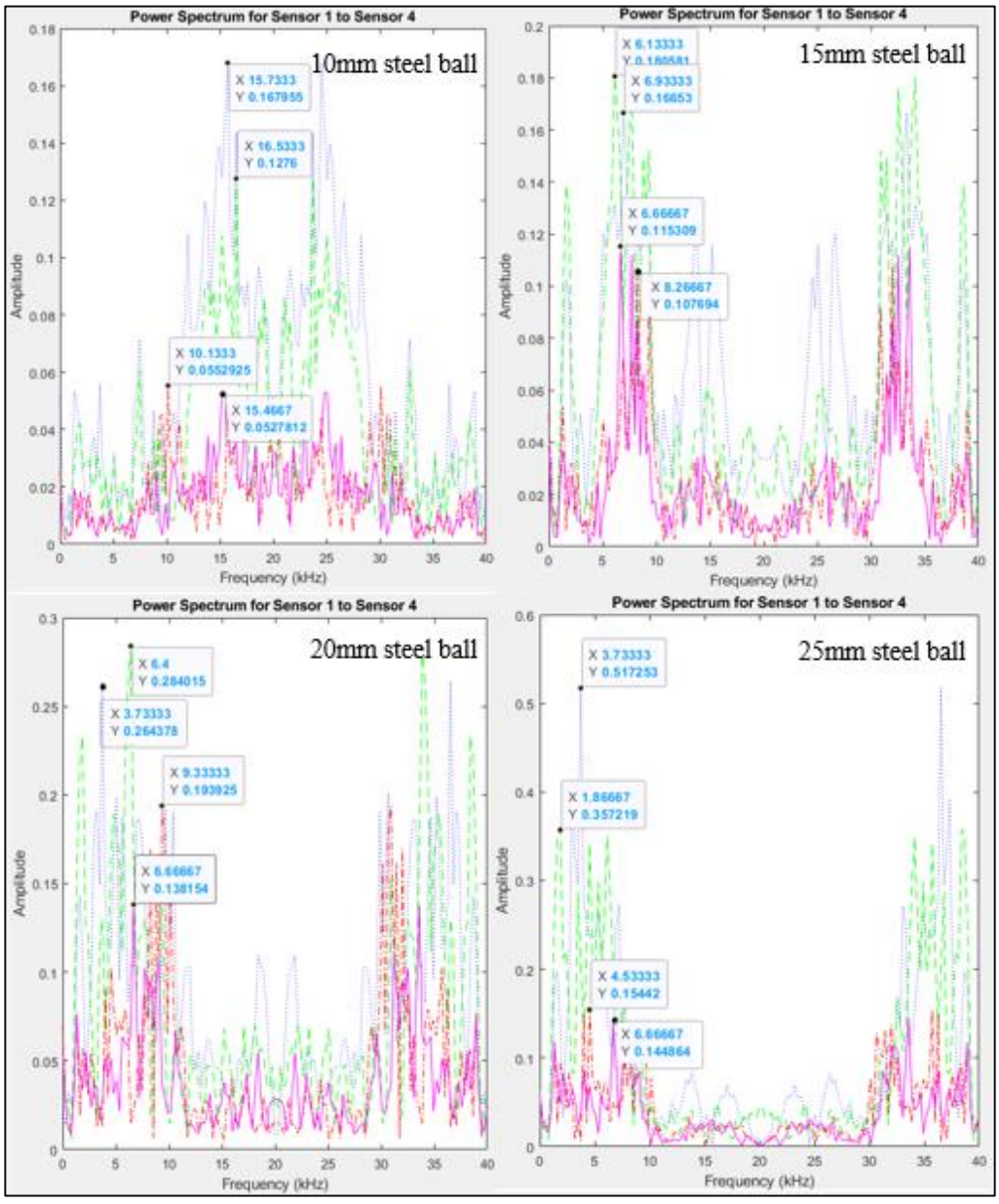
Power Spectrum for Sensor 1 to Sensor 4
10mm steel ball
X 15.7333
Y 0.167955
X 16.5333
Y 0.1276
X 10.1333
Y 0.0552925
X 15.4667
Y 0.0527812
Amplitude
Frequency (kHz)
Power Spectrum for Sensor 1 to Sensor 4
15mm steel ball
X 6.13333
X 6.93333
Y 0.16653
X 6.66667
Y 0.115309
X 8.26667
Y 0.107694
Amplitude
Frequency (kHz)
Power Spectrum for Sensor 1 to Sensor 4
20mm steel ball
X 6.4
Y 0.284015
X 3.73333
Y 0.264378
X 9.33333
Y 0.193925
X 6.66667
Y 0.138154
Amplitude
Frequency (kHz)
Power Spectrum for Sensor 1 to Sensor 4
25mm steel ball
X 3.73333
Y 0.517253
X 1.86667
Y 0.357219
X 4.53333
Y 0.15442
X 6.66667
Y 0.144864
Amplitude
Frequency (kHz)

(a)

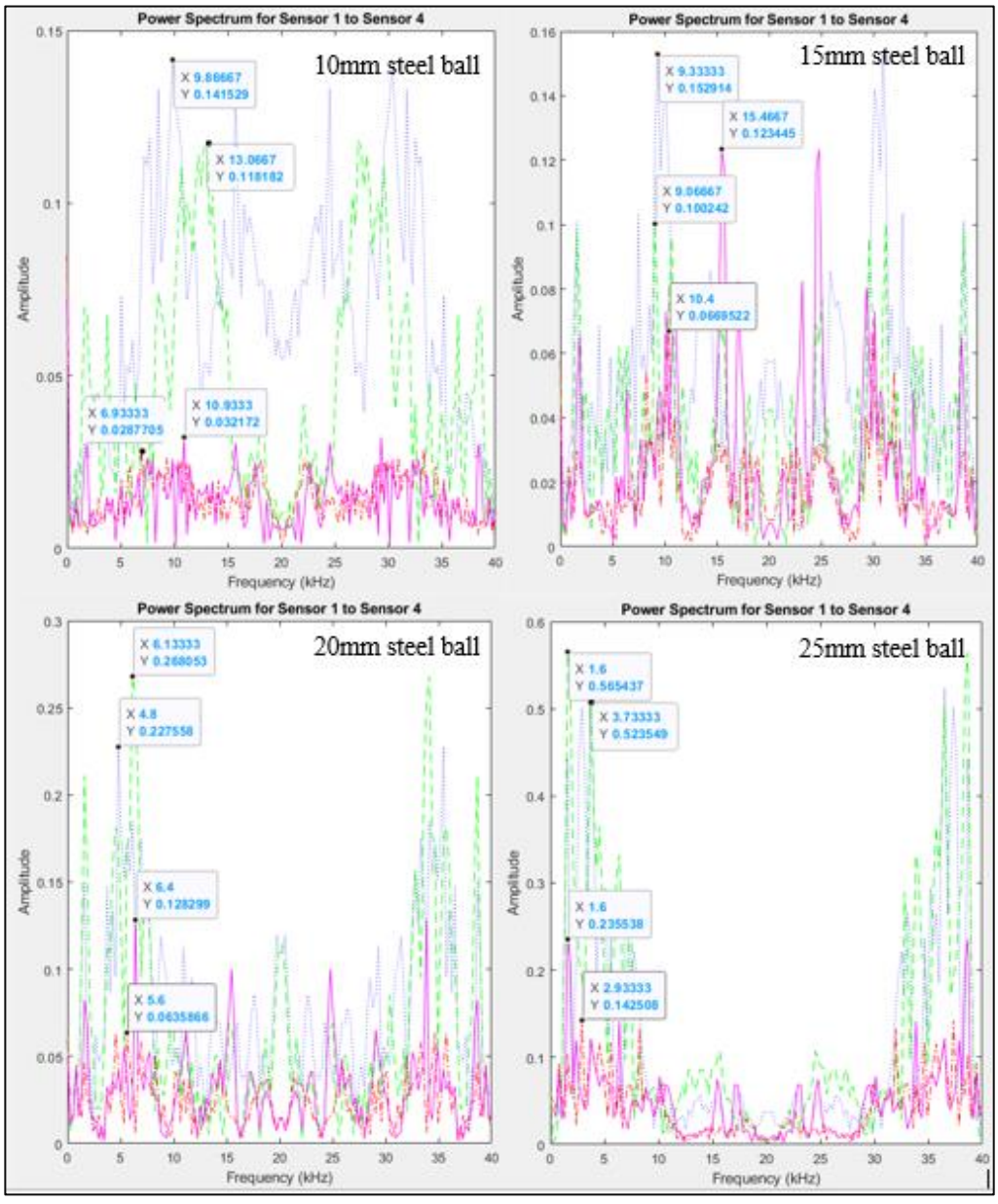
Power Spectrum for Sensor 1 to Sensor 4
10mm steel ball
X 9.86667
Y 0.141529
X 13.0667
Y 0.118182
X 6.93333
Y 0.0287705
X 10.9333
Y 0.032172
Power Spectrum for Sensor 1 to Sensor 4
15mm steel ball
X 9.33333
Y 0.152914
X 15.4667
Y 0.123445
X 9.06667
Y 0.100242
X 10.4
Y 0.0669522
Power Spectrum for Sensor 1 to Sensor 4
20mm steel ball
X 6.13333
Y 0.268053
X 4.8
Y 0.227558
X 6.4
Y 0.128299
X 5.6
Y 0.0635866
Power Spectrum for Sensor 1 to Sensor 4
25mm steel ball
X 1.6
Y 0.565437
X 3.73333
Y 0.523549
X 1.6
Y 0.235538
X 2.93333
Y 0.142508
Amplitude
Frequency (kHz)

(b)

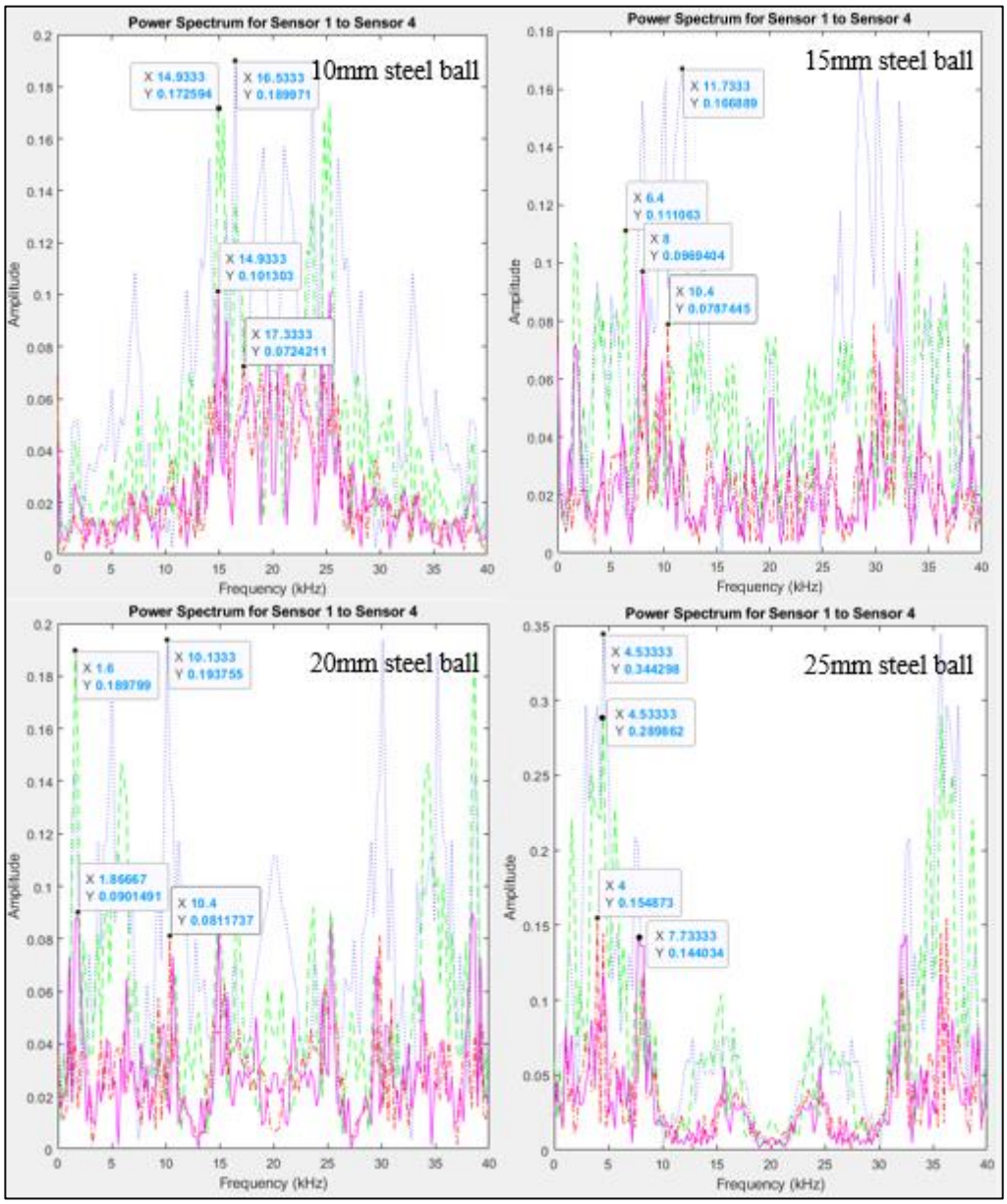
Power Spectrum for Sensor 1 to Sensor 4
10mm steel ball
X 14.9333
Y 0.172594
X 16.5333
Y 0.189971
X 14.9333
Y 0.101303
X 17.3333
Y 0.0724211
Power Spectrum for Sensor 1 to Sensor 4
15mm steel ball
X 11.7333
Y 0.166889
X 6.4
Y 0.111063
X 8
Y 0.0969404
X 10.4
Y 0.0787445
Power Spectrum for Sensor 1 to Sensor 4
20mm steel ball
X 1.6
Y 0.189799
X 10.1333
Y 0.193755
X 1.86667
Y 0.0901491
X 10.4
Y 0.0811737
Power Spectrum for Sensor 1 to Sensor 4
25mm steel ball
X 4.53333
Y 0.344298
X 4.53333
Y 0.289862
X 4
Y 0.154873
X 7.73333
Y 0.144034
Amplitude
Frequency (kHz)

(c)

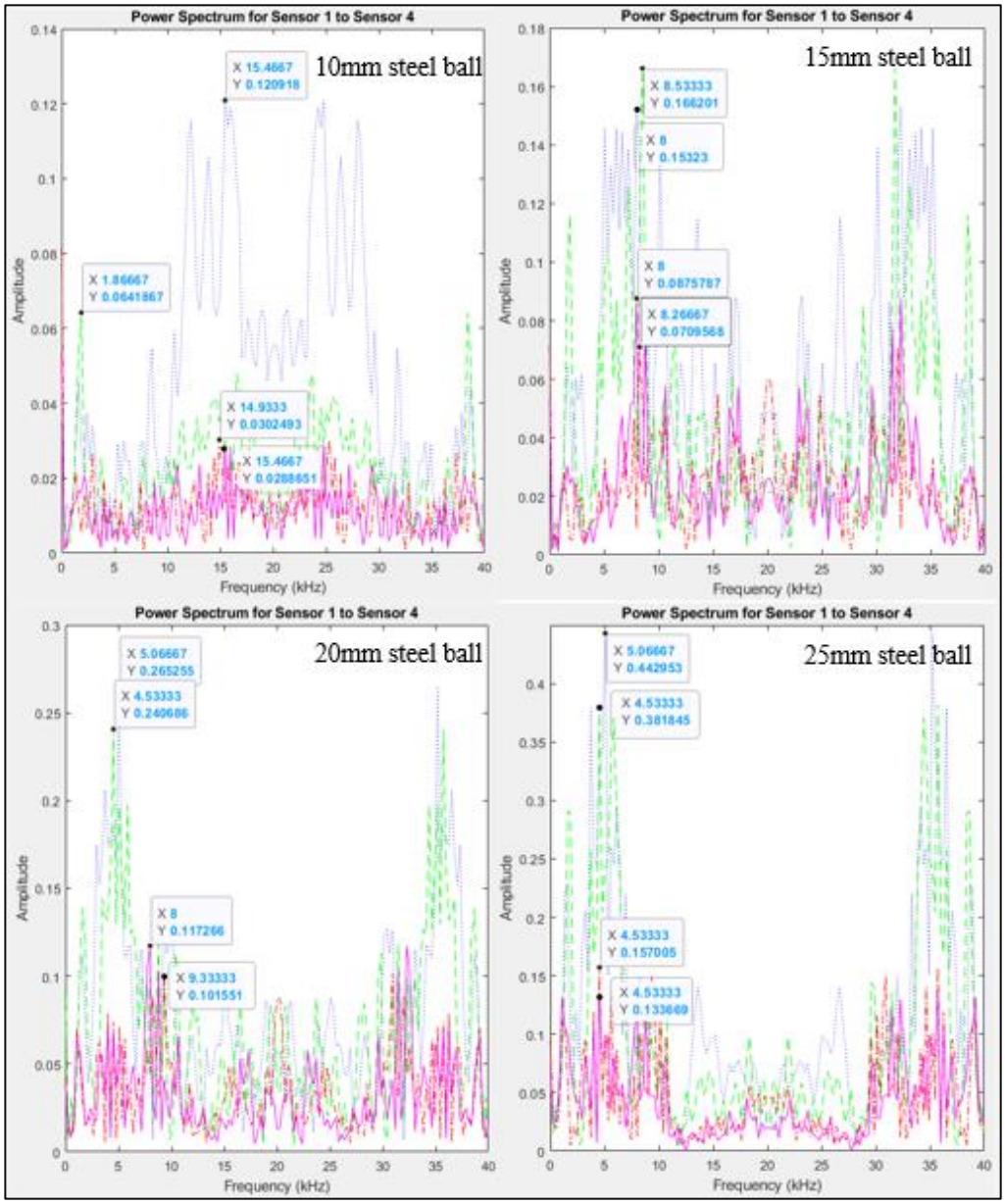

(d)

Appendix B-5: Power Spectrum for 825 mm Depth of Delamination and (a) 100 mm, (b) 200 mm, (c) 300 mm, and (d) 400 mm Diameter of Delamination.

APPENDIX C: Peak Frequency (Section 4.5.2).

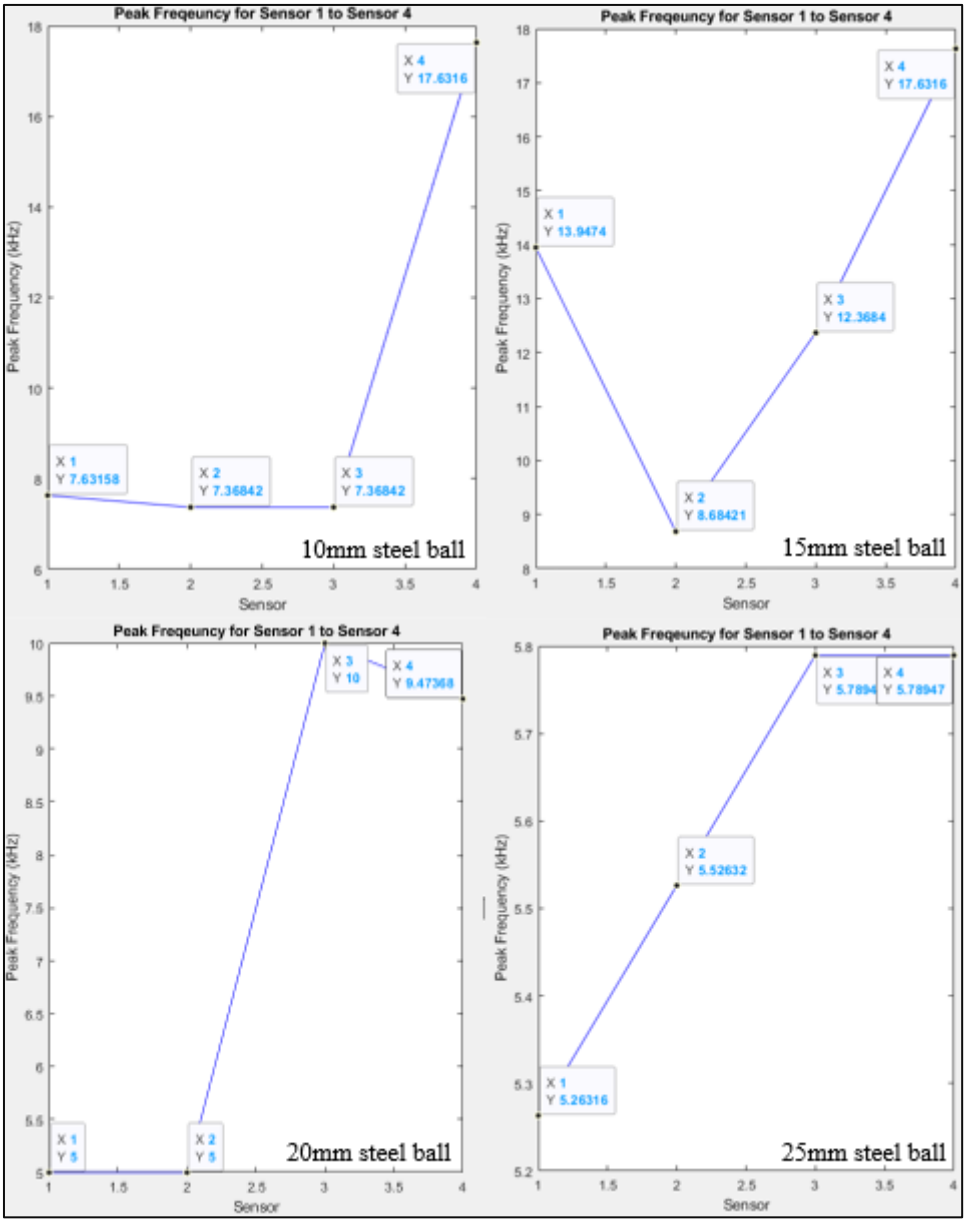

(a)

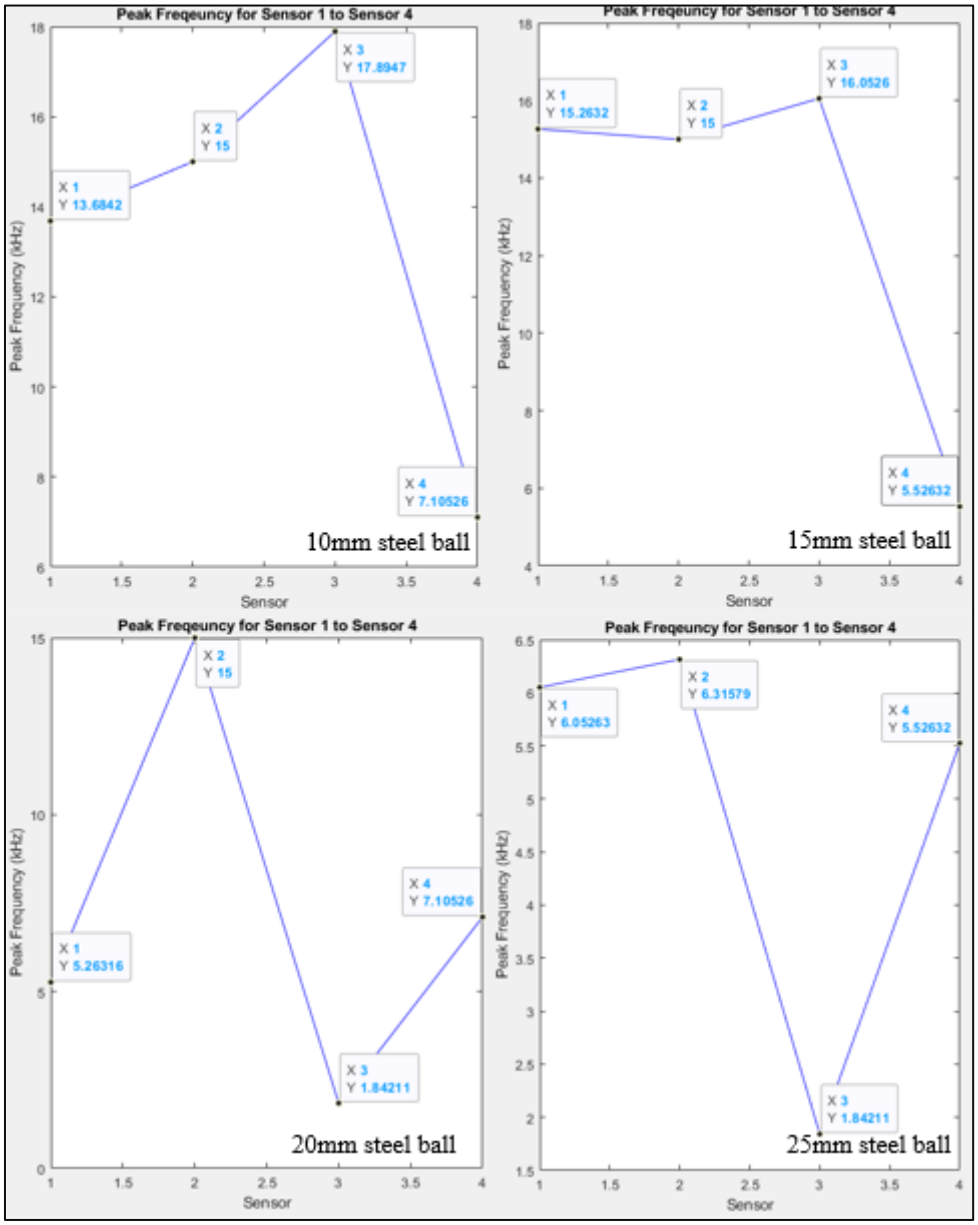
Peak Freqeuncy for Sensor 1 to Sensor 4
X 1
Y 13.6842
X 2
Y 15
X 3
Y 17.8947
X 4
Y 7.10526
10mm steel ball
Peak Freqeuncy for Sensor 1 to Sensor 4
X 1
Y 15.2632
X 2
Y 15
X 3
Y 16.0526
X 4
Y 5.52632
15mm steel ball
Peak Freqeuncy for Sensor 1 to Sensor 4
X 1
Y 5.26316
X 2
Y 15
X 3
Y 1.84211
X 4
Y 7.10526
20mm steel ball
Peak Freqeuncy for Sensor 1 to Sensor 4
X 1
Y 6.05263
X 2
Y 6.31579
X 3
Y 1.84211
X 4
Y 5.52632
25mm steel ball
Peak Frequency (kHz)
Sensor

(b)

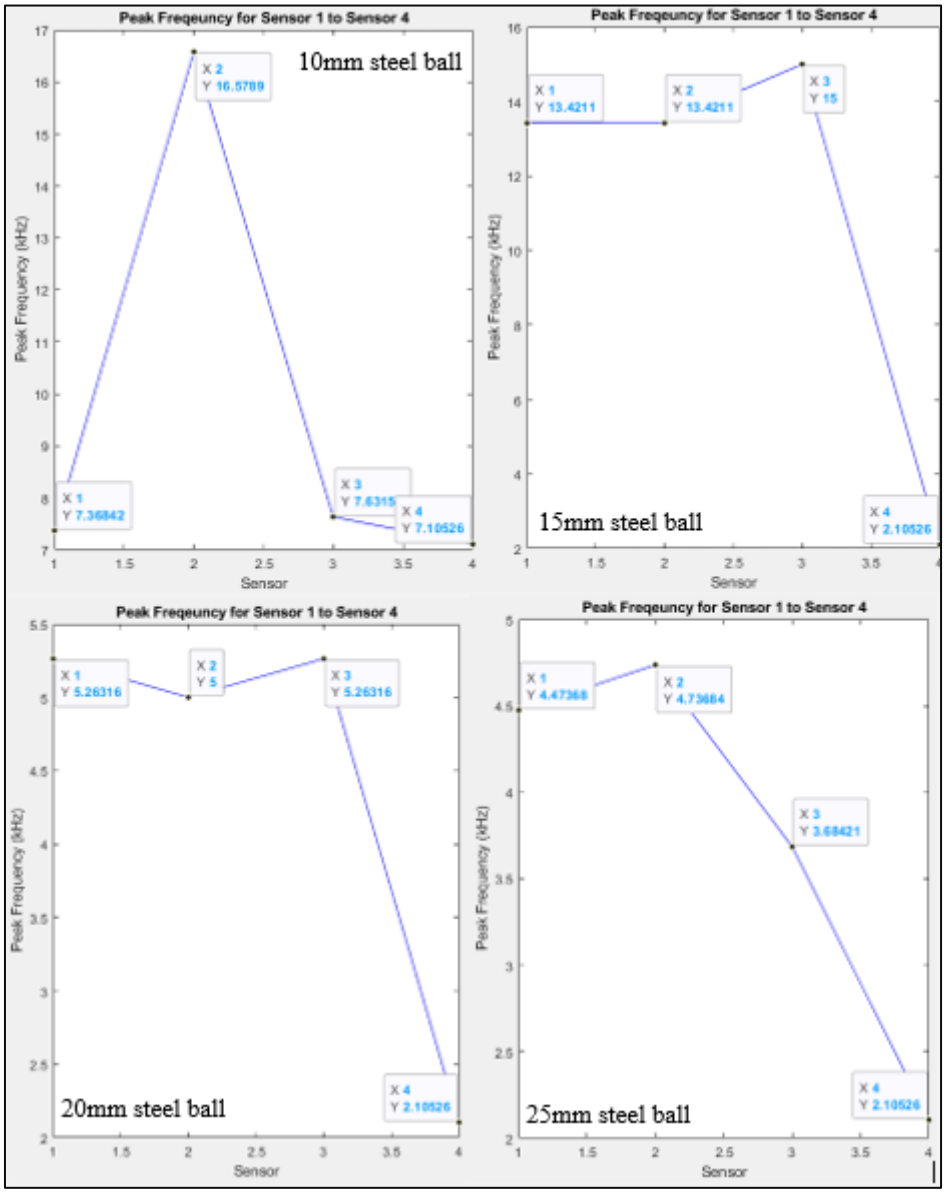
Peak Freqeuncy for Sensor 1 to Sensor 4
10mm steel ball
X 2
Y 16.5789
X 1
Y 7.36842
X 3
Y 7.6315
X 4
Y 7.10526
Peak Frequency (kHz)
Sensor
Peak Freqeuncy for Sensor 1 to Sensor 4
X 1
Y 13.4211
X 2
Y 13.4211
X 3
Y 15
15mm steel ball
X 4
Y 2.10526
Peak Frequency (kHz)
Sensor
Peak Freqeuncy for Sensor 1 to Sensor 4
X 1
Y 5.26316
X 2
Y 5
X 3
Y 5.26316
20mm steel ball
X 4
Y 2.10526
Peak Frequency (kHz)
Sensor
Peak Freqeuncy for Sensor 1 to Sensor 4
X 1
Y 4.47368
X 2
Y 4.73684
X 3
Y 3.68421
25mm steel ball
X 4
Y 2.10526
Peak Frequency (kHz)
Sensor

(c)

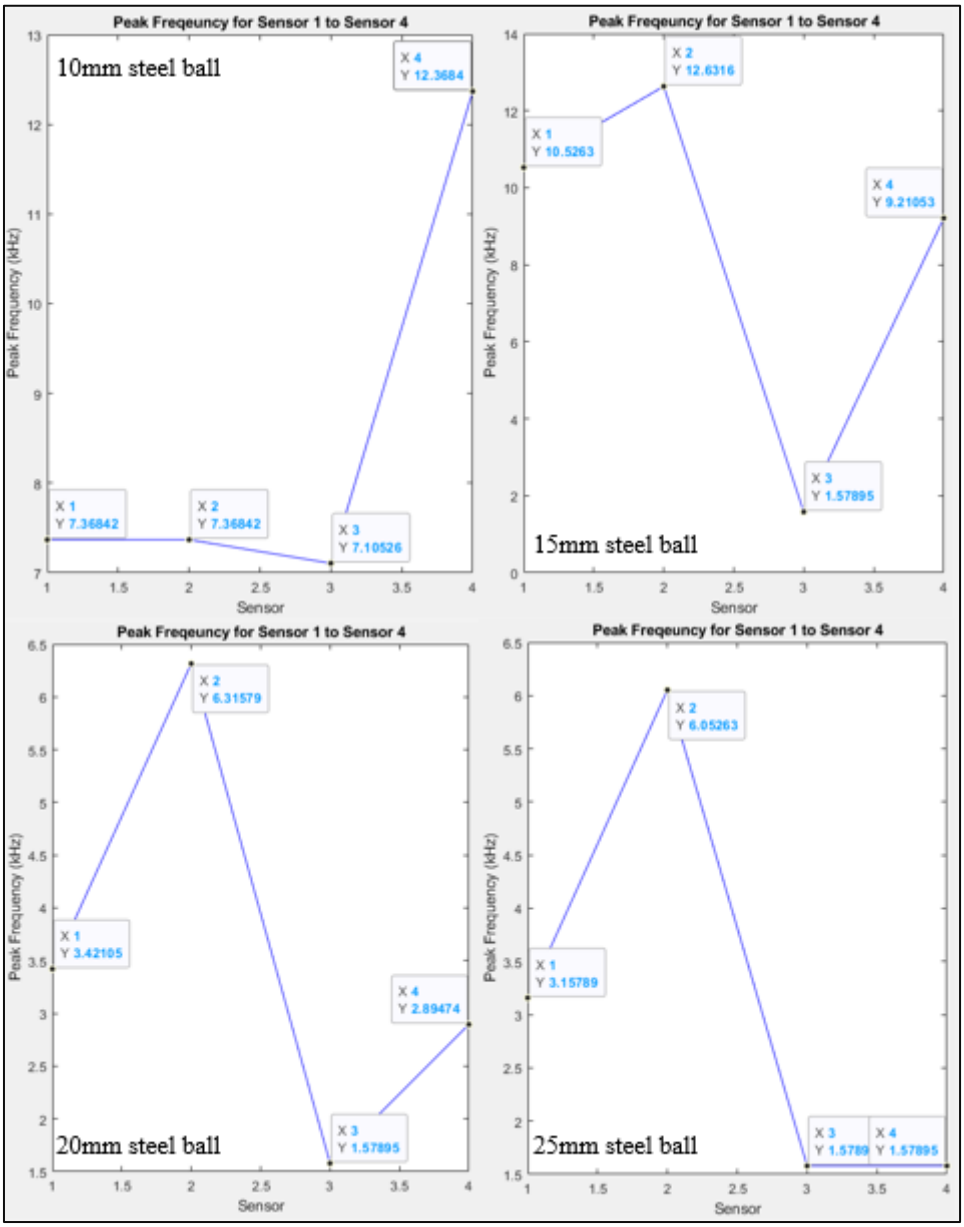
Peak Freqeuncy for Sensor 1 to Sensor 4
10mm steel ball
X 4
Y 12.3684
X 1
Y 7.36842
X 2
Y 7.36842
X 3
Y 7.10526
Peak Frequency (kHz)
Sensor
Peak Freqeuncy for Sensor 1 to Sensor 4
X 2
Y 12.6316
X 1
Y 10.5263
X 4
Y 9.21053
X 3
Y 1.57895
15mm steel ball
Peak Frequency (kHz)
Sensor
Peak Freqeuncy for Sensor 1 to Sensor 4
X 2
Y 6.31579
X 1
Y 3.42105
X 4
Y 2.89474
X 3
Y 1.57895
20mm steel ball
Peak Frequency (kHz)
Sensor
Peak Freqeuncy for Sensor 1 to Sensor 4
X 2
Y 6.05263
X 1
Y 3.15789
X 3
Y 1.5789
X 4
Y 1.57895
25mm steel ball
Peak Frequency (kHz)
Sensor

(d)

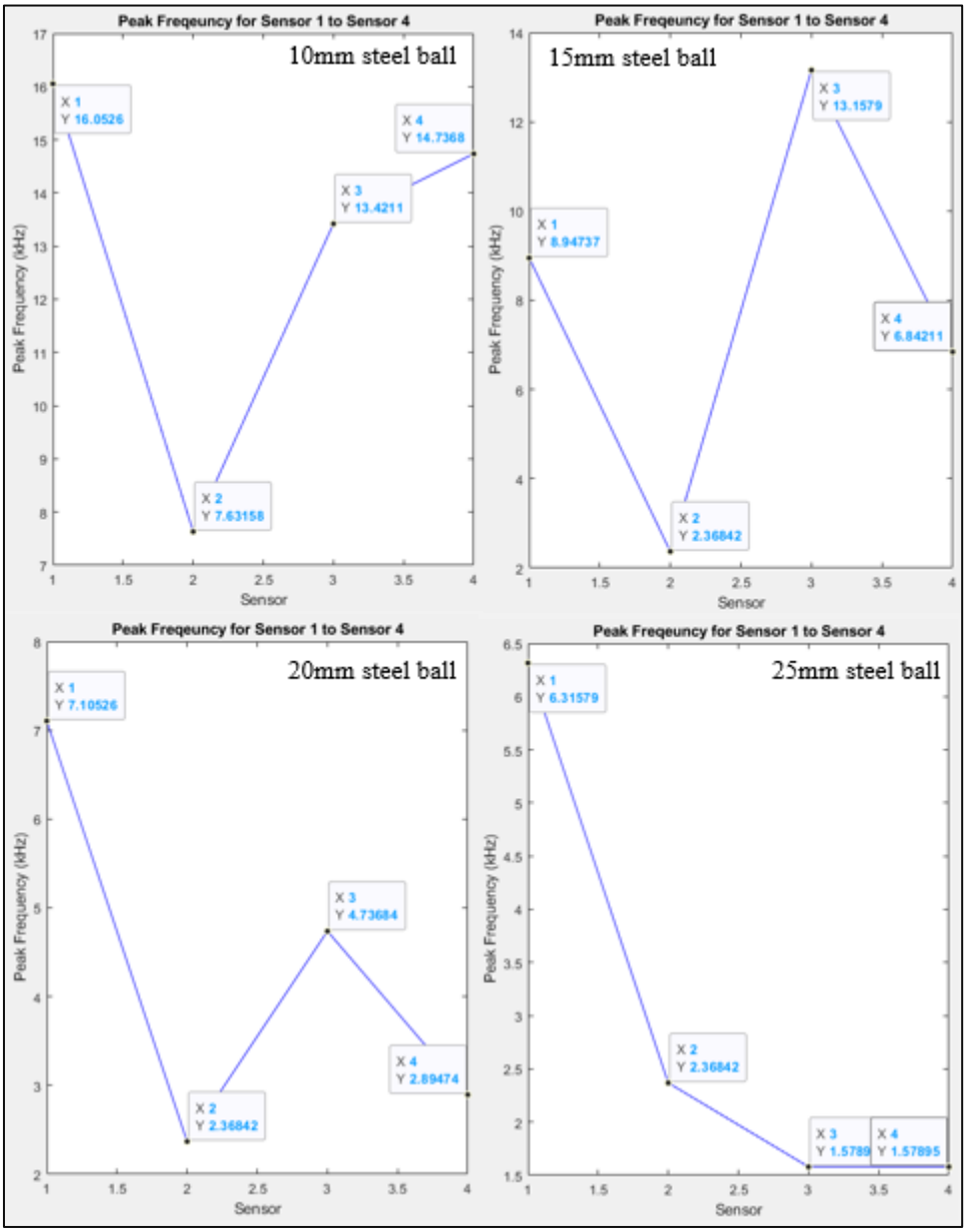

(e)

Appendix C-1: Peak Frequency for 25 mm Depth of Delamination and (a) 100 mm, (b) 200 mm, (c) 300 mm, (d) 400 mm, and (e) 500 mm Diameter of Delamination.

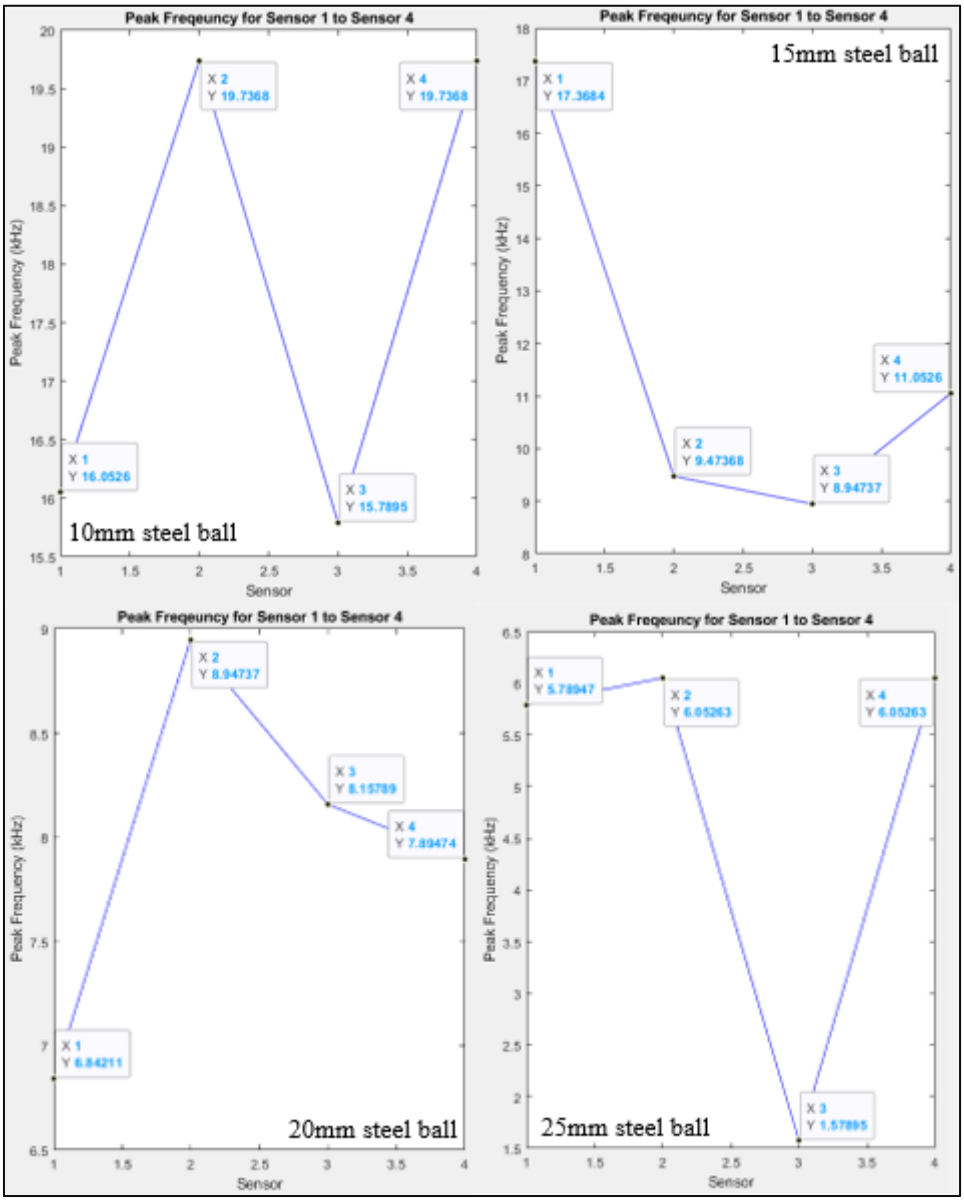
Peak Freqeuncy for Sensor 1 to Sensor 4
Peak Frequency (kHz)
Sensor
X 1
Y 16.0526
X 2
Y 19.7368
X 3
Y 15.7895
X 4
Y 19.7368
10mm steel ball
Peak Freqeuncy for Sensor 1 to Sensor 4
15mm steel ball
X 1
Y 17.3684
X 2
Y 9.47368
X 3
Y 8.94737
X 4
Y 11.0526
Peak Freqeuncy for Sensor 1 to Sensor 4
X 1
Y 6.84211
X 2
Y 8.94737
X 3
Y 8.15789
X 4
Y 7.89474
20mm steel ball
Peak Freqeuncy for Sensor 1 to Sensor 4
X 1
Y 5.78947
X 2
Y 6.05263
X 3
Y 1.57895
X 4
Y 6.05263
25mm steel ball

(a)

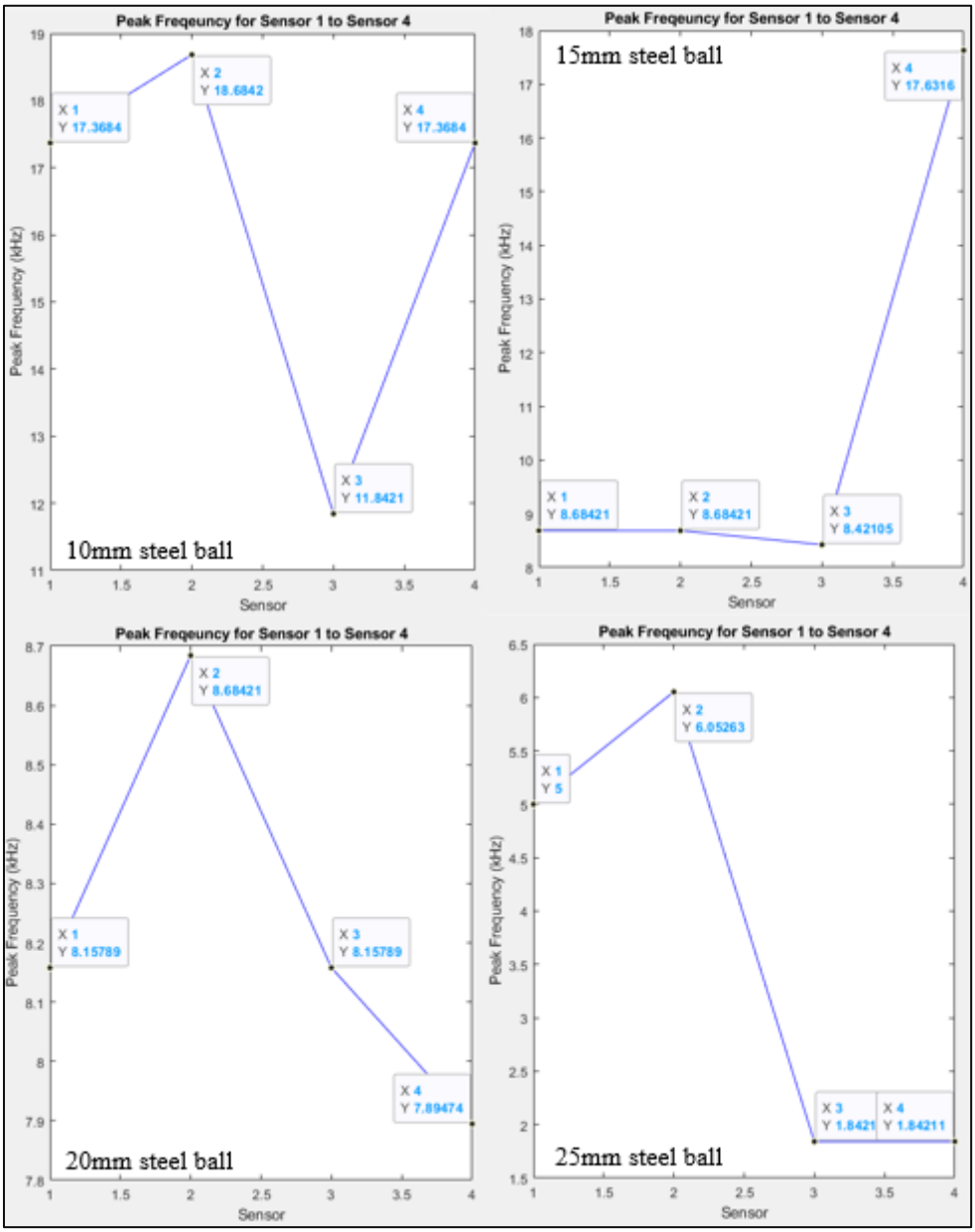
Peak Freqeuncy for Sensor 1 to Sensor 4
X 1
Y 17.3684
X 2
Y 18.6842
X 3
Y 11.8421
X 4
Y 17.3684
10mm steel ball
Peak Frequency (kHz)
Sensor
Peak Freqeuncy for Sensor 1 to Sensor 4
15mm steel ball
X 1
Y 8.68421
X 2
Y 8.68421
X 3
Y 8.42105
X 4
Y 17.6316
Peak Frequency (kHz)
Sensor
Peak Freqeuncy for Sensor 1 to Sensor 4
X 1
Y 8.15789
X 2
Y 8.68421
X 3
Y 8.15789
X 4
Y 7.89474
20mm steel ball
Peak Frequency (kHz)
Sensor
Peak Freqeuncy for Sensor 1 to Sensor 4
X 1
Y 5
X 2
Y 6.05263
X 3
Y 1.8421
X 4
Y 1.84211
25mm steel ball
Peak Frequency (kHz)
Sensor

(b)

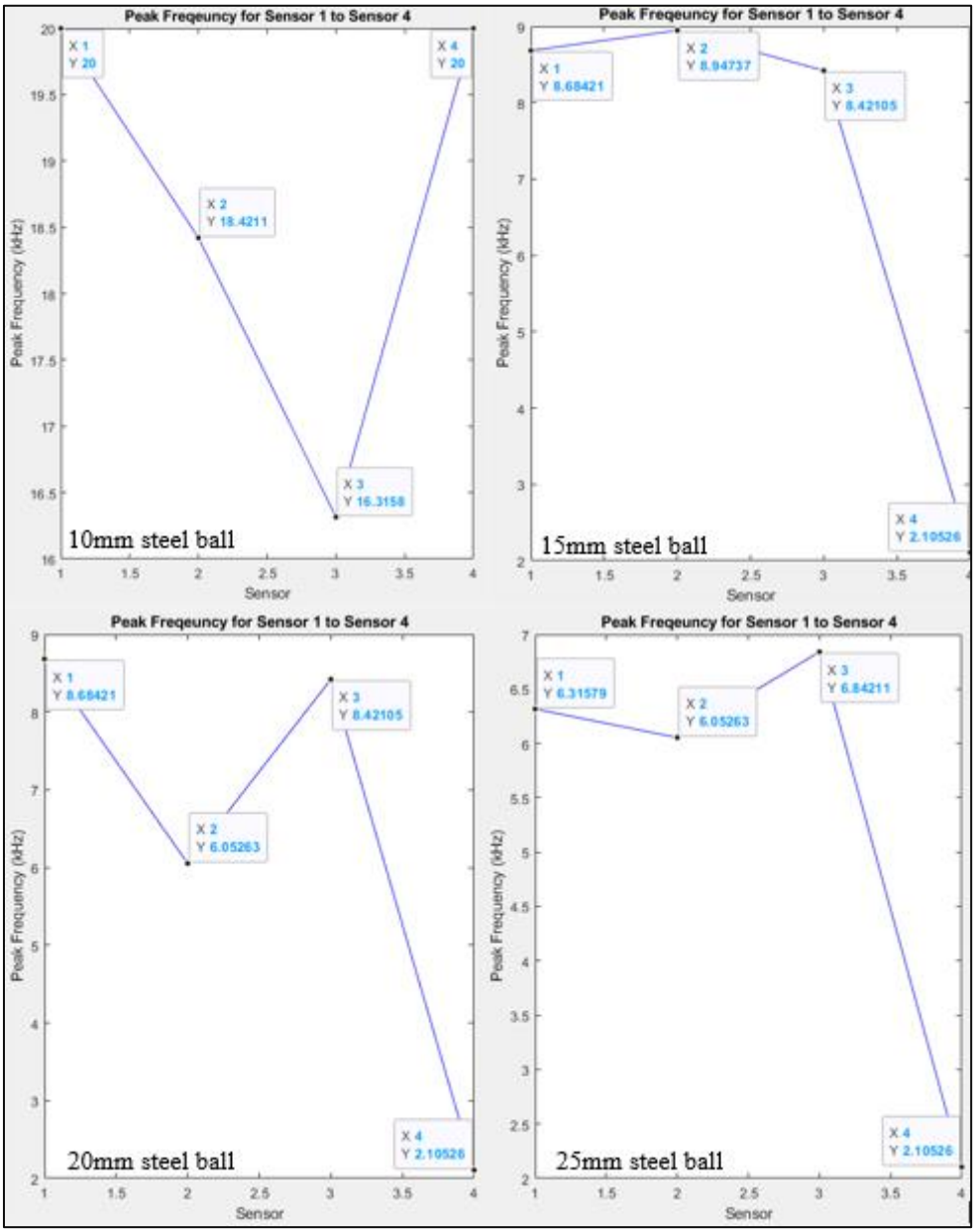
Peak Freqeuncy for Sensor 1 to Sensor 4
X 1
Y 20
X 2
Y 18.4211
X 3
Y 16.3158
X 4
Y 20
10mm steel ball
Peak Frequency (kHz)
Sensor
Peak Freqeuncy for Sensor 1 to Sensor 4
X 1
Y 8.68421
X 2
Y 8.94737
X 3
Y 8.42105
X 4
Y 2.10526
15mm steel ball
Peak Frequency (kHz)
Sensor
Peak Freqeuncy for Sensor 1 to Sensor 4
X 1
Y 8.68421
X 2
Y 6.05263
X 3
Y 8.42105
X 4
Y 2.10526
20mm steel ball
Peak Frequency (kHz)
Sensor
Peak Freqeuncy for Sensor 1 to Sensor 4
X 1
Y 6.31579
X 2
Y 6.05263
X 3
Y 6.84211
X 4
Y 2.10526
25mm steel ball
Peak Frequency (kHz)
Sensor

(c)

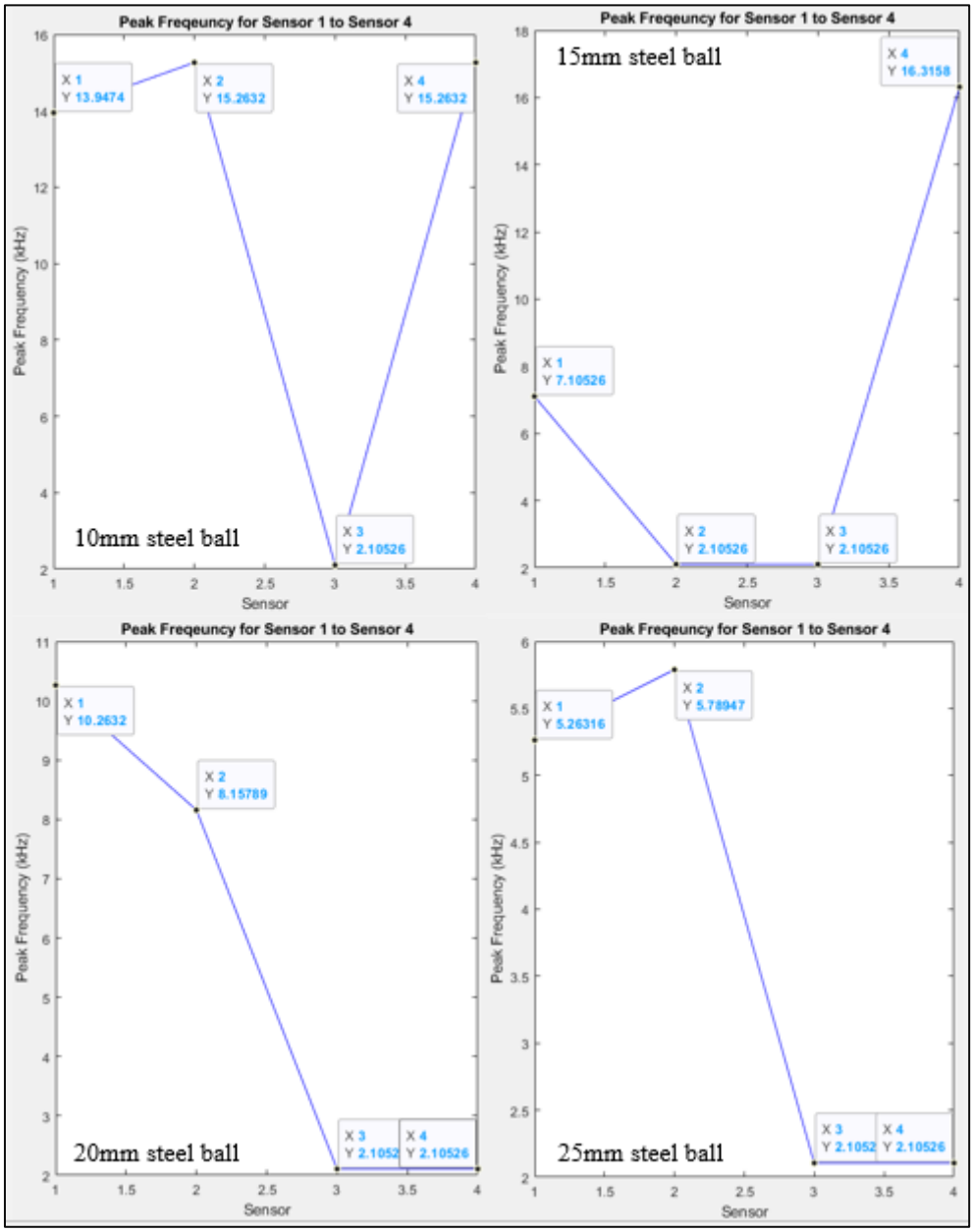

(d)

Appendix C-2: Peak Frequency for 225 mm Depth of Delamination and (a) 100 mm, (b) 200 mm, (c) 300 mm, and (d) 400 mm Diameter of Delamination.

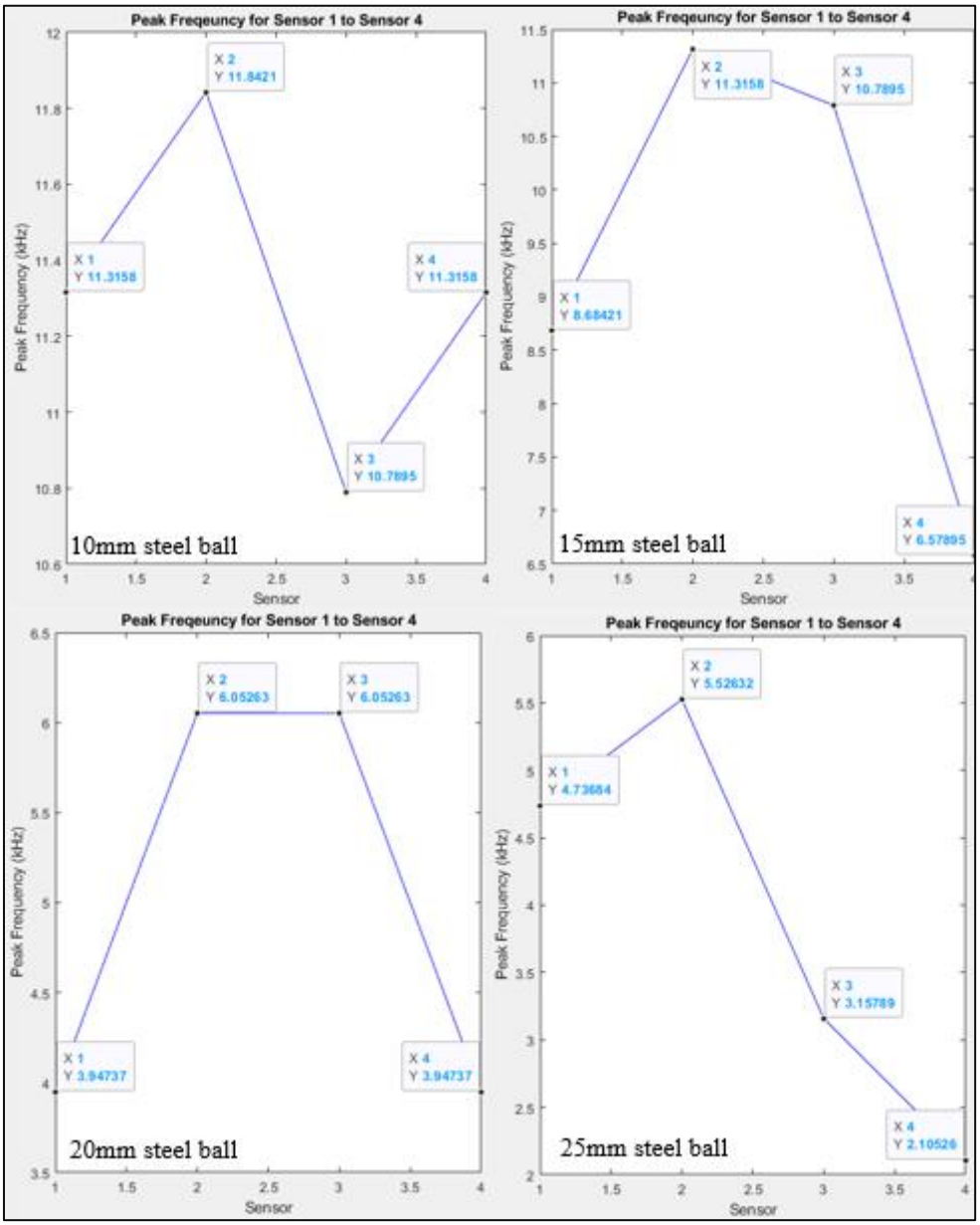
Peak Freqeuncy for Sensor 1 to Sensor 4
X 2
Y 11.8421
X 1
Y 11.3158
X 4
Y 11.3158
X 3
Y 10.7895
10mm steel ball
Peak Freqeuncy for Sensor 1 to Sensor 4
X 2
Y 11.3158
X 3
Y 10.7895
X 1
Y 8.68421
X 4
Y 6.57895
15mm steel ball
Peak Freqeuncy for Sensor 1 to Sensor 4
X 2
Y 6.05263
X 3
Y 6.05263
X 1
Y 3.94737
X 4
Y 3.94737
20mm steel ball
Peak Freqeuncy for Sensor 1 to Sensor 4
X 2
Y 5.52632
X 1
Y 4.73684
X 3
Y 3.15789
X 4
Y 2.10526
25mm steel ball
Peak Frequency (kHz)
Sensor

(a)

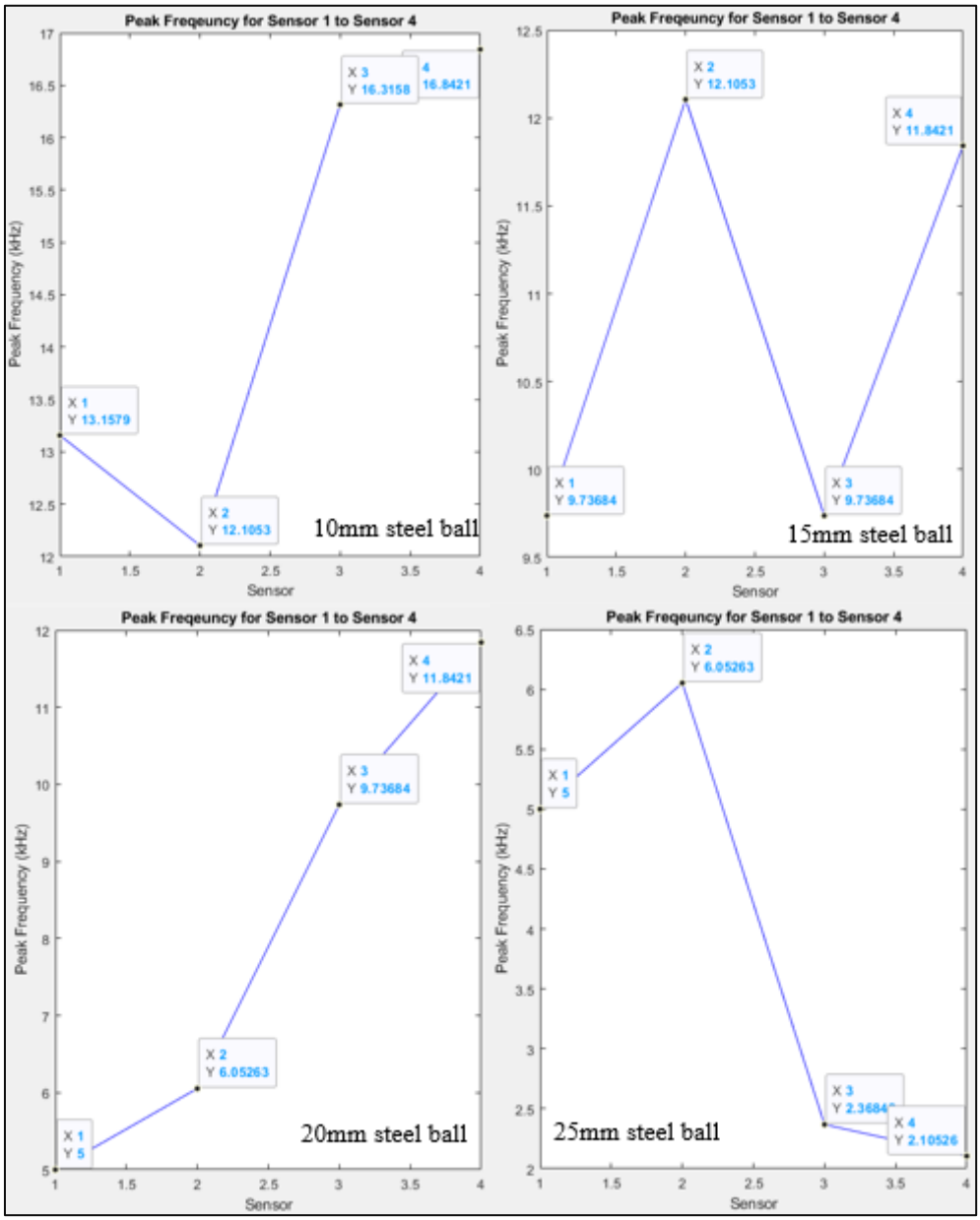
Peak Freqeuncy for Sensor 1 to Sensor 4
Peak Frequency (kHz)
Sensor
X 1
Y 13.1579
X 2
Y 12.1053
X 3
Y 16.3158
4
16.8421
10mm steel ball
Peak Freqeuncy for Sensor 1 to Sensor 4
Peak Frequency (kHz)
Sensor
X 1
Y 9.73684
X 2
Y 12.1053
X 3
Y 9.73684
X 4
Y 11.8421
15mm steel ball
Peak Freqeuncy for Sensor 1 to Sensor 4
Peak Frequency (kHz)
Sensor
X 1
Y 5
X 2
Y 6.05263
X 3
Y 9.73684
X 4
Y 11.8421
20mm steel ball
Peak Freqeuncy for Sensor 1 to Sensor 4
Peak Frequency (kHz)
Sensor
X 1
Y 5
X 2
Y 6.05263
X 3
Y 2.3684
X 4
Y 2.10526
25mm steel ball

(b)

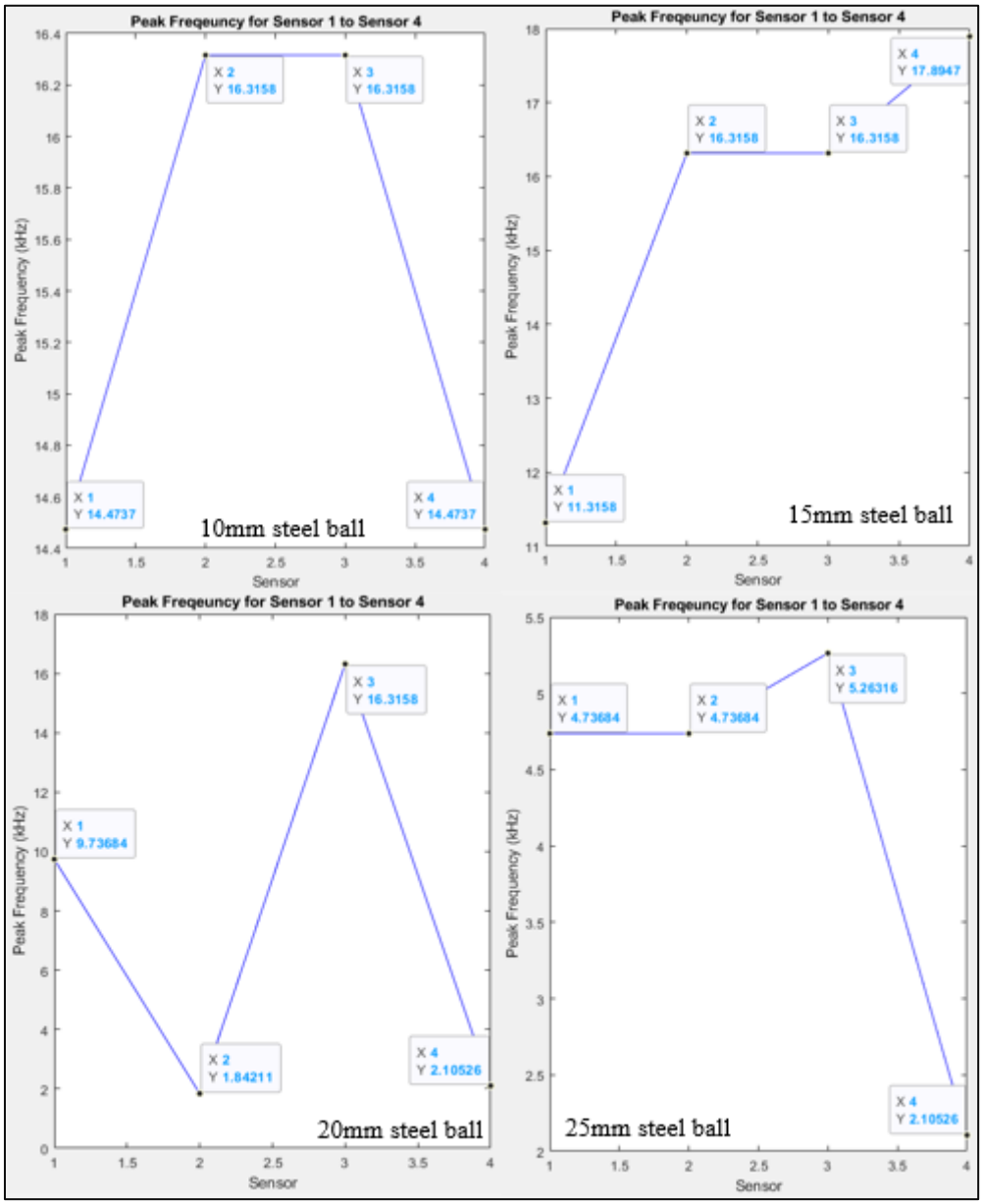
Peak Freqeuncy for Sensor 1 to Sensor 4
Peak Frequency (kHz)
Sensor
X 1
Y 14.4737
X 2
Y 16.3158
X 3
Y 16.3158
X 4
Y 14.4737
10mm steel ball
Peak Freqeuncy for Sensor 1 to Sensor 4
Peak Frequency (kHz)
Sensor
X 1
Y 11.3158
X 2
Y 16.3158
X 3
Y 16.3158
X 4
Y 17.8947
15mm steel ball
Peak Freqeuncy for Sensor 1 to Sensor 4
Peak Frequency (kHz)
Sensor
X 1
Y 9.73684
X 2
Y 1.84211
X 3
Y 16.3158
X 4
Y 2.10526
20mm steel ball
Peak Freqeuncy for Sensor 1 to Sensor 4
Peak Frequency (kHz)
Sensor
X 1
Y 4.73684
X 2
Y 4.73684
X 3
Y 5.26316
X 4
Y 2.10526
25mm steel ball

(c)

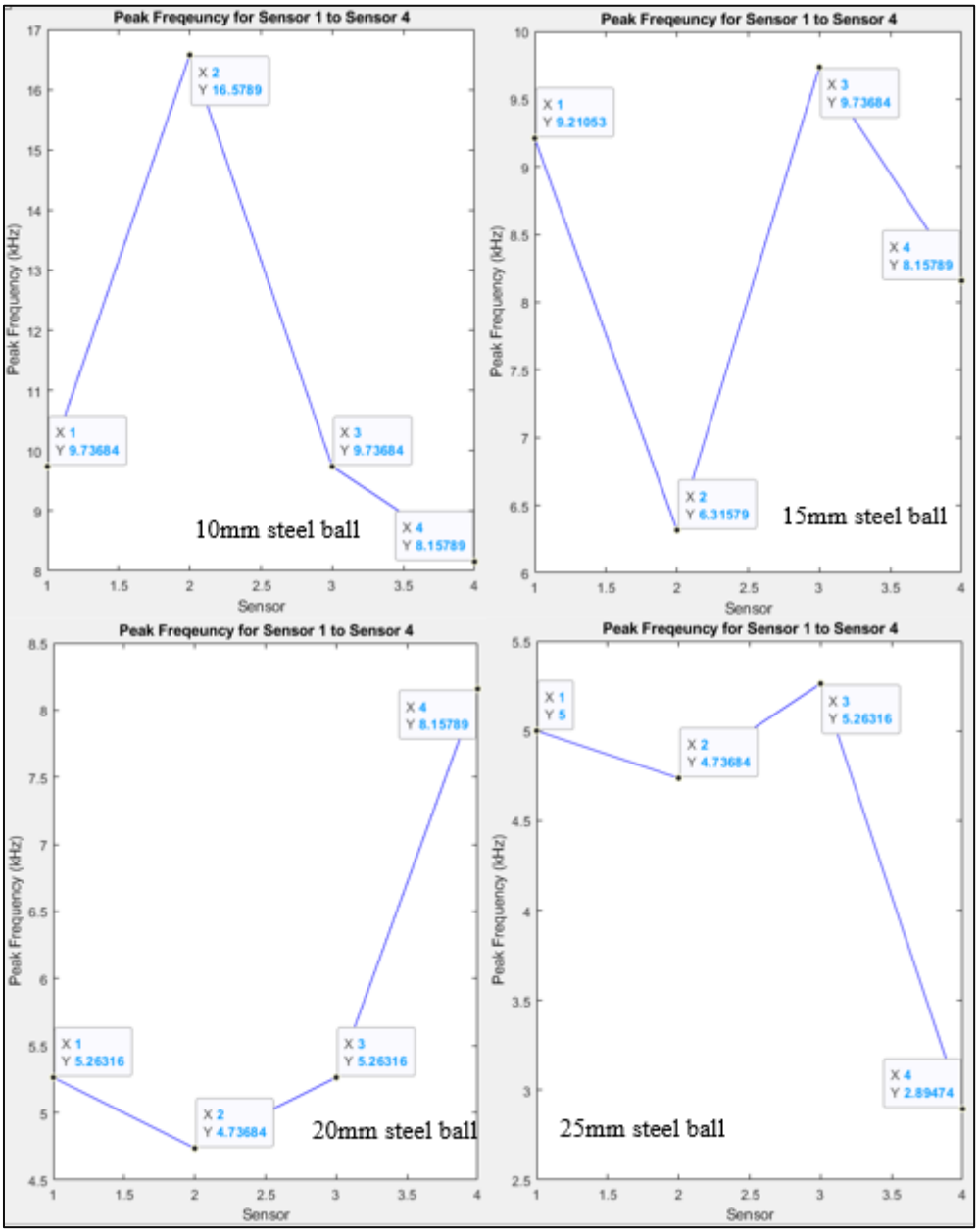
Peak Freqeuncy for Sensor 1 to Sensor 4
Peak Frequency (kHz)
Sensor
X 1
Y 9.73684
X 2
Y 16.5789
X 3
Y 9.73684
X 4
Y 8.15789
10mm steel ball
Peak Freqeuncy for Sensor 1 to Sensor 4
Peak Frequency (kHz)
Sensor
X 1
Y 9.21053
X 2
Y 6.31579
X 3
Y 9.73684
X 4
Y 8.15789
15mm steel ball
Peak Freqeuncy for Sensor 1 to Sensor 4
Peak Frequency (kHz)
Sensor
X 1
Y 5.26316
X 2
Y 4.73684
X 3
Y 5.26316
X 4
Y 8.15789
20mm steel ball
Peak Freqeuncy for Sensor 1 to Sensor 4
Peak Frequency (kHz)
Sensor
X 1
Y 5
X 2
Y 4.73684
X 3
Y 5.26316
X 4
Y 2.89474
25mm steel ball

(d)

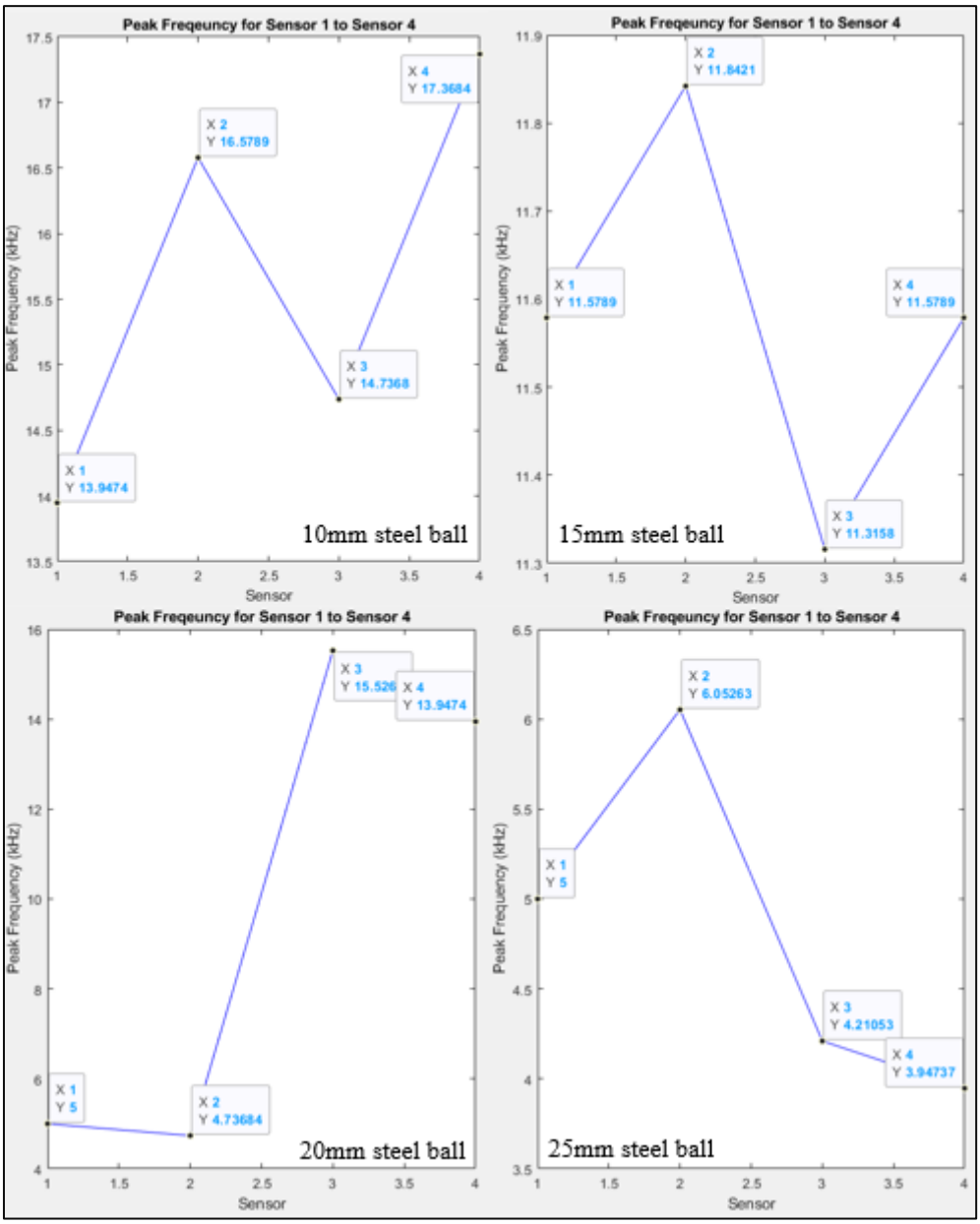

(e)

Appendix C-3: Peak Frequency for 425 mm Depth of Delamination and (a) 100 mm, (b) 200 mm, (c) 300 mm, (d) 400 mm, and (e) 500 mm Diameter of Delamination.

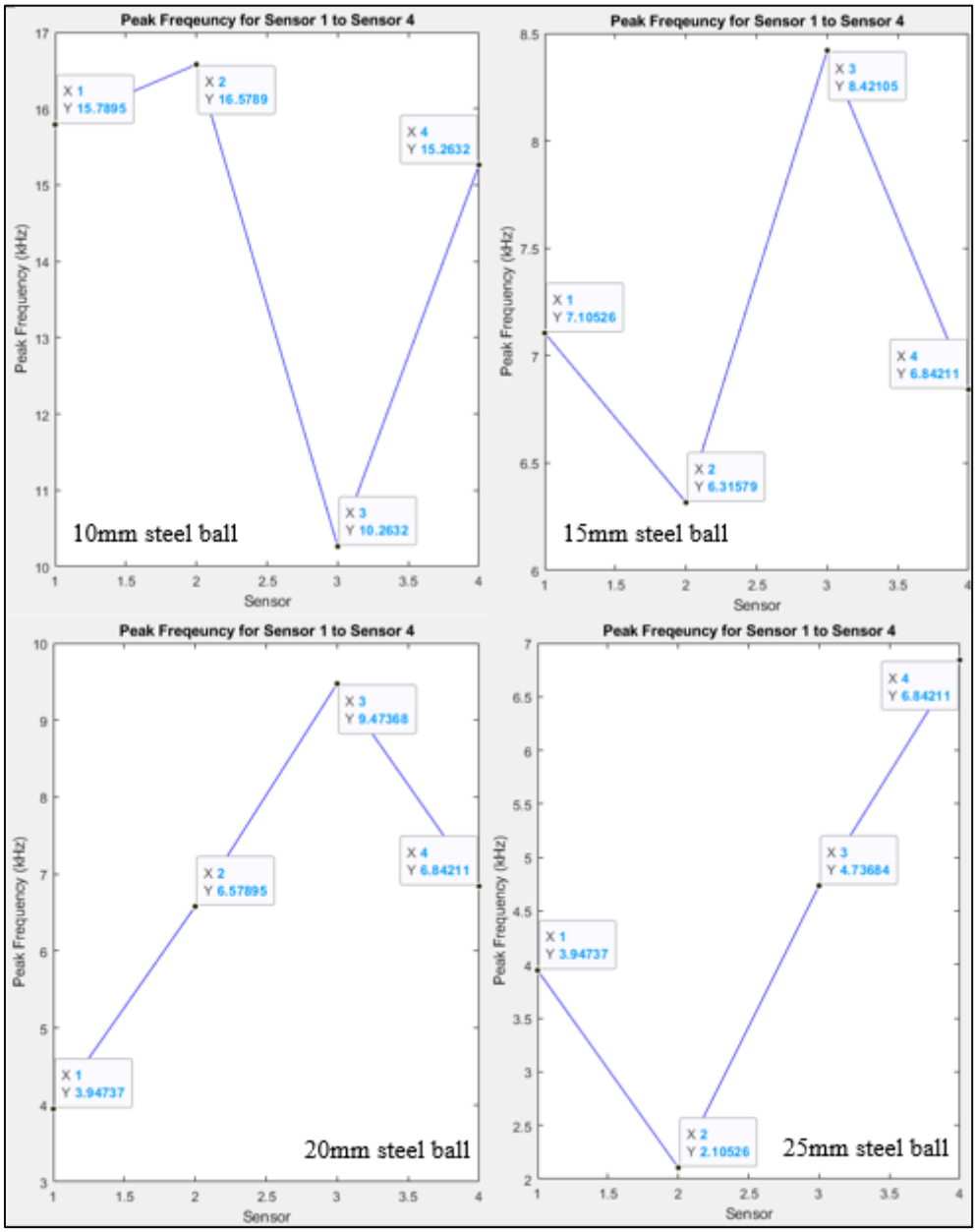
Peak Freqeuncy for Sensor 1 to Sensor 4
Peak Frequency (kHz)
Sensor
X 1
Y 15.7895
X 2
Y 16.5789
X 3
Y 10.2632
X 4
Y 15.2632
10mm steel ball
Peak Freqeuncy for Sensor 1 to Sensor 4
Peak Frequency (kHz)
Sensor
X 1
Y 7.10526
X 2
Y 6.31579
X 3
Y 8.42105
X 4
Y 6.84211
15mm steel ball
Peak Freqeuncy for Sensor 1 to Sensor 4
Peak Frequency (kHz)
Sensor
X 1
Y 3.94737
X 2
Y 6.57895
X 3
Y 9.47368
X 4
Y 6.84211
20mm steel ball
Peak Freqeuncy for Sensor 1 to Sensor 4
Peak Frequency (kHz)
Sensor
X 1
Y 3.94737
X 2
Y 2.10526
X 3
Y 4.73684
X 4
Y 6.84211
25mm steel ball

(a)

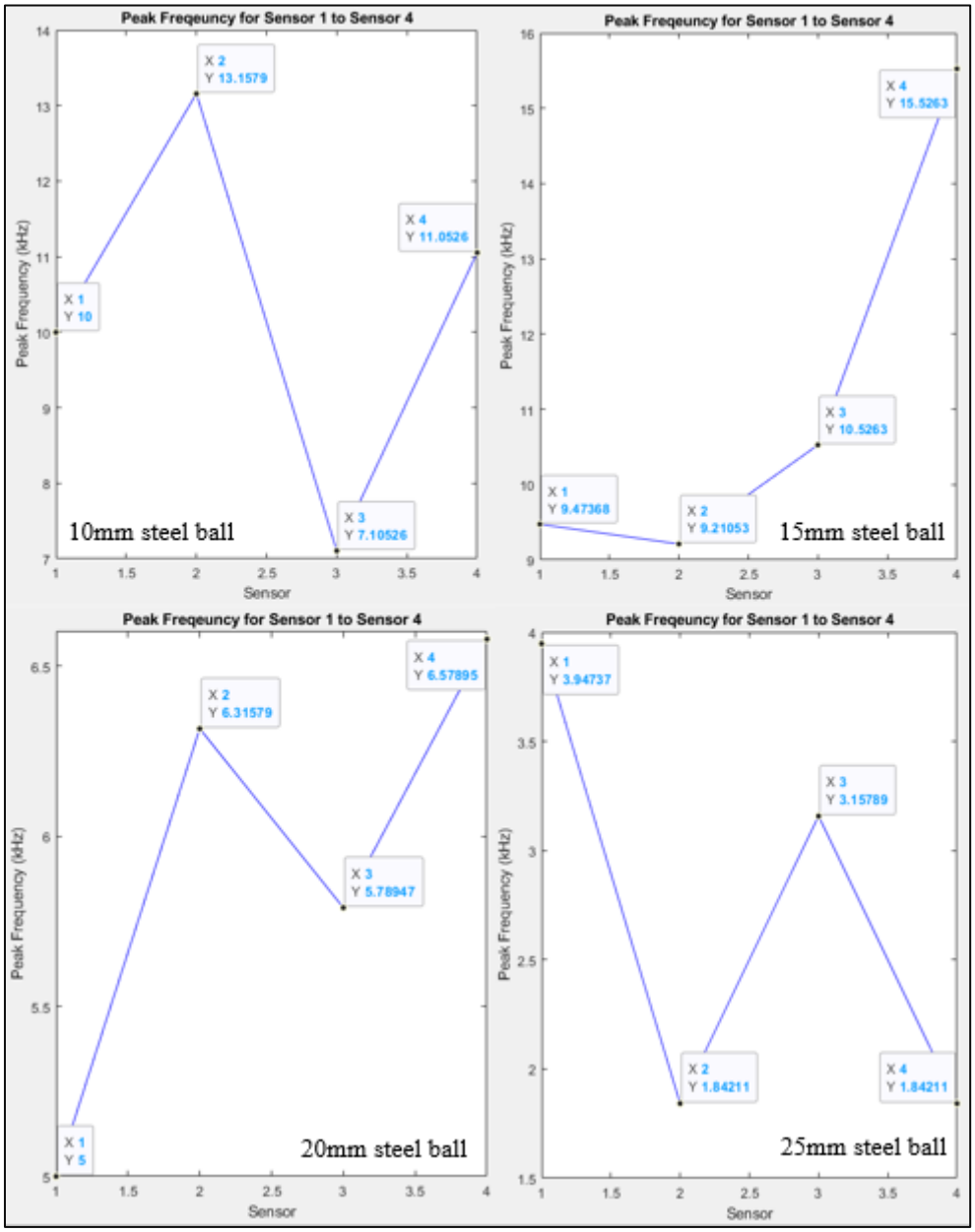
Peak Freqeuncy for Sensor 1 to Sensor 4
X 2
Y 13.1579
X 4
Y 11.0526
X 1
Y 10
X 3
Y 7.10526
10mm steel ball
Peak Frequency (kHz)
Sensor
Peak Freqeuncy for Sensor 1 to Sensor 4
X 4
Y 15.5263
X 3
Y 10.5263
X 1
Y 9.47368
X 2
Y 9.21053
15mm steel ball
Peak Frequency (kHz)
Sensor
Peak Freqeuncy for Sensor 1 to Sensor 4
X 4
Y 6.57895
X 2
Y 6.31579
X 3
Y 5.78947
X 1
Y 5
20mm steel ball
Peak Frequency (kHz)
Sensor
Peak Freqeuncy for Sensor 1 to Sensor 4
X 1
Y 3.94737
X 3
Y 3.15789
X 2
Y 1.84211
X 4
Y 1.84211
25mm steel ball
Peak Frequency (kHz)
Sensor

(b)

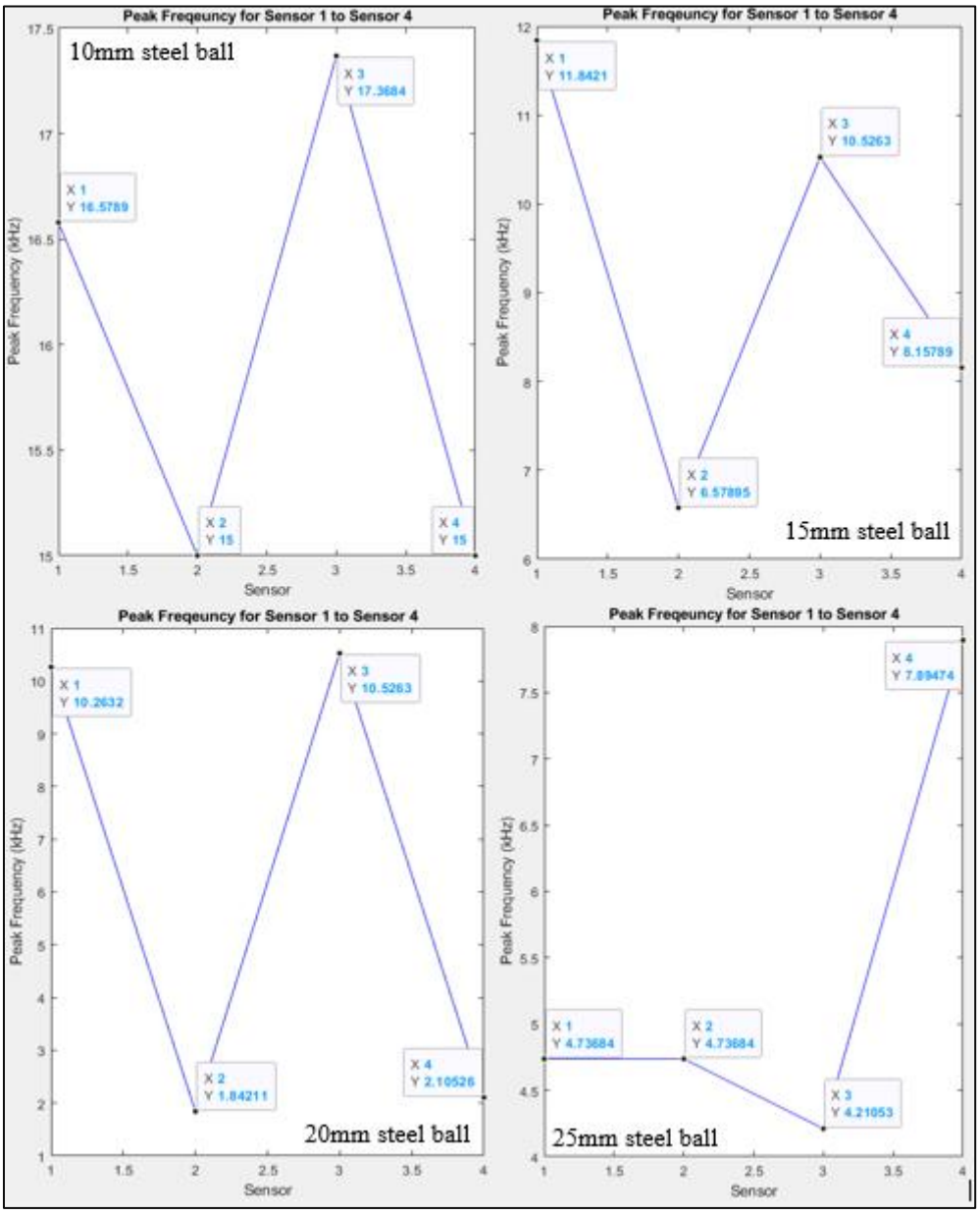
Peak Freqeuncy for Sensor 1 to Sensor 4
10mm steel ball
X 1
Y 16.5789
X 2
Y 15
X 3
Y 17.3684
X 4
Y 15
Peak Frequency (kHz)
Sensor
Peak Freqeuncy for Sensor 1 to Sensor 4
X 1
Y 11.8421
X 2
Y 6.57895
X 3
Y 10.5263
X 4
Y 8.15789
15mm steel ball
Peak Frequency (kHz)
Sensor
Peak Freqeuncy for Sensor 1 to Sensor 4
X 1
Y 10.2632
X 2
Y 1.84211
X 3
Y 10.5263
X 4
Y 2.10526
20mm steel ball
Peak Frequency (kHz)
Sensor
Peak Freqeuncy for Sensor 1 to Sensor 4
X 1
Y 4.73684
X 2
Y 4.73684
X 3
Y 4.21053
X 4
Y 7.89474
25mm steel ball
Peak Frequency (kHz)
Sensor

(c)

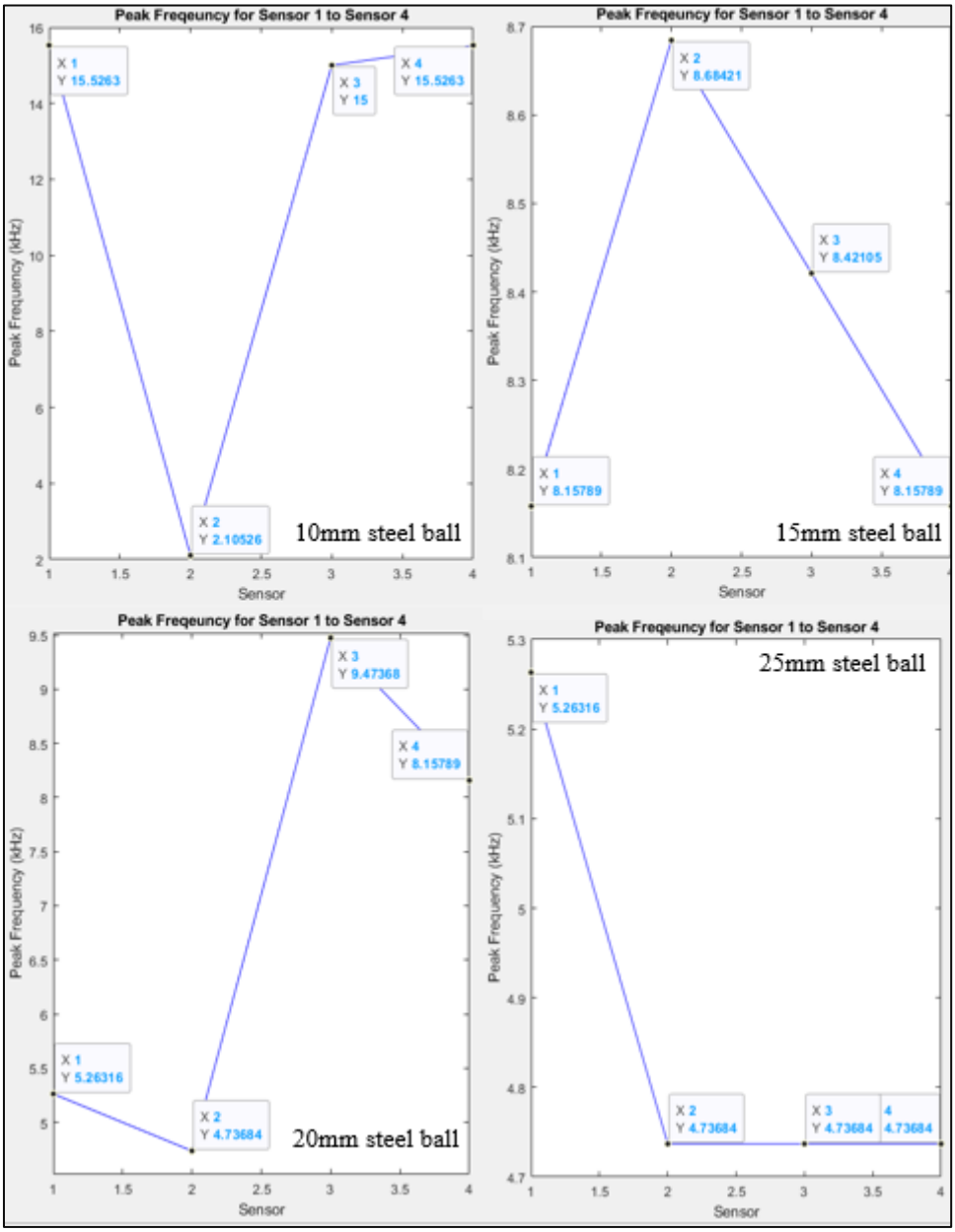

(d)

Appendix C-4: Peak Frequency for 25 mm Depth of Delamination and (a) 100 mm, (b) 200 mm, (c) 300 mm, and (d) 400 mm Diameter of Delamination.

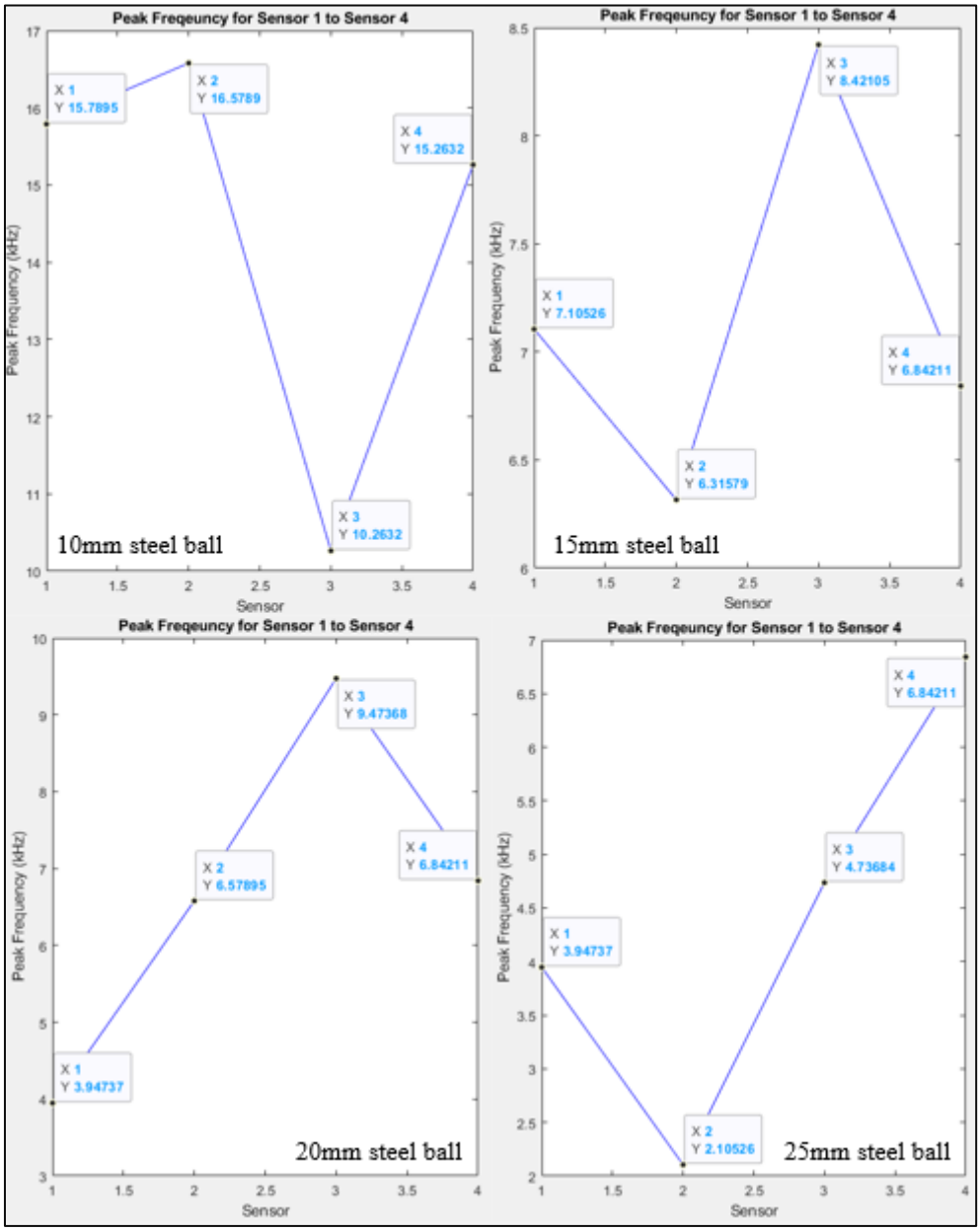
Peak Freqeuncy for Sensor 1 to Sensor 4
X 1
Y 15.7895
X 2
Y 16.5789
X 3
Y 10.2632
X 4
Y 15.2632
10mm steel ball
Peak Frequency (kHz)
Sensor
Peak Freqeuncy for Sensor 1 to Sensor 4
X 1
Y 7.10526
X 2
Y 6.31579
X 3
Y 8.42105
X 4
Y 6.84211
15mm steel ball
Peak Frequency (kHz)
Sensor
Peak Freqeuncy for Sensor 1 to Sensor 4
X 1
Y 3.94737
X 2
Y 6.57895
X 3
Y 9.47368
X 4
Y 6.84211
20mm steel ball
Peak Frequency (kHz)
Sensor
Peak Freqeuncy for Sensor 1 to Sensor 4
X 1
Y 3.94737
X 2
Y 2.10526
X 3
Y 4.73684
X 4
Y 6.84211
25mm steel ball
Peak Frequency (kHz)
Sensor

(a)

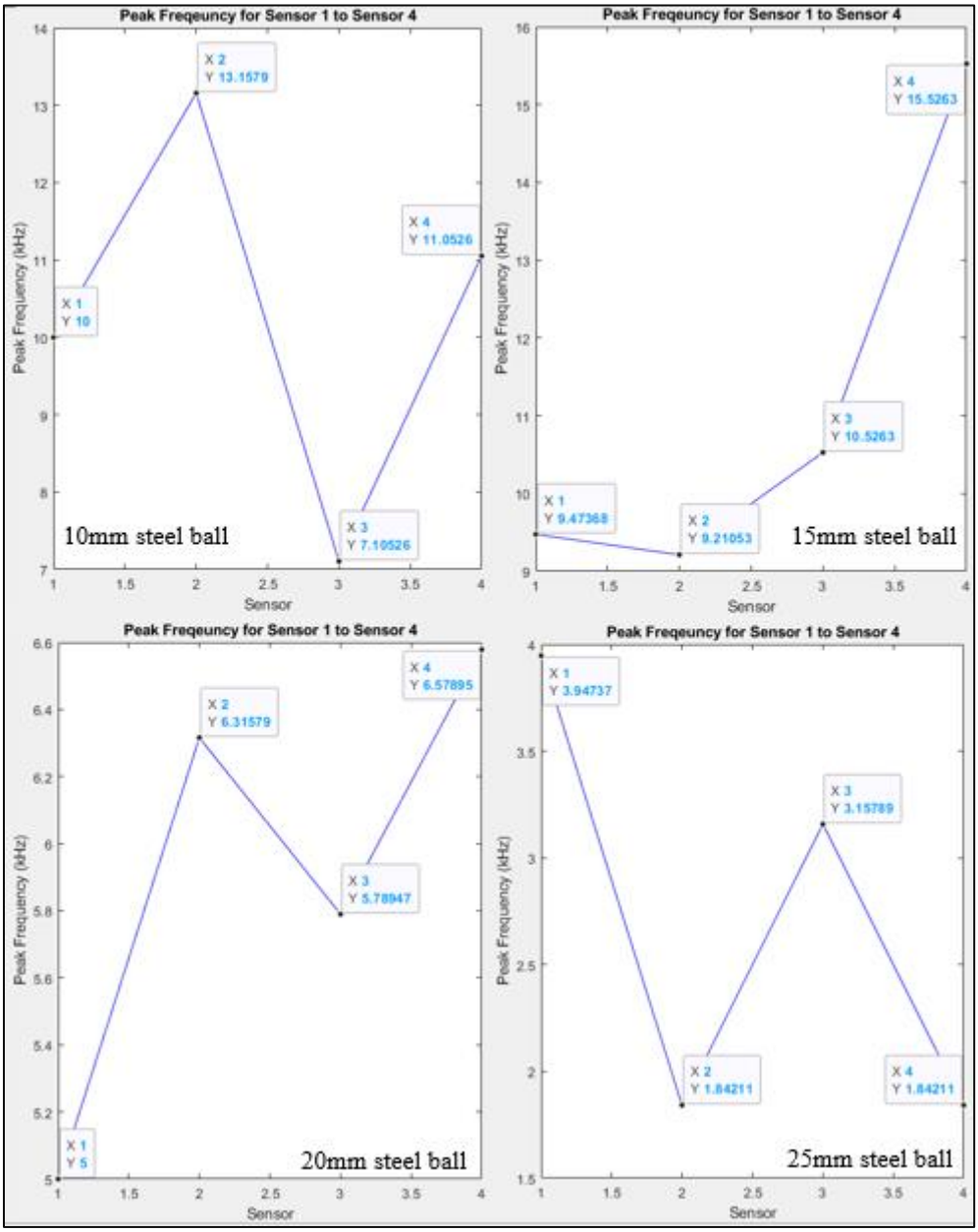
Peak Freqeuncy for Sensor 1 to Sensor 4
X 1
Y 10
X 2
Y 13.1579
X 3
Y 7.10526
X 4
Y 11.0526
10mm steel ball
Peak Frequency (kHz)
Sensor
Peak Freqeuncy for Sensor 1 to Sensor 4
X 1
Y 9.47368
X 2
Y 9.21053
X 3
Y 10.5263
X 4
Y 15.5263
15mm steel ball
Peak Frequency (kHz)
Sensor
Peak Freqeuncy for Sensor 1 to Sensor 4
X 1
Y 5
X 2
Y 6.31579
X 3
Y 5.78947
X 4
Y 6.57895
20mm steel ball
Peak Frequency (kHz)
Sensor
Peak Freqeuncy for Sensor 1 to Sensor 4
X 1
Y 3.94737
X 2
Y 1.84211
X 3
Y 3.15789
X 4
Y 1.84211
25mm steel ball
Peak Frequency (kHz)
Sensor

(b)

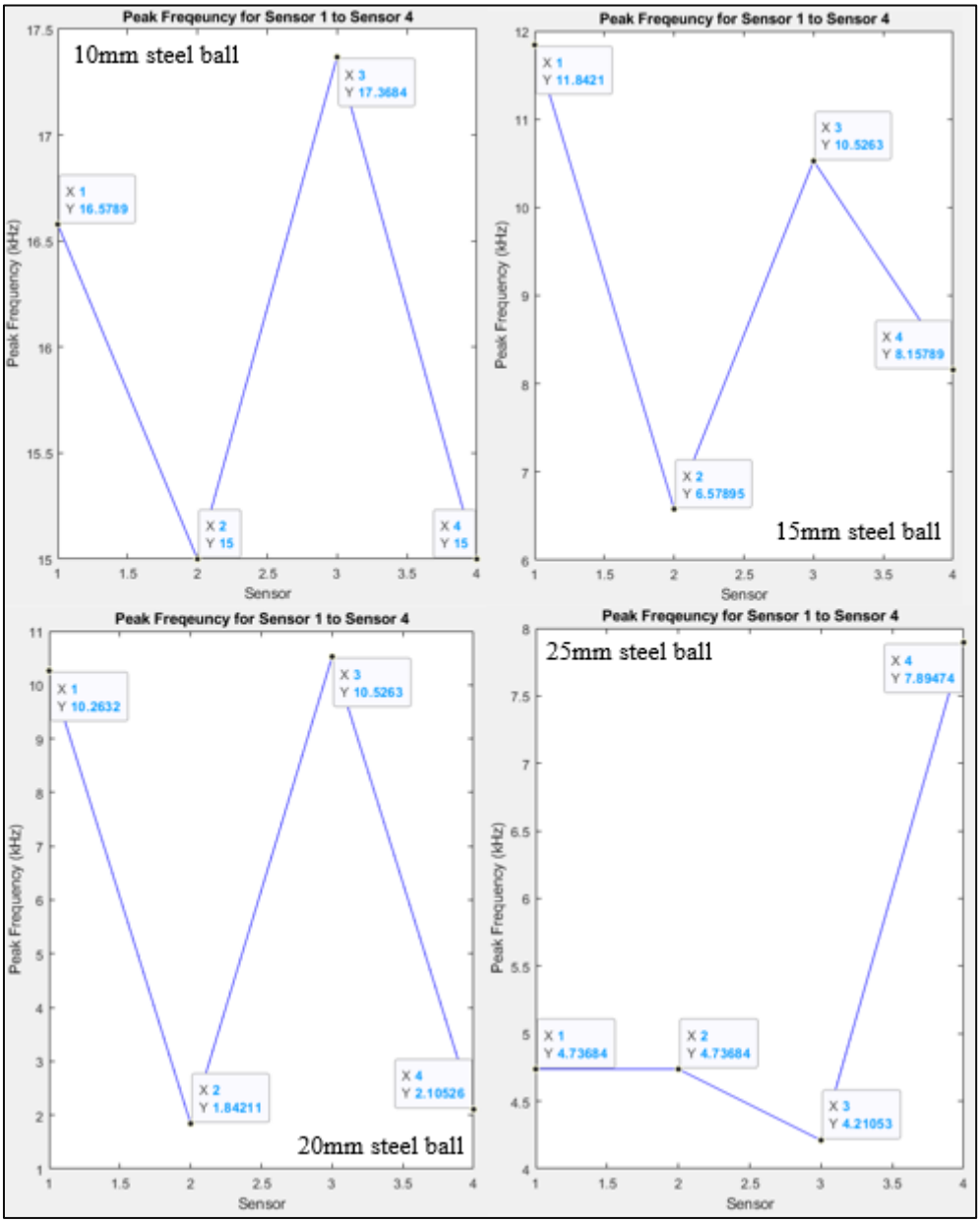
Peak Freqeuncy for Sensor 1 to Sensor 4
10mm steel ball
X 1
Y 16.5789
X 2
Y 15
X 3
Y 17.3684
X 4
Y 15
Peak Freqeuncy for Sensor 1 to Sensor 4
X 1
Y 11.8421
X 2
Y 6.57895
X 3
Y 10.5263
X 4
Y 8.15789
15mm steel ball
Peak Freqeuncy for Sensor 1 to Sensor 4
X 1
Y 10.2632
X 2
Y 1.84211
X 3
Y 10.5263
X 4
Y 2.10526
20mm steel ball
Peak Freqeuncy for Sensor 1 to Sensor 4
25mm steel ball
X 1
Y 4.73684
X 2
Y 4.73684
X 3
Y 4.21053
X 4
Y 7.89474
Peak Frequency (kHz)
Sensor

(c)

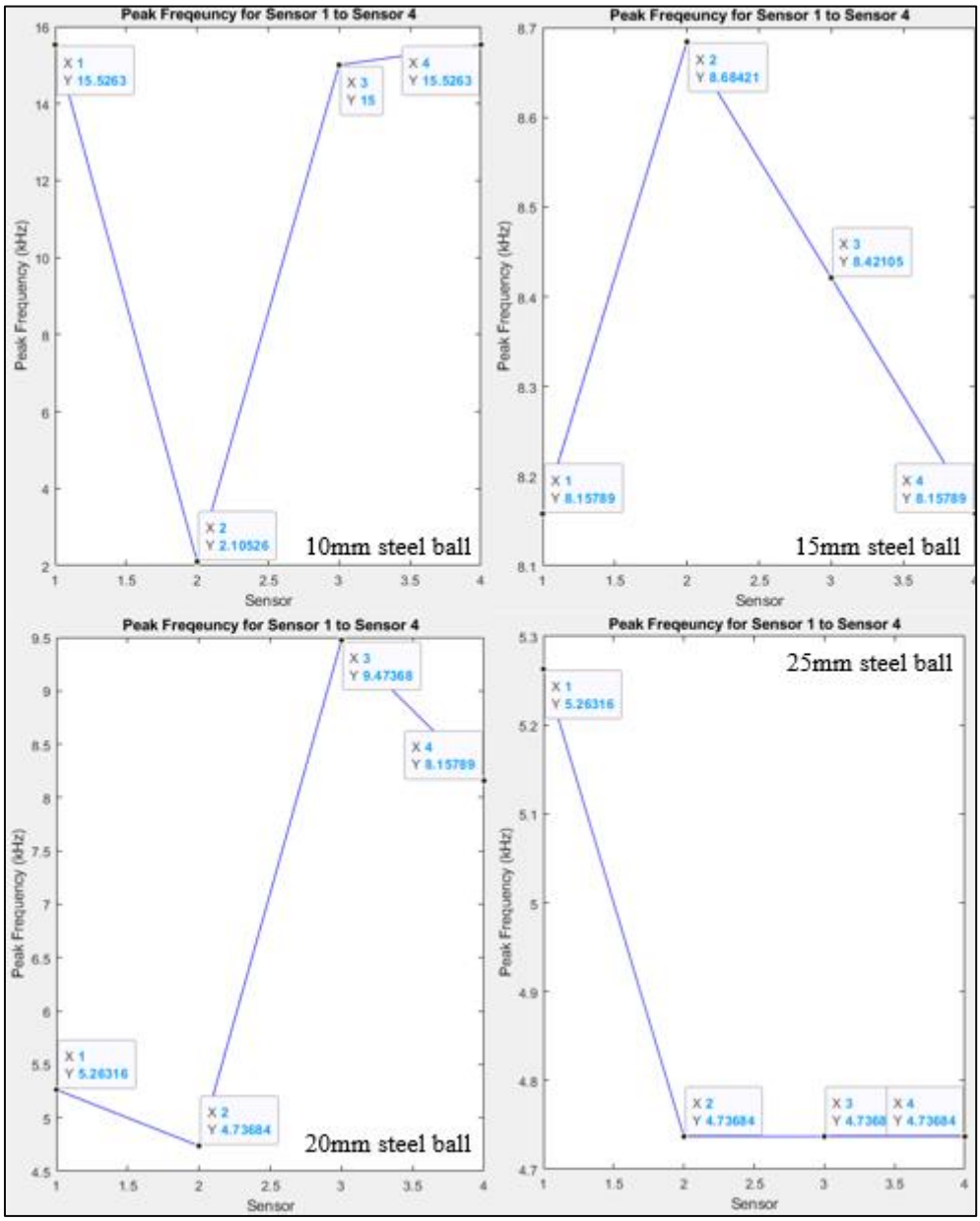

(d)

Appendix C-5: Peak Frequency for 825 mm Depth of Delamination and (a) 100 mm, (b) 200 mm, (c) 300 mm, and (d) 400 mm Diameter of Delamination.

APPENDIX D: Table of Amplitude and Time Received by each Sensor with respective Depth and Diameter of Delamination (Section 4.4).

Diameter of Delamination (mm)	Ball Diameter (mm)	Amplitude and time received by each sensor for 25 mm depth of delamination							
		Sensor 1		Sensor 2		Sensor 3		Sensor 4	
		Amplitude (V)	Time (s)	Amplitude (V)	Time (s)	Amplitude (V)	Time (s)	Amplitude (V)	Time (s)
100	10	0.0154	0.000755	-0.0898	0.00103183	-0.1982	0.00251667	-0.2984	0.00276833
	15	0.0308	0.000755	-0.0892	0.00103183	-0.196	0.0024915	-0.2964	0.00274317
	20	0.0464	0.000755	-0.075	0.00100667	-0.195	0.00261733	-0.2934	0.00266767
	25	0.0534	0.000755	-0.0652	0.00103183	-0.1982	0.0024915	-0.294	0.002718
200	10	0.0442	0.000755	-0.0866	0.00100667	-0.197	0.00244117	-0.2966	0.002718
	15	0.0658	0.000755	-0.0606	0.00100667	-0.196	0.00244117	-0.2958	0.00269283
	20	0.0808	0.000755	-0.0502	0.0010067	-0.1882	0.00244117	-0.2914	0.002718
	25	0.0876	0.000755	-0.0544	0.00100667	-0.1916	0.00244117	-0.2912	0.002718
300	10	0.041	0.000755	-0.0766	0.00100667	-0.1928	0.00244117	-0.293	0.002718
	15	0.0446	0.000755	-0.0648	0.00100667	-0.192	0.00244117	-0.2916	0.002718
	20	0.0604	0.000755	-0.0464	0.00100667	-0.1902	0.00244117	-0.289	0.002718
	25	0.067	0.000755	-0.0474	0.00100667	-0.1908	0.00244117	-0.2886	0.002718
400	10	0.0474	0.000755	-0.0732	0.00100667	-0.193	0.00244117	-0.2948	0.002718
	15	0.0648	0.000755	-0.0742	0.00100667	-0.193	0.00244117	-0.2944	0.002718
	20	0.0628	0.000755	-0.0568	0.00103183	-0.1932	0.00244117	-0.293	0.002718
	25	0.0738	0.000755	-0.0582	0.00103183	-0.1944	0.00244117	-0.2938	0.002718
500	10	0.046	0.000755	-0.0856	0.00100667	-0.1966	0.002416	-0.2978	0.00274317
	15	0.0582	0.000755	-0.0696	0.00100667	-0.1942	0.002416	-0.2942	0.00269283
	20	0.0734	0.000755	-0.0722	0.00100667	-0.1902	0.00246633	-0.2906	0.00274317
	25	0.0624	0.000755	-0.061	0.00100667	-0.1904	0.00244117	-0.2908	0.002718

Diameter of Delamination (mm)	Ball Diameter (mm)	Amplitude and time received by each sensor for 225 mm depth of delamination							
		Sensor 1		Sensor 2		Sensor 3		Sensor 4	
		Amplitude (V)	Time (s)	Amplitude (V)	Time (s)	Amplitude (V)	Time (s)	Amplitude (V)	Time (s)
100	10	0.0388	0.000755	-0.0948	0.00100667	-0.1978	0.002416	-0.296	0.00269283
	15	0.0704	0.000755	-0.0924	0.00100667	-0.1974	0.0026425	-0.2956	0.00269283
	20	0.0818	0.000755	-0.0524	0.00103183	-0.1896	0.00246633	-0.2922	0.002718
	25	0.0966	0.000755	-0.0148	0.00100667	-0.1912	0.00244117	-0.2894	0.002718
200	10	0.0354	0.000755	-0.0886	0.00100667	-0.1974	0.002416	-0.2966	0.00269283
	15	0.0438	0.000755	-0.0812	0.000906	-0.1974	0.00269283	-0.2984	0.00296967
	20	0.0674	0.000755	-0.079	0.00100667	-0.194	0.002416	-0.2944	0.00266767
	25	0.0652	0.000755	-0.05	0.00100667	-0.1908	0.002416	-0.2926	0.00269383
300	10	0.0422	0.000755	-0.0766	0.00100667	-0.1942	0.002416	-0.297	0.00269283
	15	0.0518	0.000755	-0.0584	0.00100667	-0.1918	0.002416	-0.2954	0.00269283
	20	0.0812	0.000755	-0.0728	0.00100667	-0.1876	0.002416	-0.2908	0.00269283
	25	0.1088	0.000755	-0.017	0.00103183	-0.1938	0.002567	-0.2908	0.00269283
400	10	0.0418	0.000755	-0.0796	0.00100667	-0.1962	0.00236567	-0.2988	0.00251667
	15	0.06	0.000755	-0.0856	0.00103183	-0.1968	0.00244117	-0.2942	0.002718
	20	0.0666	0.000755	-0.0722	0.00103183	-0.194	0.00244117	-0.2926	0.002718
	25	0.0808	0.000755	-0.0524	0.00103183	-0.189	0.00246633	-0.2858	0.00289417
500	10	0.032	0.000755	-0.0868	0.00100667	-0.1974	0.00244117	-0.2946	0.0026425
	15	0.0484	0.000755	-0.0804	0.00100667	-0.1942	0.00244117	-0.2972	0.00269283
	20	0.0652	0.000755	-0.0654	0.00103183	-0.1918	0.00244117	-0.2984	0.00266767
	25	0.0874	0.000755	-0.041	0.00103183	-0.1836	0.00244117	-0.298	0.002718

Diameter of Delamination (mm)	Ball Diameter (mm)	Amplitude and time received by each sensor for 425 mm depth of delamination							
		Sensor 1		Sensor 2		Sensor 3		Sensor 4	
		Amplitude (V)	Time (s)	Amplitude (V)	Time (s)	Amplitude (V)	Time (s)	Amplitude (V)	Time (s)
100	10	0.0324	0.000755	-0.0788	0.00103183	-0.1974	0.00246633	-0.2976	0.00274317
	15	0.0348	0.000755	-0.0886	0.000880833	-0.1922	0.00201333	-0.2954	0.00208883
	20	0.0428	0.000755	-0.0794	0.00100667	-0.1946	0.00239083	-0.2942	0.00246633
	25	0.038	0.000755	-0.0694	0.00103183	-0.1938	0.0026425	-0.291	0.00269283
200	10	0.0322	0.000755	-0.0828	0.00103183	-0.1952	0.00246633	-0.2958	0.00274317
	15	0.0316	0.000755	-0.086	0.000931167	-0.1958	0.00246633	-0.2944	0.00274317
	20	0.0328	0.000755	-0.0856	0.000855667	-0.194	0.00261733	-0.2952	0.002869
	25	0.0418	0.000755	-0.072	0.00103183	-0.1928	0.00246633	-0.2972	0.00274317
300	10	0.0268	0.000755	-0.0888	0.00100667	-0.1996	0.00261733	-0.2978	0.00274317
	15	0.0428	0.000755	-0.0812	0.00103183	-0.1956	0.00246633	-0.296	0.00274317
	20	0.0298	0.000755	-0.0886	0.000805333	-0.1974	0.0024915	-0.2948	0.00274317
	25	0.0382	0.000755	-0.0762	0.00103183	-0.1934	0.0026425	-0.2956	0.00291933
400	10	0.0266	0.000755	-0.0896	0.00103183	-0.1976	0.00246633	-0.2972	0.00274317
	15	0.0482	0.000755	-0.0916	0.00100667	-0.1972	0.00302	-0.297	0.003171
	20	0.0456	0.000755	-0.0842	0.00103183	-0.198	0.00261733	-0.2968	0.00274317
	25	0.0592	0.000755	-0.0616	0.00103183	-0.1932	0.0026425	-0.2906	0.00291933
500	10	0.033	0.000755	-0.093	0.00103183	-0.196	0.00246633	-0.2978	0.002718
	15	0.0422	0.000755	-0.0884	0.00100667	-0.1992	0.00269283	-0.296	0.00274317
	20	0.0448	0.000755	-0.076	0.00100667	-0.195	0.00239083	-0.2948	0.0026425
	25	0.0374	0.000755	-0.0708	0.00103183	-0.1938	0.00244117	-0.296	0.00269283

Diameter of Delamination (mm)	Ball Diameter (mm)	Amplitude and time received by each sensor for 625 mm depth of delamination							
		Sensor 1		Sensor 2		Sensor 3		Sensor 4	
		Amplitude (V)	Time (s)	Amplitude (V)	Time (s)	Amplitude (V)	Time (s)	Amplitude (V)	Time (s)
100	10	0.043	0.000755	-0.085	0.000956333	-0.1948	0.00244117	-0.2964	0.002718
	15	0.0538	0.000755	-0.0712	0.00103183	-0.1972	0.00254183	-0.2954	0.00266767
	20	0.0554	0.000755	-0.0662	0.00103183	-0.1872	0.00244117	-0.2938	0.00269283
	25	0.0622	0.000755	-0.0582	0.00100667	-0.1888	0.00244117	-0.295	0.002718
200	10	0.0432	0.000755	-0.074	0.00103183	-0.1936	0.00244117	-0.2944	0.002718
	15	0.0356	0.000755	-0.0856	0.00100667	-0.1942	0.00244117	-0.294	0.00269283
	20	0.06	0.000755	-0.0676	0.00100667	-0.1928	0.002416	-0.2942	0.00269283
	25	0.065	0.000755	-0.0506	0.00103183	-0.1874	0.00259217	-0.2898	0.002869
300	10	0.0416	0.000755	-0.0808	0.00103183	-0.195	0.00244117	-0.2992	0.00269283
	15	0.0428	0.000755	-0.0922	0.000931167	-0.1932	0.00246633	-0.2962	0.00269283
	20	0.0512	0.000755	-0.0792	0.00100667	-0.1972	0.002567	-0.2948	0.00281867
	25	0.06	0.000755	-0.0656	0.00103183	-0.1942	0.00261733	-0.2926	0.002869
400	10	0.0376	0.000755	-0.0922	0.000956333	-0.1956	0.00246633	-0.2966	0.002718
	15	0.0404	0.000755	-0.0872	0.00100667	-0.1952	0.00246633	-0.2962	0.002718
	20	0.052	0.000755	-0.0768	0.00103183	-0.1918	0.00244117	-0.2952	0.00266767
	25	0.0764	0.000755	-0.0706	0.000855667	-0.1862	0.002416	-0.2906	0.002718
500	10	0.0554	0.000755	-0.0724	0.00100667	-0.1948	0.00239083	-0.2972	0.002567
	15	0.0658	0.000755	-0.0666	0.00103183	-0.1894	0.002567	-0.2918	0.002718
	20	0.0896	0.000755	0.0488	0.00103183	-0.1882	0.00246633	-0.291	0.00274317
	25	0.0928	0.000755	-0.0338	0.00103183	-0.1826	0.00246633	-0.2898	0.00274317

Diameter of Delamination (mm)	Ball Diameter (mm)	Amplitude and time received by each sensor for 825 mm depth of delamination							
		Sensor 1		Sensor 2		Sensor 3		Sensor 4	
		Amplitude (V)	Time (s)	Amplitude (V)	Time (s)	Amplitude (V)	Time (s)	Amplitude (V)	Time (s)
100	10	0.043	0.000755	-0.085	0.000956333	-0.1984	0.00244117	-0.2978	0.0026425
	15	0.0538	0.000755	-0.0712	0.00103183	-0.1972	0.00254183	-0.2954	0.00269283
	20	0.0554	0.000755	-0.0662	0.00103183	-0.1908	0.002567	-0.2928	0.00284383
	25	0.0622	0.000755	-0.0582	0.00100667	-0.1956	0.0026425	-0.2934	0.002869
200	10	0.0432	0.000755	-0.074	0.00103183	-0.1936	0.00244117	-0.2944	0.002718
	15	0.0356	0.000755	-0.0856	0.00100667	-0.1942	0.00244117	-0.294	0.00269283
	20	0.06	0.000755	-0.0676	0.00100667	-0.1928	0.002416	-0.2942	0.00269283
	25	0.065	0.000755	-0.0506	0.00103183	-0.1874	0.00259217	-0.2898	0.002869
300	10	0.0416	0.000755	-0.0808	0.00103183	-0.195	0.00244117	-0.298	0.002718
	15	0.0428	0.000755	-0.0808	0.00108217	-0.1968	0.00284383	-0.2952	0.0029445
	20	0.0512	0.000755	-0.0792	0.00100667	-0.1972	0.002567	-0.2948	0.00281867
	25	0.06	0.000755	-0.0656	0.00103183	-0.1942	0.00261733	-0.2926	0.002869
400	10	0.0376	0.000755	-0.0922	0.000956333	-0.1956	0.00246633	-0.2966	0.002718
	15	0.0404	0.000755	-0.0872	0.00100667	-0.1974	0.002567	-0.2962	0.002718
	20	0.052	0.000755	-0.0768	0.00103183	-0.1918	0.00244117	-0.2952	0.00266767
	25	0.0764	0.000755	-0.0706	0.000855667	-0.1862	0.002416	-0.2906	0.002718
500	10	0.0554	0.000755	-0.0724	0.00100667	-0.1948	0.00239083	-0.2972	0.002567
	15	0.0658	0.000755	-0.0666	0.00103183	-0.1894	0.002567	-0.2918	0.002718
	20	0.0896	0.000755	-0.0488	0.00103183	-0.1882	0.00246633	-0.2886	0.00259217
	25	0.0928	0.000755	-0.0338	0.00103183	-0.1826	0.00246633	-0.2898	0.00274317

Diameter of Delamination (mm)	Ball Diameter (mm)	Amplitude and time received by each sensor for unsound concrete							
		Sensor 1		Sensor 2		Sensor 3		Sensor 4	
		Amplitude (V)	Time (s)	Amplitude (V)	Time (s)	Amplitude (V)	Time (s)	Amplitude (V)	Time (s)
control	10	0.0382	0.000755	-0.0784	0.00100667	-0.2008	0.002265	-0.2986	0.00251667
	15	0.0336	0.000755	-0.087	0.000855667	-0.1926	0.001223317	-0.2914	0.00125833
	20	0.0546	0.000755	-0.0566	0.00118283	-0.1866	0.00145967	-0.2892	0.00153517
	25	0.0682	0.000755	-0.0638	0.000855667	-0.1932	0.00125833	-0.2958	0.00130867

APPENDIX E: Table of Calculated Attenuation Rate with Respective Depth and Diameter of Delamination (Section 4.4.1).

Diameter of Delamination (mm)	Ball Diameter (mm)	Attenuation rate of each sensor at 25 mm depth of delamination		
		Sensor 2	Sensor 3	Sensor 4
100	10	683%	1387%	2038%
	15	390%	736%	1062%
	20	262%	520%	732%
	25	222%	471%	651%
200	10	296%	546%	771%
	15	192%	398%	550%
	20	162%	333%	461%
	25	162%	319%	432%
300	10	287%	570%	815%
	15	245%	530%	754%
	20	177%	415%	578%
	25	171%	385%	531%
400	10	254%	507%	722%
	15	215%	398%	554%
	20	190%	408%	567%
	25	179%	363%	498%
500	10	286%	527%	747%
	15	220%	434%	605%
	20	198%	359%	496%
	25	198%	405%	566%

Diameter of Delamination (mm)	Ball Diameter (mm)	Attenuation rate of each sensor at 225 mm depth of delamination		
		Sensor 2	Sensor 3	Sensor 4
100	10	344%	610%	863%
	15	231%	380%	520%
	20	164%	332%	457%
	25	115%	298%	400%
200	10	350%	658%	938%
	15	285%	551%	781%
	20	217%	388%	537%
	25	177%	393%	549%
300	10	282%	560%	804%
	15	213%	470%	670%
	20	190%	331%	458%
	25	116%	278%	367%
400	10	290%	569%	815%
	15	243%	428%	590%
	20	208%	391%	539%
	25	165%	334%	454%
500	10	371%	717%	1021%
	15	266%	501%	714%
	20	200%	394%	558%
	25	147%	310%	441%

Diameter of Delamination (mm)	Ball Diameter (mm)	Attenuation rate of each sensor at 425 mm depth of delamination		
		Sensor 2	Sensor 3	Sensor 4
100	10	343%	709%	1019%
	15	355%	652%	949%
	20	286%	555%	787%
	25	283%	610%	866%
200	10	357%	706%	1019%
	15	372%	720%	1032%
	20	361%	691%	1000%
	25	272%	561%	811%
300	10	431%	845%	1211%
	15	290%	557%	792%
	20	397%	762%	1089%
	25	299%	606%	874%
400	10	437%	843%	1217%
	15	290%	509%	716%
	20	285%	534%	751%
	25	204%	426%	591%
500	10	382%	694%	1002%
	15	309%	572%	801%
	20	270%	535%	758%
	25	289%	618%	891%

Diameter of Delamination (mm)	Ball Diameter (mm)	Attenuation rate of each sensor at 625 mm depth of delamination		
		Sensor 2	Sensor 3	Sensor 4
100	10	298%	553%	789%
	15	232%	467%	649%
	20	219%	438%	630%
	25	194%	404%	574%
200	10	271%	548%	781%
	15	340%	646%	926%
	20	213%	421%	590%
	25	178%	388%	546%
300	10	294%	569%	819%
	15	315%	551%	792%
	20	255%	485%	676%
	25	209%	424%	588%
400	10	345%	620%	889%
	15	316%	583%	833%
	20	248%	469%	668%
	25	192%	344%	480%
500	10	231%	452%	636%
	15	201%	388%	543%
	20	46%	310%	425%
	25	136%	297%	412%

Diameter of Delamination (mm)	Ball Diameter (mm)	Attenuation rate of each sensor at 825 mm depth of delamination		
		Sensor 2	Sensor 3	Sensor 4
100	10	298%	561%	793%
	15	232%	467%	649%
	20	219%	444%	629%
	25	194%	414%	572%
200	10	271%	548%	781%
	15	340%	646%	926%
	20	213%	421%	590%
	25	178%	388%	546%
300	10	294%	569%	816%
	15	289%	560%	790%
	20	255%	485%	676%
	25	209%	424%	588%
400	10	345%	620%	889%
	15	316%	589%	833%
	20	248%	469%	668%
	25	192%	344%	480%
500	10	231%	452%	636%
	15	201%	388%	543%
	20	154%	310%	422%
	25	136%	297%	412%

Diameter of Delamination (mm)	Ball Diameter (mm)	Attenuation Rate of each sensor for unsound concrete		
		Sensor 2	Sensor 3	Sensor 4
control	10	305%	626%	882%
	15	359%	673%	967%
	20	204%	442%	630%
	25	194%	383%	534%

APPENDIX F: Table of Calculated R-wave Velocity with Respective Depth and Diameter of Delamination (Section 4.4.2).

Diameter of Delamination (mm)	Ball Diameter (mm)	Velocity of propagated wave at 25 mm depth of delamination (m/s)		
		Sensor 2	Sensor 3	Sensor 4
100	10	361.23	336.74	397.36
	15	361.23	342.54	397.35
	20	397.35	310.43	1986.49
	25	361.23	342.54	441.50
200	10	397.35	348.55	361.23
	15	397.35	348.55	397.36
	20	397.30	348.56	361.23
	25	397.35	348.55	361.23
300	10	397.35	348.55	361.23
	15	397.35	348.55	361.23
	20	397.35	348.55	361.23
	25	397.35	348.55	361.23
400	10	397.35	348.55	361.23
	15	397.35	348.55	361.23
	20	361.23	354.78	361.23
	25	361.23	354.78	361.23
500	10	397.35	354.78	305.65
	15	397.35	354.78	361.23
	20	397.35	342.55	361.22
	25	397.35	348.55	361.23

Diameter of Delamination (mm)	Ball Diameter (mm)	Velocity of propagated wave at 225 mm depth of delamination (m/s)		
		Sensor 2	Sensor 3	Sensor 4
100	10	397.35	354.78	361.23
	15	397.35	305.66	1986.89
	20	361.23	348.55	397.35
	25	397.35	348.55	361.23
200	10	397.35	354.78	361.23
	15	662.25	279.83	361.22
	20	397.35	354.78	397.35
	25	397.35	354.78	359.93
300	10	397.35	354.78	361.23
	15	397.35	354.78	361.23
	20	397.35	354.78	361.23
	25	361.23	325.70	794.72
400	10	397.35	367.92	662.25
	15	361.23	354.78	361.23
	20	361.23	354.78	361.23
	25	361.23	348.55	233.73
500	10	397.35	348.55	496.70
	15	397.35	348.55	397.36
	20	361.23	354.78	441.50
	25	361.23	354.78	361.23

Diameter of Delamination (mm)	Ball Diameter (mm)	Velocity of propagated wave at 425 mm depth of delamination (m/s)		
		Sensor 2	Sensor 3	Sensor 4
100	10	361.23	348.55	361.22
	15	794.70	441.50	1324.50
	20	397.35	361.23	1324.50
	25	361.23	310.43	1986.89
200	10	361.23	348.55	361.22
	15	567.64	325.70	361.22
	20	993.37	283.82	397.35
	25	361.23	348.55	361.22
300	10	397.35	310.43	794.66
	15	361.23	348.55	361.22
	20	1986.77	296.53	397.35
	25	361.23	310.43	361.23
400	10	361.23	348.55	361.22
	15	397.35	248.34	662.25
	20	361.23	315.36	794.66
	25	361.23	310.43	361.23
500	10	361.23	348.55	397.35
	15	397.35	296.53	1986.49
	20	397.35	361.23	397.35
	25	361.23	354.78	397.36

Diameter of Delamination (mm)	Ball Diameter (mm)	Velocity of propagated wave at 625 mm depth of delamination (m/s)		
		Sensor 2	Sensor 3	Sensor 4
100	10	496.69	336.74	361.23
	15	361.23	331.13	794.66
	20	361.23	354.78	397.36
	25	397.35	348.55	361.23
200	10	361.23	354.78	361.23
	15	397.35	348.55	397.36
	20	397.35	354.78	361.23
	25	361.23	320.44	361.23
300	10	361.23	354.78	397.36
	15	567.64	325.70	441.50
	20	397.35	320.45	397.35
	25	361.23	315.36	397.35
400	10	496.69	331.13	397.35
	15	397.35	342.55	397.35
	20	361.23	354.78	441.50
	25	993.37	320.44	331.13
500	10	397.35	361.23	567.63
	15	361.23	325.70	662.25
	20	361.23	348.55	361.22
	25	361.23	348.55	361.22

Diameter of Delamination (mm)	Ball Diameter (mm)	Velocity of propagated wave at 825 mm depth of delamination (m/s)		
		Sensor 2	Sensor 3	Sensor 4
100	10	496.69	336.74	496.70
	15	361.23	331.13	662.25
	20	361.23	325.70	361.23
	25	397.35	305.66	441.50
200	10	361.23	354.78	361.23
	15	397.35	348.55	397.36
	20	397.35	354.78	361.23
	25	361.23	320.44	361.23
300	10	361.23	354.78	361.23
	15	305.65	283.82	993.34
	20	397.35	320.45	397.35
	25	361.23	315.36	397.35
400	10	496.69	331.13	397.35
	15	397.35	320.45	662.25
	20	361.23	354.78	441.50
	25	993.37	320.44	331.13
500	10	397.35	361.23	567.63
	15	361.23	325.70	662.25
	20	361.23	348.55	794.66
	25	361.23	348.55	361.22

Diameter of Delamination (mm)	Ball Diameter (mm)	Velocity of propagated wave for unsound concrete (m/s)		
		Sensor 2	Sensor 3	Sensor 4
control	10	397.35	397.35	397.35
	15	993.37	1359.99	2856.08
	20	233.74	1806.10	1324.50
	25	993.37	1241.73	1986.49

APPENDIX G: Table of Peak Amplitude and Peak Frequency with Respective Depth and Diameter of Delamination (Section 4.5.1 and Section 4.5.2).

Diameter of Delamination (mm)	Ball Diameter (mm)	Peak amplitude and peak frequency for 25 mm depth of delamination							
		Sensor 1		Sensor 2		Sensor 3		Sensor 4	
		Amplitude (V)	Peak Frequency (kHz)	Amplitude (V)	Peak Frequency (kHz)	Amplitude (V)	Peak Frequency (kHz)	Amplitude (V)	Peak Frequency (kHz)
100	10	0.0980489	7.63158	0.100969	7.36842	0.0278078	7.36842	0.0229281	17.6316
	15	0.106654	13.9474	0.0668788	8.68421	0.0432039	12.3684	0.0579886	17.6316
	20	0.230652	5	0.196081	5	0.0998749	10	0.10484	9.47368
	25	0.295621	5.26316	0.262088	5.52632	0.0648651	5.78947	0.0640653	5.78947
200	10	0.200767	13.6842	0.196344	15	0.05117888	17.8947	0.00332838	7.10526
	15	0.257731	15.2632	0.31091	15	0.062649	16.0526	0.0454925	5.52632
	20	0.352076	5.26316	0.29762	15	0.0839132	1.84211	0.084289	7.10526
	25	0.500653	6.05263	0.559298	6.31579	0.109231	1.84211	0.101068	5.52632
300	10	0.18787	7.36842	0.16469	16.5789	0.0487632	7.6315	0.0331558	7.10526
	15	0.376535	13.4211	0.33606	13.4211	0.0667266	15	0.0552045	2.10526
	20	0.395629	5.26316	0.293768	5	0.0816449	5.26316	0.0935912	2.10526
	25	0.459029	4.47368	0.396812	4.73684	0.135726	3.68421	0.158777	2.10526
400	10	0.216705	7.36842	0.193237	7.36842	0.0511053	7.10526	0.0291844	12.3684
	15	0.270889	10.5263	0.1929	12.6316	0.0451063	1.57895	0.0352122	9.21053
	20	0.393507	3.42105	0.353382	6.31579	0.0992719	1.57895	0.0629127	2.89474
	25	0.440061	3.15789	0.403188	6.05263	0.131395	1.57895	0.0881136	1.57895
500	10	0.149853	16.0526	0.12003	7.63158	0.0397736	13.4211	0.0318434	14.7368
	15	0.236655	8.94737	0.217354	2.36842	0.0522758	13.1579	0.046915	6.84211
	20	0.378786	7.10526	0.401593	2.36842	0.072968	4.73684	0.0811461	2.89474
	25	0.456333	6.31579	0.442082	2.36842	0.0988865	1.57895	0.134102	1.57895

Diameter of Delamination (mm)	Ball Diameter (mm)	Peak amplitude and peak frequency for 225 mm depth of delamination							
		Sensor 1		Sensor 2		Sensor 3		Sensor 4	
		Amplitude (V)	Peak Frequency (kHz)	Amplitude (V)	Peak Frequency (kHz)	Amplitude (V)	Peak Frequency (kHz)	Amplitude (V)	Peak Frequency (kHz)
100	10	0.191025	16.0526	0.13686	19.7368	0.0403924	15.7895	0.0596109	19.7368
	15	0.268615	17.3684	0.193942	9.47368	0.0803089	8.94737	0.066005	11.0526
	20	0.332879	6.84211	0.394157	8.94737	0.12555	8.15789	0.098458	7.89474
	25	0.620291	5.78947	0.581546	6.05263	0.902551	1.57895	0.101723	6.05263
200	10	0.165968	17.3684	0.167098	18.6842	0.0470092	11.8421	0.0889618	17.3684
	15	0.214483	8.68421	0.28539	8.68421	0.0709542	8.42105	0.140298	17.6316
	20	0.370831	8.15789	0.235337	8.68421	0.0905794	8.15789	0.0669405	7.89474
	25	0.542486	5	0.584412	6.05263	0.166741	1.84211	0.244455	1.84211
300	10	0.286276	20	0.108371	18.4211	0.0368245	16.3158	0.032171	20
	15	0.275855	8.68421	0.213875	8.94737	0.064513	8.42105	0.0970148	2.10526
	20	0.410093	8.68421	0.335926	6.05263	0.10905	8.42105	0.166987	2.10526
	25	0.663836	6.31579	0.768927	6.05263	0.161749	6.84211	0.274703	2.10526
400	10	0.152075	13.9474	0.0991923	15.2632	0.0389109	2.10526	0.0527024	15.2632
	15	0.191059	7.10526	0.153072	2.10526	0.0772329	2.10526	0.125227	16.3158
	20	0.257785	10.2632	0.260379	8.15789	0.150491	2.10526	0.129714	2.10526
	25	0.491897	5.26316	0.455389	5.78947	0.316152	2.10526	0.287248	2.10526
500	10	0.15322	17.8947	0.0694774	15.5263	0.0659516	15	0.0759115	15.7895
	15	0.148082	14.4737	0.107186	1.84211	0.105616	15	0.07284	14.2105
	20	0.272125	6.84211	0.282277	8.15789	0.136058	2.10526	0.156504	2.10526
	25	0.555633	3.15789	0.467634	1.84211	0.244116	2.10526	0.286665	2.10526

Diameter of Delamination (mm)	Ball Diameter (mm)	Peak amplitude and peak frequency for 425 mm depth of delamination							
		Sensor 1		Sensor 2		Sensor 3		Sensor 4	
		Amplitude (V)	Peak Frequency (kHz)	Amplitude (V)	Peak Frequency (kHz)	Amplitude (V)	Peak Frequency (kHz)	Amplitude (V)	Peak Frequency (kHz)
100	10	0.147797	11.3158	0.143259	11.8421	0.0527389	10.7895	0.0502528	11.3158
	15	0.15608	8.68421	0.107116	11.3158	0.0717904	10.7895	0.0713002	6.57895
	20	0.253503	3.94737	0.1858	6.05263	0.0679708	6.05263	0.0634729	3.94737
	25	0.417428	4.73684	0.460236	5.52632	0.104784	3.15789	0.112348	2.10526
200	10	0.146119	13.1579	0.126011	12.1053	0.0409548	16.3158	0.0483175	16.8421
	15	0.165353	9.73684	0.153097	12.1053	0.0491891	9.73684	0.0639557	11.8421
	20	0.175828	5	0.24218	6.05263	0.0695004	9.73684	0.0520808	11.8421
	25	0.345046	5	0.316144	6.05263	0.0825113	2.36849	0.118871	2.10526
300	10	0.112236	14.4737	0.135475	16.3158	0.0713375	16.3158	0.0413788	14.4737
	15	0.176276	11.3158	0.130381	16.3158	0.0938273	16.3158	0.065265	17.8947
	20	0.157063	9.73684	0.126453	1.84211	0.0597997	16.3158	0.0941876	2.10526
	25	0.351202	4.73684	0.297907	4.73684	0.109727	5.26316	0.122679	2.10526
400	10	0.121744	9.73684	0.0866981	16.5789	0.0430334	9.73684	0.0341751	8.15789
	15	0.202003	9.21053	0.090292	6.31579	0.0828111	9.73684	0.0818249	8.15789
	20	0.205844	5.26316	0.118863	4.73684	0.062955	5.26316	0.0599217	8.15789
	25	0.346468	5	0.298281	4.73684	0.128095	5.26316	0.0935891	2.89474
500	10	0.139928	13.9474	0.0849365	16.5789	0.0424794	14.7368	0.0595221	17.3684
	15	0.255601	11.5789	0.180623	11.8421	0.0910763	11.3158	0.0857474	11.5789
	20	0.220931	5	0.221139	4.73684	0.0585488	15.5263	0.0673656	13.9474
	25	0.233542	5	0.251169	6.05263	0.0917214	4.21053	0.0822631	3.94737

Diameter of Delamination (mm)	Ball Diameter (mm)	Peak amplitude and peak frequency for 625 mm depth of delamination							
		Sensor 1		Sensor 2		Sensor 3		Sensor 4	
		Amplitude (V)	Peak Frequency (kHz)	Amplitude (V)	Peak Frequency (kHz)	Amplitude (V)	Peak Frequency (kHz)	Amplitude (V)	Peak Frequency (kHz)
100	10	0.167955	15.7895	0.1276	16.5789	0.0552925	10.2632	0.0529492	15.2632
	15	0.16653	7.10526	0.180581	6.31579	0.107694	8.42105	0.115309	6.84211
	20	0.264378	3.94737	0.284015	6.57895	0.193925	9.47368	0.138154	6.84211
	25	0.517253	3.94737	0.35533	2.10526	0.15442	4.73684	0.144864	6.84211
200	10	0.141529	10	0.118182	13.1579	0.0287705	7.10526	0.032172	11.0526
	15	0.152914	9.47368	0.100242	9.21053	0.0669522	10.5263	0.123445	15.5263
	20	0.227558	5	0.268053	6.31579	0.0635866	5.78947	0.128299	6.57895
	25	0.523549	3.94737	0.565437	1.84211	0.142508	3.15789	0.235538	1.84211
300	10	0.189971	16.5789	0.172594	15	0.0724211	17.3684	,101303	15
	15	0.166889	11.8421	0.111063	6.57895	0.0787445	10.5263	0.0969404	8.15789
	20	0.193755	10.2632	189799	1.84211	0.0811737	10.5263	0.0901491	2.10526
	25	0.344298	4.73684	0.290962	4.73684	0.154873	4.21053	0.144034	7.89474
400	10	0.120918	15.5263	0.0641867	2.10526	0.0302493	15	0.0288651	15.5263
	15	0.15323	8.15789	0.166201	8.68421	0.0709568	8.42105	0.0875787	8.15789
	20	0.265255	5.26316	0.240686	4.73684	0.101551	9.47368	0.117266	8.15789
	25	0.442953	5.26316	0.381845	4.73684	0.157005	4.73684	0.133669	4.73684
500	10	0.22272	14.4737	0.0982745	15.7895	0.0410081	14.2105	0.0658641	18.4211
	15	0.240761	7.36842	0.0230594	7.36842	0.140493	11.0526	0.0824016	6.57895
	20	0.3722	7.10526	0.390304	6.31579	0.165779	11.0526	0.160252	6.57895
	25	0.579222	5.26316	0.535232	4.73684	0.154712	5.26316	0.181146	1.84211

Diameter of Delamination (mm)	Ball Diameter (mm)	Peak amplitude and peak frequency for 825 mm depth of delamination							
		Sensor 1		Sensor 2		Sensor 3		Sensor 4	
		Amplitude (V)	Peak Frequency (kHz)	Amplitude (V)	Peak Frequency (kHz)	Amplitude (V)	Peak Frequency (kHz)	Amplitude (V)	Peak Frequency (kHz)
100	10	0.167955	15.7895	0.1276	16.5789	0.0552925	10.2632	0.0527812	15.2632
	15	0.16653	7.10526	0.180581	6.31579	0.107694	8.42105	0.115309	6.84211
	20	0.264378	3.94737	0.284015	6.57895	0.193925	9.47368	0.138154	6.84211
	25	0.517253	3.94737	0.357219	2.10526	0.15442	4.73684	0.144864	6.84211
200	10	0.141529	10	0.118182	13.1579	0.032172	7.10526	0.0287705	11.0526
	15	0.152914	9.47368	0.100242	9.21053	0.123445	10.5263	0.0669522	15.5263
	20	0.227558	5	0.268053	6.31579	0.0635866	5.78947	0.128299	6.57895
	25	0.523549	3.94737	0.565437	1.84211	0.142508	3.15789	0.235538	1.84211
300	10	0.189971	16.5789	0.172594	15	0.0724211	17.3684	0.101303	15
	15	0.166889	11.8421	0.111063	6.57895	0.787445	10.5263	0.0969404	8.15789
	20	0.193755	10.2632	0.189799	1.84211	0.0811737	10.5263	0.0901491	2.10526
	25	0.344298	4.73684	0.289862	4.73684	0.154873	4.21053	0.144034	7.89474
400	10	0.120918	15.5263	0.0641867	2.10526	0.0302493	15	0.0288651	15.5263
	15	0.15323	8.15789	0.166201	8.68421	0.0709568	8.42105	0.0875787	8.15789
	20	0.265255	5.26316	0.240686	4.73684	0.101551	9.47368	0.117266	8.15789
	25	0.442953	5.26316	0.381845	4.73684	0.157005	4.73684	0.133669	4.73684
500	10	0.22272	14.4737	0.0982745	15.7895	0.0410081	14.2105	0.0658641	18.4211
	15	0.240761	7.36842	0.230594	7.36842	0.140493	11.0526	0.0824016	6.57895
	20	0.390304	7.10526	0.3722	6.31579	0.165779	11.0526	0.160252	6.57895
	25	0.579222	5.26316	0.535232	4.73684	0.154712	5.26316	0.181146	1.84211

Diameter of Delamination (mm)	Ball Diameter (mm)	Peak amplitude and peak frequency at unsound concrete							
		Sensor 1		Sensor 2		Sensor 3		Sensor 4	
		Amplitude (V)	Peak Frequency (kHz)	Amplitude (V)	Peak Frequency (kHz)	Amplitude (V)	Peak Frequency (kHz)	Amplitude (V)	Peak Frequency (kHz)
control	10	0.260076	16.5789	0.204189	16.5789	0.0807123	11.0526	0.0737996	11.5789
	15	0.182323	5.26316	0.168856	6.84211	0.118719	9.73684	0.0725452	9.47368
	20	0.424485	3.68421	0.474221	6.84211	0.371545	8.42105	0.26414	8.42105
	25	0.637658	3.68421	0.423477	4.21053	0.204294	8.42105	0.150521	8.42105